INSTITUTE

FOR

COSMIC RAY RESEARCH

THE UNIVERSITY OF TOKYO

ANNUAL REPORT
(APRIL 2012 – MARCH 2013)

5-1-5, Kashiwanoha, Kashiwa, Chiba 277-8582, Japan

Telephone: (81) 4-7136-3102
Facsimile: (81) 4-7136-3115
WWW URL: http://www.icrr.u-tokyo.ac.jp/

TABLE OF CONTENTS

PREFACE

This report summarizes the scientific activities of the Institute for Cosmic Ray Research (ICRR) of the University of Tokyo in the Japanese FY 2012.

ICRR is an inter-university research institute for studies of cosmic rays. The headquarters of ICRR is located in Kashiwa, Chiba prefecture, Japan. In order to promote various cosmic-ray-related studies efficiently, ICRR has three research divisions; Neutrino and Astroparticle division, High Energy Cosmic Ray division, and Astrophysics and Gravity division. ICRR has 3 observatories in Japan; Kamioka Observatory (Kamioka underground, Gifu prefecture), Norikura Observatory (2770 meters above sea level, Mt. Norikura, Gifu prefecture), and Akeno Observatory (Yamanashi prefecture), together with 1 research center; Research Center for Cosmic Neutrinos (Kashiwa, Chiba prefecture). In addition, there are 2 major experimental facilities outside of Japan. They are located in Utah in USA, and Yangbajing in Tibet, China.

More than 300 researchers from various Japanese institutions are involved in the research programs of ICRR. It should be noted that most of the scientific outputs from this institute are the results of the collaborative efforts by many scientists from various institutions. In order to produce outstanding results, it is very important to carry out an experiment by an international collaboration composed of top-level researchers all over the world. Hence, most of the experimental collaborations that ICRR is involved are international ones. For example, the number of collaborators in the Super-Kamiokande experiment is about 120; about a half of them are from abroad (USA, Korea, China, Poland and Spain).

Many exciting scientific activities of ICRR are described in this report. One of the highlights in FY 2012 is the results from the Telescope Array experiment, which studies the highest-energy cosmic rays in detail. Another highlight is the the construction of the large-scale cryogenic gravitational wave telescope (KAGRA), which intends to detect gravitational waves for the first time and open a new field of ”gravitational wave astronomy”.
It is very important that the activities of ICRR are evaluated by top-level researchers in the world in order to make the decisions on the proper direction of the research activities. Therefore, the External Review Committee was formed in 2012. The review meeting was held on January 16, 17, and 18, 2013 at ICRR. The reveiw report, which was released in May 2013, is copied in this annual report. In addition, ICRR Future Project Evaluation Committee was formed in 2012. The Committee has been evaluating various possible future projects of ICRR. It is expected that the report from this Committee will be published soon.
We hope that this report is useful for the understanding of the current research activities of ICRR. Finally, we appreciate very much the strong support of our colleagues in this research field, the University of Tokyo and the Japanese Ministry of Education, Culture, Sports, Science and Technology. They are indispensable for the continuing, and exciting scientific outcome of ICRR.

Takaaki Kajita,
Director,
Institute for Cosmic Ray Research,
The University of Tokyo

The ICRR building at Kashiwa, Chiba, Japan.

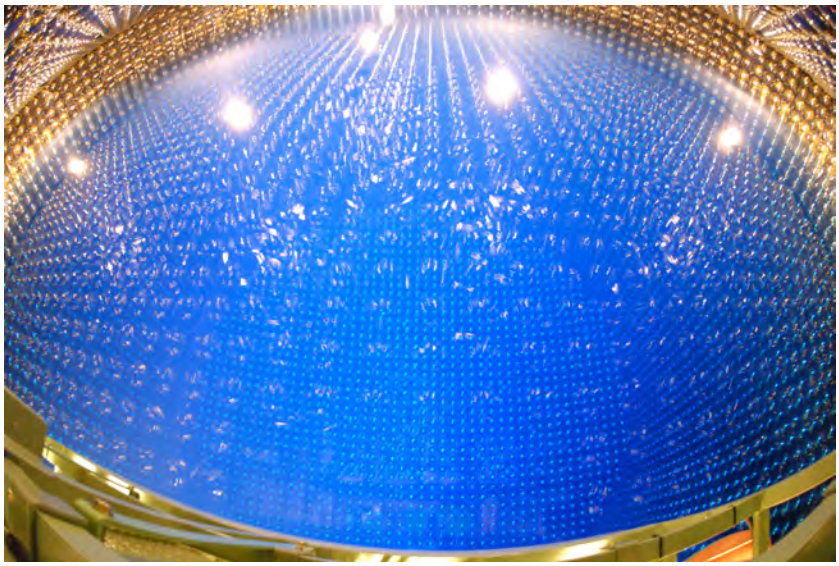

The inner detector of Super-Kamiokande-III during the full reconstruction. The purified water is under filling.

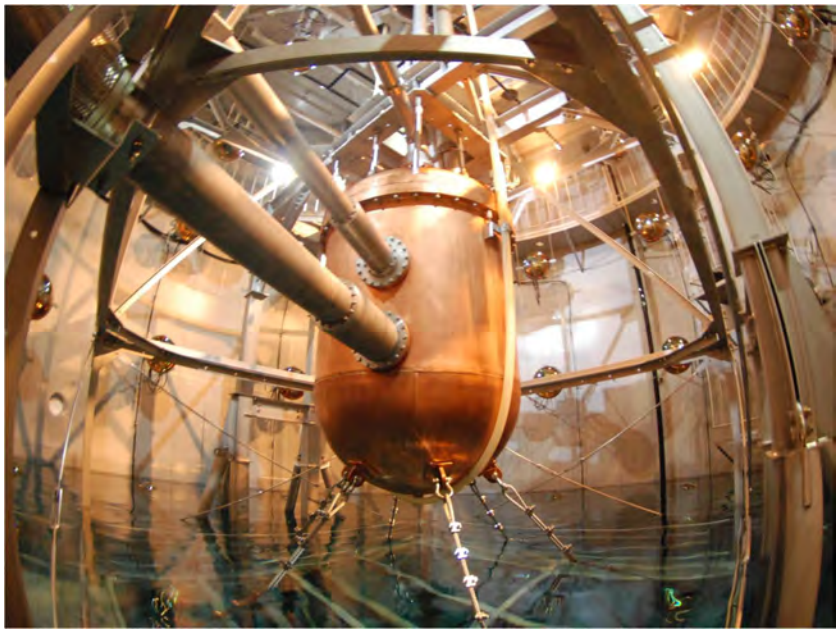

XMASS detector using 835 kg of liquid xenon. Radiations are shielded and cosmic-ray muons can be vetoed by a water-Cherenkov detector outside.

The system of four imaging atmospheric Cherenkov telescopes of 10m diameter of CANGAROO project for detection of very high energy gamma-rays The whole system is in operation since March 2004 in Woomera, South Australia.

Tibet-III air shower array (37000 m^2) at Yangbajing, Tibet (4300 m in altitude).

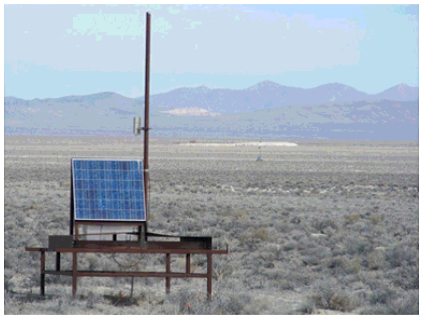

Air fluorescence telescopes (left) and a scintillator surface detector (right) of the Telescope Array experiment in Utah, USA to explore the origin of extremely high energy cosmic rays.

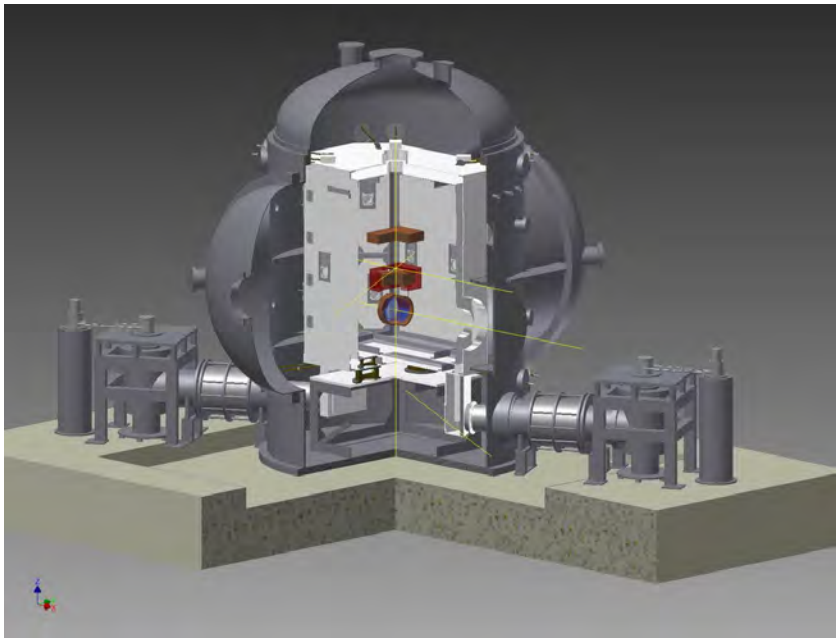

Cryogenic mirror sysytem for KAGRA with a cryostat and a cryocooler.

A public lecture held by Research Center for Cosmic Neutrinos.

Organization

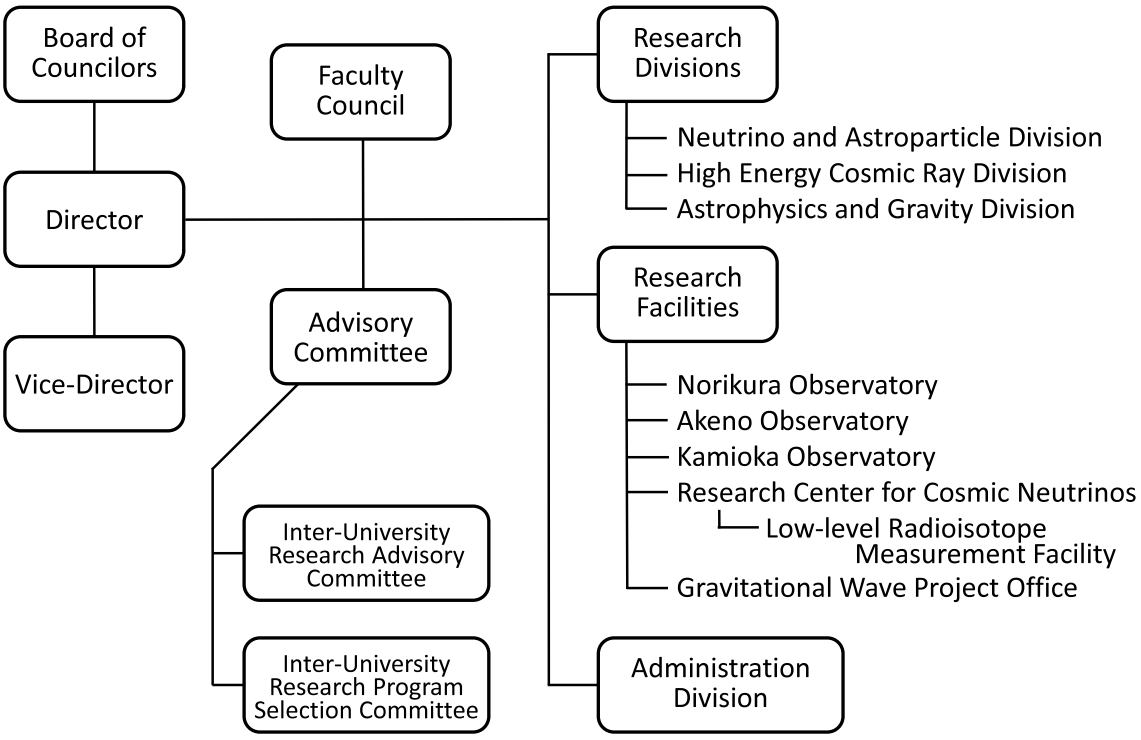

Number of Staff Members (As of May 1, 2012)

	Scientific Staff	Technical Staff	Research Fellows	Administrators and Secretaries	Total
Neutrino and Astroparticle Div.	24	4	3	17	48
High Energy Cosmic Ray Div.	16	11	6	3	36
Astrophysics and Gravity Div.	13	3	5	3	24
Administration	1	0	0	12	13
Total	54	18	14	35	121

FY 2006–2012 Budget

	2006	2007	2008	2009	2010	2011	2012
Personnel expenses	566 000	624 000	632 000	590 000	576 000	653 000	658 000
Non-personnel expenses	812 000	1 253 000	1 121 000	1 292 000	1 048 000	1 400 000	1 172 000
Total	1 378 000	1 877 000	1 753 000	1 882 000	1 624 000	2 053 000	1 830 000

(in 1 000 yen)

RESEARCH DIVISIONS

Neutrino and Astroparticle Division

Overview
Super-Kamiokande
T2K Experiment
XMASS Experiment
Hyper-Kamiokande R&D

High Energy Cosmic Ray Division

Overview
Cherenkov Cosmic Gamma-Ray Group
TA: Telescope Array Experiment
Tibet ASγ Project
The Ashra Project
High Energy Astrophysics Group

Astrophysics and Gravity Division

Overview
Gravitational Wave Group
- Gravitational Wave Project Office
- KAGRA Project Status
- CLIO Project

Observational Cosmology Group
Primary Cosmic Ray Group
Theory Group
- Particle Phenomenology
- Astrophysics and Cosmology

NEUTRINO AND ASTROPARTICLE DIVISION

Overview

This division aims to study particle physics with prime interests in physics of neutrinos and proton decay, and astroparticle physics with the use of underground experimental facilities.

Our most important facility is the Super-Kamiokande (SK) detector. It is a 50 kton water Cherenkov detector using 11,129 50 cm-diameter photomultipliers (PMTs) for its inner detector and 1,885 20 cm-diameter PMTs for its outer detector. The data taking of SK started in April 1996. The neutrino oscillations in atmospheric neutrinos were discovered in 1998 and thereby demonstrating that neutrinos have a finite mass. In 2001, the accurate measurements of the ^{8}B solar neutrino flux by SK and SNO discovered that neutrino oscillations are the solution of the solar neutrino problem beyond doubt. After those discoveries, precise measurements of atmospheric neutrinos and solar neutrinos have been performed and they unraveled various phenomena of neutrino oscillations. In 2012, excess of events induced by ν_τ appearance was observed in atmospheric neutrinos, and the day/night difference of the solar neutrino flux, which is expected from the matter effect of neutrino oscillations, was observed in the precise solar neutrino measurement.

The search for nucleon decay at SK gives the current best limit which strongly constrains the grand unification scenario of particle interactions. SK has been searching for neutrinos from supernovae by two methods, one is a search for burst neutrinos orignate from nearby supernovae, another is so-called supernova relic neutrinos, which is an accumulated supernova burst neutrinos from the biginning of the universe.

A high intensity neutrino beam experiment using the J-PARC accelerator (T2K) was started in 2009. The T2K experiment uses the SK detector as the far detector. Electron neutrino appearance (the effect of the mixing angle θ_{13}) and the high precision measurement of oscillation parameters are main physics subjects in T2K. An indication of electron neutrino appearance was found in June 2011, and the significance of the appearance has been improved to the discovery level in 2012.

Another activity of the Neutrino and Astroparticle division is a multi-purpose experiment using liquid xenon aiming at the detection of cold dark matter, neutrino absolute mass using neutrinoless double beta decay, and low energy solar neutrinos. The construction of a 800 kg liquid xenon detector was completed at the end of 2010 and subsequent commissioning run continued by June 2012. With the commissioning data, low-mass WIMPs, annual modulation of event rate, and axions were studied. In Aug. 2012, detector refurbishment to reduce the surface background started.

In addition to those on-going projects, some R&D projects are also proceeded. GADZOOKS! is a project to add 0.1% of gadolinium into the Super-K tank in order to tag neutrons for $\bar{\nu}_e$ detection. It should enable us to detect supernova relic neutrinos. A feasibility study for GADZOOKS! has been performed using a 200 ton tank which mimics the Super-K detector. The Hyper-Kamiokande (Hyper-K) detector is proposed as a next generation underground water Cherenkov detector. The detector is approximately 20 times larger in volume than Super-K and has discovery potential of leptonic CP violation and proton decays. New photosensor R&D and physics potential studies for Hyper-K has been performed in 2012.

SUPER-KAMIOKANDE

[Spokesperson : Yoichiro Suzuki]
Kamioka Observatory, ICRR, The University of Tokyo

Results obtained with the Super-Kamiokande detector in 2012 are reviewed for each topic.

Atmospheric neutrinos

Cosmic ray interactions in the atmosphere produce neutrinos. The prediction of the absolute flux has an uncertainty of at least $\pm 20\,\%$. However, the flavor ratio of the atmospheric neutrino flux, $(\nu_\mu + \bar{\nu}_\mu)/(\nu_e + \bar{\nu}_e)$, has been calculated to an accuracy of better than $5\,\%$. Another important feature of atmospheric neutrinos is that the fluxes of upward and downward going neutrinos are expected to be nearly equal for $E_\nu >$(a few GeV) where the effect of the geomagnetic field on primary cosmic rays is negligible.

Neutrino oscillation was discovered in the study of atmospheric neutrinos in SK in 1998 [1]. We have continued observing atmospheric neutrino events in Super-Kamiokande from 1996.

The SK atmospheric neutrino data has been successfully described with two flavor $\nu_\mu \to \nu_\tau$ oscillation hypothesis with maximum mixing angle (θ_{23}=π/4). However, according to recent measurements of the mixing angle between the first and third generations (θ_{13}) by the accelerator and reactor neutrino experiments, $\nu_\mu \to \nu_e$ oscillation channel due to the finite value of θ_{13} will provide us the opportunity to probe the unknown properties such as *CP* violation and mass hierarchy in lepton sector, which may be a hint for solving the origin of the matter.

We have analyzed the atmospheric neutrino data accumulated of SK-I+II+III+IV ($1489 + 799 + 518 + 1097$ days for full-contained (FC) / patially-contained (PC) and $1646 + 828 + 636 + 1097$ days for upward-going muons). We studied oscillation effects in all types of data that are categorized into FC events, PC events, and upward-going muons. FC events are characterized by the primary vertex position that is located inside the 22.5 kton fiducial volume of the detector and all the

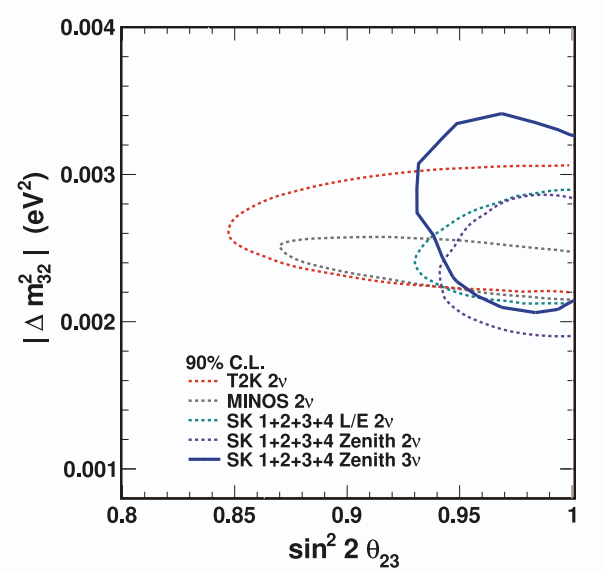

Fig. 2. Allowed oscillation parameter regions of 90% confidence levels obtained by oscillation analyses based on the Super-Kamiokande-I+II+III+IV data. The regions allowed by SK L/E analysis, $\nu_\mu \to \nu_\tau$ two flavor oscillation analysis, and full parameter three flavor oscillation analysis are shown along with T2K, MINOS results.

visible secondary particles stopped in the inner detector. PC events have the primary vertex position in the fiducial volume but at least one charged particle escaping from the inner detector. In most cases, the escaping particle is a muon. Upward-going muons originate from high energy muon-neutrino interactions in the rock surrounding the detector. Only the muon traveling through the detector upward is identified.

FC sample are divided into sub-GeV and multi-GeV according to the visible energy, and also separated into electron-like and muon-like events by particle identificantion algorithm. Though it is difficult to distinguish neutrino and antineutrino interactions on an event-by-event basis in the water Cherenkov detector, the statistical separation between ν_e and $\bar{\nu}_e$ in multi-GeV sample are carried out by using the difference of their kinematics properties at interactions in order to improve the sensitivity of the mass hierarchy determination.

Fig. 1 compares the zenith angle and lepton momentum distributions of the atmospheric neutrino data with Monte Carlo (MC) expectations with and without neutrino oscillations for FC, PC and upward-going muon events. This demonstrates that the presence of neutrino oscillation, and the atmospheric neutrino data is consistent with oscillation hypothesis in a wide energy range from sub-GeV to several 10 TeV energy range. Fig. 2 shows the allowed regions of neutrino oscillation parameters obtained by two flavor $\nu_\mu \to \nu_\tau$ oscillation and three flavor oscillation. Though the allowed region by three flavor oscillation is slightly extended compared to those by two flavor oscillation due to additional uncertainties of other oscillation parameters, they are consistent with the results from accelerator experiments.

We aimed at probing the unknown oscillation parameters, such as leptonic CP violation and mass hierarchy, by measuring $\nu_\mu \to \nu_e$ oscillation other than $\nu_\mu \to \nu_\tau$ oscillation in the atmospheric neutrino data. Several effects as listed below will be expected based on the standard three flavor oscillation framework:

- A resonant enhancement by the matter effect is expected in $\nu_\mu \leftrightarrow \nu_e$ oscillation driven by θ_{13} in the 5 to 10 GeV energy range. This effect will be observable as an excess of electron-like events in the upward-going direction, and to some degree in the oscillations of multi-GeV muon-like events.
- The above ν_e enhancement is selective for either ν_e or $\bar{\nu}_e$ depending on mass hierarchy.
- The effects of the solar oscillation parameters and non-maximal mixing are observable as a ν_e oscillation effect on the event rate of the Sub-GeV electron-like samples.
- If the CP violating term δ_{cp} is also considered, there are additional sub-dominant oscillation effects predicted across many of the SK atmospheric neutrino samples.

We have performed an extended oscillation analysis including all the mixing parameters and the CP violating term, δ_{cp}. In the oscillation analysis, the matter effect in the Earth is considered, and both the normal and inverted mass hierarchies are tested. In order to consider the θ_{13} constraint according to the recent precise measurements by the reactor experiments, θ_{13} is fixed to be $\sin^2\theta_{13}$=0.025.

Table 1 shows the oscillation parameters at the global best fit point and their allowed ranges for each hierarchy assumption.

Table 1. Oscillation parameters at best fit and of 90% C.L. allowed region obtained by three flavor oscillation analysis for normal and inverted hierarchy assumptions, respectively. The oscillation fits are performed with the constraint of $\sin^2\theta_{13}$=0.025.

	Normal		Inverted	
	best fit	90% C.L.	best fit	90% C.L.
Δm^2_{32} ($\times 10^{-3}$eV^2)	2.82	2.25 - 3.22	2.66	2.21 - 3.02
$\sin^2\theta_{23}$	0.60	0.39 - 0.45	0.60	0.41 - 0.64
δ_{CP}	220°	all allowed	220°	$0° - 9°$, $80° - 360°$

Fig. 3 shows $\Delta\chi^2$ as a function of $\sin^2\theta_{23}$ and δ_{CP} parameters with normal and inverted hierarchy assumptions, respectively, with and without reactor θ_{13} constraint. Still CP violation parameter and octant of $\sin^2\theta_{23}$ cannot be constraint more than 90% C.L., however some indications on those parameters can be seen. $\sin^2\theta_{23}$ at best fit point is slightly deviated from the maximal mixing (θ_{23}=$\pi/4$). The second octant of $\sin^2\theta_{23}$ is favored in inverted hierarchy while the first octant becomes preferred by introducing θ_{13} constraint in normal hierarchy. The large region of δ_{CP} is preferred for both hierarchy assumptions.

Fig. 4 shows the comparison of fitted χ^2 value as a function of δ_{CP} between normal and inverted hierarchy assumptions. The global minimum χ^2 value is slightly smaller for inverted hierarchy by 1.5 .

It becomes possible to search for CPT violation effects in the neutrino system via differences in the oscillation probabilities of neutrinos and antineutrinos. By inspiring oscil-

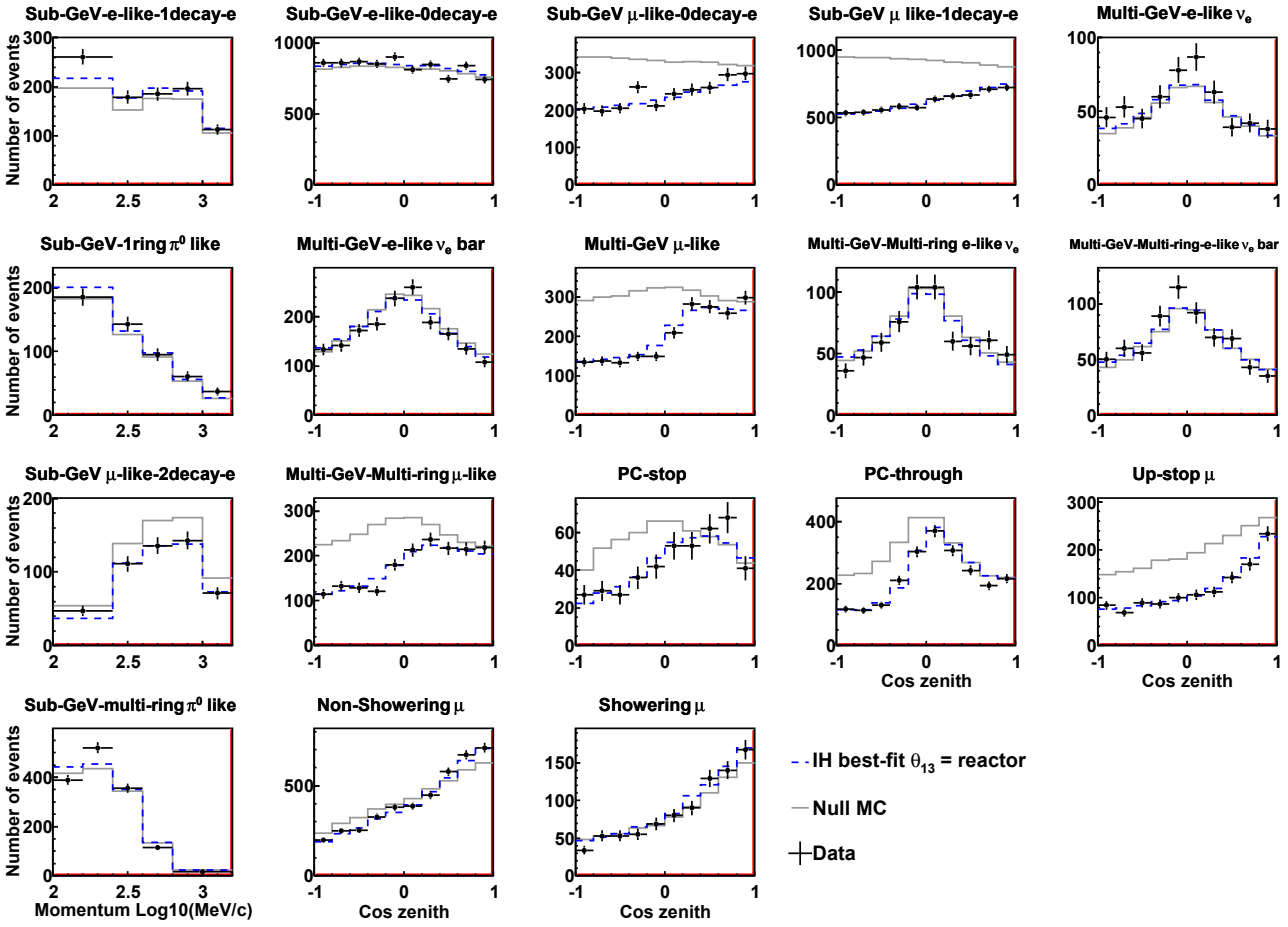

Fig. 1. The zenith angle and lepton momentum distributions for atmospheric neutrino events observed in Super-Kamiokande-I+II+III+IV. In zenith angle distributions, $\cos\Theta$ =1(-1) corresponds to vertically down-going (up-going) direction. Points with error bars are data with statistical error. The grey histograms show the MC predictions without neutrino oscillation and the blue histograms show the MC predictions for the best−fit point of 3-flavor oscillation assuming inverted hierarchy.

lation result by MINOS [1], we also performed a *CPT* violation test of the atmospheric neutrino data using separated two-neutrino disappearance model, which allows neutrino and antineutrino to oscillate with different parameter sets of (Δm^2, θ) and ($\Delta\bar{m}^2$, $\bar{\theta}$), respectively. According to the fitting result, the allowed region for antineutrino mixing parameters is shown in Fig. 5. The atmospheric mixing parameters for antineutrino oscillations are consistent with those for neutrinos and therefore no evidence for *CPT* violation is found [2].

Tau events, which are produced via ν_τ charge current (CC) interactions oscillated from ν_μ, are expected to be observed in SK. It would bring the direct evidence of $\nu_\mu \to \nu_\tau$ oscillation, however, the detection of ν_τ CC events in SK is challenging; the interaction rate of ν_τ charged current events is low since the neutrino energy threshold is 3.5 GeV and the atmospheric neutrino flux above this energy is relatively low. Also tau events are difficult to be identified individually because they tend to produce multiple particles. Tau analysis is performed employing neural network technique to discriminate tau events of hadronic decay from backgrounds of atmospheric ν_e and ν_μ events. Fig. 6 shows the zenith angle distribution of tau-selected events. Tau events are expected to appear in the upword-going events because they originates $\nu_\mu \to \nu_\tau$ oscillation. The zenith angle shape of data is fitted with the MC expectation including tau signal and background with their normalizations free. According to the fitting result, the signal excess is estimated to 180.1 $\pm$ 4.3 (stat) $^{+17.8}_{-15.2}$ (syst) events compared to an expectation of 120.2 $^{+34.2}_{-34.8}$ (syst) and the detection significance correspond to 3.8 σ [3].

From recent observations, Weakly Interacting Massive Particles (WIMPs) are considered a favorite candidate for cold dark matter. From the viewpoint of minimum supersymmetric extensions of the Standard Model, the most well-motivated candidate for WIMPs in the universe is the lightest supersymmetric neutral particle (LSP). One method of searching for a WIMP dark matter signal is an indirect search where decay or annihilation products from WIMPs are observed as originating from the center of a gravitational potential well such as a celestial body. WIMP annihilation products in the form of muon-neutrinos are an excellent instrument for indirect searches since they can pass thorough the matter of the Sun, and interact in the Earth. Here we investigate upward-going muons(upmus) which are generated from high energy neutrinos come from the WIMP annihilations using Super-Kamiokande [4]. We search in the direction of the Sun, and an excess of neutrino flux above the atmospheric neutrino back-

*1 P. Adamson *et al.* (MINOS), Phys. Rev. Lett. 107, 021801 (2011)

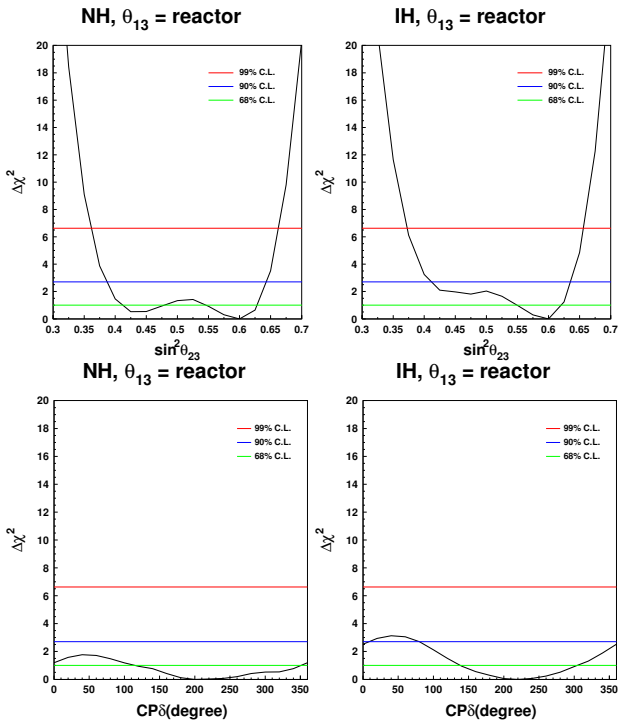

Fig. 3. Left two figures show distributions of $\Delta\chi^2$ versus $\sin^2\theta_{23}$, and right two figures show $\Delta\chi^2$ versus δ_{CP}, for normal (left) and inverted (right) hierarchy assumption. $\Delta\chi^2$ means the difference from the minimum χ^2 among the oscillation fits in each hierarchy assumption. The region below green (blue) line is allowed by 68% (90%) confidence level.

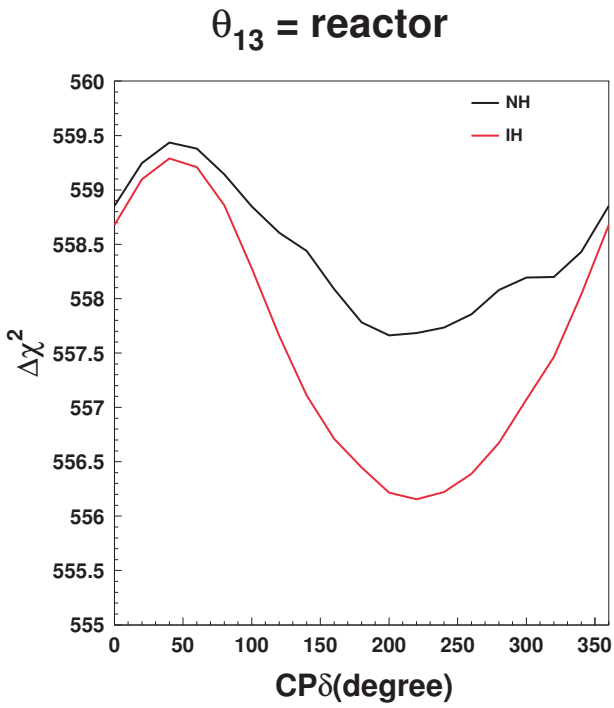

Fig. 4. χ^2 distributions as a function of CP violating term, δ_{CP} for normal (black) and inverted (red) hierarchy assumption. In each δ_{CP} point, other oscillation parameters are marginalized with fixed θ_{13}.

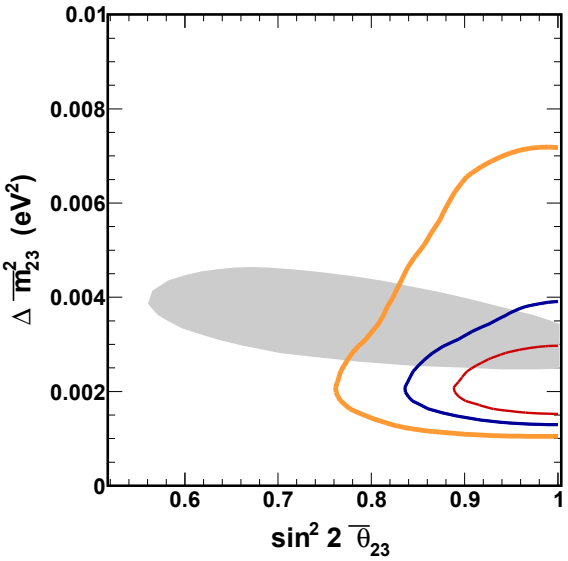

Fig. 5. Allowed regions for the antineutrino mixing parameters for SK-I+II+III data set. The 68%, 90%, and 99% allowed region appear in red thin, blue medium, and orange thick lines, respectively. The shaded region shows the 90% C.L. allowed region for antinuetrino disappearance in an antineutrino beam from MINOS.

ground is sought in the upmu events. Although volume array detectors such as IceCube have larger acceptances for higher mass WIMPs, SK is better equipped for the search of lower mass WIMPs (<100 GeV) due to its lower energy threshold for neutrino signals. The calculated upper limit is shown in Fig. 7 with the results from direct detection experiments.

Solar Neutrinos

Solar neutrino flux measurements from Super-Kamiokande (SK) [5] and the Sudbury Neutrino Observatory(SNO) [6] have provided direct evidence for solar neutrino flavour conversion. However, there is still no clear evidence that this solar neutrino flavour conversion is indeed due to neutrino oscillations and not caused by any other mechanism. Currently there are two testable signatures unique to neutrino oscillations. The first is the observation and precision test of the MSW resonance curve [7]. Based on oscillation parameters extracted from solar neutrino and reactor anti-neutrino measurements, there is an expected characteristic energy dependence of the flavour conversion. The higher energy solar neutrinos (higher energy ^{8}B and hep neutrinos) undergo complete resonant conversion within the sun, while the flavour changes of the lower energy solar neutrinos (pp, ^{7}Be, pep, CNO and lower energy ^{8}B neutrinos) arise only from vacuum oscillations, which limits the average electron flavour survival probability to exceed 50%. The transition from the matter dominated oscillations within the sun, to the vacuum dominated oscillations, should occur near 3 MeV, making ^{8}B neutrinos the best choice when looking for a transition point within the energy spectrum. A second signature unique to oscillations arises from the effect of the terrestrial matter density on solar neutrino oscillations. This effect is tested directly by comparing solar neutrinos which pass through the Earth at nighttime to those which do not during the daytime. Those neutrinos which pass

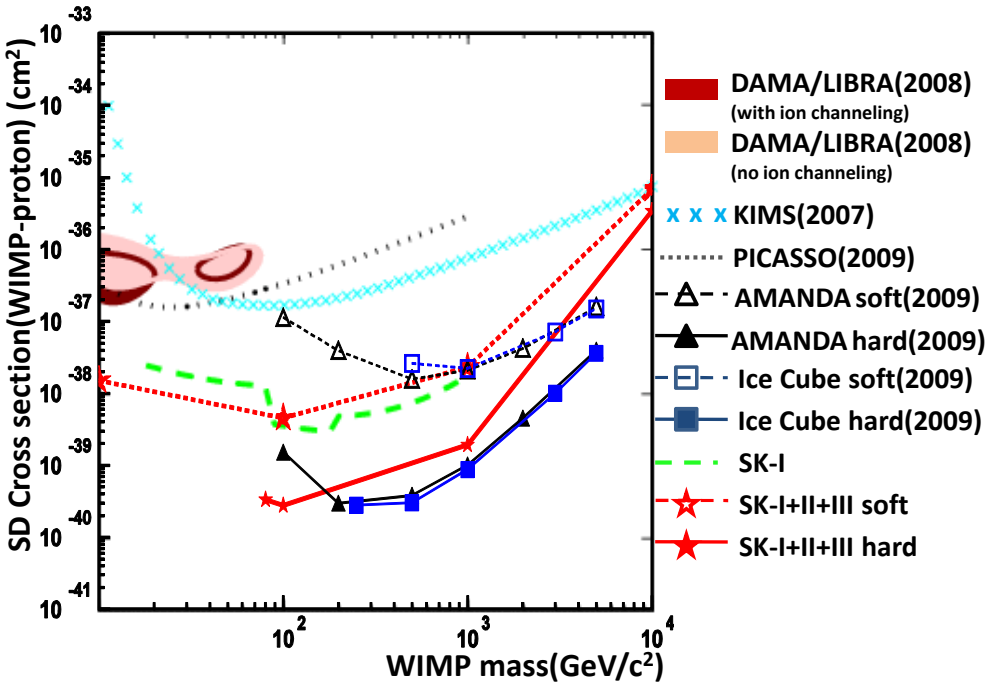

Fig. 7. Limit on the WIMP-proton spin-dependent cross section as a function of WIMP mass. Limits from direct detection experiments: DAMA/LIBRA allowed region (dark red and light red filled, for with and without ion channeling, respectively), KIMS (light blue crosses), and PICASSO (grey dotted line) are shown. Also we show here the results of indirect detection (neutrino telescopes): AMANDA (black line with triangles), IceCube (blue line with squares), and this analysis (red line with stars). Two annihilation senarios, soft channel ($b\bar{b}$) and hard channel (W^+W^-), are considered. Also the previous limit from Super-K (green dashed line) is shown.

through the Earth will in general have an enhanced electron neutrino content compared to those which do not, leading to an increase in the nighttime electron elastic scattering rate (or any charged-current interaction rate), and hence a negative "day/night asymmetry". SK detects ^{8}B solar neutrinos over a wide energy range in real time, making it a prime detector to search for both solar neutino oscillation signatures.

The start of physics data taking of SK-IV occurred on October 6th, 2008, with this report including data taken until March 31st, 2012. The total livetime is 1069.3 days. The entire data period was taken using the same low energy threshold, with 99% triggering efficiency at 4.0-4.5 MeV kinetic energy and 100% above 4.5 MeV kinetic energy. In the case of ν-e interactions of solar neutrinos in SK, the incident neutrino and recoil electron directions are highly correlated. Fig.8 shows the $\cos\theta_{\rm sun}$ distribution for events between 4.0.-19.5 MeV as well as the definition of $\cos\theta_{\rm sun}$. In order to obtain the number of solar neutrino interactions, an extended maximum likelihood fit is used. This method is also used in the SK-I [5], II [8], and III [9] analyses. The red line of Fig.8 is the best fit to the data. The blue line shows the background component of that best fit. SK-IV has $N_{\rm bin} = 22$ energy bins; 19 bins of 0.5 MeV width between 4.0-13.5 MeV, two energy bins of 1 MeV between 13.5 and 15.5 MeV, and one bin between 15.5 and 19.5 MeV.

The combined systematic uncertainty of the total flux in SK-IV is found to be 1.7% as the quadratic sum of all components. This is the best value seen throughout all phases of SK, much improved over 2.2% in SK-III. The main contributions to the reduction come from improvements in the uncertainties arising from the energy-correlated uncertainties (energy scale and resolution), the vertex shift, trigger efficiency and the angular resolution. SK-III data below 6.0 MeV recoil electron kinetic energy has only about half the livetime as the data above, while SK-IV's livetime is the same for all energy bins. As a consequence, the energy scale and resolution uncertainties lead to a smaller systematic uncertainty of the flux in SK-IV than in SK-III. The higher efficiency of SK-IV between 5.0 and 6.0 MeV (kinetic) of SK-IV and the addition of the 4.0 to 4.5 MeV data lessens the impact of energy scale and resolution uncertainty on the flux determination even further. The number of solar neutrino events (between 4.0 and 19.5 MeV) is $19,811^{+220}_{-218}(\text{stat.}) \pm 337(\text{syst.})$. This number corresponds to a ^{8}B solar neutrino flux of $\Phi_{^8B} = (2.34 \pm 0.03(\text{stat.}) \pm 0.04(\text{syst.})) \times 10^6/(\text{cm}^2\text{sec})$, assuming a pure ν_e flavor content.

Fig.9 shows the resulting SK-IV energy spectrum, where below. To test the expected "upturn" below ~6 MeV from the MSW resonance effects, the best fit oscillation parameters of solar + KamLAND(described later) was fitted to all the SK-I to SK-IV spectra, and it is disfavored by 1.8σ so far.

The SK-IV livetime during the day (night) is 506.5 days (562.8 days). The solar neutrino flux between 4.5 and 19.5 MeV and assuming no oscillations is measured as $\Phi_D = (2.27 \pm 0.04(\text{stat.}) \pm 0.05(\text{sys.})) \times 10^6/(\text{cm}^2\text{sec})$ during the day and $\Phi_N = (2.39 \pm 0.04(\text{stat.}) \pm 0.05(\text{sys.})) \times 10^6/(\text{cm}^2\text{sec})$ during the night. A more sophisticated method to test the day/night effect is given in [5, 10]. For a given set of oscillation parameters, the interaction rate as a function of the solar zenith angle is predicted. Only the shape of the caluclated solar zenith

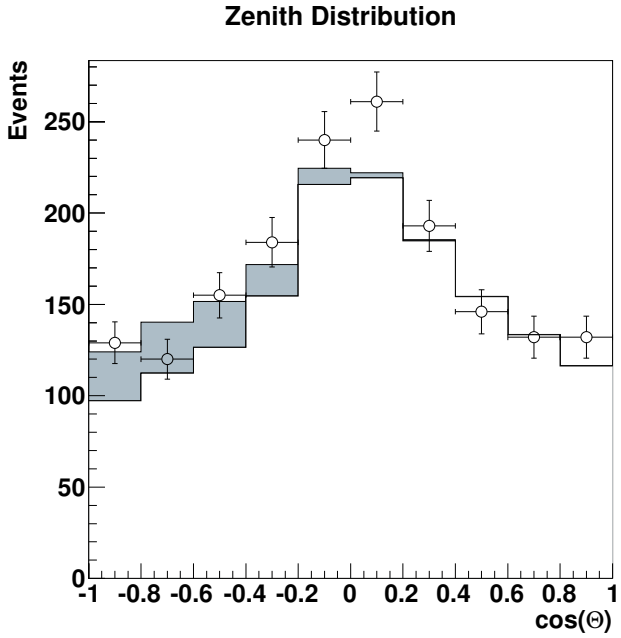

Fig. 6. Zenith angle distribution of tau-selected events by neural network method. SK-I, II, III dataset is used. Zenith angle $\cos(\theta)$=-1 (1) indicates upward-going (downward-going) direction. The data (dot with error bar) and the best-fit MC including tau signal (shaded region) and background from atmospheric neutrinos (ν_e and ν_μ) are shown.

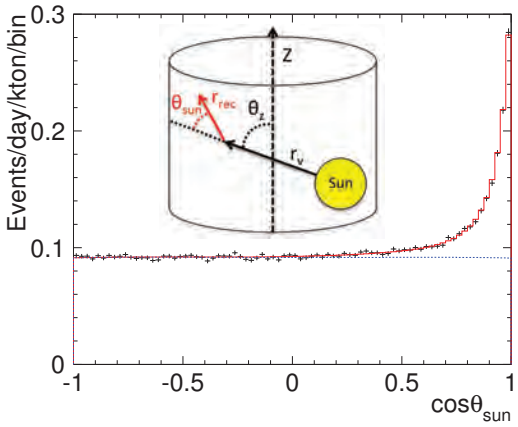

Fig. 8. Solar angle distribution for 4.0-19.5 MeV. $\theta_{\rm sun}$ is the angle between the incoming neutrino direction r_ν and the reconstructed recoil electron direction $r_{\rm rec}$. (θ_z is the solar zenith angle). Black points are data while the blue and red histograms are best fits to the background and signal plus background, respectively.

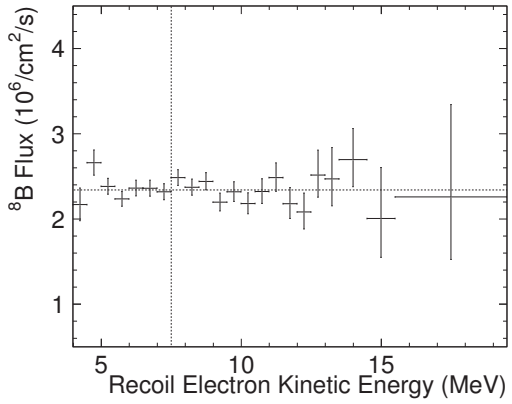

Fig. 9. SK-IV energy spectrum using MSG below 7.5 MeV. The horizontal dashed line gives the SK-IV total flux average $(2.34 \times 10^6/(\mathrm{cm}^2\mathrm{sec}))$. Error bars shown are statistical plus energy-uncorrelated systematic uncertainties.

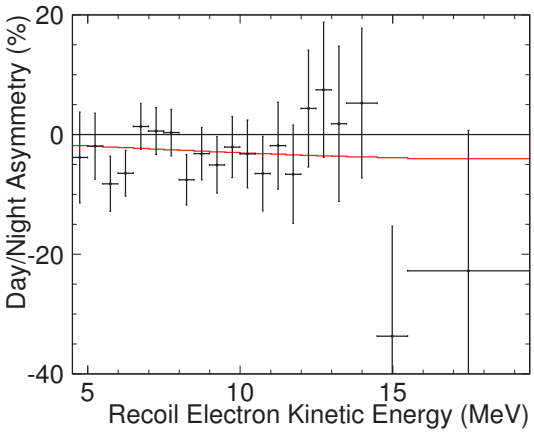

Fig. 10. SK combined energy dependence of the fitted day/night asymmetry (measured day/night amplitude times the expected asymmetry (red)) for $\Delta m^2_{21} = 4.84 \times 10^{-5}\mathrm{eV}^2$, $\sin^2\theta_{23} = 0.314$ and $\sin^2\theta_{13} = 0.025$. The error bars shown are statistical uncertainties only.

angle variation is used, the amplitude of it is scaled by an arbitrary parameter. The extended maximum likelihood fit to extract the solar neutrino signal is expanded to allow time-varying signals. The likelihood is then evaluated as a function of the average signal rates, the background rates and the scaling parameter which is called the "day/night amplitude". The equivalent day/night asymmetry is calculated by multiplying the fit scaling parameter with the expected day/night asymmetry. In this manner the day/night asymmetry is measured more precisely statistically. Because the amplitude fit depends on the assumed shape of the day/night variation, it necessarily depends on the oscillation parameters, although with very little dependence expected on the mixing angles (in or near the large mixing angle solutions and for θ_{13} values consistent with reactor neutrino measurements [11]).

The day/night asymmetry coming from the SK-I to IV combined amplitude fit can be seen as a function of recoil electron kinetic energy in Fig.10, for $\Delta m^2_{21} = 4.84 \times 10^5\mathrm{eV}^2$, $\sin^2_{12} = 0.314$ and $\sin^2_{13} = 0.025$. The day/night asymmetry in this figure is found by multiplyng the fitted day/night amplitude from each energy bin, to the expected day/night asymmetry (red distribution) from the corresponding bin.

Fig.11 shows the Δm^2_{21} dependence of the SK all phases combined day/night asymmetry for $\sin^2\theta_{12} = 0.314$ and $\sin^2\theta_{13}$ = 0.025. Here the day/night asymmetry is found by multiplying the fitted day/night amplitude by the expected day/night asymmetry (red curve). The point where the best fit crosses the expected curve represents the value of Δm^2_{21} where the measured day/night asymmetry is equal to the expectation. Superimposed are the allowed ranges in Δm^2_{21} from the global

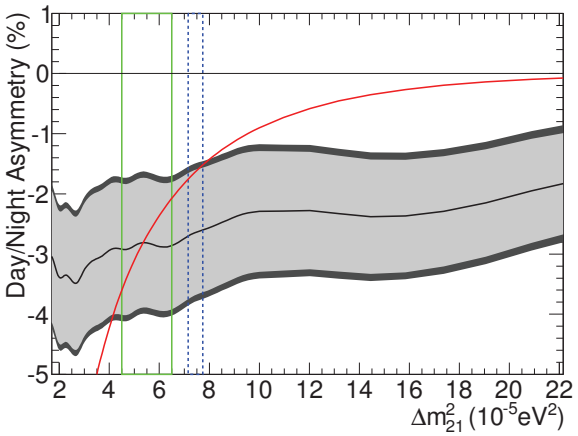

Fig. 11. Dependence of the measured day/night asymmetry (fitted day/night amplitude times the expected day/night asymmetry (red)) on Δm^2_{21} (light gray band=stat. error, dark gray band=stat.+syst. error) for $\sin^2\theta_{12} = 0.314$ and $\sin^2\theta_{13} = 0.025$. Overlaid are the allowed ranges from solar neutrino data (green band) and KamLAND (blue band).

solar neutrino data fit (green) and from KamLAND (blue). The amplitude fit shows no dependence on the values of θ_{12} (within the LMA region of the MSW plane) or θ_{13}.

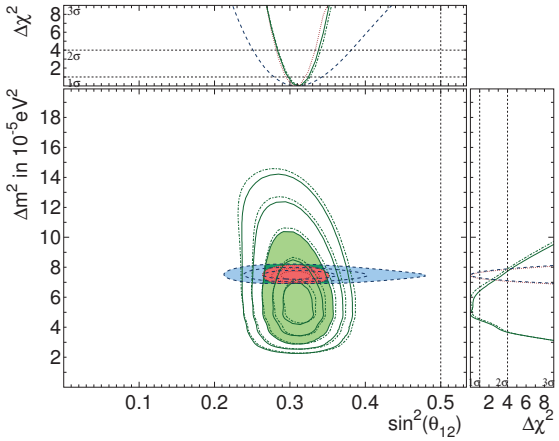

Fig. 12. Allowed contours of Δm^2_{21} vs. $\sin^2\theta_{12}$ from solar neutrino data (green) at 1, 2, 3, 4 and 5 σ and Kam-LAND data (blue) at the 1, 2 and 3 σ confidence levels. Also shown are the combined results in red. For comparison, the almost identical results of the SK+SNO combined fit are shown by the dashed dotted lines. θ_{13} is constrained by $\sin^2\theta_{13} = 0.0242 \pm 0.0026$.

We analysed the SK-IV elastic scattering rate, the recoil electron spectral shape and the day/night variation to constrain the solar neutrino oscillation parameters. We then combined the SK-IV constraints with those of previous SK phases, as well as other solar neutrino experiments. The allowed contours of all solar neutrino data (as well as KamLAND's constraints) are shown in Fig.12 and 13. In Fig.12 the contours from the fit to all solar neutrino data are almost identical to the ones of the SK+SNO combined fit. In the right panel some tension between the solar neutrino and reactor anti-neutrino measururements of the solar Δm^2_{21} is evident. This tension is

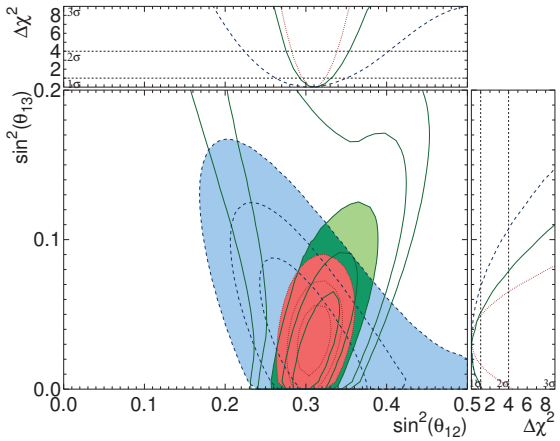

Fig. 13. Allowed contours of $\sin^2\theta_{13}$ vs. $\sin^2\theta_{12}$ from solar neutrino data (green) at 1, 2, 3, 4 and 5 σ and KamLAND measurements (blue) at the 1, 2 and 3 σ confidence levels. Also shown are the combined results in red.

mostly due to the SK day/night measurement. Even though the expected amplitude agrees well within $1\sigma$with the fitted amplitude for any Δm^2_{21} in either the KamLAND or the SK range, the SK data somewhat favor the shape of the variation predicted by values of Δm^2_{21} that are smaller than KamLAND's. The significance of non-zero θ_{13} from the solar + KamLAND data combined fit is about 2σ.

In the fourth phase of SK, we measured the solar ^{8}B neutrino-electron elastic scattering rate with the highest precison yet, $(2.34\pm0.03(\text{stat.})\pm0.04(\text{syst.}))\times10^6$ /(cm^{2}sec). We find a 2.4 σ hint for the existence of a solar day/night effect in the SK solar neutrino data, measured as the solar neutrino elastic scattering day/night rate asymmetry of -2.9 ± 1.1(stat.) ±0.5(syst.) %. SK's solar zenith angle variation data results in the world's most precise measurement of $\Delta m^2_{21} = 4.68^{+1.80}_{-0.83} \times 10^{-5}$eV^2, using neutrinos rather than antineutrinos. A fit to all solar neutrino data and KamLAND yields $\sin^2\theta_{12} = 0.304 \pm 0.013$, $\sin^2\theta_{13} = 0.030^{+0.017}_{-0.015}$ and $\Delta m^2_{21} = 7.44^{+0.20}_{-0.19} \times 10^{-5}$eV^2. This value of θ_{13} is in agreement with reactor neutrino measurements.

Search for nucleon decay

Proton decays and bound neutron decays (nucleon decays in general) is the most dramatic prediction of Grand Unified Theories in which three fundamental forces of elementary particles are unified into a single force. Super-Kamiokande (SK) is the world's largest detector to search for nucleon decays. Various nucleon decay modes have been looked for, but we have found no significant signal excess so far. In 2012, the official results has not been updated, but some studies have been carried out to improve analysis.

A proton decay into one positron and one neutral pion ($p \to e^+\pi^0$) is one of the most popular decay modes. This decay mode is mediated by super-heavy gauge bosons and discovery of the signal would give us the information of the mass of the gauge mesons. To discriminate the signal from the atmospheric neutrino background, we reconstruct the num-

ber of particles (Cherenkov rings) and reconstruct the total visible energy corresponding to parent proton mass and total momentum corresponding to the proton's Fermi momentum. If a proton decays in an oxygen with this mode, generated π^0 is affected by various interactions (scattering, absorption, charge exchange, multi pion production) with nucleus before go out from the oxygen. Recently, we have studied pion interaction cross sections which have been done by other experiments and re-tune final state interaction of pion, which is important also for atmospheric ν analysis. Fig. 14 shows cross sections of pion interaction in nucleus before (dot line) and after (solid line) the tuning. The data points shows experimental results and they show we should increase absorption and charge exchange. It will affect on number of ring distribution of $p \to e^+\pi^0$ and more signal will be rejected at selecting 2 or 3 rings in the selection criteria. Also kinematics of scattered π^0 has been tuned to adjusting experimental data. As a result, large angle scattering is increased and it also contribute to reduce efficiency because proton mass and momentun reconstruction are failed if π^0 is scattered largely. In conclusion, the selection efficiency for $p \to e^+\pi^0$ is estimated to be decreased from 45 % to 40 %. To use new pion interaction, it is needed to reprocess all proton decay MC and atmospheric ν MC for SK1 to SK4.

In addition, we looked for SUSY favored decay modes which include K mesons in the final state, $p \to \bar{\nu}K^+$. In this mode, we tag the signal by decay products from K^+. The momentum of K^+ is below the Cherenkov threshold, and is stopped in the water and decay into $\mu^+\nu$ or $\pi^+\pi^0$ with monochromatic momenta. The residual nucleus after proton decay emits γ ray (40% probability) and it is also useful to tag proton decay signal. There were several improvements in this analysis. In the conventional method to tag the prompt γ signal with $K^+ \to \mu^+\nu$, a sliding time window with 12 nsec width was used to find γ hit cluster. But because of time resolution of PMT, the γ hits which were overlapped by μ tail cannot be detected. To improved γ tagging efficiency, μ hits in 50 degree from μ direction were masked. In the atmospheric ν background, CCQEμ with invisible μ is one of the dominant source because a recoiled proton is taken as a ring and fitted as μ, then the Cherenkov angle of proton is smaller than μ case and the vertex is shifted to forward to adjust the ring edge. This vertex shift may make fake γ hits cluster in backward direction of μ after subtracting over-estimated TOF. To reject proton ring, a proton ring tagging algorism [12]is introduced.

For $K^+ \to \pi^+\pi^0$, we choose two ring sample because π^+ is just above Cherenkov threshold and π^0 decays into two γs. But if opening angle between γ is small or energy of one γ is small, sometimes π^0 reconstructed as one ring. To include the one ring sample, the π^0 fitter, which is used for rejecting background of ν_e appearance in T2K analysis is introduced. It helps to increase efficiency. To tag π^+, charge sum in backward of the π^0 is used in the conventional method. A new idea to separate signal and background is to use angular distribution. Fig. 15 shows pe distribution and horizontal axis shows angle from π^+ direction. In the signal case, there is a bump around 30 degree which is made by π^+, on the other hand, background doesnt have it. From this figure, likelihood functions assuming signal and background can be created and we

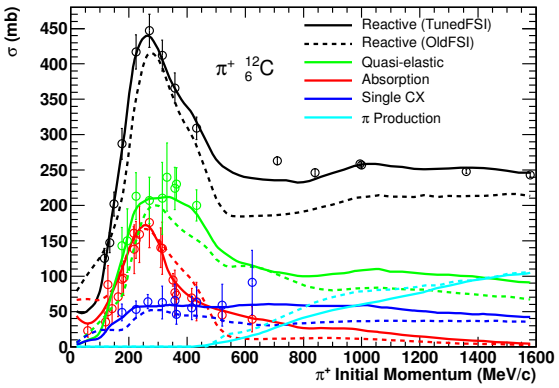

Fig. 14. Cross section of π interaction in nucleus as a function of π momentum. Plots show experimental data, solid lines show tuned simulation, and dotted lines show old simulation. Red lines are absorption and blue lines are charge exchange and they are increased in the new tune above 500 MeV/c.

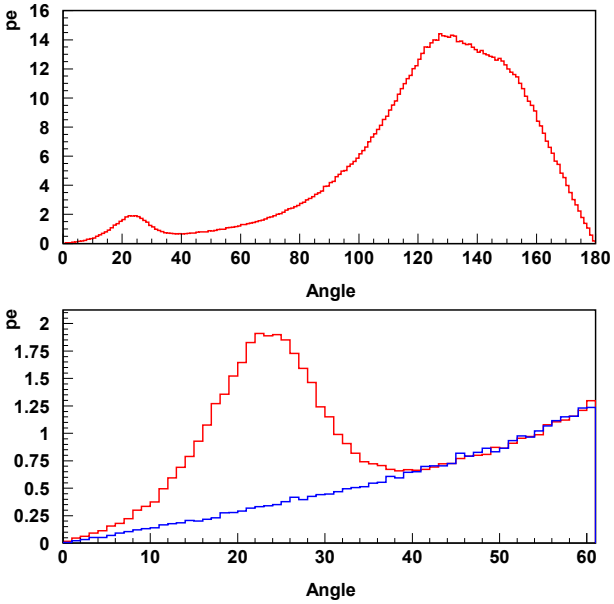

Fig. 15. Charge distribution in angle from π^+. Upper figure shows distribution of signal in entire region and lower figure shows signal (red) and background (blue) around a bump due to $\pi+$.

can separate signal and background from these function.

Those improvements will be taken into analysis then data, signal MC and background MC will be reprocessed from SK1 to SK4, and update official results in the next year.

Supernova neutrinos

Kamiokande and IMB observed the neutrino burst from supernova 1987a. This observation confirmed that the energy released by neutrinos is about several$\times 10^{53}$ergs. However, the observed number of events were only 11 by Kamiokande and 8 by IMB, respectively. Super-Kamiokande would be able to detect several thousand neutrino events if a supernova happened near the centre of our galaxy. Such an observation would enable us to investigate in detail the mechanics of the

supernova explosion.

Previously, the SK supernova search was running on an offline system. Now, galactic supernovae are searched in real time. A dedicated program called SNWATCH searches for time clustered events. The current criteria of SNWATCH are (1) more than or equal to 7 events within 0.5 sec, (2) more than or equal to 8 events within 2 sec, and (3) more than or equal to 13 events within 10 sec. When at least one of these criteria are met, SNWATCH reconstructs vertex position and energy of the events together with neighbouring cosmic ray muons. In most cases, these clusters are due to spallation products whose vertex positions are aligned with their parent cosmic ray muon. Since all the SNWATCH processes are now running on online machines, if a supernova happens, we will be able to detect it within about one minute.

If SNWATCH finds an event cluster whose vertex spread is larger than a given criterion, an alarm signal is sent to experts by e-mail and an automatic call to their cellphones. Then, the experts check whether it is a real supernova signal or not by looking at various plots which are uploaded to a secured site accessible from the Internet. These alarms are usually due to the accidental coincidence of two cosmic ray induced clusters. We have a supernova drill at least once per year. So far, no real supernova neutrino burst signal has been observed at Super-Kamiokande.

In the drill, the SNWATCH conveners and the executive committee members meet via TV conference system, and discuss to make a decision for a prompt announcement to outside researchers and the press. We practice this drill as if a real supernova happened. We also have SK shift training by illuminating an LED in the SK detector a few times every month. SK shift members are notified by a dummy alarm that SNWATCH makes when the LED is illuminated. The shift members then call to the SNWATCH experts and give a report. The SK collaborators will be ready for the real supernovae through the drill and the training.

We also search for neutrinos from old supernovae, which are called Supernova Relic Neutrinos (SRNs). The SRN signal is the diffuse supernova neutrino background from all the supernovae in the past. This signal has never been detected, but it is expected to be detectable in the 16-30 MeV energy region, which is the gap between the energy ranges of solar neutrinos and atmospheric neutrinos. We have applied carefully tuned data selection to enhance the SRN candidates, improving the efficiency of our search by over 20% compared to the 2003 SK-I study, which currently provides the world's best limit on SRN flux. Our improved data selection also allows us to now search the 16-18 MeV positron energy region, which was previously unusable due to spallation background. Our updated search utilizes SK-II and SK-III data as well as SK-I, considers two new background channels, and performs a sophisticated maximum likelihood search in multiple regions of the Cherenkov angle distribution to extract the most accurate flux limit possible(Fig.16). Multiple systematic errors are considered. A flux limit of between 2.7 and 3.0 $\bar{\nu} cm^{-2} s^{-1}$ (positron energy $>$ 16 MeV) is our new result, with the exact value depending on the shape of the neutrino spectrum assumed. This new result will replace the 2003 study to be the most accurate measure of the SRN signal ever performed.

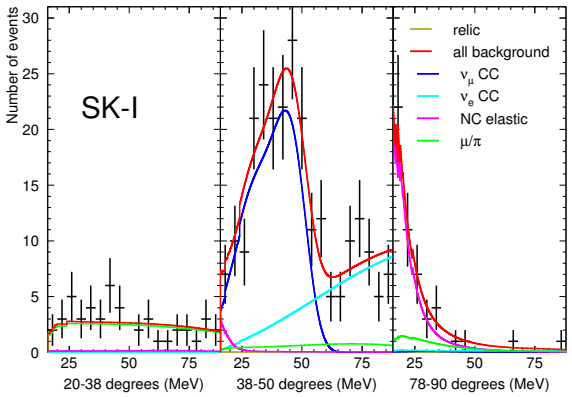

Fig. 16. SK-I best fit result, assuming Ando et al's LMA model. The relic best fit is negative, so a relic fit of 0 is shown. SK-II and SK-III have small but positive relic best fits.

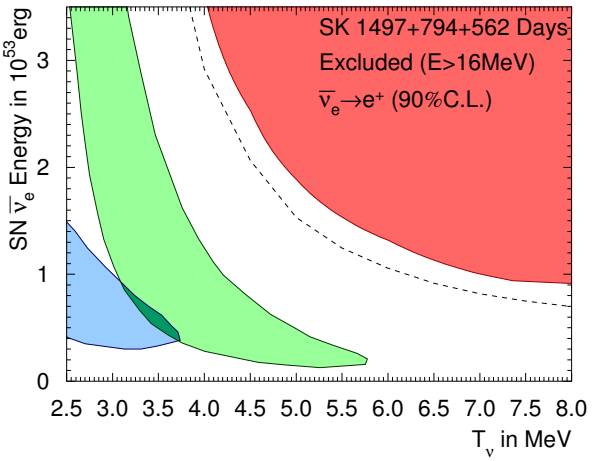

Fig. 17. Results plotted as an exclusion contour in SN neutrino luminosity vs. neutrino temperature parameter space. The green and blue contours show IMB and Kamiokande allowed areas for 1987a data, respectively. The red shows our new 90% c.l. result. The dashed line shows the individual 90% c.l. results of each temperature considered separately, which is not a true 2-D exclusion contour.

Furthermore, a new method of presenting the SRN flux limit is also ready which is of great use to theorists and does no depend on any particular model (Fig.17).

R&D for the gadolinium project

As mentioned above, although at SK a few SRN events a year are expected, SRNs have not been detected yet because the large backgrounds constrain our search. The main goal of our research is to reduce these backgrounds and be able to detect SRNs. The observation of SRNs in general or neutrinos from distant supernovae in particular, would give us some information about the universe, for example the core collapse rate from SRNs, and about the neutrino itself too, for example its lifetime. Since most of the neutrinos that can be detected at SK undergo inverse beta decay, electron anti-neutrinos are

Fig. 18. In the new cavern the Gd pre-mixing and pre-treatment 15 ton tank (front left), the selective filtration system (front right) and the 200 ton tank (rear of the hall) have been installed.

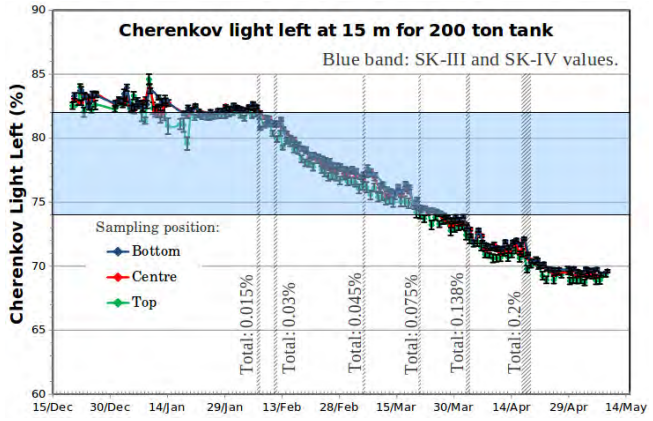

Fig. 19. Cherenkov light left at 15 m for gadolinium loaded water from the 200 ton tank. The horizontal blue bands are the values at SK-III and SK-IV. The vertical lines show the injection dates, where we also indicate the concentration (% in mass) in the 200 ton tank.

the most copiously detected neutrinos:

$$\bar{\nu}_e + p \rightarrow e^+ + n \qquad (1)$$

Presently, the SK detector can only detect the positrons efficiently but if we could detect the neutrons, we could greatly reduce the backgrounds that constrain our SRN search. This could be attained by the coincidence detection of positron and neutron (in space, vertices within tens of cm and in time, with the neutron capture delayed about 20 μsec). By adding 0.2% of gadolinium (Gd) sulfate into the water tank we could achieve this goal. Gadolinium has a neutron capture cross section of 49.000 barns (about 5 orders of magnitude larger than of protons) and emits a gamma cascade of 8 MeV that can be easily detected at SK.

We want to show that adding Gd into the SK water, SK will become an electron anti-neutrino detector, able to tag inverse beta decays, while keeping all its previous capabilities in the other analyses like solar and atmospheric neutrinos.

The EGADS (Evaluation Gadolinium's Action on Detector Systems) project was funded in 2009. Since then, a new hall near the SK detector has been excavated and a 200 ton tank with its ancillary equipment has been installed, see Fig.18, to mimic the conditions at SK. Of special importance is the selective water filtration system, that filters out water impurities while it keeps the Gd in the water.

From January 2010 to July 2011 we circulated pure water through the 200 ton tank and proved that our water system is stable and achieves a high water quality. Next we circulated Gd loaded water through the pre-treatment 15 ton tank where we gained very valuable experience running with Gd before starting our test with the 200 ton stainless steel tank (for more details see the last two annual reports).

In 2013, from February 6th to April 20th, the 200 ton tank has been stepwise loaded with Gd until the final 0.2% concentration was reached. Each batch was dumped into the 15 ton tank and then stirred until completely dissolved. Next, the loaded water was circulated through the pre-treatment system (with 0.2 μm and 0.3 μm filters) to remove dust and other impurities mainly coming from the gadolinium sulfate salt itself. Finally, the Gd loaded water was injected into the 200 ton tank after being processed at least once through the main water system.

We learnt two important lessons: the Gd sulfate dissolves homogeneously in the 200 ton tank and we can achieve and maintain a good water quality, see Fig.19.

This summer we will install 240 photomultipliers and towards end of this year 2013, we will load the water with Gd again. Next year we will upgrade the electronics and EGADS will thus become a detector with instant supernova detection capabilities.

Bibliography

[1] Y. Fukuda *et al.*, Phys. Rev. Lett. **81** 1562 (1998).

[2] K. Abe *et al.*, Phys. Lev. Lett. **107**, 241801 (2011)

[3] K. Abe *et al.*, Phys. Lev. Lett. **110**, 181802 (2013)

[4] T. Tanaka *et al.*, Astrophys. J. **742**, 78 (2011)

[5] J.Hosaka et al., Phys. Rev. D73, 112001 (2006).

[6] Q.R.Ahmad et al., Phys. Rev. Lett. 87 071301 (2001).

[7] S.P.Mikheyev and A.Y.Smirnov, Sov. Jour. Nucl. Phys. 42, 913 (1985); L.Wolfenstein, Phys. Rev. D17, 2369 (1978).

[8] J.P.Cravens et al., Phys. Rev. D 78, 032002(2008).

[9] K.Abe et al., Phys. Rev. D 83 052010 (2011).

[10] M.B.Smy et al., Phys. Rev. D. 69, 011104(R) (2004).

[11] F.P.An et al., arXiv:1210.6327 (2012); J.K.Ahn et al., Phys.Rev.Lett. 108 191802 (2012); Y.Abe et al.,Phys.Rev. D86 052008 (2012).

[12] M. Fechner *et al.* [Super-Kamiokande Collaboration], Phys. Rev. D **79**, 112010 (2009) [arXiv:0901.1645 [hep-ex]].

T2K EXPERIMENT

[Spokesperson : Takashi Kobayashi]
High Energy Accelerator Research Organization (KEK)

The T2K (Tokai-to-Kamioka) experiment [1] is a long-baseline neutrino oscillation experiment, employing a high-intensity muon neutrino beam from the J-PARC facility in Tokai sent to the Super-Kamiokande (SK) water Cherenkov detector 295 km away in Kamioka. The primary goal of T2K is to measure the last unknown mixing angle θ_{13} by observing electron neutrino appearance. T2K also aims to make a precision measurement of the known neutrino oscillation parameters with precision of $\delta(\Delta m^2_{32}) \sim 10^{-4}\,\mathrm{eV}^2$ and $\delta(\sin^2 2\theta_{23}) \sim 0.01$ via muon neutrino disappearance studies.

For producing the T2K neutrino beam, 30 GeV protons are extracted from the J-PARC Main Ring (MR) accelerator [2] and then sent to collide into a graphite target. Charged particles produced by the collisions are sign selected and focused into the 96 m long decay volume by three magnetic horns pulsed at 250 kA. Neutrinos are primarily produced in the decays of charged pions and kaons.

T2K is the first long-baseline experiment which adopts the off-axis technique [3]: the neutrino beam is purposely directed at a 2.5° angle with respect to the baseline connecting the proton target and the SK far detector. Although it reduces the total neutrino flux at the far detector, this technique allows to select the energy of the neutrinos, producing a narrow-band muon neutrino beam with the energy peaked at the first oscillation maximum $E_\nu \sim 0.6$ GeV, reducing backgrounds from higher energy neutrino interactions.

The near detector site at ~ 280 m from the production target houses two detector systems. The on-axis Interactive Neutrino GRID (INGRID [4]), composed of an array of iron/scintillator sandwiches, monitors the neutrino beam intensity, direction and profile. The off-axis ND280 detector situated along the same direction as SK measures the neutrino beam composition and energy spectrum prior to oscillations and is used to study neutrino interactions. The ND280 detector utilizes a 0.2 T magnetic field generated by the refurbished UA1 / NOMAD magnet and consists of two fine-grained scintillator bar detectors (FGDs [5]) sandwiched between three gaseous time projection chambers (TPCs [6]), side muon range detectors (SMRDs [7]), electromagnetic calorimeters (ECALs), and a π^0-optimized detector (P0D [8]).

The far detector, SK [9], is a 50 kton water Cherenkov detector located in the Kamioka Observatory. The T2K trigger records all the photomultiplier hits within $\pm 500\,\mu$s of the beam arrival time at SK. Beam timing information is measured spill-by-spill at J-PARC and immediately passed to the online computing system at SK. The time synchronization between the two sites is done using the Global Positioning System (GPS) with < 150 ns precision and is monitored with the Common-View method [10]. Spills used for the far detector data analysis are selected by beam and SK quality cuts. The largest source of spill loss at SK is the requirement that there are no events in the $100\,\mu$s before the beam window which is necessary to reject decay electrons from cosmic-ray muons.

Table 2. T2K data taking periods and the integrated protons on target (POT) for SK data collected in those periods.

Run Period	Dates	Integrated POT
Run 1	Jan. 2010 - Jun. 2010	0.32×10^{20}
Run 2	Nov. 2010 - Mar. 2011	1.11×10^{20}
Run 3	Mar. 2012 - Jun. 2012	1.58×10^{20}

The neutrino flux at the near and far detectors in the absence of neutrino oscillations is predicted by a Monte Carlo (MC) simulation of the T2K beamline, which includes the interactions of particles in the target, beamline components, decay volume walls and beam dump, and their decays. The simulation and its associated uncertainties are driven by measurements of the primary proton beam profile, measurements of the magnetic fields of the T2K horns, and hadron production data, including NA61/SHINE measurements [11, 12]. The predicted neutrino flux is predominantly ν_μ with $< 1\,\%\,\nu_e$ contamination.

The predicted neutrino flux at the ND280 and SK detectors is input to the NEUT neutrino interaction generator [13] to simulate neutrino interactions in the detectors. The dominant interaction at the T2K beam peak energy is charged current quasi-elastic scattering (CCQE) : $\nu_l + N \rightarrow l + N'$, where l is the corresponding charged lepton associated with the neutrino's flavor (electron or muon), and N and N' are the initial and final state nucleons. Above the pion production threshold, single pion production contributes to charged current interaction (CC1π) and neutral current interactions (NC1π). The systematic uncertainties in modeling neutrino interactions are derived from comparisons of NEUT to external data or alternative models.

For oscillation studies in JFY2012, the CCQE-like and CCnonQE-like ν_μ data measured at the ND280 detector are fit to determine tuned values of the ν_μ and ν_e flux parameters and cross section model parameters. The tuned parameters are then applied to predict the signal and background interactions at SK for ν_e appearance and ν_μ disappearance measurements. The fit also incorporates constraints on the flux and cross section models determined independently from the ND280 data constraint to properly propagate all constraints to the SK event rate predictions.

In 2011, the T2K experiment reported the first clear indication of the non-zero θ_{13} by measuring electron neutrino appearance in the 1.43×10^{20} protons on target (POT) beam data collected before the Tohoku earthquake [14]. Later, in 2012, the non-zero θ_{13} was firmly established by reactor $\bar{\nu}_e$ disappearance measurements [15, 16, 17]. In JFY2012, T2K updated the electron neutrino appearance measurement using neutrino data collected during the three run periods listed in Table 2. The total SK data set corresponds to 3.01×10^{20} POT or 4% of the T2K design exposure. A detailed description of the T2K JFY2012 ν_e appearance analysis can be found in the published paper [18]. A brief summary is provided here.

The electron neutrino appearance analysis produces a SK

Table 3. Summary of the contributions to the total uncertainty on the predicted number of events, assuming $\sin^2 2\theta_{13} = 0$ and 0.1, separated by sources of systematic uncertainty. The total error size in the 2011 analysis is also shown for comparison.

	$\sin^2 2\theta_{13} =$	
Error source	0	0.1
Beam flux & ν int. (ND280 meas.)	8.5%	5.0%
ν int. (from other exp.)	6.0%	7.5%
Final state interactions	2.9%	2.3%
Far detector	6.8%	3.0%
Total	13.0%	9.9%
(T2K 2011 results)	(23%)	(18%)

event sample enhanced in ν_e CCQE interactions arising from $\nu_\mu \to \nu_e$ oscillations. The main background are intrinsic ν_e contamination in the beam and neutral-current (NC) interactions with a misidentified π^0. The criteria for selecting ν_e appearance candidate events at SK are unchanged from those for the T2K 2011 analysis : (1) beam on-timing, (2) fully-contained fiducial volume, (3) single e-like ring, (4) visible energy $E_{vis} > 100$ MeV, (5) no delayed electron, (6) non-π^0-like, and (7) reconstructed neutrino energy $E_\nu^{rec} < 1250$ MeV. In run 1-3 data, 11 events passed all the selection cuts. The predicted number of events for $\sin^2 2\theta_{13} = 0$ is 3.3 ± 0.4(syst.). Table 3 summarizes the uncertainty on the predicted number of events for each systematic error source. The probability to observe 11 candidate events when 3.3 ± 0.4(syst.) background events are expected is 0.09%, equivalent to a 3.1σ significance. The T2K experiment found the first evidence of electron neutrino appearance in a muon neutrino beam at the atmospheric mass splitting.

To extract the confidence interval for $\sin^2 2\theta_{13}$, the ν_e candidate sample was fit in the three neutrino mixing paradigm. The dominant effect of a non-zero $\sin^2 2\theta_{13}$ is to increase the overall rate of ν_e events. However, spectral information can be used to further separate the signal from background. Hence, in addition to the fit using rate-only information, two independent fits using rate+spectral information were performed : one using electron momentum and angle with respect to the T2K beam direction (p_e, θ_e), the other using reconstructed neutrino energy E_ν^{rec}. The three analyses gave consistent results with each other. Fig. 20 shows the observed E_ν^{rec} distribution for the ν_e events with the best fit of the E_ν^{rec} analysis applied. Assuming $\sin^2 2\theta_{23} = 1.0$ and $\delta_{CP} = 0$, the best fit values of $\sin^2 2\theta_{13}$ with the 68% confidence intervals are :

$$\sin^2 2\theta_{13} = 0.092^{+0.049}_{-0.039} \quad \text{(normal hierarchy)}$$
$$\sin^2 2\theta_{13} = 0.112^{+0.058}_{-0.047} \quad \text{(inverted hierarchy)}.$$

Fig. 21 shows the 68 % and 90 % confidence intervals for $\sin^2 2\theta_{13}$ and the best fit $\sin^2 2\theta_{13}$ for each value of δ_{CP}.

The T2K ν_μ disappearance measurement was also updated using the whole run 1-3 data. The cuts for producing a ν_μ CCQE enriched sample are unchanged from the previous analysis : (1) beam on-timing, (2) fully-contained fiducial volume, (3) single μ-like ring, (4) reconstructed muon momentum $>$ 200 MeV/c, and (5) number of delayed electron signals is 0

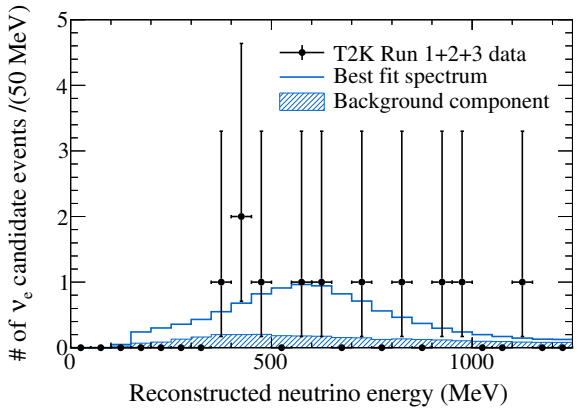

Fig. 20. The observed E_ν^{rec} distribution and prediction, assuming $\sin^2 2\theta_{13} = 0.092$, $\delta_{CP} = 0$, and normal hierarchy. The background component is also shown.

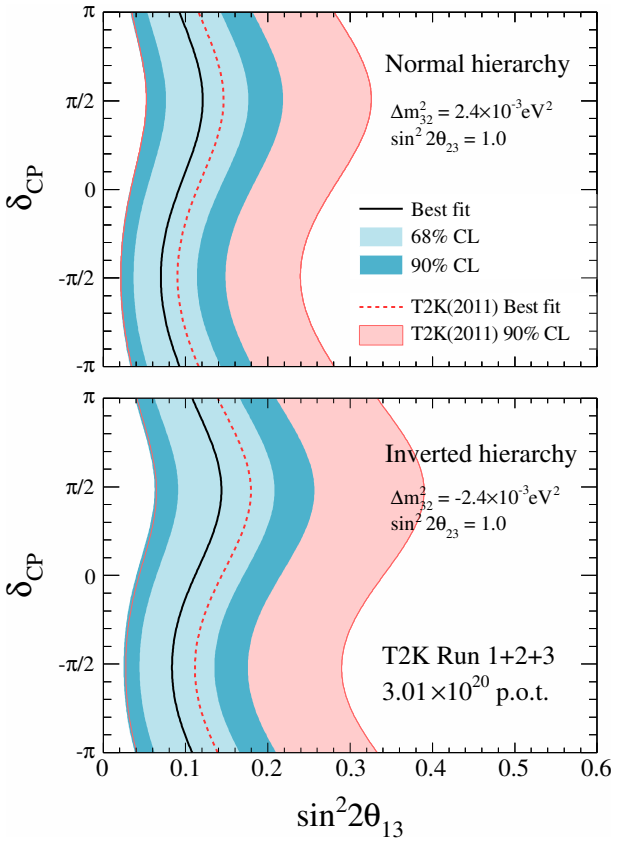

Fig. 21. The 68% and 90% confidence intervals for $\sin^2 2\theta_{13}$ scanned over values of δ_{CP} assuming $\sin^2 2\theta_{23} = 1.0$ and normal hierarchy (top) and inverted hierarchy (bottom).

or 1. Two independent analyses were performed to determine the allowed region in the parameter space $|\Delta m^2_{32}| - \sin^2 2\theta_{23}$: one is a likelihood ratio method with binned E_ν^{rec} spectrum, and the other is a maximum likelihood method with unbinned E_ν^{rec} shape. The preliminary 90% confidence region obtained by the two analyses is shown in Fig. 22.

T2K has also performed the first measurement of ν_μ inclusive charged current interactions on carbon at neutrino energies of ~ 1 GeV where the measurement is reported as flux-averaged double differential cross section in muon momentum and angle. The result can be found elsewhere [19]. A

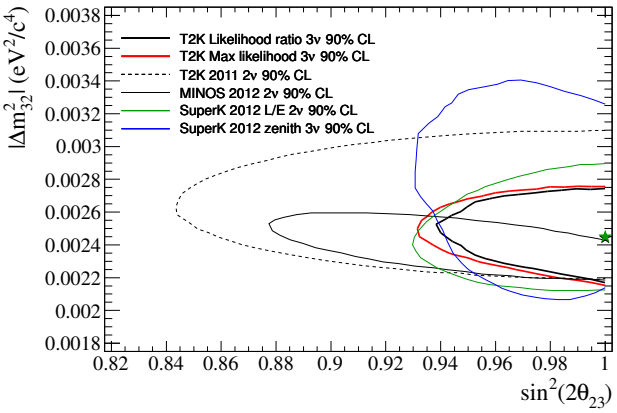

Fig. 22. Preliminary 90% confidence region for the two T2K ν_μ disappearance analyses in JFY2012, combined with the allowed region from an earlier result and allowed regions from other experiments.

measurement of neutrino-oxygen NC cross sections is also on-going by observing nuclear de-excitation gamma-rays in the beam data at SK.

The T2K run 4 period started in October 2012. It is expected that T2K will increase the accumulated data to more than twice of the run 1-3 data and reject the "no ν_e appearance" hypothesis with $> 5\sigma$ significance by summer 2013. T2K electron neutrino appearance measurements will be an important input to global fits which also combine muon neutrino disappearance measurements and reactor-based measurements of θ_{13} via $\bar{\nu}_e$ disappearance to begin to constrain δ_{CP} and the octant of θ_{23}.

Bibliography

[1] K. Abe *et Hal.* [T2K Collaboration], Nucl. Instrum. Meth. A **659**, 106 (2011) [arXiv:1106.1238 [physics.ins-det]].

[2] Y. Yamazaki *et al.*, KEK Report 2002-13 and JAERI-Tech 2003-44 and J-PARC-03-01 (2003).

[3] D. Beavis, A. Carroll, I. Chiang, *et al.*, Long Baseline Neutrino Oscillation Experiment at the AGS (Proposal E889), 1995. Physics Design Report, BNL 52459.

[4] M. Otani, N. Nagai, D. Orme, A. Minamino, K. Nitta, O. Drapier, F. Moreau and M. Besnier *et al.*, Nucl. Instrum. Meth. A **623**, 368 (2010).

[5] P. A. Amaudruz *et al.* [T2K ND280 FGD Collaboration], Nucl. Instrum. Meth. A **696**, 1 (2012) [arXiv:1204.3666 [physics.ins-det]].

[6] N. Abgrall *et al.* [T2K ND280 TPC Collaboration], Nucl. Instrum. Meth. A **637**, 25 (2011) [arXiv:1012.0865 [physics.ins-det]].

[7] S. Aoki, G. Barr, M. Batkiewicz, J. Blocki, J. D. Brinson, W. Coleman, A. Dabrowska and I. Danko *et al.*, Nucl. Instrum. Meth. A **698**, 135 (2013) [arXiv:1206.3553 [physics.ins-det]].

[8] S. Assylbekov, G. Barr, B. E. Berger, H. Berns, D. Beznosko, A. Bodek, R. Bradford and N. Buchanan *et al.*, Nucl. Instrum. Meth. A **686**, 48 (2012) [arXiv:1111.5030 [physics.ins-det]].

[9] Y. Fukuda *et al.* (Super-Kamiokande Collaboration), Nucl. Instrum. Meth. A501, 418 (2003).

[10] D. W. Allan and M. A. Weiss, Proceedings of the 34th Annual Symposium on Frequency Control, 334 (1980).

[11] N. Abgrall *et al.* [NA61/SHINE Collaboration], Phys. Rev. C **84**, 034604 (2011) [arXiv:1102.0983 [hep-ex]].

[12] N. Abgrall *et al.* [NA61/SHINE Collaboration], Phys. Rev. C **85**, 035210 (2012) [arXiv:1112.0150 [hep-ex]].

[13] Y. Hayato, Nucl. Phys. (Proc. Suppl.) B112, 171 (2002).

[14] K. Abe *et al.* [T2K Collaboration], Phys. Rev. Lett. **107**, 041801 (2011) [arXiv:1106.2822 [hep-ex]].

[15] F. P. An *et al.* [DAYA-BAY Collaboration], Phys. Rev. Lett. **108**, 171803 (2012) [arXiv:1203.1669 [hep-ex]].

[16] J. K. Ahn *et al.* [RENO Collaboration], Phys. Rev. Lett. **108**, 191802 (2012) [arXiv:1204.0626 [hep-ex]].

[17] Y. Abe *et al.* [DOUBLE-CHOOZ Collaboration], Phys. Rev. Lett. **108**, 131801 (2012) [arXiv:1112.6353 [hep-ex]].

[18] K. Abe *et al.* [T2K Collaboration], arXiv:1304.0841 [hep-ex].

[19] K. Abe *et al.* [T2K Collaboration], arXiv:1302.4908 [hep-ex].

XMASS EXPERIMENT

[Spokesperson : Yoichiro Suzuki]

Kamioka Observatory, ICRR, The University of Tokyo

XMASS is a multi-purpose experiment (detection of dark matter, neutrino-less double beta decay, and ^{7}Be/pp solar neutrinos) using ultra-pure liquid xenon [1]. The first stage of XMASS experiment is for dark matter searches using 800 kg liquid xenon detector (100 kg fiducial-mass detector). The detector construction in the Kamioka mine was funded and started in April 2007. Construction work was completed in September 2010 and commissioning data was taken from October 2010 to May 2012. Based on calibration data we took, we found that the detector has the largest photoelectron yield ($\approx$14 photoelectrons/keV). This enables us to realize low-energy threshold which is important for dark matter search. In the following sections, we describe results on searches for dark matter and axion-like particles as well as a next stage detector, XMASS 1.5.

Several astronomical observations indicate that the universe contains a large amount of nonbaryonic dark matter. One of the most plausible candidates for the nonbaryonic dark matter is a weakly interacting massive particle (WIMP) provided by the supersymmetry in the form of the lightest supersymmetric particle. WIMPs can be directly detected through their elastic scattering off target nuclei in a detector. XMASS searches for the WIMP-xenon nucleus interaction in liquid xenon. Liquid xenon has the several advantages for dark matter searches. Large amount of scintillation light (42,000 photons/MeV), which is as good as NaI(Tl) scintillator enables us to detect small energy signals such as dark matter recoil.

The XMASS detector consists of the cylindrical water tank with 72 50 cm PMTs and spherical liquid xenon detector with 642 2 inch PMTs as shown in Fig. 23. This is the first case to adopt a pure-water tank as an active and passive shield for dark matter experiments. The spherical array of PMTs is contained in a double wall vessel. The vessel consisting of inner and outer vacuum chamber is made from oxygen free high conductivity copper. The gap between IVC and OVC is kept vacuum for thermal isolation. Details of the detector are described in Ref. [2].

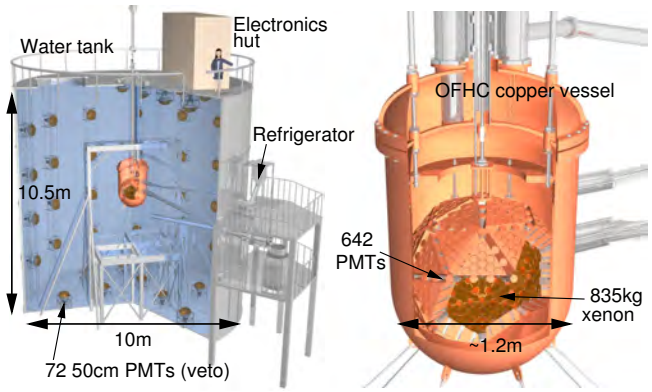

Fig. 23. Schematic view of the water tank and the liquid xenon vessel.

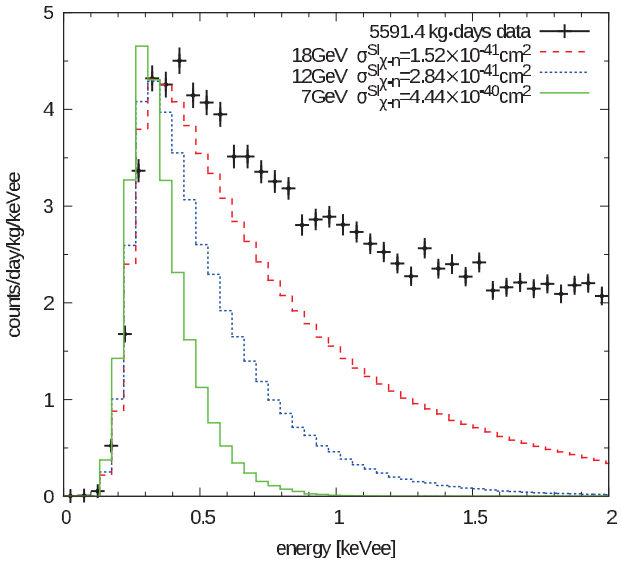

Fig. 24. Observed energy spectrum and predictions for various mass of dark matter.

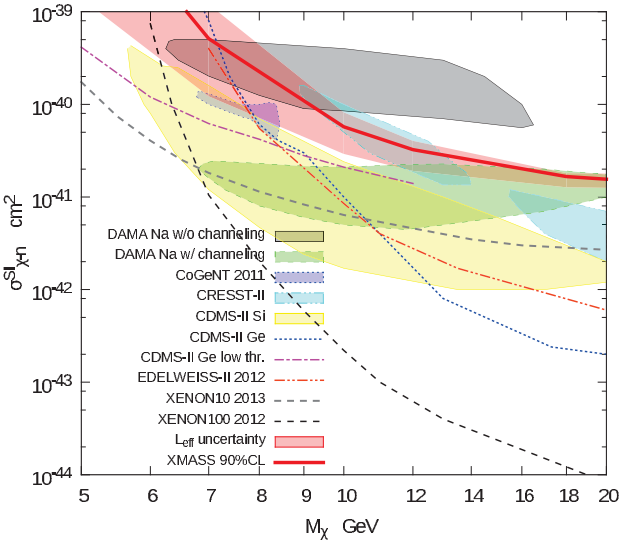

Fig. 25. Preliminary result of constraints on low mass WIMPs (red thick line) with uncertainties of scintillation efficiency (red dark region). Allowed region for DAMA (gray area) and CoGeNT (blue area) are also shown.

Results using commissioning data

A search for light WIMPs has been carried out by taking advantage of the high light yield. Since the energy threshold is low (0.3 keV electron-equivalent, keVee), the detector is sensitive to low mass WIMPs. We used whole the detector volume since fiducial volume cut based on the event reconstruction cannot be used due to a limited number of photoelectrons at the lowest energy range. Fig.24 shows the energy spectrum after rejection of noisy events and Cherenkov events mainly caused by potassium in photo cathodes. In the same figure, expectations of dark matter signals are shown. Since the signals cannot exceed the observed energy spectrum, limits on the cross section for the light WIMPs have been derived. Fig.25 shows the limit on the cross section. Though we have uncertainty originated from the scintillation efficiency for nuclear recoil (red band), some part of allowed region by the DAMA experiment was excluded. See Ref. [3] for more details.

Some studies have been done to search axion-like particle. One study is for the candidate of dark matter which might cause the annual modulation observed by DAMA group. If the dark matter consists of such particles, their signal would be detected through axio-electric effect. The data set for the light WIMPs search was used to find the mono-energetic signals which correspond to rest mass of the non-relativistic dark matter. Since there is no prominent peak in the observed data, limits on the axion-electron coupling are given as shown in Fig.26.

Another study is for the solar axions. Axions produced by bremsstrahlung and Compton process in the Sun could be observed by axio-electric effect. By taking into account the ef-

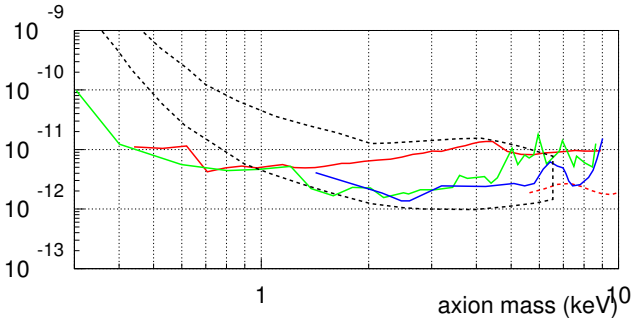

Fig. 26. Limit on the axion-electron coupling constant assuming the dark matter consists of axions. The red line shows the constraint with our data set. The black-dotted area shows the parameter space which is argued to cause annual modulation in DAMA experiment. The solid green and blue lines are showing constraints by CoGeNT and CDMS experiments. The red dashed line shows a result of sensitivity study with a model of background.

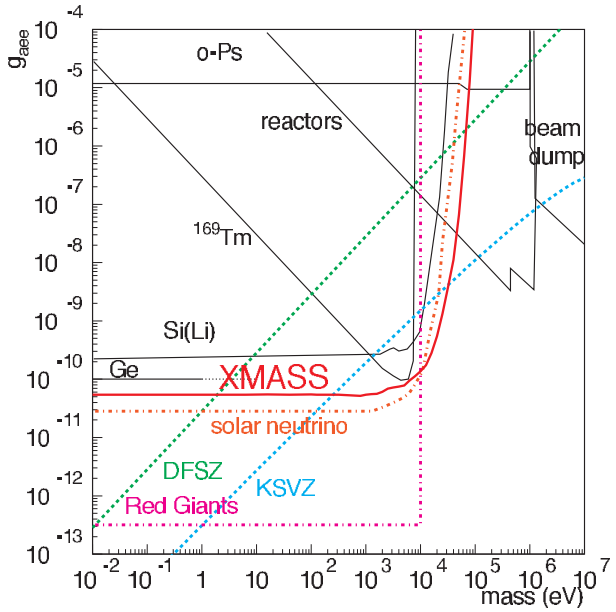

Fig. 27. Result of the search for solar axions produced by bremsstrahlung and Compton effect in the Sun. The red line shows the limit with our data set and other lines are from other experiments, astrophysical arguments, and theoretical predictions.

fect of the mass of axions on the production in the Sun and the detection in the laboratory, comparison between expected signals and the observed spectrum was performed. Since no indication of signals in the observed energy spectrum was found, the corresponding limit of axion-electron coupling is also derived (Fig.27). Details can be found in Ref. [4].

We found unexpected background on the inner surface and studied the origin of background. As a conclusion, one source is aluminum sealing material between PMT window and its body. Significant amount of ^{238}U and ^{210}Pb was found by a measurement with a germanium detector. Another source is the radon daughters attached on the inner surface of the detector. To reduce these background, we plan to place metal covers on top of aluminum seal of the photomultiplier tubes as well as all the inner surface. Significant reduction of background is expected.

XMASS 1.5

We are planning to build the next stage detector, XMASS1.5, with 1 ton fiducial mass. Increasing the fiducial mass is indispensable to examine cross sections smaller than current constraints. XMASS 1.5 is expected to have a sensitivity around 10^{-46}cm^2 for the WIMPs with a mass of 100 GeV.

The basic design of the detector is same as the one for the 100 kg fiducial mass detector but with an improvement of the discrimination between the surface background and the inner events. For that purpose, we are developing a new type of PMTs. They have convex-shape photocathodes which has advantage to detect direct light from the inner surface of the detector. The new PMT design is expected to enforce the discrimination between events around the wall and inner volume, and minimizes leakage events from undesirable surface background after the fiducial volume cut. A detailed design is underway based on the knowledge of the current detector.

Bibliography

[1] Y. Suzuki *et al.*, "Low energy solar neutrino detection by using liquid xenon", Aug. 2000, hep-ph/0008296.

[2] K. Abe *et al.*, the XMASS collaboration, Nucl. Instr. Meth. A 716 (2013) 78.

[3] K. Abe *et al.*, the XMASS collaboration, Phys. Lett. B 719 (2013) 78.

[4] K. Abe *et al.*, the XMASS collaboration, Phys. Lett. B 724 (2013) 46.

HYPER-KAMIOKANDE R&D

[[Project Leader: Masato Shiozawa]
Kamioka Observatory, ICRR, The University of Tokyo

The Hyper-Kamiokande is the third generation nucleon decay and neutrino detector at Kamioka that aims to explore unification of elementary particles and full picture of neutrino masses and mixings [1, 2, 3]. The schematic view of the Hyper-K detector is illustrated in Fig. 28 and 29. We released a letter of intent [4] in which the detectors baseline design and physics potential of Hyper-K are described. The water Cherenkov detector with the dimension of 1 million tones has capability of exploring nucleon lifetimes about 10 times as long as the limits set by the Super-Kamiokande. For example, the sensitivity for the decay mode $p \to e^+\pi^0$ is expected to be beyond 1×10^{35} years [4]. The detector also aims to study neutrino properties such as Dirac *CP* phase, mass hierarchy, octant of θ_{23}, and so on by using a high power accelerator

based neutrino beam and atmospheric neutrinos. Fig.30 shows the expected size of allowed regions for the parameter space of θ_{13} and δ_{CP} by using upgraded J-PARC neutrino beam with the power of 0.75 MW $\times$10 years and the Hyper-Kamiokande detector with the fiducial volume of 0.56 Megaton [4]. The high statistics data sample of atmospheric neutrinos obtained by Hyper-K will also allow us to extract information on the mass hierarchy and the octant of θ_{23}. With a full 10 year period of data taking, the significance for the mass hierarchy determination is expected to reach 3σ or greater as is shown in Fig. 31.

T2K presented an evidence for $\nu_\mu \to \nu_e$ oscillations in 2012. Furthermore the Reactor Neutrino Experiments announced that they have observed $\bar{\nu}_e$ disappearance and the measured θ_{13} value is consistent with the ν_e appearance observed in T2K [5]. The observed nonzero θ_{13} opened the possibility of exploring remaining neutrino parameters, *i.e. CP* phase and mass hierarchy. The large size of θ_{13} is really encouraging and it boosted the activities toward realization of the future detector.

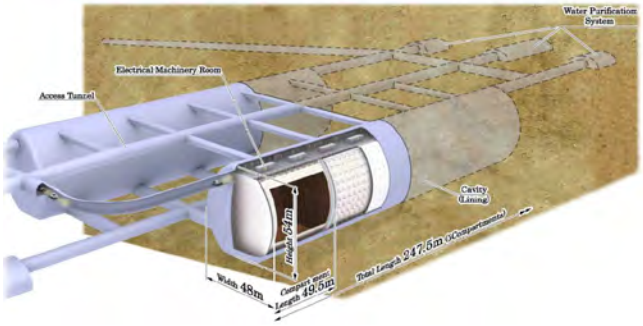

Fig. 28. Schematic view of the Hyper-Kamiokande. The detector consists of two cylindrical tanks holding 500 kton ultrapure water (1 Mton in total). The each tank is divided by segmentation walls every 50 m.

Extensive development works by the Hyper-Kamiokande working group have been performed on geological surveys in the candidate sites, design of cavern and tank, water purification and circulation system design, new photon sensor and DAQ system, detector calibration system, analysis software, and physics sensitivities. The 20-inch PMTs which have been used in the Super-K satisfy necessary requirement of Hyper-K. However, lower-cost higher-sensitivity photo-sensors are preferred because one of main cost drivers is the PMT. A hybrid photo-detector (HPD) using a photocathode and an avalanche photo-diode with 8 kV high voltage is being developed 33. Proof-test will be conducted in 2013 by long term operation of several prototypical HPDs installed in a 100 ton scale water Cherenkov detector. Photo-sensors using other techniques are also being developed. In parallel, many development works are going on or starting mainly to enhance the physics potential of the detector and optimize its construction cost. DAQ electronics and computer system design was made based upon the Super-K. R&D of the front-end electronics under water is being started. The design of water purification system is going on with companies in Japan and US. The water flow control in the big tank is under investigation. Moreover, sophisticated detector calibration system and dedicated software development are also under discussions.

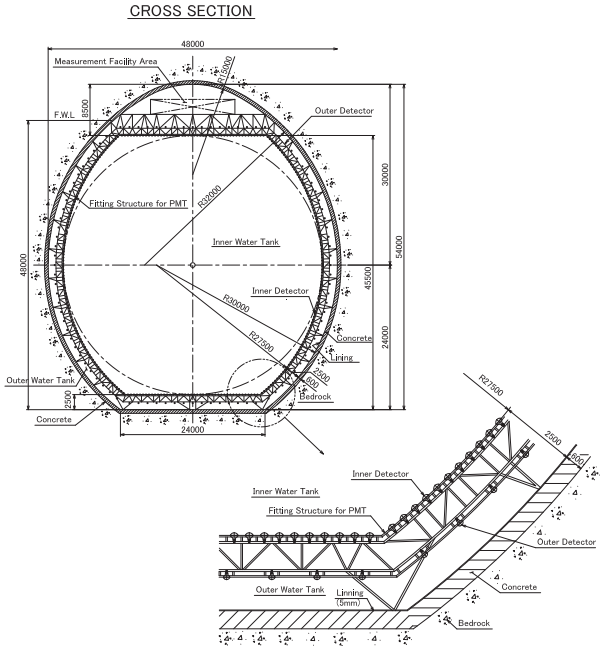

Fig. 29. The cross section view of the Hyper-Kamiokande water tank.

Various development and detector design optimization works are performed in an international Hyper-K working group. The results of the works will be summarized in a design report in near future.

Bibliography

[1] M. Shiozawa, "Large Underground Water Cherenkov Detectors", Proceeding of the XXIV International Conference on Neutrino Physics and Astrophysics (Neutrino2010), June, 2010. to be published in Nuclear Physics B Proceedings Supplement.

[2] M. Diwan, R. Edgecock, T. Hasegawa, T. Patzak, M. Shiozawa and J. Strait, "Future long-baseline neutrino facilities and detectors," Adv. High Energy Phys. **2013**, 460123 (2013).

[3] M. Shiozawa, "The Hyper-Kamiokande project," Nucl. Phys. B (Proc. Suppl.) **237-238**, 289-294 (2013).

[4] K. Abe, T. Abe, H. Aihara, Y. Fukuda, Y. Hayato, K. Huang, A. K. Ichikawa and M. Ikeda *et al.*, "Letter of Intent: The Hyper-Kamiokande Experiment — Detector Design and Physics Potential —," arXiv:1109.3262 [hep-ex].

[5] K. Abe *et al.* [T2K Collaboration], "Indication of Electron Neutrino Appearance from an Accelerator-produced Off-axis Muon Neutrino Beam," arXiv:1106.2822 [hep-ex].

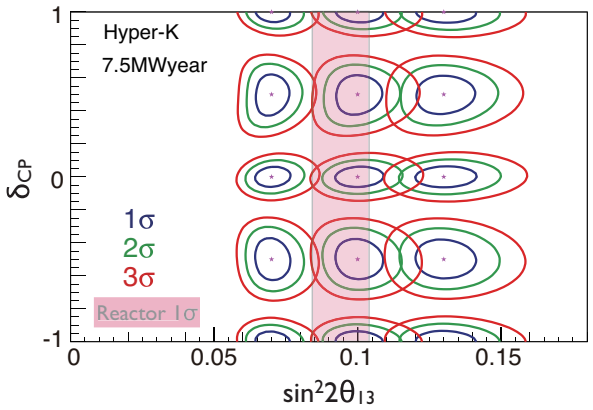

Fig. 30. Expected sensitivity for $\sin^2 2\theta_{13}$ and CP phase δ assuming the 2.25 Mton·years of ν and 5.25 Mton·years of $\bar{\nu}$ runs. The pink band represents the measurement by Daya Bay reactor experiment. Hyper-K has a good sensitivity in the whole relevant θ_{13} and δ_{CP} parameter space.

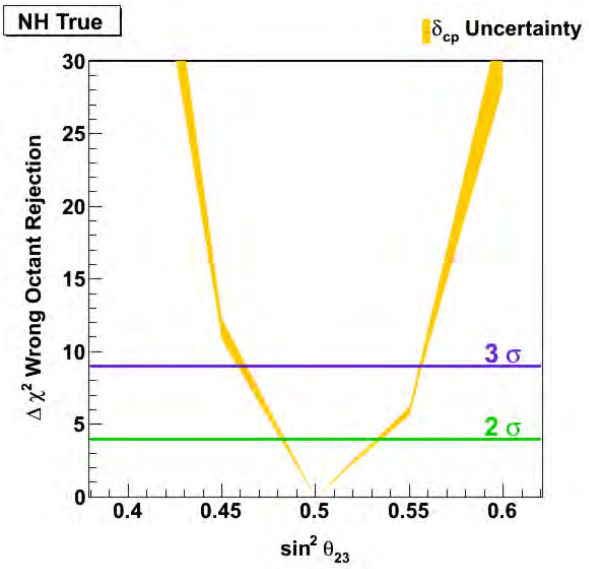

Fig. 32. Expected discrimination power for θ_{23} octant as a function of $\sin^2\theta_{23}$ by 10 years exposure of Hyper-K. The band width corresponds to the variation of the CP phase value. Note that $\sin^2\theta_{23} = 0.45$ or 0.55 in the horizontal axis corresponds to $\sin^2 2\theta_{23} = 0.99$.

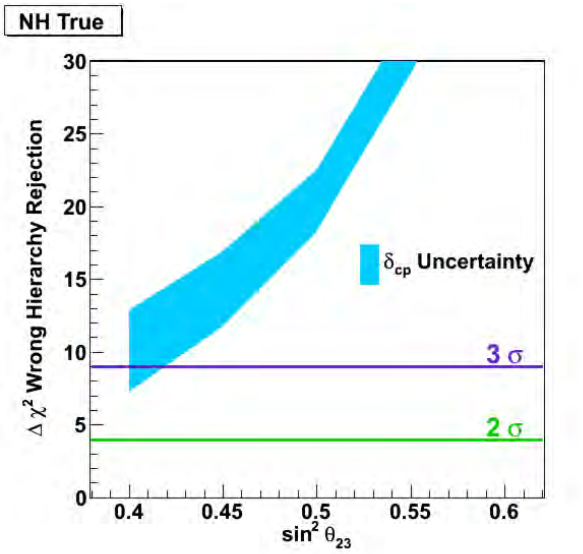

Fig. 31. Expected discrimination power for neutrino mass hierarchy as a function of $\sin^2\theta_{23}$ by 10 years exposure of Hyper-K. The blue band shows expected $\Delta\chi^2$ to reject wrong hierarchy scenario with the width corresponding to the variation of the CP phase value.

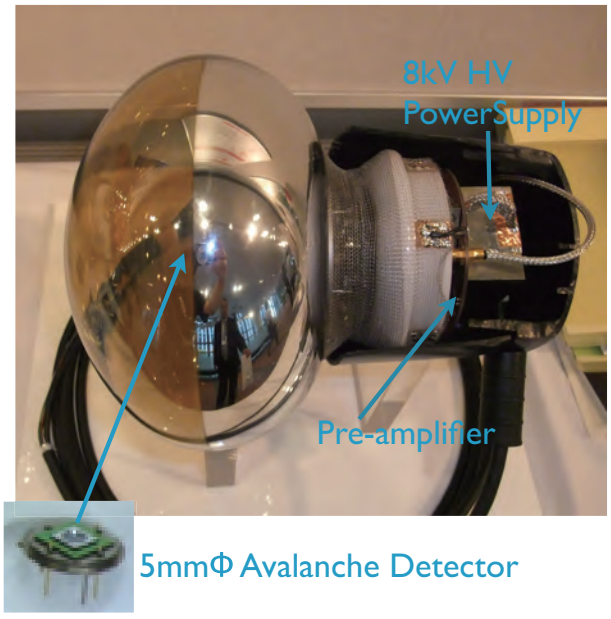

Fig. 33. 8-inch hybrid photo detector prototype.

HIGH ENERGY COSMIC RAY DIVISION

Overview

There are three major experimental research activities in the High Energy Cosmic Ray Division, the study of high energy gamma rays and the development of the next generation gamma-ray telescopes by the Cherenkov Cosmic Gamma Ray group, the study of extremely high energy cosmic rays by the Telescope Array (TA) group, and the study of very high energy cosmic rays and gamma rays by the Tibet ASγ group.

Other activities, such as experiments utilizing the Akeno observatory, the Norikura observatory, the Mt. Chacaltaya observatory (jointly operated with Bolivia) are closely related to inter-university joint research programs. Also an all-sky high resolution air-shower detector (Ashra) is in partial operation on the Hawaii island.

The High Energy Astrophysics group created in the fiscal year 2009 aims to explore various high energy astrophysical phenomena, through theoretical and observational approaches.

The CANGAROO telescopes had been in operation in South Australia since 1992, with a 3.8 m small telescope and then with four 10 m telescopes. The major scientific objective was the study of Very High Energy (VHE) gamma-ray sources in our galaxy in the southern hemisphere. The mission of these telescopes was completed and the CANGAROO observation site was closed in 2011.

For further development of VHE gamma-ray astronomy, the Cherenkov Cosmic Gamma Ray group is working on the design study and development of the next generation international ground-based gamma-ray observatory CTA which will offer an order of magnitude better sensitivity than currently running Cherenkov telescopes, three times better angular resolution, and wider energy coverage from 20 GeV to 100 TeV or higher.

At the Akeno observatory, a series of air shower arrays of increasing geometrical sizes were constructed and operated to observe extremely high energy cosmic rays (EHECRs). The Akeno Giant Air Shower Array (AGASA) was operated from 1991 to January 2004 and covered the ground area of 100 km^2 as the world largest air shower array. In 13 years of operation, AGASA observed a handful of cosmic rays exceeding the theoretical energy end of the extra-galactic cosmic rays (GZK cutoff) at 10^{20} eV.

The Telescope Array (TA), a large plastic scintillator array with air fluorescence telescopes, has been constructed in Utah, USA, which succeeds AGASA and measures the EHECRs with an order of magnitude larger aperture than that of AGASA for the further study of EHECRs. The full-scale TA is accumulating data as the largest array viewing the northern sky and observed the energy spectrum with high statistics, which is in good agreement with the GZK suppression.

An air shower experiment aiming to search for celestial gamma-ray point sources started in 1990 with Chinese physicists at Yangbajing (Tibet, 4,300 m a.s.l.). This international collaboration is called the Tibet ASγ Collaboration. An extension of the air shower array was completed in 1995 and an emulsion chamber has been combined with this air shower array since 1996 to study the primary cosmic rays around the knee energy region. After successive extensions carried out in 1999, 2002 and 2003, the total area of the air shower array amounts to 37,000 m^2. The sun's shadow in cosmic rays affected by the solar magnetic field was observed for the first time in 1992, utilizing its good angular resolution at multi-TeV energy region.

A new type of detector, called Ashra (all-sky survey high resolution air-shower detector), was developed. The first-phase stations were installed near the Mauna Loa summit in the Hawaii Island and high-efficiency observation is continuing. It monitors optical and particle radiation from high-energy transient objects with a wide field-of-view.

The High Energy Astrophysics group is conducting theoretical researches on fundamental processes responsible for non-thermal particle acceleration in various astrophysical environments, including first-order diffusive shock acceleration, second-order stochastic acceleration in shock downstream regions, modification of shock structure by pick-up interstellar neutrals, as well as injection processes of suprathermal particles. In addition to these theoretical works, R/D studies for radio observations of pulsars and cosmic ray air showers are also being made.

Cherenkov Cosmic Gamma-Ray Group

CANGAROO-III

[Spokespersons: R.W. Clay, T. Tanimori, and T. Yoshikoshi]

Collaboration list:
Institute for Cosmic Ray Research, University of Tokyo, Chiba, Japan; School of Chemistry and Physics, University of Adelaide, Australia; Mt Stromlo and Siding Spring Observatories, Australian National University, Australia; Australia Telescope National Facility, CSIRO, Australia; Faculty of Science, Ibaraki University, Ibaraki, Japan; Department of Physics, Konan University, Hyogo, Japan; Department of Physics, Kyoto University, Kyoto, Japan; Solar-Terrestrial Environment Laboratory, Nagoya University, Aichi, Japan; National Astronomical Observatory of Japan, National Institutes of Natural Sciences, Tokyo, Japan; Department of Physics, Tokai University, Kanagawa, Japan; Department of Radiation Oncology, Tokai University, Kanagawa, Japan; Department of Physics, Yamagata University, Yamagata, Japan; Faculty of Management Information, Yamanashi Gakuin University, Yamanashi, Japan; Faculty of Medical Engineering and Technology, Kitasato University, Kanagawa, Japan; Department of Physics, Ritsumeikan University, Shiga, Japan; Institute of Particle and

Nuclear Studies, High Energy Accelerator Research Organization (KEK), Ibaraki, Japan; Department of Applied Physics, Waseda University, Tokyo, Japan [1].

Status of the Project

CANGAROO is the acronym for the Collaboration of Australia and Nippon (Japan) for a GAmma-Ray Observatory in the Outback. The collaboration started in 1992 with a single Imaging Atmospheric Cherenkov Telescope (IACT) of 3.8 m diameter called CANGAROO-I in the desert area near Woomera, South Australia (136°47′E, 31°06′S, 160 m a.s.l.). As its third-generation experimental setup, the CANGAROO-III stereoscopic IACT system has been in operation since March 2004 with four IACTs of 10 m diameter. Stereoscopic observations of atmospheric Cherenkov light images produced by air showers caused by high-energy particles bombarding the earth allow effective discrimination of gamma rays from charged cosmic rays which are the overwhelming backgrounds. Two of the four telescopes (called T3 and T4 in the order of construction) have been used in observations since May 2008, as the first and second telescopes have degraded. A stereoscopic triggering system was installed at the beginning of 2005 and has been working properly, rejecting most single muon events, which are the major background component at low energies. Observations of various candidates of celestial gamma-ray emitters have been carried out on moonless, clear nights.

Since the CANGAROO-III telescopes, which, due to financial considerations, were not sheltered from the harsh desert environment, have seriously deteriorated over time from their original performance, we have stopped observations in 2011 and the telescopes were demolished in 2012. A paper summarizing the CANGAROO activity for about 20 years is being prepared for publication.

Results from CANGAROO-III

Blazars H 2356−309, PKS 2155−304, PKS 0537−441, and 3C 279

We have observed four selected blazars, H 2356−309, PKS 2155−304, PKS 0537−441, and 3C 279, with the CANGAROO-III IACTs from 2005 to 2009. No statistically significant excess of events above 510–720 GeV from the direction of any of these objects was found, and we derived flux upper limits for very high energy (VHE) gamma-ray emissions [2]. In addition, we analyzed GeV gamma-ray data between 0.2 and 300 GeV taken with Fermi/LAT from August 2008 to May 2011.

To derive some important physical parameters of these blazars, we consider a simple leptonic jet model to explain the multiwavelength spectral energy distributions (SEDs) including GeV and TeV spectra, even though non-simultaneous. The observed SED of H 2356-309 (HBL) could be explained by a simple synchrotron-self-Compton (SSC) model with a single power-law electron spectrum, and to keep a consistency with GeV spectrum, we need to assume a large beaming factor $\delta = 59$ and weak magnetic field strength of 0.012 G. Radiation from PKS 2155−304, a nearby HBL, was well modeled by the SSC scenario, and obtained parameters are consistent with earlier works. PKS 0537−441, a luminous LBL, was studied and we found SSC + EC (external Compton) model could explain the observed multiwavelength spectrum where the EC component is dominant in the gamma-ray photons. The SED of one of the distant FSRQ, 3C 279, were also well explained by the SSC + EC model.

Additionally, from our parameter fit results as the HBL to the FSRQ of blazar sub-classes, it is seen that the beaming factor becomes smaller, and in contrast the strength of the magnetic field becomes stronger and the size of blob becomes larger. Although we could not take into account of the uncertainties such as simultaneity of the data and the differences of models, these latter two tendencies are in agreement with the proposed blazar sequence.

Bibliography

[1] Collaboration website: `http://vesper.icrr.u-tokyo.ac.jp/`.

[2] Y. Mizumura et al., Astropart. Phys. **35**, 563–572 (2012).

CTA Project (Cherenkov Telescope Array)

CTA-Japan Consortium
[Spokespersons : M.Teshima and H.Kubo]

Collaboration list:
Institute for Cosmic Ray Research, The University of Tokyo, Chiba, Japan; Department of Physics, Yamagata University, Yamagata, Japan; Faculty of Science, Ibaraki University, Ibaraki, Japan; Institute of Particle and Nuclear Studies, High Energy Accelerator Research Organization (KEK), Ibaraki, Japan; Department of Physics, The University of Tokyo, Tokyo, Japan; Interactive Research Center of Science, Tokyo Institute of Technology, Tokyo, Japan; Department of Physics, Aoyama Gakuin University, Tokyo, Japan; Faculty of Science and Engineering, Waseda University, Tokyo, Japan; Department of Physics, Saitama University, Saitama, Japan; Institute of Space and Astronautical Science, JAXA, Kanagawa, Japan; Department of Physics, Tokai University, Kanagawa, Japan; Department of Radiation Oncology, Tokai University, Kanagawa, Japan; Faculty of Medical Engineering and Technology, Kitasato University, Kanagawa, Japan; Faculty of Management Information, Yamanashi Gakuin University, Yamanashi, Japan; Department of Physics, Nagoya University, Aichi, Japan; Solar-Terrestrial Environment Laboratory, Nagoya University, Aichi, Japan; Kobayashi-Maskawa Institute, Nagoya University, Aichi, Japan; Department of Astronomy, Kyoto University, Kyoto, Japan; Department of Physics, Kyoto University, Kyoto, Japan; Yukawa Institute for Theoretical Physics, Kyoto University, Kyoto, Japan; Department of Earth and Space Science, Osaka University, Japan; Department of Physics, Kinki University, Osaka, Japan; Department of Physics, Konan University, Hyogo, Japan; Department of Physics, Hiroshima University, Hiroshima, Japan; Hiroshima Astrophysical Science Center, Hiroshima University, Hiroshima, Japan; Faculty of Integrated Arts and Sciences, The University of

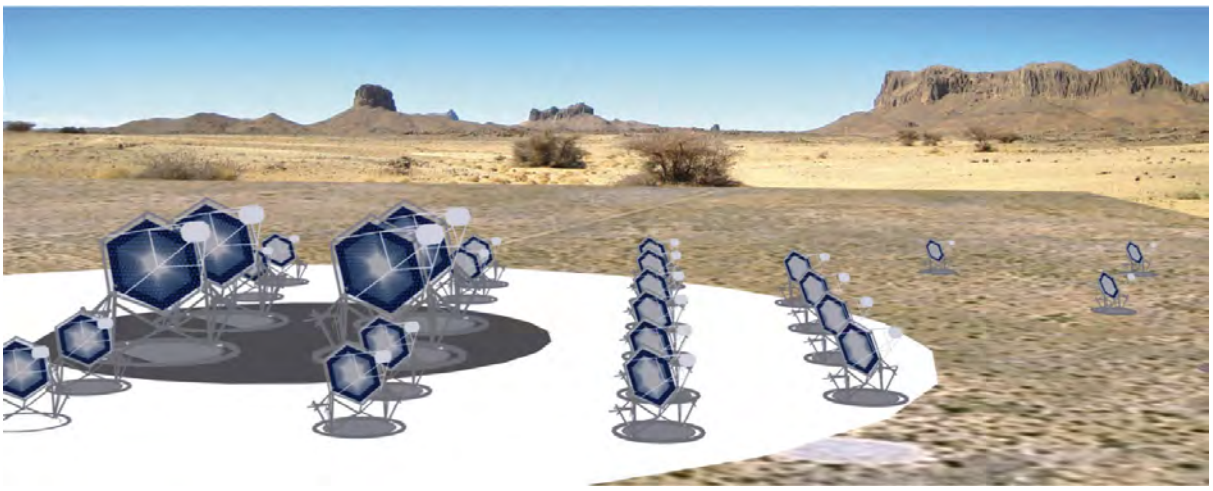

Fig. 1. Artist view of the CTA observatory. CTA consists of three types of telescopes, Large Size Telescopes (23m diameter), Mid Size Telescopes (12m) and Small Size Telescopes (6m), and covers the broad energy band from 20GeV to 100TeV.

Tokushima; Department of Applied Physics, University of Miyazaki, Miyazaki, Japan; Graduate School of Science and Technology, Kumamoto University, Kumamoto, Japan; Center for Cosmology and AstroParticle Physics, Ohio State University, Ohio, USA; Max-Planck-Institute for Physics, Munich, Germany [1].

CTA Project

During the past few years, Very High Energy (VHE) gamma ray astronomy has made spectacular progress and has established itself as a vital branch of astrophysics. To advance this field even further, we propose the Cherenkov Telescope Array (CTA) [2], the next generation VHE gamma ray observatory, in the framework of a worldwide, international collaboration. CTA is the ultimate VHE gamma ray observatory, whose sensitivity and broad energy coverage will attain an order of magnitude improvement above those of current Imaging Atmospheric Cherenkov Telescopes (IACTs). By observing the highest energy photons known, CTA will clarify many aspects of the extreme Universe, including the origin of the highest energy cosmic rays in our Galaxy and beyond, the physics of energetic particle generation in neutron stars and black holes, as well as the star formation history of the Universe. CTA will also address critical issues in fundamental physics, such as the identity of dark matter particles and the nature of quantum gravity.

VHE gamma rays from 100GeV to 10TeV can be observed with ground-based IACTs. The history of VHE gamma ray astronomy began with the discovery of VHE gamma rays from the Crab Nebula by the Whipple Observatory in 1989. To date, the current generation IACTs featuring new technologies, such as H.E.S.S., MAGIC, VERITAS, and CANGAROO, have discovered more than 100 Galactic and extragalactic sources of various types.

CTA is designed to achieve superior sensitivity and performance, utilizing established technologies and experience gained from the current IACTs. The project is presently in its preparatory phase, with international efforts from Japan, the US and EU. It will consist of several 10s of IACTs of three different sizes (Large Size Telescopes, Mid Size Telescopes, and Small Size Telescopes). With a factor of 10 increase in sensitivity (1m Crab $\sim 10^{-14} erg\ s^{-1}\ cm^{-2}$), together with a much broader energy coverage from 20GeV up to 100TeV, CTA will bring forth further dramatic advances for VHE gamma ray astronomy. The discovery of more than 1000 Galactic and extragalactic sources is anticipated with CTA.

CTA will allow us to explore numerous diverse topics in physics and astrophysics. The century-old question of the origin of cosmic rays is expected to be finally settled through detailed observations of supernova remnants and other Galactic objects along with the diffuse Galactic gamma ray emission, which will also shed light on the physics of the interstellar medium. Observing pulsars and associated pulsar wind nebulae will clarify physical processes in the vicinity of neutron stars and extreme magnetic fields. The physics of accretion onto supermassive black holes, the long-standing puzzle of the origin of ultrarelativistic jets emanating from them, as well as their cosmological evolution, will be addressed by extensive studies of active galactic nuclei (AGN). Through dedicated observing strategies, CTA will also elucidate many aspects of the mysterious nature of gamma ray bursts (GRBs), the most energetic explosions in the Universe. Detailed studies of both AGNs and GRBs can also reveal the origin of the highest energy cosmic rays in the Universe, probe the cosmic history of star formation including the very first stars, as well as provide high precision tests of theories of quantum gravity. Finally, CTA will search for signatures from elementary particles constituting dark matter with the highest sensitivity yet. Realization of the rich scientific potential of CTA is very much feasible, thanks to the positive experience gained from the current IACTs.

The CTA-Japan consortium [1] is aiming at contributing in particularly to the construction of the Large Size Telescopes (LSTs) and is involved in their development. The LST covers the low energy domain from 20GeV to 1000GeV and is especially important for studies of high redshift AGNs and GRBs. The diameter and area of the mirror are 23m and 400m^2, respectively, in order to achieve the lowest possible

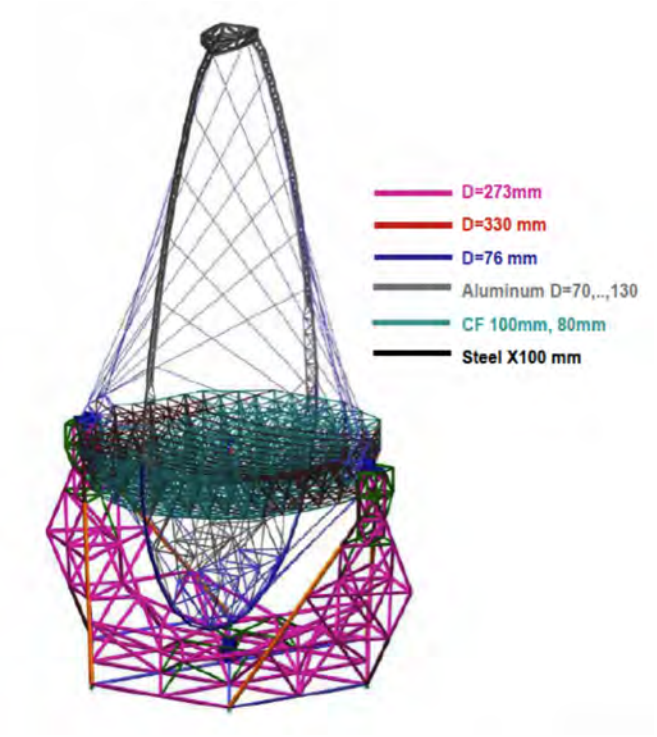

Fig. 2. Large Size Telescope (23m diameter) designed by Max–Planck-Institute for Physics. CTA Japan is contributing to the design and prototyping of the imaging camera at the focal plane, ultrafast readout electronics, and high precision segmented mirrors.

energy threshold of 20GeV. All optical elements/detectors require high specifications, for example, high reflectivity, high collection efficiency, high quantum efficiency and ultra fast digitization of signal, etc. For this purpose, CTA-Japan is developing high quantum efficiency photomultipliers, ultrafast readout electronics and high precision segmented mirrors. On the strength of their experience gained from construction of the MAGIC telescope, the Max-Planck-Institute for Physics in Munich is responsible for the design of the 23m diameter telescope structure, based on a carbon fiber tube space frame. The LSTs require very fast rotation (180 degrees/20seconds) for promptly observing GRBs.

The Cherenkov Cosmic Gamma Ray group is also operating the MAGIC Telescopes [5] on La Palma, Canary Islands. This facility is used not only for scientific observations but also for technological development toward the future observatory CTA.

Bibliography

[1] CTA Consortium website: `http://www.cta-observatory.jp/` and `http://www.cta-observatory.org/`.

[2] Design Concepts for The Cherenkov Telescope Array, The CTA Consortium, Exper. Astron. 32 (2011) 193-316.

[3] Status of Very High Energy Gamma Ray Astronomy and Future Prospects, M. Teshima, The Astronomical Herald, 104 (2011) 333-342.

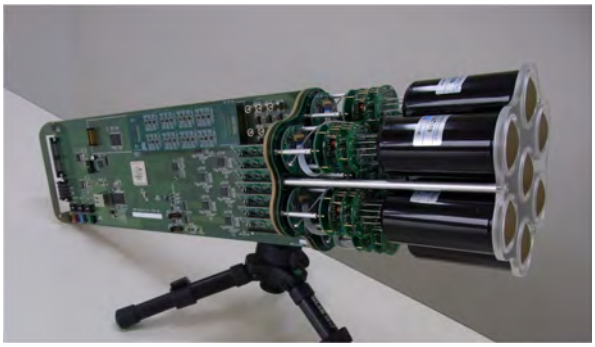

Fig. 3. Camera cluster for the Large Size Telescope (LST) developed by CTA-Japan. This cluster consists of seven high quantum efficiency photomultipliers (R11920-100), CW High Voltages, pre-amplifier, Slow Control Board, DRS4 Ultra fast waveform recording system and Trigger. The LST camera can be assembled with 400 of these clusters, cooling plates and camera housing.

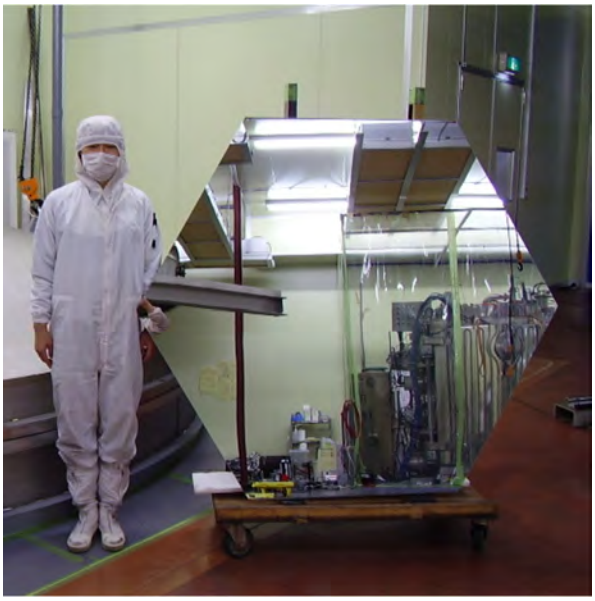

Fig. 4. Prototype of the high precision segmented mirror for the Large Size Telescope (LST) developed by CTA-Japan in cooperation with Sanko Co.LTD. The mirror is made of a 60mm thick aluminum honeycomb sandwiched by 3mm thin glass on both sides. A surface protection coat consisting of the materials SiO2 and HfO2 will be applied to enhance the reflectivity and to elongate the lifetime.

[4] Design Study of a CTA Large Size Telescope, Proc. of ICRC2012 at Beijing China, M. Teshima, arXiv:1111.2183.

[5] MAGIC Collaboration website: `http://magic.mppmu.mpg.de/`.

Other Activities

As a test bench of domestic R & D activities for future ground-based gamma-ray observatory projects, a used atmospheric Cherenkov telescope of a 3 m diameter was obtained and placed at the Akeno Observatory in November 2010. This is currently the only atmospheric Cherenkov telescope located in Japan. In the fiscal year 2012, we completed recoating its 18 deteriorated segment mirrors at the Okayama Astrophysi-

Fig. 5. Akeno atmospheric Cherenkov telescope with 18 segment mirrors recoated and assembled back to the structure.

cal Observatory (OAO), the National Astronomical Observatory of Japan (NAOJ), and assembled them back to the telescope structure (Fig. 5). A new telescope operation system has also been rebuilt for tracking celestial objects, adding a PC with interfaces to the old positioner and encoder. Some prototype imaging cameras and electronics systems are planned to be installed to this telescope (e.g. [1]), and test observations will be carried out in the near future.

Bibliography

[1] T. Yoshikoshi et al., Proc. of 32nd Internat. Cosmic Ray Conf. (Beijing), **9**, 226–229 (2011).

TA: Telescope Array Experiment

[Spokespersons: H. Sagawa[1], G. B.Thomson[2]]

1 : ICRR, The Univ. of Tokyo, Kashiawa, Chiba 277-8582
2 : Dept. of Physics, University of Utah

Collaborating Institutions:

Chiba Univ., Chiba, Japan; Chungnam Nat. Univ., Daejeon, Korea; Earthquake Research Institute, Univ. of Tokyo, Tokyo, Japan; Ehime Univ., Matsuyama, Japan; Ewha W. Univ., Seoul, Korea; Hiroshima City Univ., Hiroshima, Japan; Hanyang Univ., Seoul, Korea; ICRR, Univ. of Tokyo, Kashiwa, Japan; INR, Moscow, Russia; IPMU, Univ. of Tokyo, Kashiwa, Japan; Kanagawa Univ., Yokohama, Japan; KEK/IPNS, Tsukuba, Japan; Kinki Univ., Higashi-Osaka, Japan; Kochi Univ., Kochi, Japan; Kyoto Univ., Kyoto, Japan; Nat. Inst. of Rad. Sci., Chiba, Japan; Osaka City Univ., Osaka, Japan; RIKEN, Wako, Japan; Ritsumeikan Univ., Kusatsu, Japan; Rutgers Univ., Piscataway, NJ, USA; Saitama Univ., Saitama, Japan; Tokyo City Univ., Tokyo, Japan; Tokyo Inst. of Tech., Tokyo, Japan; Tokyo Univ. of Science, Noda, Japan; ULB, Brussels, Belgium; Univ. of Utah, Salt Lake City, UT, USA; Univ. of Yamanashi, Kofu, Japan; Waseda Univ., Tokyo, Japan; Yonsei Univ., Seoul, Korea

Overview and Status of TA

The Telescope Array (TA) is the largest Ultra-High Energy Cosmic Ray (UHECR) observatory in the northern hemisphere. The aim of the TA experiment is to explore the origin, propagation and interaction of extremely-high energy (EHE) cosmic rays by measuring energy, arrival direction and mass composition. The TA consists of a surface array of 507 plastic scintillator detectors (SD) and three stations of fluorescence detectors (FD). It is located in the desert of Utah in USA (lat. 39.3°N, long. 112.9°W, alt.∼1400 m). The TA was constructed mainly by the Grants-in-Aid for Priority Areas "The Origin of Highest Energy Cosmic Rays" (JFY2003-2008) and the fund from the US National Science Foundation (NSF). All three FD stations started the observation in November 2007. Major construction of the SD array was completed in February 2007, and started the full operation in March 2008. The TA is operated by the international collaboration of researchers from US, Russia, Korea, Belgium and Japan. The main fund for the TA operation is the Grants-in-Aid for Specially Promoted Research "Extreme Phenomena in the Universe Explored by Highest Energy Cosmic Rays" (JFY2009-2013).

Surface Detector Array

Each SD has two 1.2-cm thick layers of plastic scintillator. Signal light from energy deposited by particles is collected by wavelength shifting optical fibers in extruded grooves on the scintillator layers and brought out to a photomultiplier tube (PMT) for each layer. The resulting electronic waveforms are digitized by 12-bit FADCs at 50 MHz sampling rate. A solar photovoltaic panel provides power for the PMTs and electronics. The SDs are divided into three sub-arrays which communicate via wireless LAN each with an SD host electronics at a communication tower in their sub-array. In 2010, we installed hybrid trigger system, by which filtered FD trigger signals trigger SD data taking. In addition to shower trigger data, we collect a variety of monitor information for SD calibration and maintenance. The fraction of running time is greater than 96% . The performance of the SD is described in [1].

Fluorescence Telescope

The Middle Drum (MD) FD site is located to the north of the TA site, and is instrumented with 14 refurbished telescopes from the HiRes-I site. The cameras each contain 256 hexagonal Photonics PMTs in a 16×16 array. Each PMT views ∼1° of sky. The telescopes view from 3-31° above horizon and 114° in azimuth.

The Black Rock Mesa (BRM) and Long Ridge (LR) FD sites are located to the southeast and southwest of the TA site, respectively. They are each instrumented with 12 new telescopes [2]. The cameras use a Hamamatsu PMT with the 1° field of view. The PMTs are calibrated with a laser [3]. The relative calibration is described in [4]. The sites view 3-33° above horizon and 108° in azimuth. The trigger system is described in [5, 6]. The BRM and LR FD sites have duty cycles

of 12 and 10%, respectively.

A monostatic LIDAR (LIght Detection And Ranging) system, in which the laser and receiver are collocated, is located in the BRM site to measure atmospheric transparency [7]. The BRM site has an IR camera to monitor clouds.

A laser facility (CLF) sits at the center of the three FD sites. This allows one to measure the atmospheric transmission parameters [8] as well as to directly compare the reconstruction of the three FD sites. We installed a LIDAR system at the CLF.

No absolute energy calibration source existed on the sites of previous UHECR experiments. At KEK in Japan, we built an electron linear accelerator (ELS, Electron Light Source) for an end-to-end energy calibration of the FD [9]. The maximum beam energy is 40 MeV, and the charge of one pulse is 10^9 e^-, and the typical pulse width is 1 μsec. The ELS was installed 100 m forward from the BRM FD in March 2009. With the FD, we observed pseudo air shower induced by an electron beam that was shot vertically in the air from ELS in September, 2010. The basic idea of the end-to-end calibration of FD with the ELS is that we compare measured ADC value and that from Monte Carlo simulation and the difference is corrected for the simulation, which affects energy scale. The beam energy is measured with a bending magnet with an accuracy better than 1%. We worked with emphasis on precise measurement of the beam charge with a Faraday cup. We checked the relevant geometry and GEANT4 simulation.

Results

Here we present the recent results of energy spectrum, mass composition, and anisotropy from TA data.

Energy Spectrum

The HiRes [10] observed the GZK cutoff and Auger [11] confirmed the flux suppression consistent with HiRes result.

We measured the energy spectrum by using the SD data over approximately four years of observation between 2008 May 11 and 2012 May 20. The value of exposure for this data set is $\sim$3690 km^2 sr yr. The Monte Carlo (MC) data were generated by CORSIKA air shower simulation with QGSJET-II-03 proton model. GEANT4 simulation is used for the detector simulation. The correlation of S_{800} and zenith angle with primary energy from MC study is used for the first estimation of the CR energy. Here S_{800} is the charge density at a distance of 800 m from shower core.

We compare the FD and SD energies using hybrid events. The SD energy is 27% larger than that of FD. The SD energy is rescaled by 27%. The plot of the energies is shown in Fig. 6.

The selection criteria employed in our analysis are as follows:

- Each event must include at least five counters.
- The reconstructed primary zenith angle must be less than 45°.
- The reconstructed event core must be more than 1200 m from edge of the array.

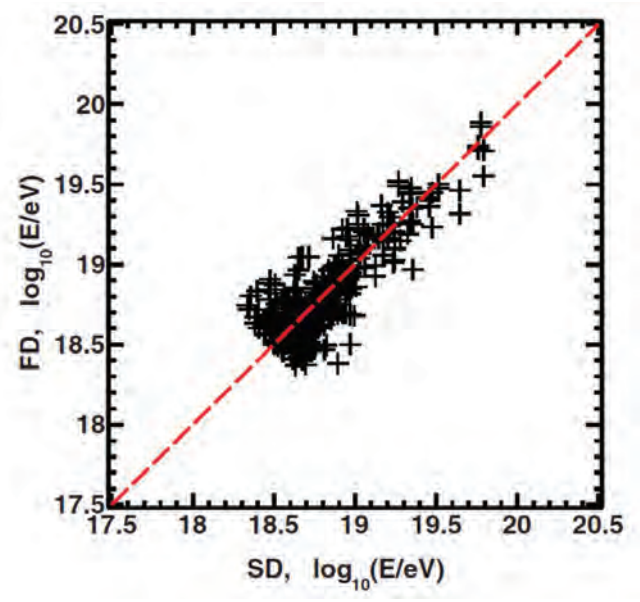

Fig. 6. The SD and FD energy comparison after applying 27% normalization to the SD. The dashed line corresponds to $E_{SD} = E_{FD}$.

The energy spectrum is shown together with other experiments in Fig. 7 [12]. The SD spectrum is consistent with HiRes spectra. Using a power-law fit, we found the two breaks at $(4.6 \pm 0.3)\times10^{18}$ eV and at $(5.4 \pm 0.6)\times10^{19}$ eV, which correspond to the ankle and the GZK suppression, respectively. We observed 21 events above the suppression while a linear extrapolation of the power law below the break predicts 58.6 events above the break. This result provides evidence for the flux suppression with the significance of 5.5σ. The difference of the TA and Auger fluxes corresponds to the difference of the TA and Auger energy scales of approximately 20%,. which is consistent with systematic energy uncertainties.

Mass Composition

The dependence of $X_{\rm max}$ on the primary energy is used to determine the mass composition. The Auger data suggests a change to a heavier composition for $E > 10^{18.5}$ eV [13] while the HiRes data is consistent with constant elongation rate which stays with proton [14].

The events simultaneously observed at two new FD stations (stereo events) from November 2007 through September 2010 have been presented [15]. The distribution of reconstructed $X_{\rm max}$ for the TA data with QGSJET-01 MC data was in good agreement with the proton distribution.

Here we show the result of X_{max} from the events simultaneously observed with the Middle Drum FD and surface detectors for the period between May 2008 and September 2011. The X_{max} distributions are shown in Fig. 8 and the data are in good agreement with the QGSJET-II-03 proton prediction. The evolution of the average $X_{\rm max}$ with energy is shown with the MC data in the energy range from $10^{18.2}$ to $10^{19.6}$ eV in Fig. 9. The observed TA data are in good agreement with proton prediction.

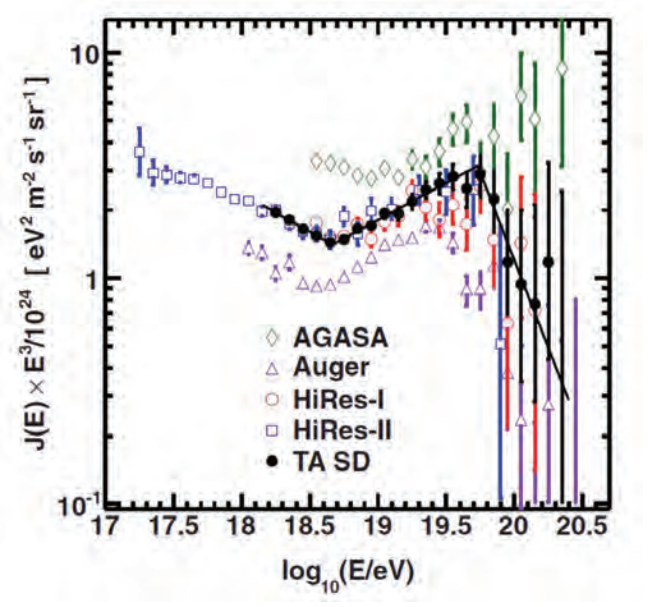

Fig. 7. The TA SD spectrum together with the spectra from other experiments: the TA SD (black filled circles), AGASA (green open diamonds), Auger (purple open triangles), HiRes-1 (red open circles), and HiRes-2 (blue open squares). Solid line shows the broken power line fit to the TA SD data.

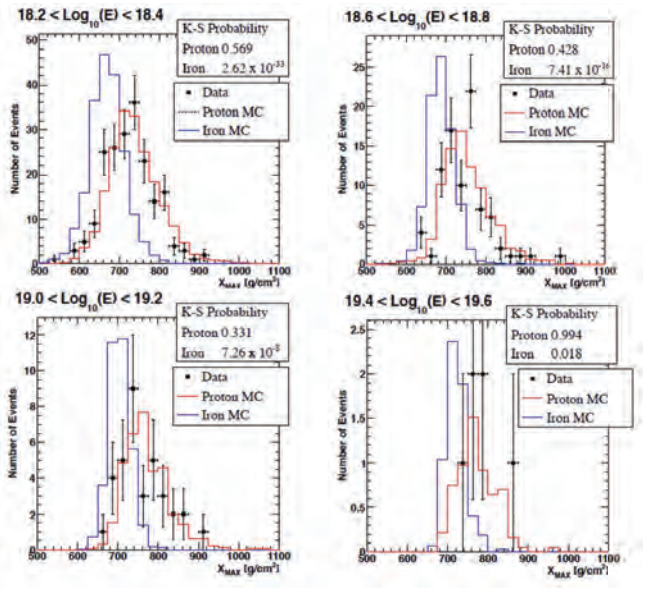

Fig. 8. The preliminary reconstructed $X_{\rm max}$ distributions for the data (points) with QGSJET-01 MC data above $10^{18.2}$ eV. The red and blue histograms are the proton and iron predictions, respectively.

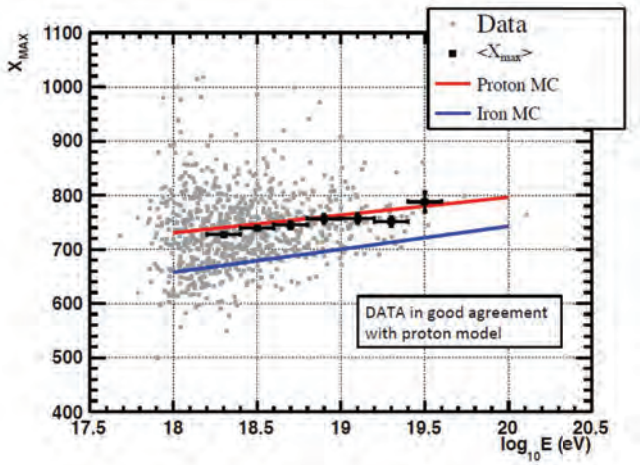

Fig. 9. The preliminary TA average reconstructed $X_{\rm max}$ (black points) as a function of energy. The red line is the prediction for pure proton with the interaction model of QGSJET-II-03. The blue line is under the assumption of iron.

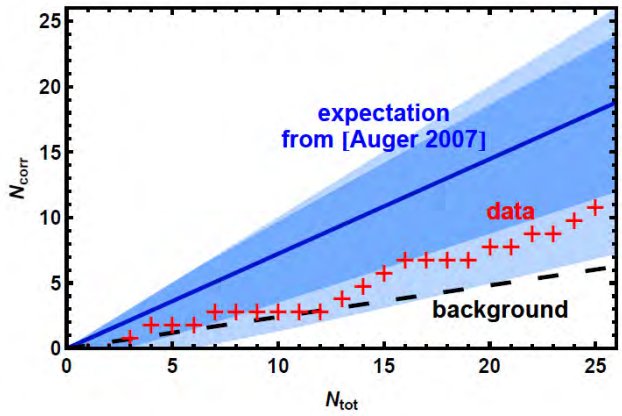

Fig. 10. The TA result of the correlations with AGN. The horizontal axis is the number of observed events and the vertical axis is the number of correlated events with AGN. The red crosses are the TA data. The black dashed line is the prediction from isotropic distribution. The expectation from the original Auger claim is represented by the blue line together with the 1- and 2-σ bands.

Arrival Directions of UHECRs

We report the analysis of UHECRs for correlations with AGNs, autocorrelations and correlations with the Large Scale Structure (LSS) [16]. The SD data set in the period between 2008 May 11 and 2011 September 15 contains 988 events above 10 EeV, 57 events above 40 EeV, and 25 events above 57 EeV.

Correlations with AGNs : The Auger reported correlations between the arrival directions of UHECRs with E $>$ 57 EeV and positions of nearby AGN from Véron 2006 catalog with $0<z\leq0.018$ in 2007 [17]. The probability that the correlations for angular separations less than 3.1° occurred by chance is 1.7×10^{-3}. The number of correlating events was 9 out of 13, which corresponds to about 69% of events. The Auger has updated the analysis and found that the number of correlating events was 21 out of 55, which corresponds to about 38% of events [18]. The HiRes reported that no correlations had been found [19]. The TA searched for AGN correlation using the same condition as Auger and found 11 correlating events (44%) out of 25 total events while the expected number of random coincidences for this total number of events is 5.9. As is seen in Fig. 10, the TA result is compatible both with isotropic distribution and the AGN hypothesis. By using binomial distribution with the probability of a single event to correlate p_{iso} = 0.24, such an excess has probability of $\sim$2% to occur by chance with isotropic distribution.

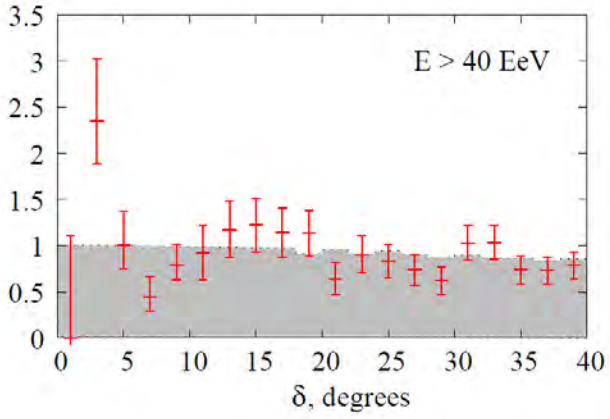

Fig. 11. The distribution of separation angles for any two cosmic rays above 40 EeV normalized by solid angle. The points are the observed data and the shaded region represents the average number of pairs expected for the uniform distribution. The expectation in the first bin is set to be one as the overall normalization.

Autocorrelations : The small-scale clusters of UHECR arrival directions were observed by the AGASA at the angular scale of 2.5° above 40 EeV [20, 21]. On the other hand, the result by the HiRes is consistent with an isotropic distribution [22]. Fig. 11 shows the distribution of separation angles for any two cosmic rays above 40 EeV for the TA data set. We find 0 pair separated by less than 2.5° while 1.5 are expected for the isotropic model. There is no excess of small-scale clusters in the TA data, and no significant excess is found for angles from 0 to 40° and for three energy thresholds of 10 EeV, 40 EeV, and 57 EeV. There is a hint of grouping of events at angular scales between 20 and 30° at the highest energies. However, the statistical significance of this feature is not sufficient.

Correlations with LSS : Next we check the compatibility of the TA event sets with the isotropic distribution at large angular scales. The flux sampling test gives the values of statistical probability (p-values) 0.5, 0.9 and 0.6 for the three energy thresholds (10 EeV, 40 EeV, 57 EeV), respectively. The data are compatible with an isotropic distribution.

At large angular scales, the anisotropy in the Auger data was claimed [23] , and that in the HiRes data was not confirmed [24]. We use the galaxies at distances from 5 to 250 Mpc and with Ks magnitudes less than 12.5 in the 2MASS Galaxy Redshift Catalog (XSCz) [25]. This catalog provides the most accurate information about three-dimensional galaxy distribution. We assume that UHECRs are protons and the effects of the Galactic and extragalactic magnetic fields on each arrival direction are approximated by a Gaussian probability density function with an angular resolution called a smearing angle θ, which is treated as a free parameter. The sky maps of the expected flux at the smearing angle of 6° are shown in Fig. 12 together with the TA events. Fig. 13 shows the p-values as a function of the smearing angle. The data both above 40 EeV and 57 EeV are compatible with LSS model even without considering the effect of regular Galactic Magnetic Field (GMF). For E $>$ 10 EeV, the data set is compatible with LSS hypothesis that includes the regular GMF with strong and thick halo component. Here we adopt the recent GMF model with the magnitude of 4 μG and the thickness of 1.5 kpc for the halo [26].

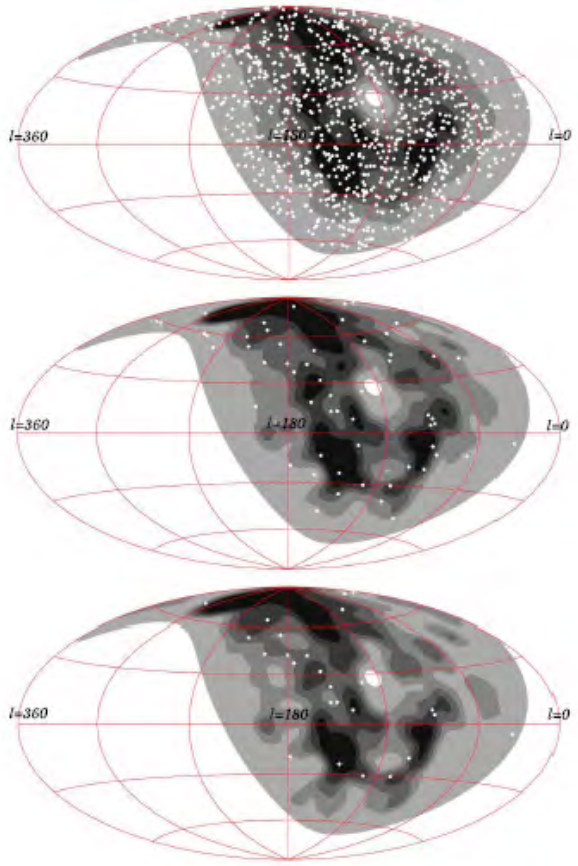

Fig. 12. The sky map of expected flux from LSS model together with the TA events (white dots) at energy thresholds of 10 EeV, 40 EeV, and 57 EeV (from top to bottom) in Galactic coordinates. The smearing angle is 6°. Darker gray region indicates larger flux and each band contains 1/5 of the total flux.

Prospects

We describe the recent joint studies with the TA and Auger collaborations to understand the discrepancies between the TA and Auger results, the TA Low-energy Extension (TALE), and the future plans.

TA and Auger joint studies

The International Symposium on Future Directions in UHECR Physics (UHECR2012) was held in CERN in February 2012 [27]. We discussed the highlights and future UHECR experiments. There are some discrepancies between the results from the TA and Auger collaborations such as energy spectrum and $X_{\rm max}$. After the symposium, the TA and Auger collaborations have begun a program of joint studies in order to understand the nature of these differences, which are related to energy spectrum, $X_{\rm max}$, and arrival directions. The following is the list of the joint studies:

- The light source developed by the Auger collaboration was brought to the TA site and measured with TA FD

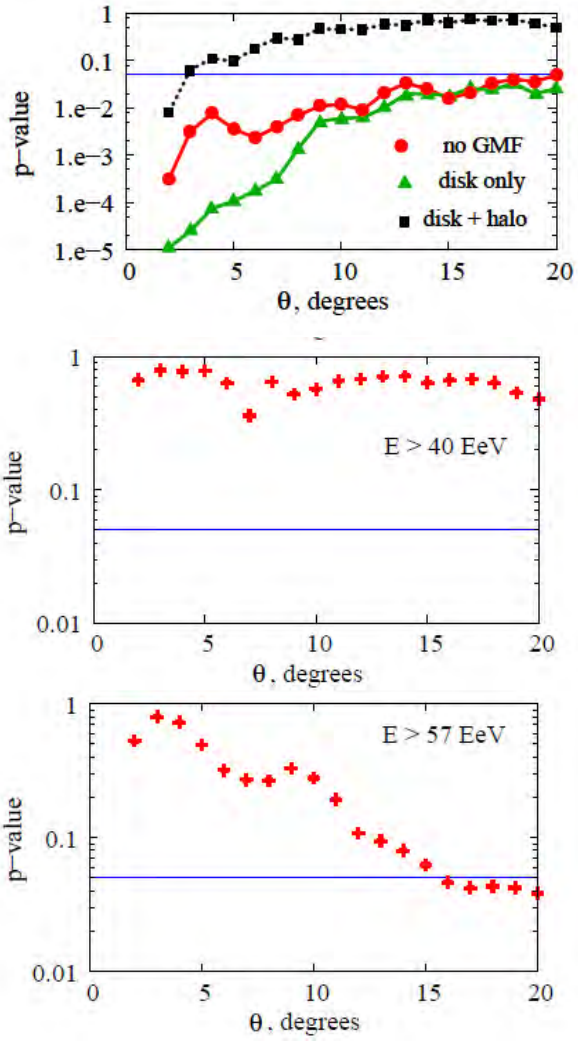

Fig. 13. The results of the statistical test for the compatibility between the data and the LSS hypothesis. The p-values are shown as a function of the smearing angle θ. The horizontal blue line shows a confidence level of 95%. The three panels correspond to energy thresholds of 10 EeV, 40 EeV, and 57 EeV from top to bottom. Red circles represent that with no regular GMF, In the upper panel with E $>$ 10 EeV, black squares represent the result of the TA events with the LSS hypothesis with disk and halo components, and green triangles represent that with disk component only.

together with the Auger members in November 2012 and in March 2013.

- The first joint anisotropy analysis meeting was held by the TA and Auger members in February in 2013 in order to obtain the large scale anisotropy result with the full sky coverage by using the TA and Auger data above 10^{19} eV.
- The $X_{\rm max}$ analysis of an adhoc data compatible with Auger composition model via TA reconstruction is being studied in order to know how well the TA SD detector distinguish between Auger mixed composition and pure proton compositions.

The progress reports from these joint studies would be presented at ICRC2013 [28].

Fig. 14. The photograph of the TALE FD

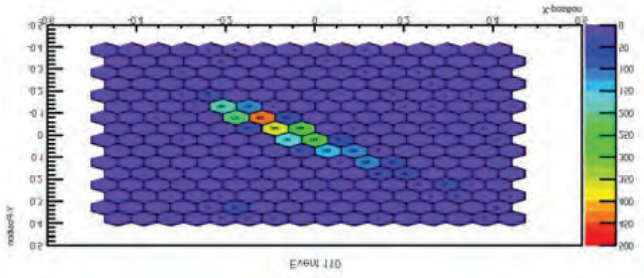

Fig. 15. A first air shower event taken with TALE FD

TA Low Energy Extension (TALE)

The TALE will give us the detailed studies of energy spectrum and composition from $10^{16.5}$ eV to the highest energies. The second knee has been observed at about 4×10^{17} eV in the cosmic-ray spectrum by previous experiments. The energy scales of these detectors differed by about a factor of two, so the energy at which this spectral break occurs is quite uncertain. There is a possibility that the transition from galactic cosmic rays to extragalactic cosmic rays occurs around this energy region. Then it is expected to observe the transition of heavier to lighter composition. The laboratory equivalent proton energy is 10^{17} eV in the center of mass energy of 14 TeV at the LHC. The cosmic-ray data to be observed by the TALE and the air shower MC simulation to be tuned by the result of the LHC forward (LHCf) experiment could be compared at about 10^{17} eV.

The mirror building of the TALE FD was constructed right next to the MD FD building in the spring of 2012. The 10 additional TALE FDs view 31°-59° in elevation angle and are constructed from refurbished HiRes-II telescopes. The TALE infill SD array consists of approximately 100 scintillation counters identical to those of the TA SD array, with graded spacings ranging from 400 m near the FD to 600 m further away, and merging with the main TA SD array of 1.2-km spacing at its northwestern corner. The TALE FDs was completed as shown in Fig. 14 and started its operation in the spring of 2013. Fig. 15 is a first air shower event with TALE FD. About the same time, the deployment of about one third of the surface detectors was planned.

Future plans

The grant of the current TA operation will end in March 2014. As described above, TA result is consistent with proton GZK model and there are hints of anisotropy. We propose to expand the aperture of the TA SD by a factor of four by building 500 additional counters, tentatively based on the existing TA SD design, but deployed in a square grid with 2.08-km spacing. Coupled with an additional FD site, the expanded TA will achieve the equivalent of 20 and 14 years of SD and hybrid exposures of the existing TA, respectively, by 2019 if the proposal is approved and we can start the construction in 2014.

The ground array 60 times that of the TA consisting of 10,000 SDs with 2 km spacing was proposed as a next generation air-shower ground array experiment first in the UHECR-2010 symposium [29]. This plan was reviewed at the CRC (Cosmic-ray Researchers Congress) future project symposium in 2012.

The merit of the ground-based observatory with huge aperture is its guaranteed ability of the conventional technique and/or possible ability of new method or new technique to be well calibrated with the existing observatories. We have already started the R&D experiments in the TA site with the group outside the TA. The R&D of the radio echo detection from air showers is being performed in the TA site [30]. An R&D of GHz radio detection in the TA site was performed first in March, 2012 together with the Auger members from the Karlsruhe Institute of Technology (KIT) and University of Chicago and the second test was performed in March, 2013.

The JEM-EUSO is the first space project to investigate EHE cosmic rays by a super-wide view (60°) telescope on the International Space Station (ISS). The advantage is its rather uniform and huge aperture (1.5×10^6 km^2 sr) in the whole sky. The ICRR TA members joined the JEM-EUSO group in December, 2012. The prototype of the JEM-EUSO has been developed and was installed on the TA site in March of 2012. It will be tested with ELS, CLF and air shower events simultaneously observed by TA.

Summary

The TA group confirmed suppression consistent with the GZK cutoff with a significance of 5.5σ and the ankle. The $X_{\rm max}$ measurement above $10^{18.2}$ eV is consistent with proton composition. The analyses of arrival directions of UHECRs for the correlations with AGNs, correlations with LSS proton model and autocorrelations show some hints of anisotropy although they are consistent with isotropic model with the current statistics.

The main aim of the TALE is to investigate the transition from galactic and extragalactic cosmic rays. The construction of TALE FD was completed and the deployment of about one third of TALE SDs was planned in the spring of 2013. Based on the UHECR2012 symposium and continuation of the working groups, the TA and Auger collaborations started joint studies to understand the discrepancies between TA and Auger. The TA results are consistent with proton GZK model, which leads to UHECR astronomy. As the next five year plan, we propose the plan of four times TA.

Bibliography

[1] T. Abu-Zayyad *et al.*, "The surface detector array of the Telescope Array experiment", *Nucl. Instrum. Methods* **A 689** (2012) 87-97.

[2] H. Tokuno *et al.*, "New air fluorescence detectors employed in the telescope Array experiment", *Nucl. Instrum. Methods* **A 676** (2012) 54-65.

[3] S. Kawana *et al.*, "Calibration of photomultiplier tubes for the fluorescence detector of telescope array experiment using a Rayleigh scattered laser beam", *Nucl. Instrum. Methods* **A 681** (2012) 68-77.

[4] H. Tokuno *et al.*, "On site calibration for new fluorescence detectors of the telescope array experiment", *Nucl. Instrum. Methods* **A 601** (2009) 364-371.

[5] Y. Tameda *et al.*, "Trigger system for the TA fluorescence detector", Proc. of nano PHYS'07, *Physica* **E 40** (2007) 430-433.

[6] Y. Tameda *et al.*, "Trigger electronics of the new Fluorescence Detectors of the Telescope Array Experiment", *Nucl. Instrum. Methods* **A 609** (2009) 227-234.

[7] T. Tomida *et al.*, "The atmospheric transparency measured with a LIDAR system at the Telescope Array experiment", *Nucl. Instrum. Methods* **A 654** (2011) 653-660.

[8] T. Tomida *et al.*, "Development of atmospheric transparency measurement system", *International Journal of Nanomanufacturing*, 2012, 047031.

[9] T. Shibata *et al.*, "End-to-end absolute energy calibration of atmospheric fluorescence telescopes by an electron linear accelerator", *Nucl. Instrum. Methods* **A 597** (2008) 61-66.

[10] R.U. Abbasi *et al.*, *Phys. Rev. Lett.* **100** (2008) 101101.

[11] J. Abraham *et al.*, *Phys. Rev. Lett.* **101** (2008) 061101.

[12] T. Abu-Zayyad *et al.*, "The COSMIC-RAY ENERGY SPECTRUM OBSERVED WITH THE SURFACE DETECTOR OF THE TELESCOPE ARRAY EXPERIMENT", *Ap. J.* Lett. 768 (2013) L1 (5pp).

[13] J. Abraham *et al.*, *Phys. Rev. Lett.* **104** (2010) 09110.

[14] R.U. Abbasi *et al.*, *Phys. Rev. Lett.* **104** (2010) 161101.

[15] Y. Tameda et al., "HiRes and TA Composition Measurements", Proc. of UHECR2012 Symposium, CERN, Geneva, Switzerland, 2012.

[16] T. Abu-Zayyad et al., "SEARCH FOR ANISOTROPY OF ULTRAHIGH ENERGY COSMIC RAYS WITH THE TELESCOPE ARRAY EXPERIMENT", *Ap. J.* 757 (2012) 26 (11pp).

[17] J. Abraham *et al.*, *Science* **318** (2007) 939; J. Abraham *et al.*, *Astropart. Phys.* **29** (2008) 188-204.

[18] P. Abreu *et al.*, *Astroparticle Phys.* **34** (2010) 315-326.

[19] R.U. Abbasi *et al.*, *Astroparticle Phys.* **30** (2008) 175-179.

[20] N. Hayashida *et al.*, *Phys. Rev. Lett.* **77** (1996) 1000-1003.

[21] M. Takeda *et al.*, *J. Phys. Soc. Jpn (Suppl.)* **B 70** (2001) 15-21.

[22] R.U. Abbasi *et al.*, *Ap. J. Lett.*, **610** (2004) 73-76.

[23] T. Kashti and E. Waxman, *JCAP* **05** (2008) 006.

[24] R.U. Abbasi *et al.*, *Ap. J. Lett.* **71B** (2010) 64-68.

[25] T. Jarrett, arXiv:astro-ph/0405069.

[26] M. Pshirkov, P. Tinyakov, P. Kronberg, K. Newton-McGee, *Ap. J.* **738** (2011) 192.

[27] `http://www.epj-conferences.org/index.php?option=com_toc&url=/articles/epjconf/abs/2013/14/contents/contents.html`

[28] http://www.cbpf.br/ icrc2013/

[29] S. Ogio, "Future Plans of the Telescope Array Experiment", Proc. of UHECR2012 Symposium, CERN, Geneva, Switzerland, 2012.

[30] J. Belz et al., "TARA: Forward-Scattered Radar Detection of UHECR at the Telescope Array", Proc. of UHECR2012 Symposium, CERN, Geneva, Switzerland, 2012.

Tibet ASγ Project

[Spokespersons : M. Takita]

ICRR, The Univ. of Tokyo, Kashiawa, Chiba 277-8582

Experiment

The Tibet air shower experiment has been successfully operated at Yangbajing (90°31' E, 30°06' N; 4300 m above sea level) in Tibet, China since 1990. It has continuously made a wide field-of-view (approximately 2 steradian) observation of cosmic rays and gamma rays in the northen sky.

The Tibet I array was constructed in 1990 and it was gradually upgraded to the Tibet II by 1994 which consisted of 185 fast-timing (FT) scintillation counters placed on a 15 m square grid covering 36,900 m^2, and 36 density (D) counters around the FT-counter array. Each counter has a plastic scintillator plate of 0.5 m^2 in area and 3 cm in thickness. All the FT counters are equipped with a fast-timing 2-inch-indiameter photomultiplier tube (FT-PMT), and 52 out of 185

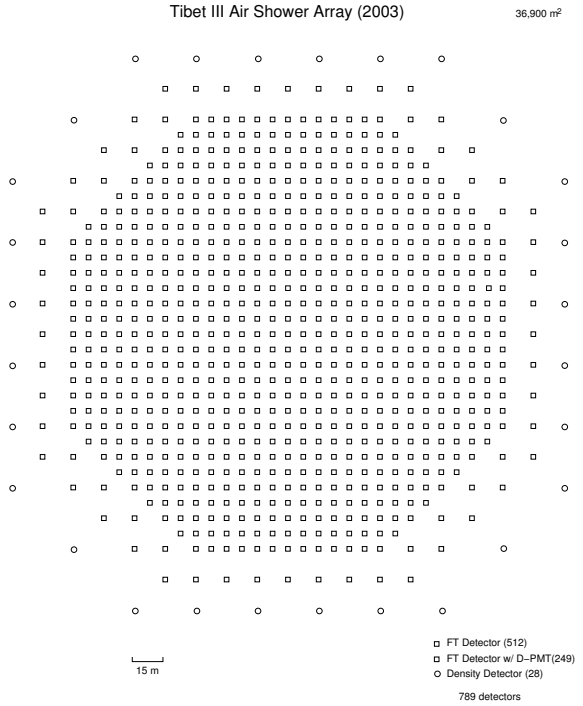

Fig. 16. Schematic view of Tibet III.

FT counters are also equipped with a wide dynamic range 1.5-inch-indiameter PMT (D-PMT) by which we measure up to 500 particles which saturates FT-PMT output, and all the D-counters have a D-PMT. A 0.5 cm thick lead plate is put on the top of each counter in order to increase the counter sensitivity by converting gamma rays into electron-positron pairs in an electromagnetic shower. The mode energy of the triggered events in Tibet II is 10 TeV.

In 1996, we added 77 FT counters with a 7.5 m lattice interval to a 5,200 m^2 area inside the northern part of the Tibet II array. We called this high-density array Tibet HD. The mode energy of the triggered events in Tibet HD is a few TeV.

In the late fall of 1999, the array was further upgraded by adding 235 FT-counters so as to enlarge the high-density area from 5,200 m^2 to 22,050 m^2, and we call this array and further upgraded one Tibet III. In 2002, all of the 36,900 m^2 area was covered by the high-density array by adding 200 FT-counters more. Finally we set up 56 FT-counters around the 36,900 m^2 high density array and equipped 8 D-counters with FT-PMT in 2003. At present, the Tibet air shower array consists of 761 FT-counters (249 of which have a D-PMT) and 28 D-counters as in Fig. 16.

The performance of the Tibet air shower array has been well examined by observing the Moon's shadow (approximately 0.5 degrees in diameter) in cosmic rays. The deficit map of cosmic rays around the Moon demonstrates the angular resolution to be around 0.9° at a few TeV for the Tibet III array. The pointing error is estimated to be better than $\sim$0.01°, as shown in Fig. 17, by displacement of the shadow's center from the apparent center in the north-south direction, as the east-west component of the geomagnetic field is very small at the experimental site. On the other hand, the shadow center displacement in the east-west direction due to the geomagnetic field enables us to spectroscopically estimate the energy

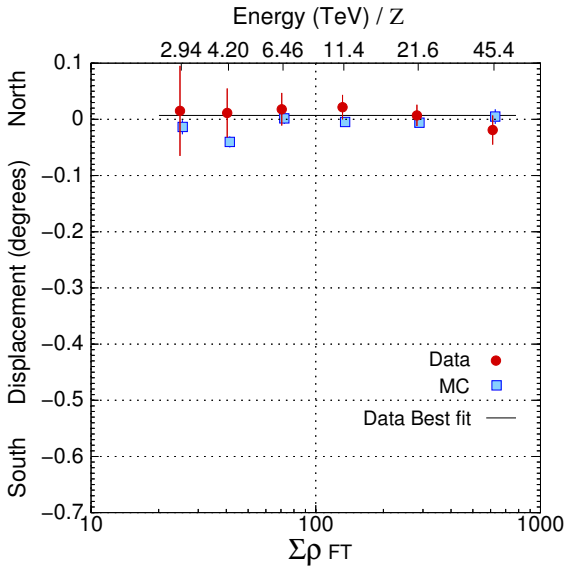

Fig. 17. From [1]. The Moon's shadow center displacement from the apparent position in the north-south direction as a function of energy, observed by Tibet III.

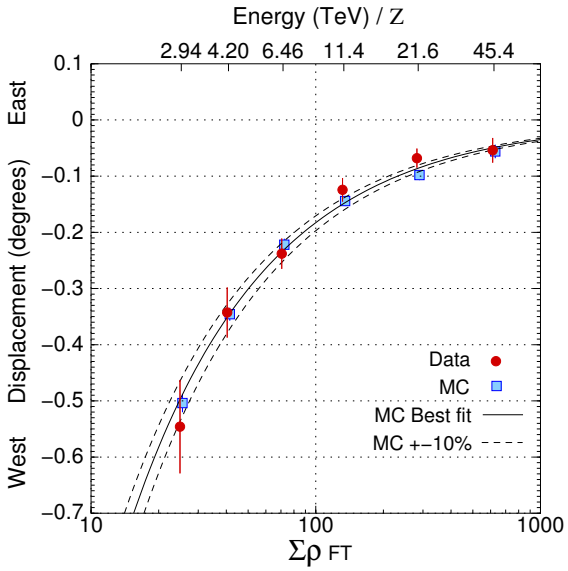

Fig. 18. From [1]. The Moon's shadow center displacement from the apparent positionin the east-west direction as a function of energy, observed by Tibet III.

scale uncertainty at ± 12 % level, as shown in Fig. 18. Thus, the Tibet air shower experiment introduces a new method for energy scale calibration other than the conventional estimation by the difference between the measured cosmic-ray flux by an air shower experiment and the higher-energy extrapolation of cosmic-ray flux measured by direct measurements by baloon-borne or satellite experiments.

Physics Results

Our current research theme is classified into 4 categories:

(1) TeV celestial gamma-ray point/diffuse sources,

(2) Chemical composition and energy spectrum of primary cosmic rays in the knee energy region,

(3) Cosmic-ray anisotropy in the multi-TeV region with high precision,

(4) Global 3-dimensional structure of the solar and interplanetary magnetic fields by observing the Sun's shadow in cosmic rays.

We will introduce a part of the results obtained in this fiscal year.

Galactic cosmic rays at TeV energies reach the Earth almost isotropically, due to galactic magnetic field disturbing the trajectory of cosmic rays. The Larmor radius of a 1 TeV proton in a lG magnetic field is 0.001 pc, many orders of magnitude shorter than the distance to any potential source of cosmic rays. Numerous experiments including the Tibet air-shower experiment, on the other hand, reported the existence of a small $\sim$0.1%) galactic cosmic- ray anisotropy at sidereal time frame. They consistently found that there are two distinct large-scale structures in the anisotropy; one is a deficit region in the cosmicray flux called the "loss-cone", distributed between 150 degrees and 240 degrees in right ascension, and the other an excess region called the "tail-in", distributed between 40 degrees and 90 degrees in right ascension. The common understanding of the origin of the anisotropy has not been established until now.

The Milagro experiment reported a steady increase in the amplitude of the loss-cone at 6 TeV from July 2000 to July 2007, in the latter half of the 23rd solar cycle. Milagro was a water Cherenkov detector located in New Mexico at the altitude of 2630 m above sea level, composed of an 80 m $\times$ 60 m $\times$ 8 m pond surrounded by a 200 m $\times$ 200 m array of 175 water tanks. Using a data set consisting of 96 billion cosmic-ray events, which is unprecedentedly large at TeV energies, Milagro significantly claimed the detection of the increase in the loss-cone amplitude at 6 TeV. The Tibet air-shower experiment would be the only experiment that operated during the corresponding period and is capable of examining Milagro's results with comparable statistics at TeV energies. We examined Milagro's claim using the data collected by the Tibet air-shower experiment during 1916 live days from November 1999 through December 2008.

Fig. 19 shows the time dependence of the loss-cone amplitude measured at 4.4, 6.2, and 11 TeV by the Tibet experiment in comparison with that measured at 6 TeV by Milagro. It can be clearly seen that, contrary to Milagro's results, the loss-cone amplitude measured by the Tibet experiment is quite stable at 4.4, 6.2, and 11 TeV during the period from 2000 to 2008. The ARGO-YBJ experiment, using the data collected from January 2008 to December 2009, also reported the observation of the sidereal anisotropy at multi-TeV energies, where the amplitude of the loss-cone remained $\sim$0.1 %. Milagro argued that variations in the heliosphere in relation to solar activities could cause the time dependence of the sidereal cosmic-ray anisotropy. In that case, the same tendency would

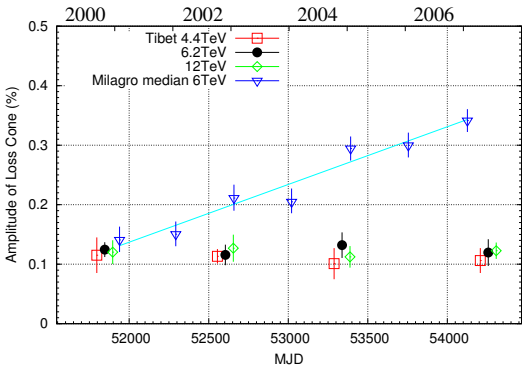

Fig. 19. From Ref. [2]. Time dependence of the loss-cone amplitude observed by the Tibet experiment at 4.4 TeV (open squares), 6.2 TeV (filled circles) and 11 TeV (open diamonds), along with Milagro's data (open inverse triangles) and the best-fit linear function to Milagro's data. The MJDs of our data points correspond to the times at the middle of each period. The upper horizontal axis represents years. All the error bars are the linear sums of the statistical and systematic errors.

be seen at sub-TeV energies, where the anisotropy is expected to be much more sensitive to solar activities. Matsushiro underground muon observatory, however, reports that the loss-cone amplitude shows no significant increase at 0.6 TeV during the corresponding period, suggesting that the steady increase in the loss-cone amplitude observed by Milagro at 6 TeV is not caused by the solar modulation effects.

Other Activities

The emulsion-pouring facilities can meet the demands for making any kind of nuclear emulsion plates which are used for cosmic ray or accelerator experiments. The thermostatic emulsion-processing facilities are operated in order to develop nuclear emulsion plates or X-ray films. Using these facilities, it is also possible to make and develop emulsion pellicles in 600-micron thickness each. In this way, these facilities have been open to all the qualified scientists who want to carry out joint research programs successfully. Of recent, however, the shrinking demand for the facilities let us decide that we should suspend calls for joint research programs to utilize the emulsion-pouring facilities, starting from 2012.

Future Plans

(1) Chemical composition of primary cosmic rays making the knee in the all-particel energy spectrum

We have measured the energy spectra of primary cosmic-ray protons, heliums, all particles around the knee energy region. The main component responsible for making the knee structure in the all particle energy spectrum is heavier nulei than helium. The next step is to identify the chemical component making the knee in the all particle energy spectrum. We have a plan to install an Yangbajing Air shower Core detector array (YAC) around the center of Tibet III to distinguish the chemical component making the knee. We set up YAC2

Fig. 20. YAC2 set up at Yangbajing.

($\sim$100 detectors over $\sim$160m^2 in area) in 2011, as is shown in Fig. 20 to mainly study the energy specta of proton and helium components in the knee energy region.

Currently, we are planning to set up YAC3 ($\sim$400 detectors over $\sim$5000m^2 in area) to measure the iron flux in the knee energy region.

(2) Gamma-ray astronomy in the 100 TeV region

We have a plan[3] to construct a large ($\sim 10,000\,\mathrm{m}^2 \times 1.5$m deep) underground ($\sim$ 2.5 m soil+concrete overburden) water Cherenkov muon detector array (Tibet MD) around an extended version (Tibet AS, $\sim$83,000 m^2) of Tibet III. By Tibet AS + MD, we aim at background-free detection of celestial point-source gamma rays in the 100 TeV region (10 TeV – 1000 TeV) with world-best sensitivity and at locating the origins of cosmic rays accelerated up to the knee energy region in the northern sky. The measurement of cut off energies in the energy spectra of such gamma rays in the 100 TeV region may contribute significantly to understanding of the cosmic-ray acceleration limit at SNRs. Search for extremely diffuse gamma-ray sources by Tibet AS + MD, for example, from the galactic plane or from the Cygnus region may be very intriguing as well. Above 100 TeV, the angular resolution of Tibet AS with 2-steradian wide field of view is 0.2° and the hadron rejection power of Tibet MD is 1/10000. The proposed Tibet AS + MD, demonstrated in Fig. 21, has the world-best sensitivity in the 100 TeV region, superior to HESS above 10-20 TeV and to CTA above 30-40 TeV.

In addition to unknown point-like sources, we expect to detect established sources in the 100 TeV region: TeV J2032 + 4130, HESS J1837-069, Crab, MGRO J2019+37, MGRO J1908+06, Milagro candidate sources, Mrk421, Mrk501 are sufficiently detectable and Cas A, HESS J1834-087,LS I+63 303, IC443 and M87 are marginal.

Furthermore, our integral flux sensitivity to diffuse gamma rays will be the world-best as well. The diffuse gamma rays from the Cygnus region reported by the Milagro group and also diffuse gamma-rays from the galactic plane will be clearly detected. Diffuse gamma-rays of extragalacitic origin may be an interesting target as well.

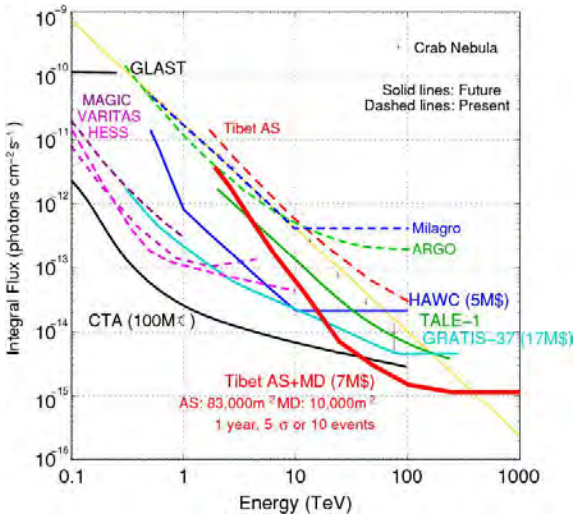

Fig. 21. Tibet AS + MD (red curve) integral flux sensitivity (5σ or 10 events/1yr) for a point source.

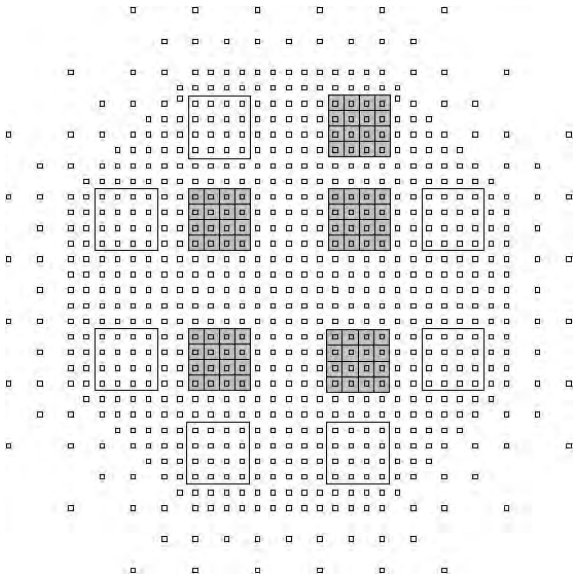

Fig. 22. The 5 shaded squares represent the constructed 5 MD pools.

In fall, 2007, a prototype underground muon detector, composed of two 52m^2 water pools, was successfully constructed in Tibet to demonstrate the technical feasibility, cost estimate, validity of our Monte Carlo simulation. Data analyses demonstrate that our MC simulation reproduces real data quite reasonably.

In 2010, construction of 5/12 of the full-scale MD, as is shown in Fig. 22, started and the concrete-based water pools were successfully completed. The remaining works are under way, as is shown in Fig. 23

Fig. 23. PMTs mounted on a MD cell.

Bibliography

Papers in refereed journals

[1] "Multi-TeV Gamma-Ray Observation from the Crab Nebula Using the Tibet-III Air Shower Array Finely Tuned by the Cosmic-Ray Moon's Shadow", M. Amenomori *et al.*, Astrophysical Journal, **692** , 61-72 (2009).

[2] "Is the large-scale sidereal anisotropy of the galactic cosmic-ray intensity really instable at TeV energies?", M. Amenomori *et al.*, Astroparticle Physics, **36** , 237-241 (2012).

[3] "Exploration of a 100 TeV gamma-ray northern sky using the Tibet air-shower array combined with an underground water-Cherenkov muon-detector array", T.K. Sako *et al.*, Astroparticle Physics, **32** , 177-184 (2009).

The Tibet ASγ Collaboration

M. Amenomori[1], X. J. Bi[2], D. Chen[3], T. L. Chen[4], W. Y. Chen[2], S. W. Cui[5], Danzengluobu[4], L. K. Ding[2], C. F. Feng[6], Zhaoyang Feng[2], Z. Y. Feng[7], Q. B. Gou[2], Y. Q. Guo[2], H. H. He[2], Z. T. He[5], K. Hibino[8], N. Hotta[9], Haibing Hu[4], H. B. Hu[2], J. Huang[2], H. Y. Jia[7], L. Jiang[2], F. Kajino[10], K. Kasahara[11], Y. Katayose[12], C. Kato[13], K. Kawata[14], M. Kozai[13], Labaciren[4], G. M. Le[2], A. F. Li[15,6,2], H. J. Li[4], W. J. Li[2,7], C. Liu[2], J. S. Liu[2], M. Y. Liu[4], H. Lu[2], X. R. Meng[4], K. Mizutani[11,16], K. Munakata[13], H. Nanjo[1], M. Nishizawa[17], M. Ohnishi[14], I. Ohta[18], S. Ozawa[11], X. L. Qian[6,2], X. B. Qu[19,2], T. Saito[20], T. Y. Saito[21], M. Sakata[10], T. K. Sako[14], J. Shao[2,6], M. Shibata[12], A. Shiomi[22], T. Shirai[8], H. Sugimoto[23], M. Takita[14], Y. H. Tan[2], N. Tateyama[8], S. Torii[11], H. Tsuchiya[24], S. Udo[8], H. Wang[2], H. R. Wu[2], L. Xue[6], Y. Yamamoto[10], Z. Yang[2], S. Yasue[25], A. F. Yuan[4], T. Yuda[14], L. M. Zhai[2], H. M. Zhang[2], J. L. Zhang[2], X. Y. Zhang[6], Y. Zhang[2], Yi Zhang[2], Ying Zhang[2], Zhaxisangzhu[4], X. X. Zhou[7]

[1] *Department of Physics, Hirosaki University, Hirosaki 036-8561, Japan*
[2] *Key Laboratory of Particle Astrophysics, Institute of High Energy Physics, Chinese Academy of Sciences, Beijing 100049, China*
[3] *National Astronomical Observatories, Chinese Academy of Sciences, Beijing 100012, China*
[4] *Department of Mathematics and Physics, Tibet University, Lhasa 850000, China*
[5] *Department of Physics, Hebei Normal University, Shijiazhuang 050016, China*

[6] *Department of Physics, Shandong University, Jinan 250100, China*
[7] *Institute of Modern Physics, SouthWest Jiaotong University, Chengdu 610031, China*
[8] *Faculty of Engineering, Kanagawa University, Yokohama 221-8686, Japan*
[9] *Faculty of Education, Utsunomiya University, Utsunomiya 321-8505, Japan*
[10] *Department of Physics, Konan University, Kobe 658-8501, Japan*
[11] *Research Institute for Science and Engineering, Waseda University, Tokyo 169-8555, Japan*
[12] *Faculty of Engineering, Yokohama National University, Yokohama 240-8501, Japan*
[13] *Department of Physics, Shinshu University, Matsumoto 390-8621, Japan*
[14] *Institute for Cosmic Ray Research, University of Tokyo, Kashiwa 277-8582, Japan*
[15] *School of Information Science and Engineering, Shandong Agriculture University, Taian 271018, China*
[16] *Saitama University, Saitama 338-8570, Japan*
[17] *National Institute of Informatics, Tokyo 101-8430, Japan*
[18] *Sakushin Gakuin University, Utsunomiya 321-3295, Japan*
[19] *College of Science, China University of Petroleum, Qingdao, 266555, China*
[20] *Tokyo Metropolitan College of Industrial Technology, Tokyo 116-8523, Japan*
[21] *Max-Planck-Institut für Physik, München D-80805, Deutschland*
[22] *College of Industrial Technology, Nihon University, Narashino 275-8576, Japan*
[23] *Shonan Institute of Technology, Fujisawa 251-8511, Japan*
[24] *Japan Atomic Energy Agency, Tokai-mura 319-1195, Japan*
[25] *School of General Education, Shinshu University, Matsumoto 390-8621, Japan*

The Ashra Project

[Spokesperson: Makoto Sasaki]
ICRR, The Univ. of Tokyo, Kashiwa, Chiba 277-8582
In collaboration with the members of:
ICRR, The University of Tokyo, Kashiwa, Japan; Toho University, Funabashi, Japan; University of Hawaii at Manoa, Honolulu, USA; University of Hawaii at Hilo, Hilo, USA; Nagoya University, Nagoya, Japan; Kanagawa University, Yokohama, Japan

Overview

Ashra (*All-sky Survey High Resolution Air-shower detector*) [1, 2, 3, 4] is a project to build an unconventional optical telescope complex that images very wide field of view, covering 77% of the sky, yet with the angle resolution of a few arcmin, sensitive to the blue to UV light with the use of image intensifier and CMOS technology.

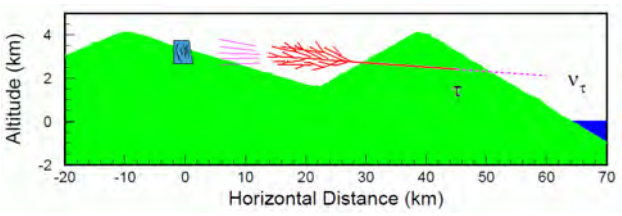

Fig. 24. Conceptual drawing of Cherenkov τ shower method. The right mountain is Mauna Kea and the left is Mauna Loa.

Fig. 25. The Ashra main and sub stations at the Mauna Loa site (top), and a light collector towards Mauna Kea (bottom).

Detection of PeV-EeV neutrinos (ν's) is direct evidence for the acceleration of hadrons into the EeV range and of photo-pion interactions in a violent object such as GRBs[5]. The earth-skimming tau neutrino technique, which detects extensive air showers [6], has the advantage of providing a large target mass. The technique uses air shower produced by decay particles of tau leptons in the atmosphere as the observed signal. The air shower emits intense Cherenkov lights in front, which could be detected by the mountain or the ground faced detector (Fig. 24). The method is realized by Ashra-1 experiment [7]. The air shower also emits isotropic fluorescence lights. In order to enhance the tau neutrino detectability, the detector should be capable of detecting fluorescence signal.

The observatory firstly consists of one main station having 12 detector units and two sub-stations having 8 and 4 detector units. One detector unit has a few light collecting systems with segmented mirrors. The main station and one of the sub stations were constructed on Mauna Loa (3,300 m) on Hawaii Island in 2007 as shown in Fig. 25.

Since January 2012, we highly efficiently made physics observation runs (Observation03) with triple types of triggers for Cherenkov tau showers induced by earth-skimming tau neutrinos, Cherenkov cosmic ray showers, and optical flashes from transient objects like GRBs.

Ashra detector

All-sky survey high-resolution air-shower detector (Ashra) is designed to hold 77% of the entire night sky in the field of view with a resolution of a few arcminutes. Ashra detector is a complex of unconventional optical light collectors (LCs) , each of those has 42° diameter field of view. An image of the optical collector is focused on the large electrostatic lens [8] followed by the image pipeline, which is shown in Fig. 26. The image pipeline split and transport the image to both a trigger device and a high-gain, high-resolution complementary metal-oxide semiconductor image sensor.

Ashra will acquire optical images every 1 second with 1-second exposure without dead time. This enables us to explore optical transients, possibly associated with gamma ray bursts (GRBs), flares of soft gamma-ray repeaters (SGRs), supernovae explosion, and so on, in so far as they are brighter than $B \simeq 13$ mag, for which we expect 3-σ signals.

The split image is transported a trigger device via the 4m long optical fiber bundle. The bundle is made of 500 $\mu m\phi$ optical fiber. 64×64 optical fibers are arranged to have $32mm \times 32mm$ square cross section. Central position of each fiber is arranged according to 500 μm lattice within the accuracy of less than $100\mu m$. The transmittance is measured to be greater than 85% including coupling loss at each end of the fiber.

One end of the bundle is connected to multi-anode PMTs. PMT signal is injected to the custom made trigger LSI . Each LSI chip has 16×16 pixels, each size of those is $500\mu m \times 500\mu m$. Total 4096 channels of 16 LSI chips are implemented on the ceramic board. In order to process different time scale lights, Cherenkov light and fluorescence light, band-pass frequency of the filter is designed to be adjustable by external voltage. The threshold level on each pixel can be chosen from 8 levels to compensate pixel-to-pixel sensitivity discrepancy.

"Wired OR" signal, summed signal of 64 pixels along axes, are sent to the FPGA based trigger circuit. Decision of the first level Cherenkov trigger is based on geometrical criteria. The aperture of one trigger pixel is $\sim 0.65^\circ \times 0.65^\circ$, adjacent two of which well contain Cherenkov lights from an air shower.

The calibration chain is designed to obtain not only an absolute energy scale to air shower measurement, but also uniformed sensitivity over the large field of view (positional) and in time (temporal). Environmental monitors systems, a cloud monitor, weather monitors, a far Lider and a near Lidar have already been installed or are ready for installation. Especially Ashra detector observes stars in the view every 1 second, which would give us an absolute calibration of the transparency of atmosphere. LED flasher system was developed in order to obtain positional and temporal flat calibration of the detector sensitivity.

LED flasher is composed of a LED, a photo diode and optical lenses in a black box. Collimated light of $\lambda = 405nm$ is divided by a half mirror in two directions. One illuminates a photo diode monitoring LED luminous intensity and the other illuminates the input window of the photoelectric tube via off -focusing optical lenses. Thermal variations of LED luminosity and photo diode sensitivity were carefully studied using a thermostatic chamber. LED luminosity variable coefficient (Photo diode output variable coefficient) was measured to be -0.21ppc/$^\circ C$(-0.07ppc/$^\circ C$) in the temperature range from 35$^\circ C$ to 47$^\circ C$. Radiance uniformity was also measured to be sufficiently flat in the view; namely the variation was less than 1%.

Experiment and Observation

Experiment of the Cherenkov light trigger was carried out at Ashra observational site on Mauna Loa in Hawaii. The trigger LSI module and the trigger board were installed on one LC and a half of the PMT channels are read out in place of old handmade discriminator module. The LC which dedicates

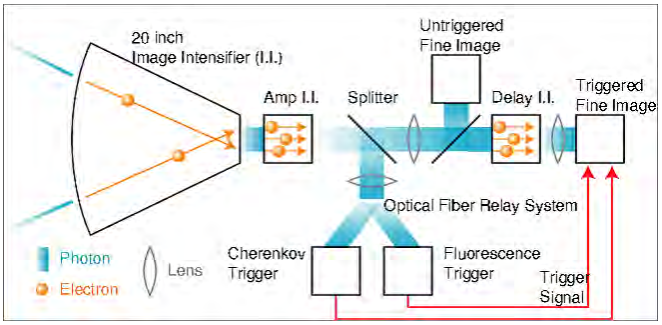

Fig. 26. Schematic view of Ashra image pipeline

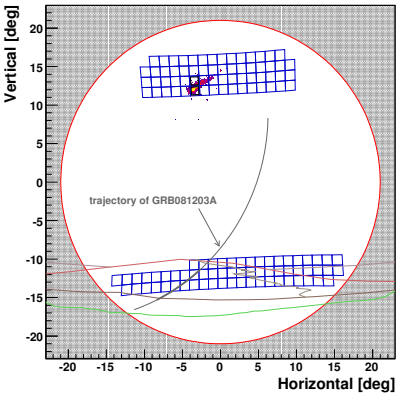

Fig. 27. Trigger pixel configuration in Ashra FOV. GRB081203A trajectry and the form of Mauna Kea is also drawn.

Mauna Kea and the above sky to the view allows to observe the earth skimming tau neutrino and also extensive air showers. Pilot observation was carried out for a total of 44.4 hours in 2008 December [5, 7] Data was also taken in the 3rd observation period from January 2012 to end of February 2013, more than 1720 hours.

Arrays of trigger pixels and their aperture are shown in the field of view of the detector (Fig. 27). Cherenkov light observation was carried out using this trigger pixel configuration. In Fig. 27, shown are the boundary (large red circle) between the inside (open circle) and outside (hatched area) of the FOV of the Ashra-1 light collector, which faces Mauna Kea, and the layout of trigger pixel FOVs and blue boxes for Cherenkov τ shower observation [7]. We repositioned array of the trigger pixel FOVs (upper blue boxes) to check the detection sensitivity with ordinary cosmic-ray air showers at a higher elevation. Firing trigger pixels (thick blue boxes) of an observed image of a cosmic-ray air shower readout along the trigger (points) is overlaid. An extended portion of the trajectory of GRB081203A counterpart (circular arc), the segment of this trajectory used in the ν_τ search (thick circular arc), the ridge lines of Mauna Kea (red) and Mauna Loa (green) mountains, the horizon, and Mauna Kea access road are shown. Observed cosmic-ray flux was consistent with Monte Carlo simulation

Satellite	GRB Name	$t_{inFOV} - t_0$ [sec]
Swift	GRB081203A	$-1.2\times10^4 - 5.6\times10^3$
Fermi	GRB090428	$-8.1\times10^3 - 5.9\times10^3$
Fermi	GRB090429C	$-4.1\times10^3 - 1.7\times10^3$
Swift	GRB091024	$-1.6\times10^3 - 3.3\times10^2$
Fermi	GRB100216A	$-4.0\times10^3 - 1.1\times10^4$
Swift	GRB100906A	$-1.0\times10^4 - 4.0\times10^3$
Fermi	GRB120120	$-1.4\times10^3 - 8.9\times10^3$
Fermi	GRB120129	$-1.6\times10^3 - 6.7\times10^3$
Fermi	GRB120327	$-9.9\times10^3 - 8.2\times10^1$
Swift	GRB120911	$-2.4\times10^4 - 6.8\times10^1$
Fermi	GRB121019	$-1.7\times10^3 - 7.3\times10^3$
Swift	GRB121212A	$-5.8\times10^3 - 2.6\times10^4$
Fermi	GRB130206	$-3.3\times10^3 - 7.5\times10^4$
Fermi	GRB130215	$-2.7\times10^3 - 4.3\times10^2$

Table 1. Summary of coincidence events with satellite GRB triggers [16, 17]. List of gold-plated events which must be observable geometrically within the FOV of our light collector at satellite triggers during our observation time.

in PeV to EeV region [7].

Gamma-ray bursts (GRBs) eject the most energetic outflows in the observed universe, with jets of material expanding relativistically into the surrounding interstellar matter with a Lorentz factor Γ of 100 or more. Energy dissipation processes involving nonthermal interactions between particles are thought to play an important role in GRBs. The GRB standard model [9], which is based on internal/external shock acceleration, has been used to describe the general features of a GRB, but the jet structure and particle acceleration details remain observationally unresolved. In the context of the GRB standard model, the interaction of an expanding relativistic shell with the intersteller medium (ISM) involves two shocks: the forward shock, which explains observed multi-wavelength afterglow, and the reverse shock, which is predicted to produce a strong optical flash [10, 11]. The explanation of optical flashes by the reverse shock has led to some estimates of the initial Lorentz factor η [11, 12]. The presence of accelerated protons at the GRB site must be a reality. The detection of PeV–EeV neutrinos (νs) from a GRB provides direct evidence for the acceleration of hadrons into the EeV range, and of photopion interactions in the GRB. Even the non-detection of neutrino can provide valuable information about GRB's key physical parameters such as the emission radius R_d, and the bulk Lorentz factor Γ [13].

Ashra-1 acquires optical images every 1$\sim$6 s with short readout deadtime. This enables us to explore optical transients, possibly associated with violent objects such as GRBs in so far as they are brighter than $B = 12 \sim 13$ mag, for which we expect 3σ signals assuming 4 s exposure. The unique advantage is the on-time detection of the events without resorting to usual satellite alerts. In each detector unit FOV, 1$\sim$2 events per year are expected in coincidence with the Swift gamma-ray events. The total Ashra field of view that is wider than satellite instruments allows to detect more optical transients, including an interesting possibility for an optical flash, not visble with gamma-rays.

The earth-skimming tau neutrino (ν_τ) technique, which detects extensive air showers [6], has the advantage of a large target mass, since it uses air showers produced by decay particles of tau leptons (τs) in the atmosphere as the observed signals. τs emerge out of the side of the mountain or the ground facing the detector; they are the product of interactions between VHE ν_τ and the earth matter they traverse. Above 1 EeV, air fluorescence observations based on the earth-skimming ν_τ technique have been reported [14]. Ashra-1 has reported the first observational search for ν_τ from a GRB based on the earth-skimming ν_τ technique with air showers induced by τ decays (hereafter referred to as the Cherenkov τ shower method) [15]. It can achieve sufficient detection sensitivity in the PeV–EeV region to be useful in the search for νs originating from hadrons accelerated to EeV at astronomical objects. Additional advantages of the Cherenkov τ shower method are its perfect shielding of cosmic-ray secondary particles, highly precise arrival direction determination for primary ν_τ and negligible background contamination by atmospheric νs in the PeV–EeV energy range.

Two of the Ashra-1 light collectors has been used for optical flash observation, of which FOV centers are in the direction of 60° (0°N) and 12° (22.5°N) in the elevation (azimuthal) angles respectively. We recorded more than 3 million non-trigger reccuring images of the FOV of 0.83 sr for 5637 hr of 1121 night runs between June 28 in 2008 and March 23 in 2013. The observation time corresponds to 20 % of all time without the shutdown period for the maintenance and 95 % of the maximum observable time defined by the solar and the lunar conditions where the altitudes of the sun and the moon must be lower than -18° and 0° respectively with the moon fraction less than 0.2.

To investigate GRB optical emission, we define three specific observational time domains with respect to satellite triggers; precursor ($0<t_0-t_e<24$ hr), prompt ($t_s<t_0<t_e$), and afterglow ($0<t_s-t_0<3$ hr) where t_0 is a satellite trigger time, t_s is the time when the trajectry of the center position of GRB counter part object triggered by the satellite enters into a FOV of an Ashra-1 light collector and t_e is the time when it exits the FOV. Throughout the above observation time for optical flashes and afterglows, we preselected and categolized 32 (86), 6 (21), and 1 (4) GRBs triggers by Swift (Fermi) satellite, which were circulated through The Gamma-ray Coordinates Network (GCN) [16, 17], into the three time domains respectively as optical transient cadidates. Futhermore, we selected gold-plated samples of 14 prompt GRB candidate events for our cross observation with Swift or Fermi satellites requiring the events triggered are reported as trigger type of GRB as summarized in Table1.

One of the Ashra light collectors built on Mauna Loa has the geometrical advantages of not only facing Mauna Kea, allowing it to encompass the large target mass of Mauna Kea in the observational FOV, but has also an appropriate distance of $\sim$30 km from Mauna Kea, yielding good observational efficiency when imaging air-shower Cherenkov lights which are directional with respect to the air-shower axis. Using the advanced features, we performed commissioning search for Cherenkov τ showers for 197.1 hr between October and December of 2008 and have already published [15]. We served

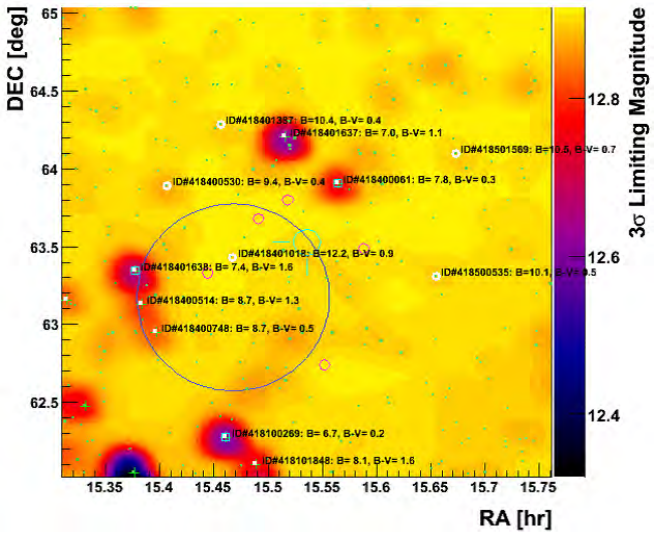

Fig. 28. 3σ limiting map for prompt optical flash GRB081203A.

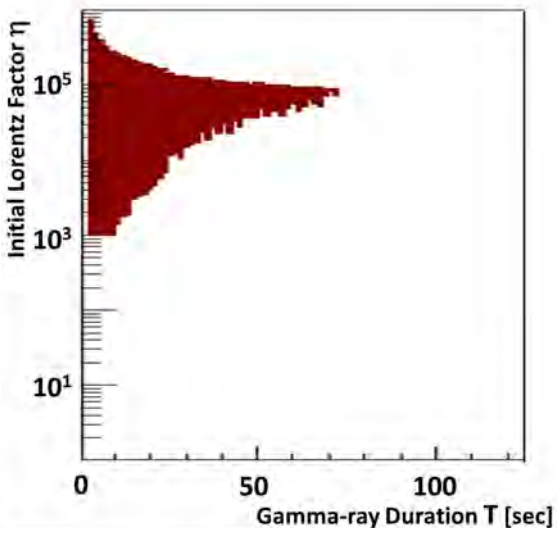

Fig. 29. Constrain of the 3σ rejection area (dark) for the initial Lorentz factor as varying the GRB duration.

limited 62 channels of photomultiplier tubes (PMTs) as trigger sensors prepared for the commissioning runs to cover the view of the surface area of Mauna Kea, maximizing the trigger efficiency for Cherenkov τ showers from Monte Carlo (MC) study. Adjacent-two logic was adopted to trigger the fine imaging, by judging discriminated waveform signals from each pixel of the multi-PMT trigger sensor. During the commissioning search period, $\sim$2 hr before the trigger of GRB081203A [21]. We accumulated nealy 44 million images with the air-shower Cherenkov light triggers for 1863 hr of 323 night runs of the ν_τ search between January 12 in 2012 and March 23 in 2013.

Analysis

Our wide field observation covered the Swift-BAT error circle at the time of GRB081203A [21]. We have searched for optical emission in the field of GRB081203A around the BAT-triggered GRB time (T0) with one of the light collector units in the Ashra-1 detector. The Ashra-1 light collector unit used in this analysis has the achieved resolution of a few arcmin, viewing 42° circle region of which center is located at Alt = 11.7°, Azi = 22.1°. The sensitive region of wavelength is similar with the B-band. We quickly analyzed 83 images covering the field of GRB081203A every 7.2s with 6s exposure time respectively during the observation between T0-300s and T0+300s. We detected no new optical object within the PSF resolution around the GRB081203A determined by Swift-UVOT. As a result of our preliminary analysis, the 3sigma limiting magnitudes were estimated in comparison with stars in Tycho-2 Catalog to be distributed between 11.7 and 12.0 for time bins corresponding to 4 s exposure time.

Our observation also covered the Swift-BAT error circle at the time of GRB100906A [22]. We searched for optical emission in the field of GRB100906A around T0 with an Ashra-1 light collector, viewing 42° circle region of which center is located at Alt = 60°, Azi = 0°. We analyzed 200 images covering the field of GRB100906A every 6s with 4s exposure time respectively during the observation between T0-600s and T0+600s. We detected no new optical object within the PSF resolution around the GRB100906A determined by Swift-UVOT. In the same manner as GRB081203A, the 3sigma limiting magnitudes were estimated and they were distributed between 12.0 and 12.2 for individual time bins corresponding to 4 s exposure time. All original RAW format images of the preselected event samples were converted into Fits format files. A set of dark image frames were prepared for every night runs at the Mauna Loa observation site. Another set of image frames for the procedure of gain flat were made for every observational season, which is defined as a period between full moon ages, using uniformly illuminating spherical plate scintilator with the same curvature radius of the input facal sphere of our photoelectric lens imaging tube (PLI). The calibration procedure was performed at the beginning and the ending of each observational season with the sherical plate scintilator put on the input window of PLI. The quantative quality of the gain calibration can be checked using the night sky background images taken as flat images with the same Ashra-1 light collector, followed by a procedure of the median flat method. The gain calibration error was confirmed to be less than several % with the comparison between the gain calibration with scintilation and checks with the median flat procedure.

Once image data are prepared after the dark and gain flat procedures, we perform two kinds of main data processes of astrometry and photometry as conventional astronomical procedure. Contrary to the astronomical convention we use so wide angle photoelectrical optics that we needed to consider gradually converging procedure of matching observed sources with catalog stars. First of all we extracted observed sources from each image using the SExtractor program [23] and compared with the positions and B and V filter brightness of stars preselected from the Tycho2 Catalog [24] to be within FOV of the light collector. The matching procedure started with the brightest stars to be in FOV and gradually compared with fainter ones until all observed sources should be matched with

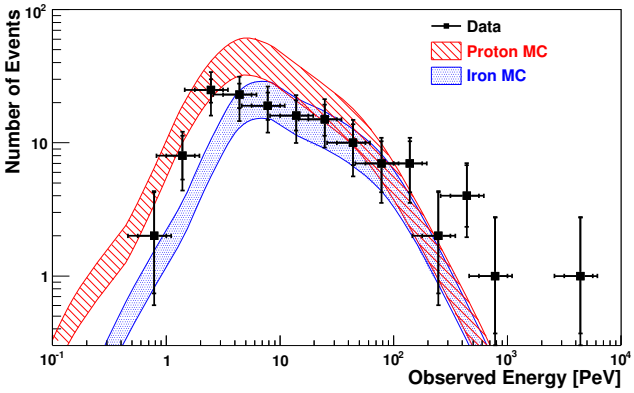

Fig. 30. Observed cosmic-ray flux spectrum (filled box) with bars indicating statistical and systematic errors and the MC predictions for proton primary (hatched band) and iron primary (shaded band) assumptions [20]. The width of the bands shows the evaluated systematic error of 30% of the MC prediction.

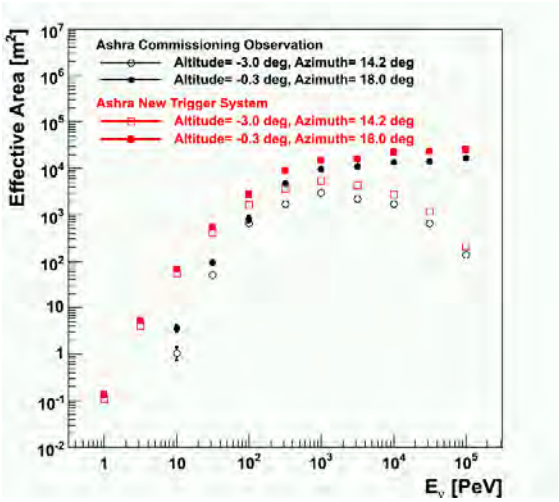

Fig. 31. Effective area of Cherenkov τ shower ES method with Ashra-1 for the Obs03 period in 2012-2013 (square) and for the past commissioning phase (circle) in 2008, in the cases of (altitude, azimuth) of (-0.3°,14.2°) (filled) and (-3.0°, 18.0°) (opened) respectively.

the preselected catalog stars. We have checked this scheme using 572 test pairs of real observed sources and tycho2 catalog stars and confirmed that the estimated source positions and magnitudes are fairly consistent with the catalog ones with negligible failures in matching. The matching error on the position is confirmed to be less than 1 CMOS pixel corresponding to the resolution of 1.4 arcmin in the Ashra-1 optical system. In the final stage of the astrometory, we determined the position of the GRB counter part at the satellite trigger time as well as the local coodinate system using at least 3 reference stars as close to the GRB position as possible in the observed image.

For the procedure of the photometory, again we used near observed stars as references, of which B and V magnitudes are well known to estimate the detection sensitivity of the Ashra-1 light collector. Adding that we checked the fluctuation of the background of each image using the output ADC values of CMOS pixels in the region not containgin effectively bright stars after applying Gaussian filter with the measured point spread to images to eliminate photon statistical flucutuation. The estimated signal to noise ratio (SNR) in the background region was confirmed to be consisitnt Gaussian distribution with the standard deviation of unity without any tailed events. Finally we made the SNR map and the map of 3σ limiting magnitude for each selected image.

For physics interpretation, we deal with the parameter of real gamma-ray duration as a free parameter taking into account the threshold effect of the satellite triggers. Following the assumption of the duration, we needed to change the time bin width to estimate the limiting magnitude of the detection sensitivity. Fig. 28 shows the map of 3σ limiting magnitude as a preliminary result of the search of prompt optical flash from GRB081203A.

The unique check of optical flash around the GRB satellite trigger time can lead to the estimates of the initial value of the Lorentz factor η with another assumed parameter of gamma-ray duration time T following the procedure described in [25] and combining with the other multi-wavelength observations of the afterglow from GRB081203A [21]. Fig. 29 shows the preliminary result of the constrain of the initial Lorentz factor as varying the parameter of gamma-ray duration from the search for optical flash from GRB081203A.

The estimation of the detection sensitivity, background, and pointing accuracy of the Ashra light collector as an ES ν_τ detector and the validity of the reconstruction procedure are described elsewhere [27]. To confirm the detection sensitivity and gain calibration for the Cherenkov τ shower, we detected and analyzed 140 events of normal cosmic-ray air-shower Cherenkov images for a total of 44.4 hr in 2008 December and 1863 hr between July 11 in 2011 and March 23 in 2013, using the same instruments used in neutrino observation, but after rearranging the trigger pixel layout to view the sky field above Mauna Kea. In the cosmic-ray observation, the trigger pixel layout is centered at zenith angle of $\sim$65°. The observed and MC cosmic-ray flux spectra are shown in Fig. 30, in which the MC prediction used the typically observed cosmic-ray flux in the knee region [18, 19]. Since the primary cosmic-ray components are observationally undefined, we present the MC prediction of cosmic-ray flux spectra, assuming either only protons or irons as the primary cosmic rays in Fig. 30. Note that the same reconstruction procedure was applied to both of the observed and MC data to extract the observed energy. In both cases, the observed data and the MC prediction agreed well on the normalization and the shape of the distribution within the expected errors.

Prospects

In this Ashra-1 experiment, we were performing device installation and specific observation in a step-by-step way to enhance the scientific impacts as shown in the previous sections. We have already made a referee journal publication of PeV-EeV tau neutrino search [20] as important physics results with the Ashra-1 detector unit adding to publications on the detector or methodorogical developments and circulations [8, 21, 22]. We are now preparing for a few physics publications from the optical observation data of the 2.5 years from

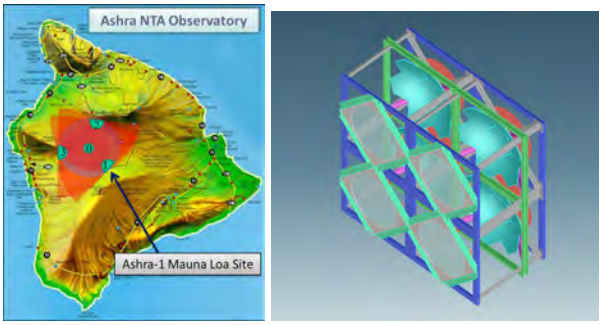

Fig. 32. Ashra NTA Observatory layout (left) and Ashra NTA detector unit of four same LCs (right).

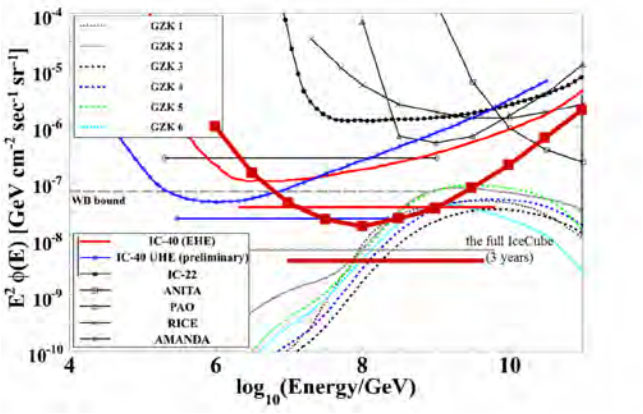

Fig. 35. Diffuse sensitivity with 3 yr observation.

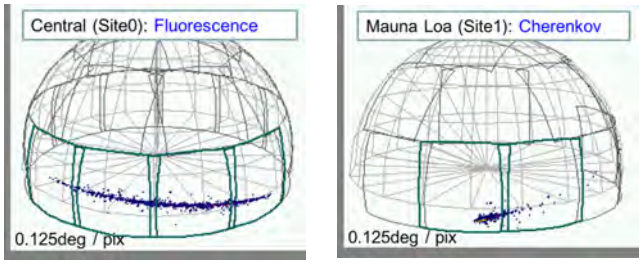

Fig. 33. Simulated event with $E_{\nu_\tau} = 10^{17}$eV: (left) fluorescence track image by Site0; (right) Cherenkov track image by Site1. Trigger pixel and fine image FOV angles are 0.5° and 0.125°, respectively.

the Obs01 to Obs02 as well as keeping highly efficient observation runs in Obs03 for optical transients, VHE CRs and tau neutrinos. Adding that, the R&D for the direct Cherenkov method applied to Ashra-1 has been granted and under development.

The planned full Ashra (Ashra NTA) observatory consists of four sites: Site0-3, as shown in Fig.32 (left), with the x-y-z coordinates and corresponding FOV coverage. Site1-3 form a 25 km triangle, observing the total air mass surrounded by Mauna Loa, Mauna Kea, and Hualalai. The central Site0 has full-sky coverage. Each site has a group of detector units each of which has several LC systems (Fig.32 (right)) instrumented with segmented mirrors. Performance was studied based on Ashra-1 experience. Detailed design studies for the Ashra NTA detector are currently underway.

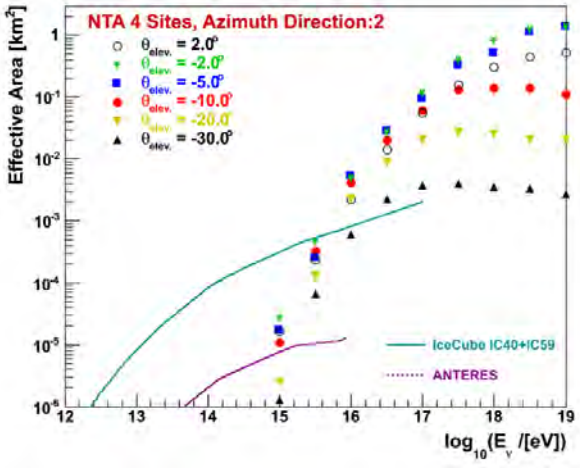

Fig. 34. Estimated effective detection areas simulated for ν_τ from point source with azimuthal arrival direction ϕ_2 of the Mauna Loa summit with respect to the central Site0, and dip angles 2.0° (black open circle), -2.0° (green star), -5.0° (blue filled box), -10.0° (red filled circle), -20.0° (yellow filled triangle), and -30.0° (black filled triangle).

The z-axis points to zenith and y-axis points north, with z-coordinates determined from topography data. Site1-3 are the vertices of an equilateral triangle of side length 25 km, with Site0 at their geometric center. Site1 is located at ML-OS (on Mauna Loa) and Site2 at 25 km distant from ML-OS in the direction of the Kilohana Girl Scout Camp. To simulate the performance of the Ashra NTA detector, we assume each LC has $32^\circ \times 32^\circ$ total FOV, $0.5^\circ \times 0.5^\circ$ for trigger pixel FOV, and $0.125^\circ \times 0.125^\circ$ image sensor pixel FOV. The Site0 system consist of 12 LCs in the lower, 8 LCs in the middle, and 4 LCs in the higher elevation angle regions which together cover the full-sky solid angle of 2π sr. The remaining sites have only 12 LCs in the lower elevation angle region covering π sr. The bottom edge of the lower elevation angle region is defined to be -9° (below the horizon).

In our simulation program, we take density profile of the Earth, use the ν_τ distribution from CTEQ4 citeGandhi96, inelasticity parameter from [29], and parameterize energy loss in Earth by citeTseng03,Dutta2001. We use τ decay from TAUOLA and air-shower generation of Gaisser-Hillas + NKG [30]. We use a constant average ν_τ energy fraction of 40% (lab frame) from τ decays. The error from this approximation is found negligible. For detector simulation, we incorporate light collection and throughput with simplified triggering logic. Event reconstruction is not yet implemented. All candidate events must satisfy the trigger conditions (1) number of detected photoelectrons per LC > 61; (2) S/N estimated in track-associated 4 pixels $\times$ 64 pixels box (air-shower track included) >4 [31].

A simulated event with primary ν_τ energy $E_{\nu_\tau} = 10^{17}$ eV consistent with the above conditions is shown in the r.h.s. of Fig.33. The error for ν_τ arrival direction reconstruction is 0.08°. Fig.35 shows Ashra NTA sensitivity for diffuse ν_τ flux (maroon squares) for 3 year ($\sim 9.5 \times 10^6$ s) observation, as-

suming duty cycle of 10Ashra NTA can survey ν_τ point source objects with the best-yet sensitivity in the detection solid angle for ν_τ defined as $-30^\circ < \theta_{elev} < 0^\circ$ and $0^\circ < \phi_{azi} < 360^\circ$, and for 10 PeV $< E_{\nu_\tau} <$ 1 EeV. The location of Ashra NTA on Hawaii Island allows us to survey the galactic center for more than several hundred hours each year.

Further discussion on angular resolution and background simulation can be found in the LOI, which would appear in 2013.

Bibliography

[1] http://www.icrr.u-tokyo.ac.jp/∼ashra

[2] Sasaki, M., Progress of Theoretical Physics Supplement, **151**, 192 (2003).

[3] Sasaki, M., et al., Proc. 29th Int. Cosmic Ray Conf. (Pune, India), Vol. 8, 197-200, 2005.

[4] M. Sasaki, 30th Intl. Cosmic Ray Conf. (Merida), ID1232, 2007.

[5] M. Sasaki *et al.*, in 32th International Cosmic Ray Conference, Rio de Janeiro 2013.

[6] D. Fargion, ApJ, 570:909, 2002.

[7] Y. Aita *et al.* ApJ, 736:L12, 2011.

[8] Y. Asaoka and M. Sasaki, Nucl. Instr. and Meth. A647, 34, 2011.

[9] Mészaros, P. 2006, Rep. Prog. Phys., 69, 2259

[10] Mészaros, P., & Rees, M.J. 1997, ApJ, 476, 232

[11] Sari, R., & Piran, T., 1999. ApJ, 517, L109

[12] Mészaros, P., & Rees, M.J. 1999, MNRAS, 306, L39

[13] Gao, S., *et al.* 2013, arXiv:1305.6055

[14] Abraham, J., et al. 2008, Phys. Rev. Lett., 100, 211101

[15] Aita, Y., et al. 2011, ApJL, 736, L12

[16] http://gcn.gsfc.nasa.gov/swift_grbs.html

[17] http://gcn.gsfc.nasa.gov/fermi_grbs.html

[18] Antoni, T., et al. 2005, Astropart. Phys., 24, 1

[19] Amenomori, M., et al. 2008, ApJ, 678, 1165

[20] Y. Aita *et al.*, ApJL**736**, L12 (2011).

[21] Y. Aita *et al.*, GCN Circ., 8632 (2008).

[22] Y. Asaoka *et al.*, GCN Circ., 11291 (2010).

[23] Bertin, E. and Arnouts, S. 1996, A&AS, 117, 393

[24] Hϕg, E., *et al.*, 2000, A&A, 355, L27

[25] Kobayashi, S. and Zhang, B., 2003, ApJ, 582, 641

[26] http://gcn.gsfc.nasa.gov/other/081203A.gcn3

[27] Asaoka, Y. and Sasaki, M., 2013, Astropart. Phys., 41, 7

[28] Sasaki, M., Manago, N., Noda, K., Asaoka, Y., GCN Circ. 3421, 2005.

[29] R. Gandhi, C. Quigg, M.H. Reno and I. Sarcevic, Phys. Rev. D **58** (1998) 093009.

[30] M. Sasaki, Y. Asaoka, M. Jobashi, Astropart. Phys. 19 (2003) 37.

[31] M. Sasaki, J. Phys. Soc. Jpn. **70** (Suppl. B) (2001) 129.

High Energy Astrophysics Group

[Spokesperson: T. Terasawa]
ICRR, The Univ. of Tokyo, Kashiawa, Chiba 277-8582

Overview

Since its creation in December 2009, the high energy astrophysics group has been making theoretical and observational studies of violent astrophysical phenomena in which nonthermal cosmic ray particles are being accelerated. Targets of the group's study include high energy astrophysical objects such as supernova explosions/pulsar magnetospheres, giant flares and repeating bursts of magnetars, jets from active galactic nuclei (AGN), star-burst galaxies, mysterious gamma ray bursts (GRB), as well as galaxy clusters. Research works on the origin of ultra high energy cosmic rays (UHECRs) are also within the coverage of the group.

Research topics: 1. Reevaluation of acceleration processes

While the diffusive shock acceleration process has been accepted as the standard model of astrophysical particle acceleration, interests are being renewed on other processes such as second-order stochastic acceleration in relativistic turbulences. To study the particle acceleration in realistic relativistic shear flow turbulence, we have made relativistic MHD simulations of the two dimensional Kelvin-Helmholtz instability and then followed test particle motions in the electromagnetic field obtained from the simulations. We have found that some particles are stochastically accelerated non-resonantly to have a log-normal distribution (Fig. 36).

Research topics: 2. Pulsars

The magnetosphere around neutron stars are candidate sites for efficient particle acceleration. We study the particle acceleration in the pulsar magnetosphere and the observational verifications of them. As an example, we have shown the possibility that cosmic-ray electrons/positrons from millisecond pulsars (MSPs), which have a higher angular frequency and a lower surface magnetic field than that of canonical pulsars, may contribute significantly to the observed spectrum. Our results are shown in Fig. 37. Recent gamma-ray observations suggest that the MSP population is separated into two subclasses with respect to the number of ejected electrons/positrons (multiplicity). In Figure 37a, the electron/positron flux from multiple MSPs with low multiplicity is shown. There is a large peak at 10–50 TeV energy range. Even if the fraction

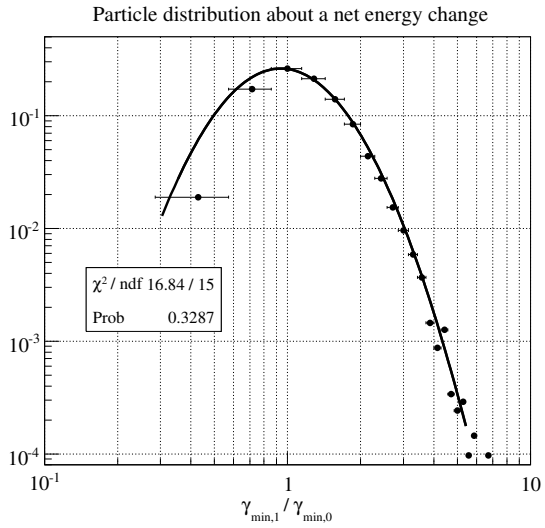

Fig. 36. The distribution of the net energy change of particles (black circles) and the fitted log-normal distribution function (black line). The horizontal and vertical axes respectively show the net energy change (as the ratios between the final and intial Lorentz factors) and the particle phase space density (in arbitrary unit). The suffix 'min' of γ indicates that these Lorentz factors are measured when the particle energy reached the minimum during one gyro-period along with their $\mathbf{E}\times\mathbf{B}$ motions.

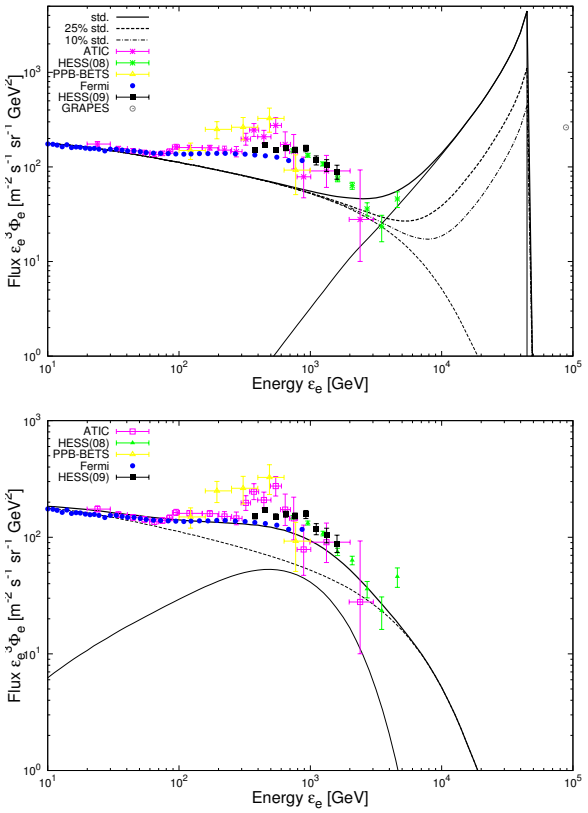

Fig. 37. a (top). Predicted cosmic ray electron/positron spectrum from MSPs. A thin solid line shows the MSP contribution if 100% of MSPs are with *low* multiplicity. A thick solid line shows the total spectra, namely the sum of the MSP contribution and the background cosmic rays electron/positron. Thick–dashed and dot—dashed lines show the total spectra, if 25% and 10% of MSPs are with low multiplicity and contribute to the spectra. Figure b (bottom). A thin solid line shows the MSP contribution if 100% of MSPs are with *high* multiplicity. A thick solid line shows the total spectra.

of their MSPs is as small as 10 per cent, this peak would be detectable in future missions such as CALET (see the later subsection) and CTA. On the other hand, MSPs with high multiplicity are expected to contribute to the excess in the energy spectrum between 100 GeV and several TeV (Figure 37b). Our results are also consistent with the observational spectrums recently reported by AMS-02.

The Crab pulsar, the remnant of the supernova explosion in 1054 A.D., is one of the most studied neutron stars. It is known that the dispersion measure (DM) of the Crab pulsar, namely the total electron content from the pulsar to the observer along the line of sight, shows temporal variations with various time scales (minutes to months) in the range of 56.7-56.9 pc cm^{-3}. To the shortest limit, Popov et al. (2009) reported that the short-term DM variations are of the order 0.001pc cm^{-3} with a few minutes timescale. Such DM variations, if confirmed, may give a clue to study the change of the physical condition within the pulsar's magnetosphere. While we have made a followup observation of the DM variation (Fig. 38), the estimated errors are $\sim$0.001pc cm^{-3} or larger, too large to confirm the results by Popov et al. We need further observations to settle this matter.

Research topics: 3. Study of solar flare neutrino generation

When a solar flare is triggered, some of the surrounding protons are accelerated up to the energy of several tens of GeV. Such energetic protons interact with the solar atmosphere, resulting in the creation of solar-flare neutrinos. We made a feasibility study for the solar-flare neutrino detection with the next-generation neutrino experiment, Hyper-Kamiokande (HK), using Geant4 toolkit. Fig. 39 shows simulated neutrino fluences on the Earth's orbit from a solar flare behind the Sun. These neutrinos have the peak energies around several tens

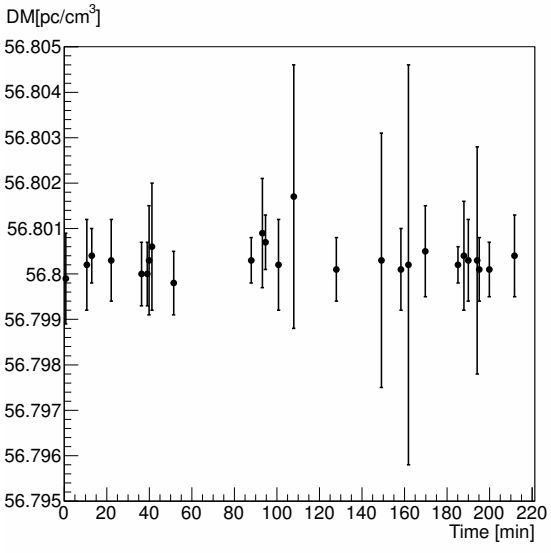

Fig. 38. Dots with 3σ errors show DM values determined from 26 Crab's giant radio pulses simultaneously observed at the NICT Kashima 34m parabola antenna (1.4 GHz band) and the JAXA Usuda 64m parabola antenna (2.2 GHz band). The observation was made on 17 October 2011 for 220 minutes.

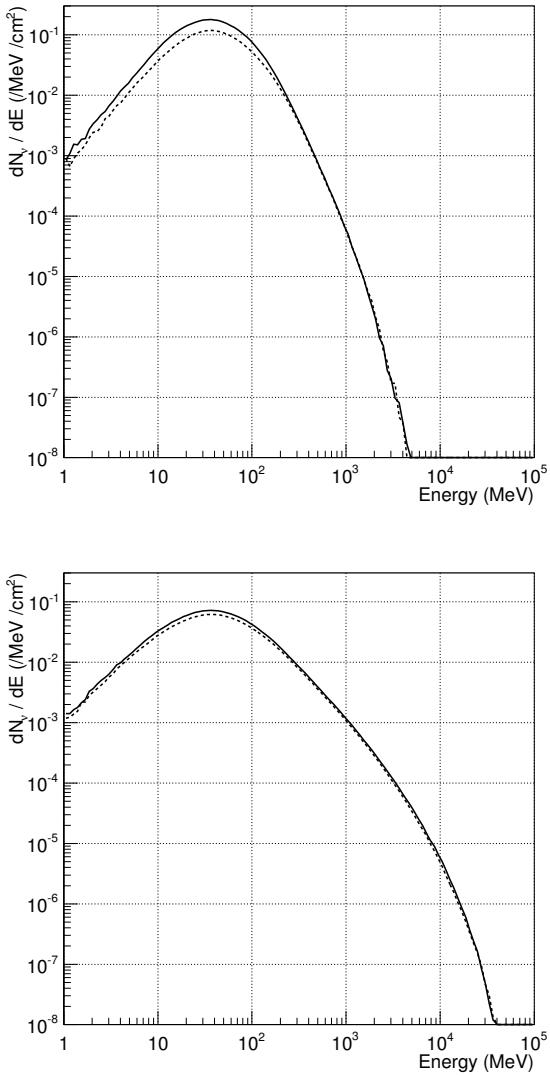

Fig. 39. a (top). Neutrino fluences on the Earth's orbit from a solar flare behind the Sun. We assume that the flare proton spectra follows a power law distribution as expected for X10 class flares. In our analysis, ν_e and ν_μ have almost the same fluences (solid line). $\overline{\nu_e}$ and $\overline{\nu_\mu}$ also have almost the same flueneces (dashed line). Figure a (bottom). The same as the top panel, but for the extremely hard proton spectra.

of MeV. We have calculated the expected event rate at HK based on these neutrino fluence calculations, and found that the event rate is less than $\sim 10^{-3}$ per flare. Therefore, the detection of solar flare neutrinos by HK is not feasible. This also means that HK will be free from the background noise from solar flare neutrinos even during the largest solar flares as ever recorded.

Research topics: 4. Search for correlation between the lightning and solar activities (in collaboration with the primary cosmic ray group, Dr. H. Miyahara)

Lightning is a discharge process neutralizing electric charge which are generated by electrification process in thunderclouds. Remote sensing measurements of global lightning activity with Schumann Resonance (SR) revealed a clear 28 day periodicity in the lightning activity obtained in a span of four years,

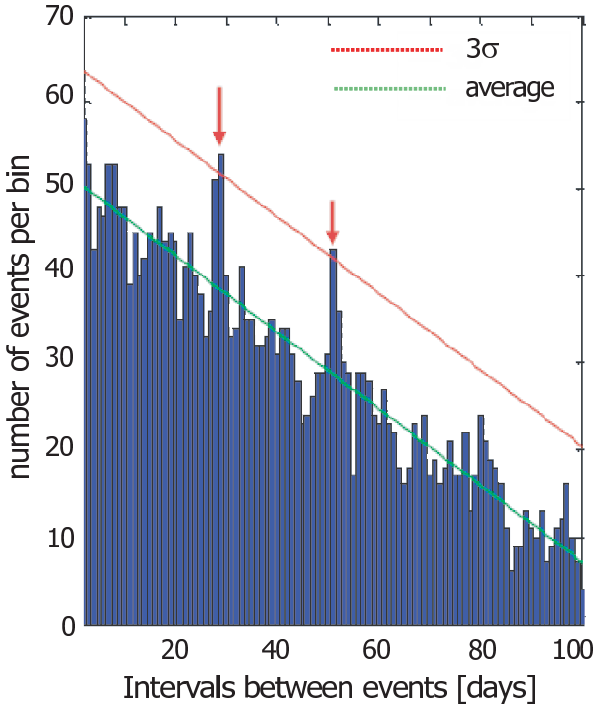

Fig. 40. Plot of histogram of intervals between 'lightning events' in Japan[2] between 1989 and 2010. Here, a 'lightning event' is defined as a event in which lightning activities are reported in more than 9 prefectures. A green line shows the average dependence of the event number on the intervals, while a red line shows 3 σ fluctuation level above the average obtained from Monte Carlo calculation.

2000-2003 (Sato, 2004). Since this 28 day periodicity is close to the apparent solar rotation period ($\sim$27 day), this observation may indicate the existense of the correlation between the lightning activity and solar (or geomagntic) activity. We have attempted to make further studies of lightning activity with longer time span, 1989-2010, for which the daily meteorological data in Japan are available. We obtain statistically significant peaks ($> 3\sigma$) at 28-29 day and 51 day periodicities (Fig. 40), where the first peak at 28-29 day seems consistent with the previous result by Sato (Note, however, there is a difference between the natures of the data sets: While Sato's is of global coverage, ours is limeted to the area of Japan). To clarify the physical mechanism to produce these periodicities, we are making correlation studies between the lightning activity and activity indices of the sun, galactic cosmic rays, and geomagnetism.

Research topics: 5. CALET project — a R/D study

The CALorimetric Electron Telescope, CALET, project is a Japan-led international mission for the International Space Station in collaboration with Italy and the United States. The instrument will be flown in 2014 and is scheduled to be operated for five years. The primary science goal of CALET is to perform high precision measurements of the electron spectrum from 1 GeV to 20 TeV to search for nearby cosmic ray sources and dark matter signatures. The unique feature of CALET is its thick, fully active calorimeter that allows mea-

[*2] We exclude the data from the area along the sea of Japan so as to avoid the winter lightnings characteristic to this area.

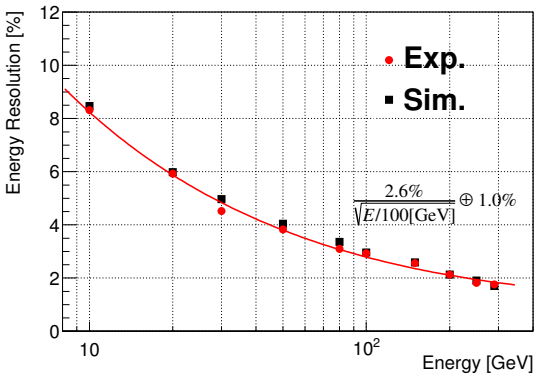

Fig. 41. The energy resolution of CALET for electrons measured at CERN-SPS with Monte Carlo simulation. We use EPICS as a detector simulation code.

surements well into the TeV energy region with excellent energy resolution and low background contamination, which are confirmed by Monte Carlo simulation. In order to assess the detector performance and the validity of our Monte Carlo simulation, a testing team of the CALET collaboration has carried out beam tests with CALET prototypes at the CERN Super Proton Synchrotron (SPS), using electron and proton beams in the energy region from 10 GeV to 290 GeV and from 30 GeV to 400 GeV, respectively. Comparing the experimental data with the simulation results, consistencies of the energy deposition, the energy resolution and lateral shower spread and so on are confirmed. Fig. 41 shows the energy resolution for electrons. We note that the energy resolution above 100 GeV is excellent, better than 3%, which will enable us to detect a distinctive feature in the energy spectrum originating from dark matter or astrophysical origins at sub-TeV energies.

Bibliography

Papers in refereed journals

1. Kisaka, S., and N. Kawanaka, TeV cosmic-ray electrons from millisecond pulsars, Monthly Notices of the Royal Astronomical Society, 421, Apr. 2012.

2. Kojima, Y., and S. Kisaka, Magnetic field decay with Hall drift in neutron star crusts, Monthly Notices of the Royal Astronomical Society, 421, 2722-2730, Apr. 2012.

3. Kero, J., C. Szasz, T. Nakamura, D. D. Meisel, M. Ueda, Y. Fujiwara, T. Terasawa, K. Nishimura, and J. Watanabe, The 2009-2010 MU radar head echo observation programme for sporadic and shower meteors: radiant densities and diurnal rates, Monthly Notices of the Royal Astronomical Society, 425, 135-146, Sep. 2012.

4. Terasawa, T., and S. Matsukiyo, Cyclotron resonant interactions in cosmic particle accelerators, Space Science Rev., 173, 623-640, Nov. 2012.

Thesis

5. Mikami, R., "Giant radio pulses from the Crab pulsar: Study of radiation mechanisms with simultaneous radio and hard X-ray observations" (in Japanese), Master thesis, Department of Physics, The University of Tokyo, March 2012.

6. Takeishi, R., "Numerical study of solar flare neutrinos" (in Japanese), Master thesis, Department of Physics, The University of Tokyo, March 2012.

Conference papers

7. Yoshida, H., T. Terasawa, H. Miyamoto, T. Usui, N. Yaguchi, and I. Yoshikawa, The Forward Scattering Meteor Radio Echo Observation Using a GPS-Synchronized Multiple Receiving Stations, Asteroids, Comets, Meteors 2012, Proceedings of the conference held May 16-20, 2012 in Niigata, Japan, LPI Contribution No. 1667, id.6187, 2012.

8. Usui, T., H. Yoshida, H. Miyamoto, N. Yaguchi, T. Terasawa, and I. Yoshikawa, Development of a Ranging System for the Forward Scattering Meteor Radio Echo Observation Using a GPS-Synchronized Multiple Receiving Stations, Asteroids, Comets, Meteors 2012, Proceedings of the conference held May 16-20, 2012 in Niigata, Japan, LPI Contribution No. 1667, id.6099, 2012.

9. Kero, J., T. Nakamura, K. Nishimura, D. Meisel, T. Terasawa, M. Ueda, Y. Fujiwara, C. Szasz, and J. Watanabe, The MU radar meteor head echo observation programme, 39th COSPAR Scientific Assembly. held 14-22 July 2012, in Mysore, India, Abstract C0.3-3-12, p.909, 2012.

10. Niita, T., H. Fuke, K. Yoshida, Y. Katayose, S. Torii, Y. Akaike, K. Kasahara, T. Tamura, Y. Ueyama, S. Ozawa, Y. Shimizu,M. Kyutan, H. Murakami, D.Ito, M. Karube,, K. Kondo, Cosmic-ray Electrons and Atmospheric Gamma-rays in 1-30 GeV observed with Balloon-borne CALET prototype detector, 39th COSPAR Scientific Assembly, held 14-22 July 2012, in Mysore, India, Abstract C2.1-5-12, p.1371, 2012.

11. Kisaka, S, and N. Kawanaka, TeV cosmic-ray electrons from millisecond pulsars, Proceedings of the International Astronomical Union, 291, pp. 419-421, 2013.

ASTROPHYSICS AND GRAVITY DIVISION

Overview

Astrophysics and Gravity Division consists of Gravitational Wave Group, The Observational Cosmology Group, Primary Cosmic Ray Group and Theory Group. The Gravitational Wave Group conducts experimental research of gravitational wave with researchers of gravitational wave experiment and theory in Japan. The main items are the construction of the large scale cryogenic interferometer(KAGRA) at Kamioka underground and the operation of CLIO. The Observational Cosmology Group has completed the planned imaging and spectroscopy observations, and it continues publishing papers in collaboration with worldwide researchers. This group has started a new optical deep survey project with the wide-field imager of Hyper Suprime-Cam mounted on the Subaru telescope. Primary Cosmic Ray Group reconstructs past cosmic ray changes and studies their impacts on climate change. Theory Group conducts both theoretical study of the Universe and astroparticle physics.

Gravitational Wave Group

Gravitational Wave Project Office (GWPO)

[Spokesperson : Kazuaki KURODA]
ICRR, The Univ. of Tokyo, Kashiwa, Chiba 277-8582

Overview

Gravitational wave project office was established at the beginning of the financial year of 2011 to assist the construction of KAGRA[3] gravitational wave telescope. The organization of this office is illustrated in Fig. 1. Main office is set in Kashiwa campus and its Kamioka branch is in Kamioka. It is an internal office placed in Astrophysics and Gravity Division of ICRR.

KAGRA project is hosted by ICRR, which means the funding comes through the University of Tokyo and all procurements are made through ICRR. However, the number of researchers working for KAGRA construction belonging to other organizations is larger than the staffs belonging to ICRR. Therefore, three collaboration members of KEK are recruited as guest researchers of ICRR and two research staffs are temporarily moved to ICRR from NAOJ.

The role of this office is to support execution of KAGRA project by ICRR staffs together with these collaboration members. Main works are

- finance planning
- management of collaboration
- support for the execution of KAGRA budget
- coordination of collaboration meetings
- technical supports for the KAGRA construction
- support for education of graduate students
- bridging collaboration members and ICRR administration office
- others

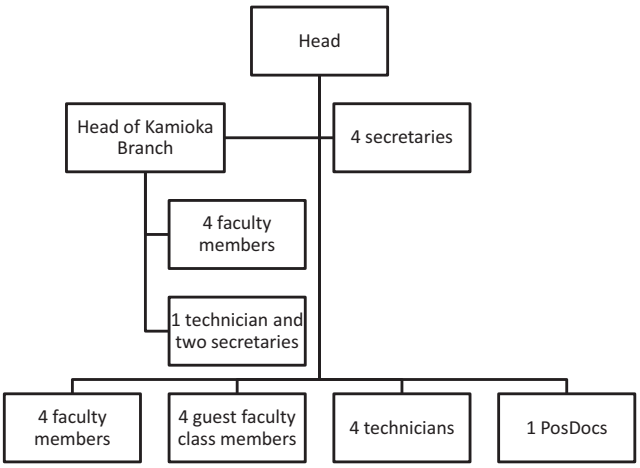

Fig. 1. Organization of the Gravitational Wave Project Office

Activity in FY 2012

We supported the collaboration meetings held in Kashiwa campus. They were two face-to-face international collaboration meetings[4] and six KAGRA collaobration remote meetings (two international and four domestic)[5]. We supported the KAGRA council meeting on 19th, June, 1st ELiTES general meeting held at Euro Tokyo delegation house on 3rd , October and at Sanjo Conferene Hall on 4th, October and Virgo-KAGRA meeting at the Hongo campus on 5th, Octoer.

We took care of travel supports for the following events:
- External Peer Review of KAGRA in April
- Workshop in collaboration with Toyama University
- 3rd Korea-Japan workshop in Seoul on 21-22 December.

We supported the execution of research programs adopted as ICRR collaborative researches listed in Table 1 in processing invoices for experimental goods and domestic travels.

*3 nicknamed in January, 2012 by public contribution for LCGT

*4 http://gwwiki.icrr.u-tokyo.ac.jp/JGWwiki/KAGRA/Meeting/F2F

*5 http://gwwiki.icrr.u-tokyo.ac.jp/JGWwiki/KAGRA/Meeting/Collaboration

Title	Representative	Affiliation
Development of optical cavities for ultranarrow stable laser	Tetsuya Ido	NICT
Gravitational Wave Detector in Kamioka	Masatake Ohashi	ICRR, UT
Study for LCGT data analysis and Research for its System (II)	Nobuyuki Kanda	OCU
Research of Large-scale Gravitational wave Telescope (II)	Kazuaki Kuroda	ICRR, UT
Development of Sapphire Mirror Suspension for LCGT (VII)	Toshikazu Suzuki	KEK/ICRR
Study of quatntum noise and quantum non-demolition scheme for LCGT	Kentaro Somiya	TITEC
Development of precision profiler for mirrors of LCGT interferometer 2	Toshiyuki Takatsuji	AIST
Data analysis using CLIO data	Hirotaka Takahashi	Yamanashi EC Nagaoka UT
Research on ultra-low frequency anti-vibration system for LCGT	Ryutaro Takahashi	ICRR, UT
Research of Earth's free oscillations based on simultaneous observations with a laser strainmeter and a superconductive gravimeter	Yoshiaki Tamura	NAOJ
Measurement of low-temperature mechnaical Q for mirror coating in gravitational-wave detector	Eiichi Hirose	ICRR, UT
Development of an evaluation system of a higher-quality sapphire for LCGT	Norikatsu Mio	PSC, UT
Real time control for interferometer using computers	Osamu Miyakawa	ICRR, UT
Research of Cryogenic Sillicon mirror for 3rd generation GWDs II	Shinji Miyoki	ICRR, UT
Research on cryogenic payload for LCGT	Kazuhiro Yamamoto	ICRR, UT
Development of Very Low Vibration Cryo-Cooler System	Nobuhiro Kimura	KEK/ICRR

Table 1. List of adopted as ICRR Cooperative researches

Kamioka branch of GWPO

The office and laboratory rooms for Kamioka branch of GWPO was created in July in Hokubu Kaikan (previous Kinder garten was refurbished) as shown in Fig. 2 and staffs moved to the office in July. One assitant professor moved from NAOJ as ICRR project staff on 1st, September. The Kamioka branch held an intorductory tour for local residents to KAGRA construction site on 2nd, December (as shown in Fig. 3). Two new secretary members joined to this branch since 1st, December.

The Kamioka branch conducted the site construction of KAGRA as the local headquarters making liaison with the comtruction company, Kamioka Observatory and local government.

KAGRA Project Status

[Spokesperson : Seiji KAWAMURA]

ICRR, The Univ. of Tokyo, Kashiwa, Chiba 277-8582

Overview

KAGRA (The new nickname has been given for LCGT : Large-scale Cryogenic Gravitational wave Telescope), as one of the world network of gravitational wave detectors, aims at the detection of gravitational waves by a 3 km baseline laser interferometer with cryogenic mirror system placed underground at Kamioka.

The development of KAGRA started as a 6.5 year project in October 2010, but later it was rescheduled as a 7.5 year project due to the suspension of the budget for the start of tunnel excavation as a result of the Great East Japan Earthquake which occurred on March 11, 2011. The KAGRA development is divided into two stages: initial KAGRA (iKAGRA) and baseline KAGRA (bKAGRA). In the 5 year iKAGRA stage the mirror system will be kept at room temperature with SAS (Seismic Attenuation System) and RSE (Resonant Sideband Extraction) not in operation while the bKAGRA is the latter 2.5 year development stage where the final goal is to be pursued with full equipment in operation including SAS, cryogenic system and RSE.

Fig. 2. Refurbished Hokubu Kaikan for Kamioka branch of GWPO

Fig. 3. An introductory tour for local residents inside KAGRA tunnel on 2nd, Decenber.

The host organization to conduct the KAGRA project is the Institute for Cosmic Ray Research, the University of Tokyo with a number of organizations both domestic and international involved. Up to now 33 Japanese and 37 overseas universities and research institutes have joined the KAGRA collaboration and still counting. The official agreements to establish international collaborations have been concluded between ICRR and 9 foreign institutes.

KAGRA, in the final configuration of bKAGRA, is designed to achieve the aim to detect gravitational-wave signals. Among several expected gravitational-wave sources, the primary observation target is selected to be an inspiral and merger of neutron-star binary. This is because it is the most certain source: its existence has been proved by radio-pulsar surveys, and its event rate has been theoretically estimated from astronomical observation results.

It is required that the KAGRA sensitivity be high enough to realize more than one detection of gravitational waves from neutron-star binaries in a one-year observation run with probability 90% or higher. For the requirement, the KAGRA duty

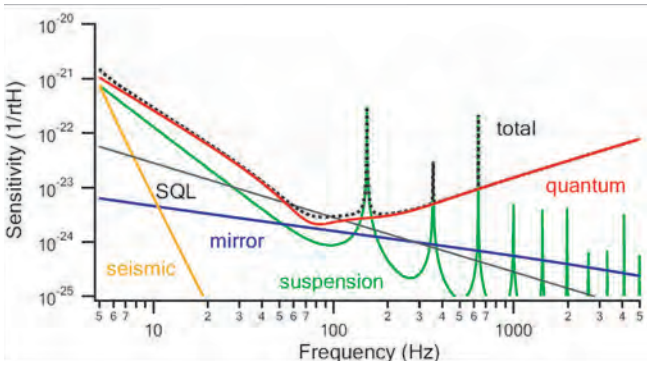

Fig. 4. Ultimate sensitivity limit of KAGRA.

factor must be higher than 80% and the observation range must be higher than 180Mpc. Here the signal-to-noise ratio is 8 and the normal incidence of gravitational waves on to the detector is assumed.

Fig. 4 shows the estimated ultimate sensitivity limits of KAGRA where incoherent sum of the fundamental noise sources is assumed. The observation range with the ultimate sensitivity limit of KAGRA is 280Mpc.

With the currently-practical design parameter set for bKAGRA, the sensitivity limited by fundamental noise sources gives the observation range of 240Mpc. The requirement allocation to each subsystem is determined in such a way as not to deteriorate the sensitivity more than 10% in total.

The observation range of bKAGRA with the 10% deterioration is 210Mpc. It is also required to each subsystem that the duty factor of KAGRA during the observation run be 80% or higher in total. More detailed requirement allocation is shown in the Interface Control Document (ICD).

The requirement for KAGRA is to be flowed down into that for each of the subsystems. Required values for the subsystem components are determined in such a way that the KAGRA target sensitivity be achieved with all the noise curves summed up in the spectrum. Some of the setup parameters are shared by multiple subsystems and those interface parameters shall be controlled by the System Engineer Office (SEO).

Major components of each subsystem are listed below.

- **Tunnel (TUN):** 3km tunnels, center room, end rooms, entrance tunnels, water drainage system
- **Facility Support (FCL):** buildings, power supply system, clean rooms, air conditioning, temperature control, humidity control
- **Vacuum (VAC):** vacuum ducts, vacuum chambers, baffles, flanges, vacuum pumps
- **Cryogenic System (CRY):** cryostats, heat link, Sapphire fibers, radiation shields, refrigerators

- **Vibration Isolation System (VIS):** Type-A/B/C SAS, suspension fibers (excl. Sapphire fibers), local controls
- **Mirror (MIR):** core optics, MC mirrors, MMT mirrors
- **Laser (LAS):** laser (1064nm, 532nm)
- **Main Interferometer (MIF):** optical layout of the main interferometer
- **Input Output Optics (IOO):** MC, OMC, Faraday isolator, EOM, MZ, BRT
- **Auxiliary Optics (AOS):** light control components (including suspended baffles), beam reducing telescopes, optical levers, moniors (CCD/CMOS cameras), viewports, automatic targets, beam shutters
- **Analog Electronics (AEL):** PD, QPD, actuators, CCD, monitors
- **Digital System (DGS):** CDS, signal transferring cables, ADC, DAC
- **Data Management (DMG):** data acquisition, archiving and distribution
- **Data Analysis (DAS):** data analysis pipelines
- **Geophysics Interferometer (GIF):** 1.5km interferometers, seismometers, environmental sensors

The rapidly changing status of KAGAR is presented in several international conferences.[1] There are also special articles presented in journals of academic societies.[2] We also present activitiy in our web-page.[3]

Bibliography

[1] S. Miyoki and LCGT collaboration, "Curent Status of LCGT project", TAUP 2011 in Minich, Munchen.

[2] K. Kuroda, "Large-scale Cryogenic Gravitational wave Telscope (LCGT) -Construction Status of LCGT project-", J. Cryo. Super. Soc. Jpn **46** (2011) 385 (in Japanese).

[3] http://gwcenter.icrr.u-tokyo.ac.jp/en/

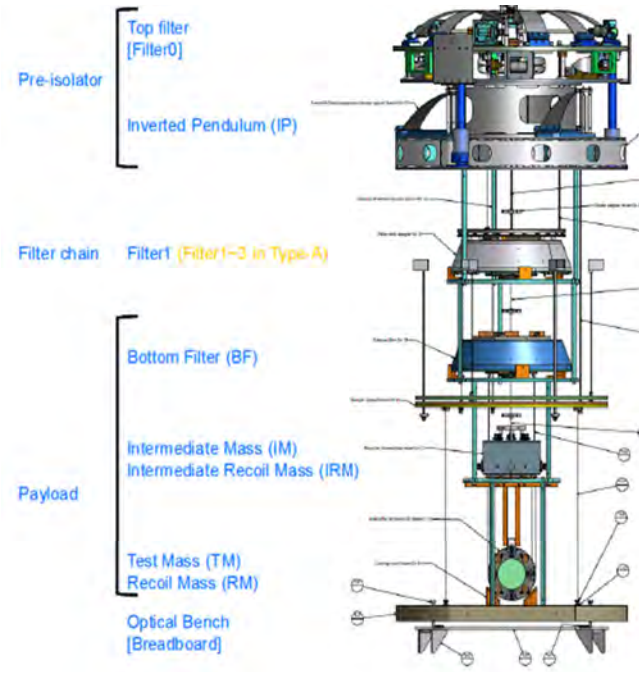

Fig. 5. Schematic view of Type-A/B system. Type-A system has additional two filters (Filter2 and 3). The payload for Type-A system is cryogenic.

Vibration Isolation Subsystem[6]

This subsystem makes vibration isolation for all optics used in KAGRA. There are two purposes required for this subsystem. One is attenuation of seismic noise in the observation band (less than 4×10^{-20} m/$\sqrt{}$ Hz at 10 Hz). The other is reduction of RMS displacement or RMS velocity of mirrors (less than 0.1μm or 0.1μm/s). Three kinds of system are disposed to 23 vacuum chambers to accomplish their purposes. Main mirrors are isolated by Type-A system, which consists of an inverted pendulum (IP), five stage geometric anti-spring (GAS) filters and a cryogenic mirror suspension. Other core optics is isolated by Type-B system, which consists of an IP, three stage GAS filters and a mirror suspension. Small opticsis isolated by Type-C system, which consists of three stage stack and a mirror suspension. Schematic view of Type-A/B system is shown in Fig.5. The mirror suspensionis called "payload". Type-A test mass is a sapphire mirror of 22 cm in diameter, 15 cm in thickness and 23 kg in weight. Type-B test mass is a silica mirror of 25 cm in diameter, 10 cm in thickness and 10 kg in weight. GAS filters are linked by connection wires each other. The GAS blades and the connection wires are made of maraging steel. The top part is called "pre-isolator" which consists of IP and top filter. The diameter of the top filter is larger than that of standard filter's to reach lower resonant frequencies and to suspend a larger total mass.[1] We have tested the pre-isolator prototype in Kashiwa. The control of the IP using an inertial sensor (geophone) was demonstrated successfully (Fig. 6).

---

*6 Ryutaro Takahashi, ICRR, The University of Tokyo

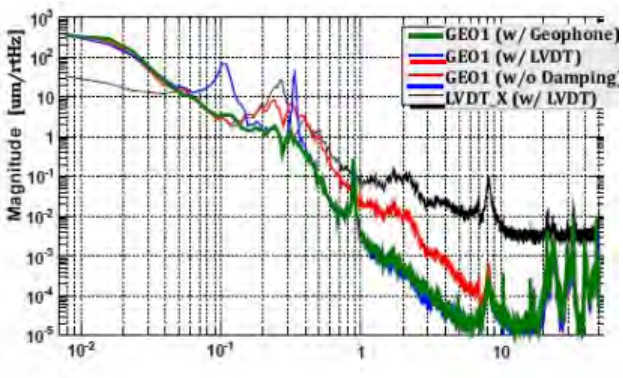

Fig. 6. Active damping using a geophone signal. Only X-DoF was controlled by the geophone. The other DoFs were controlled by the LVDTs. The motion of the top stage was reduced by the inertial damping.

Bibliography

[1] R. Takahashi, "Vibration Isolation System for Mirrors", J. Vac. Jpn **54** (2011) 24-27.

Digital system / Analog electronics[7]

KAGRA will employee an RSE interferometer with a power recycling cavity in its optical configuration. Control topology of RSE would be very complicated in kilo meter scale interferometers. The number of degrees of freedom to be controlled will be 5 in the optical length, ~ 30 in the alignment for mirrors and ~ 100 in the local damping for seismic isolations. A real time digital control system using computers will be used to control whole KAGRA interferometer. This system consists of ~ 25 real time front-end computers and ~ 15 servers to manage the front-end computers.

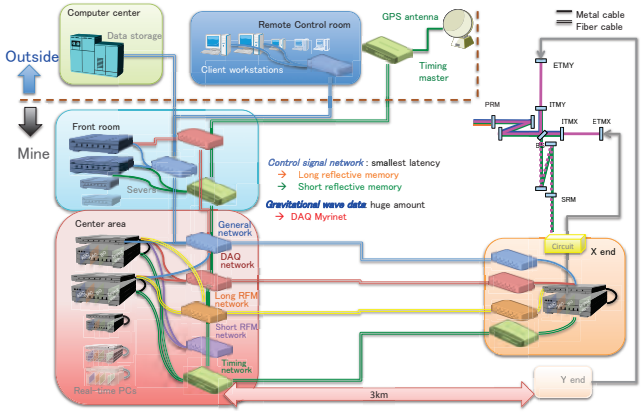

Fig. 7. Conceptual control design for KAGRA using computers.

Conceptual control network design is shown in Fig.7. In order to operate interferometers, we continuously keep controlling all degrees of freedom to maintain optical resonance in mirror cavities. The control signal is not so big amount but must be connected with very small latency. The front-end computers are connected by a reflective memory technology which has a remote memory over the network but the memory behaves as a local memory immediately reflecting the remote memory with very small latency. We will have two kinds of reflective memory network depending the distance between computers. The GE Fanuc's reflective memory will be used for connections along 3 km arms of KAGRA as a long distance reflective memory but speed is a bit slow, and the Dolphin's one is fast but only used for short distance in the center room of KAGRA.

Amount of data produced by interferometer, including gravitational wave data, will be a huge, roughly 1 Peta-byte per year or something. Transferring such a huge data from each front-end computer to a data concentrator server is realized by the DAQ network which uses Myrinet technology. Myrinet has an advantage for some low latency compared with general TCP/IP and enough band-width limit for data transfer amount. Huge gravitational wave data will be collected by these DAQ networks with small latency.

All ADC and DAC must be synchronized each other. The number of channels of ADC and DAC will be ~ 2500 in total. Synchronization whole ADC/DAC in km scale can be realized by independent timing networks with an automatic compensation system for time delay due to long distance.

This digital system involves EPICS technology and the EPICS database is used for slow data transfers. TCP/IP networks transfer general packet and EPICS data as well.

By the end of this fiscal year, we have tested above netwrok connections by the simple setup using 3 computers. The 2 real time front-end computers are connected by reflective memories and 1 master computer receives data from the front-end computers through the DAQ network. The 2 ADCs and 1 DAC are synchronized to GPS antenna through the timing network. General network and EPICS data are connected by TCP/IP. After stable operation test of this small system, then we moved on constructing a larger scale digital system. A big room for the large scale test has been prepared in a new laboratory built at Kamioka, Higashi-Mouzmi area. This large scale test will be done by the end of next fiscal year. Whole system of this large test will be moved into the KAGAR mine and used as an actual KAGRA control system.

In parallel, simple standalone digital control systems using a single computer have been prepared for developing KAGRA subsystems. We started distributing the system in 2011 to several subsystems. One of the good example is drawn in the seismic isolation subsystem's section that local damping controls for the Pre-Isolator has been performed using the standalone system at Kashiwa campus. CLIO uses the same standalone system for the control of test mass. A test observation has been scheduled and performed to test productions of frame data and establish data pipeline with the digital system.

Many kinds of and many numbers of analog circuit will be used for KAGRA to make subsystems work. We are designing circuits for each purpose of each subsystem. For example, the total amount is not so many but some special design circuits are needed for Input Output Optics subsystem. Vibration Isolation subsystem requires a huge number of circuits because the numbers of sensor/actuator in seismic isolation system is huge. To cope with making such many analog electronics, we are discussing how to design, how to manufacture and how to

*7 Osamu Miyakawa, ICRR, The University of Tokyo

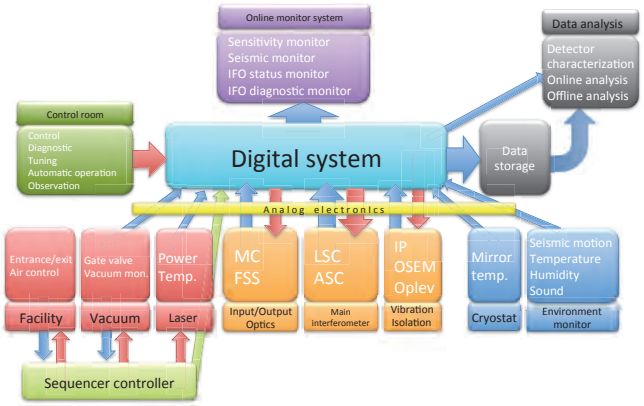

Fig. 8. Relations between digital system and other subsystems.

test all the circuits. Actually, noot a big number, but some of circuits have been already manufactured for KAGRA.

Analog circuits also offer an interface between subsystems and the digital system (see Fig.8). For example, we designed and manufactured analog filters for ADC/DAC to avoid aliases or images on digital input/output for 2500 channels. Currently we are designing a whitening filter to have a lower noise when the interferometer is switched into an observation mode.

Combined system with analog and digital will provide us not only to control the interferometer but also to collect/store all data from KAGRA, monitor/diagnostic systems as a flexible human interface, and a very good observation environment for gravitational wave detections.

Fabrication of cryostat and R&D for cryogenic items[8]

Outlines : The cryogenic mirror is one of the key features of KAGRA. In 2012, all four cryostats for KAGRA were assembled and cooling test was finished. Other R&D research was also in progress. Here, fabrication of KAGRA cryostat and R&D items are explained.

Fabrication of KAGRA cryostat : In this year, all four KAGRA cryostat were fabricated in Toshiba Keihin Product Operations. KAGRA cryostat consists of a vacuum chamber, radiation shields, and four cryocooler units.

The cryocooler units were fabricated in JECC Torisha. The cooling time is about 70 hours. The measured temperature is 3.5 K and 9 K at most without heat load and with 0.9 W, respectively. We also measured the vibration of the cryocooler units and found that the root mean square of the vibration is less than 0.1 μm. Thus, these cryocooler units satisfy our requirements.

The cooling test of KAGRA cryostat themselves was also conducted. It took about two weeks to cool the radiation shield. This is comparable with our expectation. The measured shield temperature is 10 K at most without heat load. When the heat load is 5 W (we expect that scattered light by cooled mirror is comparable with this value), it is 15 K at most. Since the mirror temperature is 20 K, it is not a serious problem.

Cryogenic duct : The radiation shields should have two large holes which are comparable with the cooled mirror diameter (220 mm) for the laser beam. The 300 K radiation invades the radiation shield through these holes. The cryogenic ducts with baffles are necessary to prevent the propagation of 300 K radiation. We proceeded with and fixed the design of the cryogenic duct. We take the scattered light by the cooling mirror into account. This light is absorbed by this duct.

Measurement of radiation shield vibration : The vibration of radiation shield could contaminate the signal of gravitational wave detector via heat link to cool the mirrors and scattered light. In order to evaluate this noise, we must measure the vibration of the radiation shield. We developed the cryogenic (horizontal) accelerometer. The vertical accelerometer was developed in University of Rome La Sapienza (Luca Naticchioni, Maurizio Perciballi, and Ettore Majorana visited to install and check their accelerometer. Their visit was supported by ELiTES). They were installed in KAGRA cryostat and measured vibration during the cooling test in Toshiba Keihin Product Operations. The analysis is in progress.

Black coating for shorter initial cooling time : The cryogenic payload (the cooled mirror is at the bottom of this payload) is in the radiation shield. It takes long time (2 months) to cool down the cryogenic payload because it is heavy and well isolated. In the initial phase of cooling, the radiation dominates the heat transfer. If the black coating (Diamond Like Carbon (DLC) or SolBalck) is deposited on the cryogenic payload, the radiation heat transfer is larger and the initial cooling time is shorter. The experiment to investigate this idea was in progress.

First of all, we prepared the copper spheres (30 mm in diameter) with and without black coating. These spheres are suspended in the evacuated hollow sphere cooled by liquid nitrogen. We confirmed that the sphere with black coating is cooled more rapidly and evaluate the emissivity of black coating as the function of temperature.

The larger aluminum sphere (100 mm in diameter) with and without black coating were also suspended in KAGRA cryostat during the cooling test and monitored the sphere temperature. The result is consistent with the experiment of small sphere.

The dummy payload (the size is half of the actual one) with black coating was suspended in the KAGRA cryostat during the cooling test. The measured result is consistent with the calculation based on the emissivity derived from the previous experiment.

Since the validity of the calculation is confirmed, we evaluated the initial cooling time of KAGRA cryogenic payload. In the case with and without the black coating, the initial cooling time is about one and two months, respectively. In short, the black coating makes the cooling time twice times shorter.

*[8] Kazuhiro Yamamoto, ICRR, The University of Tokyo

1/4 cryostat : Since the cryogenic payload is a complicate system, the test before the installation in Kamioka mine is necessary. The 1/4 cryostat for this test is under construction (JECC Torisha).

Sapphire fibers : The cooled mirror is suspended by four sapphire fibers. It must have nail head on the fiber end. Mol-Tech GmbH and IMPEX HighTech GmbH (both of them are German companies) delivered the sapphire fibers with nail head.

These sapphire fibers must have high thermal conductivity to extract heat from the mirror and high Q-values for small thermal noise. We measure these values. The thermal conductivity is slightly smaller than the required value although they are on the same order of magnitude. The measured Q-values are comparable with requirement. Although the quality improvement is necessary, the result is promising.

These experiments were conducted under the collaboration with Europe. Young researchers are exchanged for the experiments (Christian Schwarz and Gerd Hofmann visited ICRR from Jena. Their visit was supported by ELiTES.
Y. Sakakibara visited University of Glasgow and Friedrich-Schiller-Universitaet Jena.)

Fig. 9. Assembled KAGRA cryostat in Toshiba Keihin Product Operations

ELiTES activity[9]

Objective of ELiTES : The Researchers in Europe conducted the design study for Einstein Telescope (ET) from 2009 to 2011 under the Framework Programme 7 (FP7) by the European Commission. The ET project aims to the realization of a crucial research infrastructure in Europe: a third generation Gravitational Wave observatory. Some people from Japan participated in this study work. At the last ET workshop, this fruitfull collaboration between ET and LCGT (now, KAGRA) was desired to be continued because both detectors commonly utilize cryogenic mirror and underground. After a Conceptual Design Document has been released as the result of the design study, a new project, embedded in the ET framework, is now supported by the European Commission, still under FP7 (People, IRSES): ELiTES, focused on the development of the cryogenic technologies for KAGRA and ET.

Rome and NIKHEF group are familiar with anti-vibration system in frequency region at low frequency. Glasgow people promote highly sophisticated monolithic suspesnsion system with catalysis bonding technique. People in FS University in Jena developed original cryogenic measurement methods. Researchers in Sannio University develop optimized optical coating on main mirrors that can reduce thermal noise in the coating. These techniques developed in Europe are useful for KAGRA that has limited resources to develop from scratch. Contary to this, we in Japan have extensive experience on cryogenic laser interferometer. Therefore, the exchange of techniques especially by young researchers is expected to accelerates efficient R&Ds for successfull outcomes.

There are four working packages: WP: Mirror Thermal, WP: Suspension, WP3: Cooling and radiation shield, WP4: Organization. Glasgow University and FS University in Jena mainly contribute to WP1. Rome University handles WP2 with NIKHEF researchers that develop seismic anti-vibration system. Japanese group coordinates WP3.

Exchange researchers with European Universities and Institutes : Fig 10 shows researchers who were seconded under ELiTES program in 2012 (March 2012-February 2013). The main fund for Japanese researchers came form JSPS bilateral exchange program between Japan and Germany (Coordinator: Kentaro Somiya, TITECH) and two Ph.D students staying about two months were supported by Advanced Leading Graduate Course for Photon Science (ALPS) in the University of Tokyo. One of two Ph.D students participated collaborative research on measuring Q of fibers at cryogenic temperature and the other conducted a study of anti-vibration system.

The activity summarized by the coordinator of ELiTES (Michele Puntro) is shown in Fig. 11, which compares the achievement with the objective. The reason why all achievements are less than objectives is due to budget cut and a constraint on expenditure of PDs. We did not have enough fund in Japanese side in this financial year.

Meetings : Under ELiTES, each working package hold regular teleconferences and combined meetings for effective research promotion. Apart from these individual meetings, we have a general meeting based on face-to-face once in Europe and once in Japan. In this year, we have 2 days general meeting in Tokyo. On 3rd, October, the meeting started from the speech of the head of Sciencen Research Institutes Division, Research Promotion Bureau of the Ministry of Education, Culture, Sports, Science and Technology (MEXT) in the Tokyo house of Delegatgion of the Euroepan Union to Japan. We could strengthen an intimate relationship in this meeting (Fig. 12). On 4th, October, many research subjects were presented and discussed in Sanjo Kaikan hall in Hongo campus of the University of Tokyo. The general meeting held in Europe was combined to the meeting of ET project (ET workshop), which was held in Hannover in Germany in 2-5 December.

*[9] Kentaro Somiya, Tokyo Institute of Technology

Period	First Name of the research	Surname of the researcher	Gender	Type	Seconded FROM participant (Acronym)	Seconded FROM participant	Seconded TO participant	Seconded TO participant
1	Kazuhiro	Agatsuma	Male	ER	ICRR-UT	JP	IIGLASGC	UK
1	Alessandr	Bertolini	Male	ER	PHYSICS-UNIRM	IT	ICRR-UT	JP
1	Alessandr	Bertolini	Male	ER	FOM	NL	ICRR-UT	JP
1	Dan	Chen	Male	ESR	ICRR-UT	JP	FSU	DE
1	Andrea	Conte	Male	ESR	PHYSICS-UNIRM	IT	ICRR-UT	JP
1	Kieran	Craig	Male	ESR	UNIGLASGOW	UK	ICRR-UT	JP
1	Riccardo	De Salvo	Male	ER	UNISANNIO	IT	ICRR-UT	JP
1	Federico	Ferrini	Male	ER	EGO	IT	ICRR-UT	JP
1	Gilles	Hammond	Male	ER	UNIGLASGOW	UK	ICRR-UT	JP
1	Eric	Hennes	Male	ER	PHYSICS-UNIRM	IT	ICRR-UT	JP
1	Eric	Hennes	Male	ER	FOM	NL	ICRR-UT	JP
1	Eiichi	Hirose	Male	ER	ICRR-UT	JP	MPG	DE
1	Julius	Komma	Male	ESR	FSU	DE	ICRR-UT	JP
1	Kazuaki	Kuroda	Male	ER	ICRR-UT	JP	MPG	DE
1	Harald	Lueck	Male	ER	MPG	DE	ICRR-UT	JP
1	Ettore	Majorana	Male	ER	PHYSICS-UNIRM	IT	ICRR-UT	JP
1	Ettore	Majorana	Male	ER	PHYSICS-UNIRM	IT	ICRR-UT	JP
1	Nobuyuki	Matsumoto	Male	ESR	ICRR-UT	JP	FSU	DE
1	Yuta	Michimura	Male	ESR	ICRR-UT	JP	FSU	DE
1	Shinji	Miyoki	Male	ER	ICRR-UT	JP	SICS-UNI	IT
1	Peter	Murray	Male	ER	UNIGLASGOW	UK	ICRR-UT	JP
1	Luca	Naticchioni	Male	ESR	PHYSICS-UNIRM	IT	ICRR-UT	JP
1	Luca	Naticchioni	Male	ESR	PHYSICS-UNIRM	IT	ICRR-UT	JP
1	Luca	Naticchioni	Male	ESR	PHYSICS-UNIRM	IT	ICRR-UT	JP
1	Ronny	Nawrodt	Male	ER	FSU	DE	ICRR-UT	JP
1	Innocenzo	Pinto	Male	ER	UNISANNIO	IT	ICRR-UT	JP
1	Innocenzo	Pinto	Male	ER	UNISANNIO	IT	ICRR-UT	JP
1	Michele	Punturo	Male	ER	EGO	IT	ICRR-UT	JP
1	Fulvio	Ricci	Male	ER	PHYSICS-UNIRM	IT	ICRR-UT	JP
1	Nana	Saito	Male	ESR	ICRR-UT	JP	MPG	DE
1	Yusuke	Sakakibara	Male	ESR	ICRR-UT	JP	FSU	DE
1	Takanori	Sekiguchi	Male	ESR	ICRR-UT	JP	MPG	DE
1	Kazunori	Shibata	Male	ESR	ICRR-UT	JP	FSU	DE
1	Kentaro	Somiya	Male	ER	ICRR-UT	JP	FSU	DE
1	Shinichiro	Ueda	Male	ESR	ICRR-UT	JP	MPG	DE
1	Takafumi	Ushiba	Male	ESR	ICRR-UT	JP	MPG	DE
1	Jo	van den Br	Male	ER	FOM	NL	ICRR-UT	JP
1	Kazuhiro	Yamamoto	Male	ER	ICRR-UT	JP	FSU	DE

Fig. 10. Researchers list seconded each other under ELiTES program in 2012. Some of visiting researchers in Japan had extended stay for new financial year of Japan.

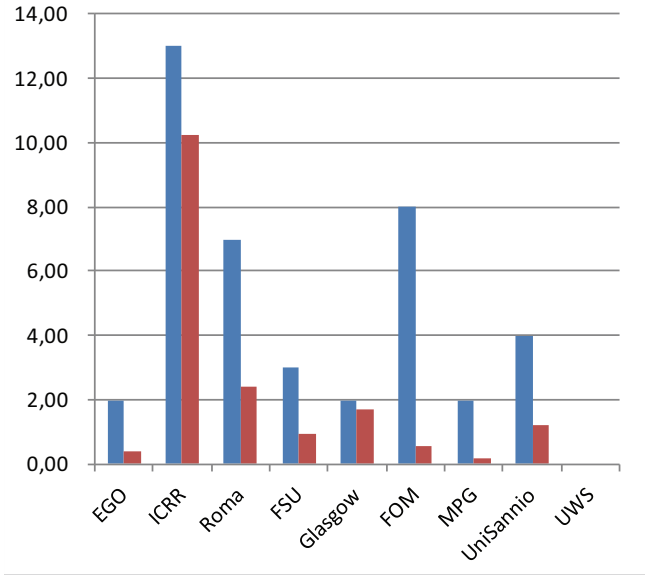

Fig. 11. Secondment status at the end of first year (28/2/2013) for seconded researchers among Universities and Institutes. Blue bar represents the total expected and the red is effective. The coordinate is in (man)×(month).

Fig. 12. 1st general meeting was held in Tokyo EU house on 3rd, October and in Hongo campus of the University of Tokyo on 4th, October.

CLIO Project

[Spokesperson : Masatake Ohashi]

ICRR, The Univ. of Tokyo, Kashiwa, Chiba 277-8582
In collaboration with members of: KEK, Tsukuba; Kyoto-U, Kyoto; ERI of UT, Tokyo

Overview

CLIO (Cryogenic Laser Interferometer Observatory) is a 100 m-baseline underground cryogenic interferometer at the Kamioka Mine. CLIO forms a bridge connecting the CLIK (7 m prototype cryogenic interferometer at Kashiwa campus) and the KAGRA (3 km cryogenic interferometer at Kamioka). The site of CLIO, near the Super-Kamiokande neutrino detector, is shown in Fig. 13. The tunnel was dug in 2002, and a strain meter for geophysics was installed in 2003 [1]. The construction of CLIO began in late 2003, and installation of the mode cleaner vacuum system was reported in the annual report (2003–2004). Four sets of cryostats and whole vacuum system were installed (annual report 2004–2005). We started the operation of CLIO in 2006 (annual report 2006).

The prime purpose of CLIO is to demonstrate mirror thermal noise reduction with cryogenic mirrors. We achieved the design sensitivity at the room temperature after noise hunting taken in 2008 (Annual report 2008) [2, 3]. After then, we started out cooling the mirrors and noise hunting with the mirrors under 20K had been done. We firstly observed the sensitivity improvement due to the mirror thermal noise reduction.

CLIO sensitivity curve with cooled mirrors (cryogenic sensitivity) and without cooling (300K sensitivity) are shown in Fig.16 with estimation curves of the mirror thermal noise. The 300K sensitivity and the cryogenic sensitivity were measured at 2008/11/5 and at 2010/03/20, respectively. When the cryogenic sensitivity was measured, two front mirrors were cooled and the rest of two end mirrors were at the room temperature. Temperature of the front mirrors were 17K and 18K. Modifications possibly affecting the sensitivity at the cryogenic sensitivity measurement are exchange of final suspension wires and addition of heat link wires to the suspension systems. Cooling the mirror took about 250 hours and vacuum pressure was better than 10^{-4}Pa for both sensitivity measurements.

The noise floor level of the cryogenic sensitivity from 90Hz to 240Hz is below the 300K sensitivity. Observation range for GWs from neutron star binary coalescence was also improved to 159kpc from 148kpc for the optimum direction. This is the first observation of sensitivity improvement by the cryogenic mirrors. The noise floor at 165Hz was reduced to

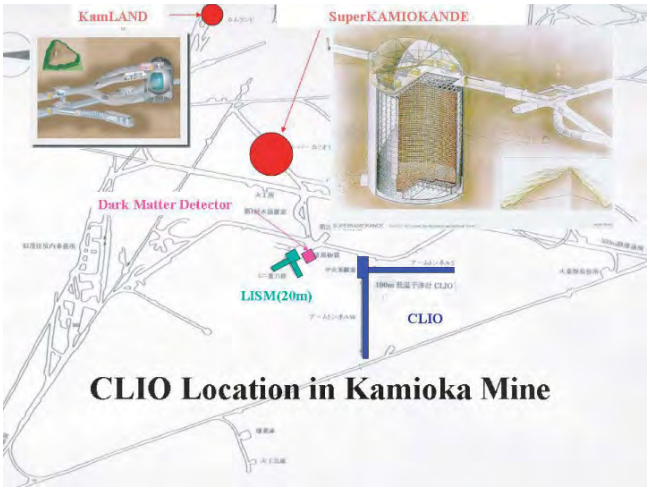

Fig. 13. Location of the CLIO interferometer.

$2.2 \times 10^{-19}\,\mathrm{m}/\sqrt{\mathrm{Hz}}$ from $3.1 \times 10^{-19}\,\mathrm{m}/\sqrt{\mathrm{Hz}}$ after cooling the front mirrors. Amount of this noise floor reduction is consistent with the estimation of mirror thermal noise reduction due to cooling. This achievement has been published in 2012 [4].

Fig. 14. Overview of the CLIO interferometer.

Fig. 15. A sapphire mirror and cryogenic suspension system

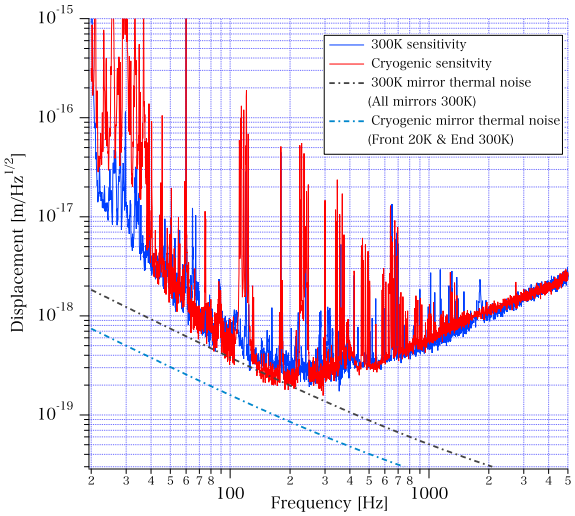

Fig. 16. Comparison of CLIO sensitivity curves. 300K sensitivity (solid blue line) and Cryogenic sensitivity (solid red line) show CLIO sensitivity curves without cooling mirrors measured at 2008/11/05 and with front mirrors under 20K measured at 2010/03/20, respectively. 300K mirror thermal noise (dot dash gray line) and Cryogenic mirror thermal noise (dot dash blue line) show estimation curve of mirror thermal noise corresponding to the each sensitivity measurements.

Detecter characterization using a digital control system

A real time control system using computers (digital control system) has been implemented into CLIO to test basic performances of the digital system for a lock acquisition, calibration and noise performance etc. of the interferometer. We performed a short term observation using this digital controls system. The purpose of this observation was to establish a data pipeline for gravitational wave data analysis in the future interferometer like KAGRA. This system is not only used for control but also for DAQ (data acquisition) system since the control signals is equivalent to the sensitivity signal in the computer.

We obtained 13 hours frame data including 2 hours continuos lock. Raw frame data from CLIO was stored into a data storage and it was calibrated into displacement/strain sensitivity using a measured calibration transfer function in the frequency domain and results are shown on a web page every 16 seconds. We also re-produced time domain transfer function in time domain and the raw frame data was calibrated into strain sensitivity in time domain by off-line data analysis. Some detecter characterization data like a laser power or a seismic motion was stored as frame data at the same time to define noise sources in the sensitivity of interferometer. This

short observation is just a first step to establish whole data pipe line. We will continue observations with better sensitivity than that obtained in this observation since the noise is currently limited by ADC and DAC. This characterizing method developed in CLIO will be used for KAGRA in the future.

Bibliography

[1] S. Takemoto, *et al.*, Journal of Geodynamics **41** (2006) 23.

[2] S. Miyoki, *et al.*, Journal of Physics: Conference Series **203** (2010) 012075.

[3] T. Uchiyama and S. Miyoki, "Experimental Demonstration of Cryogenic Mirror Technique - Achievements of CLIO-", J. Cryo. Super. Soc. Jpn., **46** (2011) 392-399.

[4] Takashi Uchiyama, Shinji Miyoki, Souichi Telada, Kazuhiro Yamamoto, Masatake Ohashi, Kazuhiro Agatsuma, Koji Arai, Masa-Katsu Fujimoto, Tomiyoshi Haruyama, Seiji Kawamura, Osamu Miyakawa, Naoko Ohishi, Takanori Saito, Takakazu Shintomi, Toshikazu Suzuki, Ryutaro Takahashi, Daisuke Tatsumi, "Reduction of thermal fluctuations in a cryogenic laser interferometric gravitational wave detector", Phys. Rev. Lett. **108**, 141101 (2012) [5 pages].

Observational Cosmology Group

[Spokesperson : Yoshiaki Ono]

ICRR, The Univ. of Tokyo, Kashiwa, Chiba 277-8582

The Abundance of Star-forming Galaxies in the Redshift Range 8.5 – 12: New Results from the 2012 Hubble Ultra Deep Field Campaign [1]

In collaboration with the members of California Institute of Technology, University of Edinburgh, University of Arizona, The University of Tokyo, IPMU, Space Telescope Science Institute, University of California Los Angeles, and Institut d'Astrophysique de Paris.

We present the results of the deepest search to date for star-forming galaxies beyond a redshift $z \simeq 8.5$ utilizing a new sequence of near-infrared Wide Field Camera 3 images of the Hubble Ultra Deep Field. This 'UDF12' campaign completed in September 2012 doubles the earlier exposures with WFC3/IR in this field and quadruples the exposure in the key F105W filter used to locate such distant galaxies. Combined with additional imaging in the F140W filter, the fidelity of high redshift candidates is greatly improved. Using spectral energy distribution fitting techniques on objects selected from a deep multi-band near-infrared stack we find 7 promising $z > 8.5$ candidates. As none of the previously claimed UDF candidates with $8.5 < z < 10$ is confirmed by our deeper multi-band imaging, our campaign has transformed the measured abundance of galaxies in this redshift range. Although we recover the candidate UDFj-39546284 (previously proposed at z=10.3), it is undetected in the newly added F140W image, implying it lies at z=11.9 or is an intense emission line galaxy at $z \simeq 2.4$. Although no physically-plausible model can explain the required line intensity given the lack of Lyman α or broad-band UV signal, without an infrared spectrum we cannot rule out an exotic interloper. Regardless, our robust $z \simeq 8.5 - 10$ sample demonstrates a luminosity density that continues the smooth decline observed over $6 < z < 8$ (Fig.17). Such continuity has important implications for models of cosmic reionization and future searches for $z > 10$ galaxies with JWST.

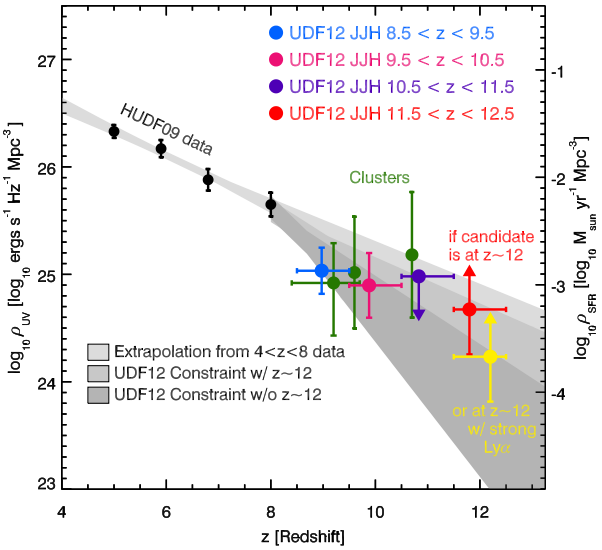

Fig. 17. Luminosity and star formation rate (SFR) density versus redshift inferred from UDF12. Reddening corrected luminosity densities are shown from the literature over the redshift range $5 < z < 8$ (black points). Extrapolating their evolution to redshift $z \sim 13$ provides the lightest gray area. Claimed estimates from the CLASH detections (green points) are shown. Luminosity densities are shown for the four $8.5 \lesssim z \lesssim 9.5$ sources (blue data point) and the two $9.5 \lesssim z \lesssim 10.5$ objects (magenta point). The non-detection at $10.5 \lesssim z \lesssim 11.5$ provides an upper limit at $z \approx 10.8$ (purple limit). The single $z \sim 12$ source provides a conservative lower limit at $z \approx 11.8$ (red point). If this source has strong Lyα emission, the luminosity density limit becomes the yellow point. Overlapping maximum likelihood 68% confidence regions on a linear trend in the luminosity density with redshift from $z \sim 8$ are shown with (medium gray) and without (dark gray) the $z \sim 12$ object. This figure is reproduced by permission of the AAS.

Bibliography

[1] Ellis, R., et al. 2013, Astrophys. J., 763, L7

Gas Motion Study of Lyα Emitters at $z \sim 2$ Using FUV and Optical Spectral Lines [2]

In collaboration with the members of The University of Tokyo, IPMU, Observatories of the Carnegie Institution of Washington, and Space Telescope Science Institute.

We present the results of Magellan/MMIRS and Keck /NIRSPEC spectroscopy for five Lyα emitters (LAEs) at $z \simeq 2.2$

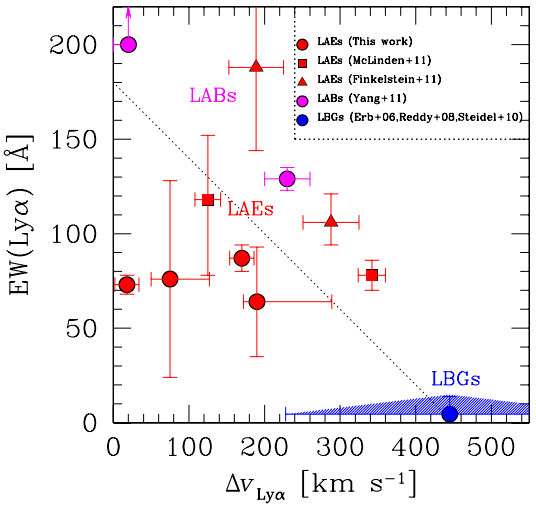

Fig. 18. Rest-frame EW(Lyα) plotted against $\Delta v_{\rm Ly\alpha}$. The red circles are our LAEs. The red square and the red triangle show the LAEs taken from the literature. The blue symbol indicates the average of 41 LBGs, with the error bars corresponding to the 68 percentiles of the $\Delta v_{\rm Ly\alpha}$ distribution and the EW distribution. The magenta circles denote the LABs. The dotted line is the best-fit linear function to all the data points. This figure is reproduced by permission of the AAS.

for which high-resolution FUV spectra from Magellan/MagE are available. We detect nebular emission lines including Hα on the individual basis and low-ionization interstellar (LIS) absorption lines in a stacked FUV spectrum, and measure average offset velocities of the Lyα line, $\Delta v_{\rm Ly\alpha}$, and LIS absorption lines, $\Delta v_{\rm abs}$, with respect to the systemic velocity defined by the nebular lines. For a sample of eight $z\sim 2-3$ LAEs without AGN from our study and the literature, we obtain $\Delta v_{\rm Ly\alpha} = 175\pm 35$ km s^{-1}, which is significantly smaller than that of Lyman-break Galaxies (LBGs), $\Delta v_{\rm Ly\alpha} \simeq 400$ km s^{-1}. The stacked FUV spectrum gives $\Delta v_{\rm abs} = -179\pm 73$ km s^{-1}, comparable to that of LBGs. These positive $\Delta v_{\rm Ly\alpha}$ and negative $\Delta v_{\rm abs}$ suggest that LAEs also have outflows. In contrast to LBGs, however, the LAEs' $\Delta v_{\rm Ly\alpha}$ is as small as $|\Delta v_{\rm abs}|$, suggesting low neutral hydrogen column densities. Such a low column density with a small number of resonant scattering may cause the observed strong Lyα emission of LAEs. We find an anti-correlation between Lyα equivalent width (EW) and $\Delta v_{\rm Ly\alpha}$ in a compilation of LAE and LBG samples (Fig.18). Although its physical origin is not clear, this anti-correlation result appears to challenge the hypothesis that a strong outflow, by means of a reduced number of resonant scattering, produces a large EW. If LAEs at $z>6$ have similarly small $\Delta v_{\rm Ly\alpha}$ values, constraints on the reionization history derived from the Lyα transmissivity may need to be revised.

Bibliography

[2] Hashimoto, T., Ouchi, M., et al. 2013, Astrophys. J., 765, 70

The First Systematic Survey for Lyα Emitters at $z=7.3$ with Red-sensitive Subaru/Suprime-Cam [3]

In collaboration with the members of The Graduate University for Advanced Studies, National Astronomical Observatory of Japan, Kyoto University, The University of Tokyo, and IPMU.

We have performed deep imaging surveys for Lyman α emitters (LAEs) at redshift ~ 7.3 in two blank fields, the Subaru Deep Field (SDF) and the Subaru/XMM-Newton Deep survey Field (SXDF), using the Subaru/Suprime-Cam equipped with new red-sensitive CCDs and a new narrow-band filter, NB1006 ($\lambda_c = 10052$Å, FWHM $\Delta\lambda = 214$Å). We identified four objects as LAE candidates that exhibit luminosity excess in NB1006. By carrying out deep follow-up spectroscopy for three of them using Subaru/FOCAS and Keck/DEIMOS, a definitively asymmetric emission line is detected for one of them, SXDF-NB1006-2. Assuming this line is Lyα, this object is a LAE at $z=7.215$ which has luminosity of $1.2^{+1.5}_{-0.6}\times 10^{43}$ erg s^{-1} and a weighted skewness $S_\omega = 4.90\pm 0.86$. Another object, SDF-NB1006-2, shows variable photometry and is thus probably a quasar (QSO) or an active galactic nucleus (AGN). It shows an asymmetric emission line at 10076Å which may be due to either Lyα at $z=7.288$ or [O II] at $z=1.703$. The third object, SDF-NB1006-1, is likely a galaxy with temporal luminosity enhancement associated with a supernova explosion, as the brightness of this object varies between the observed epochs. Its spectrum does not show any emission lines. The inferred decrease in the number density of LAEs toward higher redshift is $n^{z=7.3}_{\rm Ly\alpha}/n^{z=5.7}_{\rm Ly\alpha} = 0.05^{+0.11}_{-0.05}$ from $z=5.7$ to 7.3 down to $L^{\rm Ly\alpha} = 1.0\times 10^{43}$ erg s^{-1} (Fig.19). The present result is consistent with the interpretation in previous studies that the neutral hydrogen fraction is rapidly increasing from $z=5.7$ to 7.3.

Bibliography

[3] Shibuya, T., et al. 2012 Astrophys. J., 752, 114

Diffuse Lyα haloes around Lyα emitters at $z=3$: do dark matter distributions determine the Lyα spatial extents? [4]

In collaboration with the members of California Institute of Technology, Tohoku University, The University of Tokyo, IPMU, and University of Tsukuba.

Using stacks of Lyα images of 2128 Lyα emitters (LAEs) and 24 protocluster UV-selected galaxies (LBGs) at $z=3.1$, we examine the surface brightness profiles of Lyα haloes around high-z galaxies as a function of environment and UV luminosity. We find that the slopes of the Lyα radial profiles become flatter as the Mpc-scale LAE surface densities increase, but they are almost independent of the central UV luminosities. The characteristic exponential scale lengths of the Lyα haloes appear to be proportional to the square of the LAE surface densities (Fig.20). Including the diffuse, extended Lyα haloes, the rest-frame Lyα equivalent width of the LAEs in the densest regions approaches $EW_0 \sim 200$Å, the maximum value expected for young ($< 10^7$ yr) galaxies. This suggests

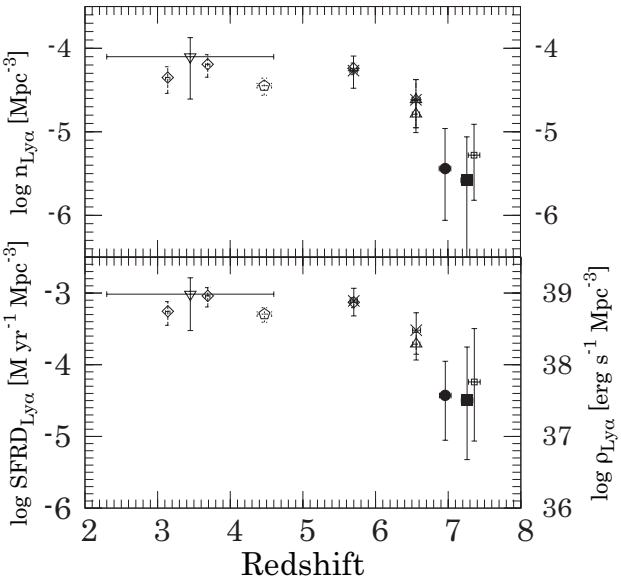

Fig. 19. Number density $n_{\mathrm{Ly}\alpha}$, and star formation rate density $\mathrm{SFRD}_{\mathrm{Ly}\alpha}$ of the LAE at $z = 7.215$, SXDF-NB1006-2 confirmed spectroscopically in this study (filled square) and those at $2.3 \leq z \leq 7$ from the spectroscopic studies down to $L^{\mathrm{Ly}\alpha} = 1.0 \times 10^{43}$ erg s^{-1}. The filled circles are those of the LAE at $z = 6.96$. The crosses show the densities at $z = 5.7$ and 6.6 in the SDF. Densities at $2.3 \leq z \leq 4.5$ and $z \sim 4.5$ are calculated using the best-fit Lyα Schechter luminosity functions (LFs) from the literatures. Also, densities at $z = 3.1, 3.7, 5.7$ (diamonds) and 6.6 (triangles) in the ~ 1.0 deg^2 of SXDF are calculated using the best-fit Lyα Schechter LFs from the literature. Each horizontal error bar shows the redshift range of each survey. The vertical error bars at $z = 5.7, 6.6, 7$ and 7.3 include both cosmic variance and Poissonian errors for small number statistics. We correct for the detection completeness of the $z = 7.3$ LAE survey. If SXDF-NB1006-1 is a real LAE at $z = 7.3$ with a brighter $L^{\mathrm{Ly}\alpha}$ than one of SXDF-NB1006-2, the number and SFR densities of SXDF-NB1006-2 becomes small the open square slightly shifted in the redshift direction for clarification. This figure is reproduced by permission of the AAS.

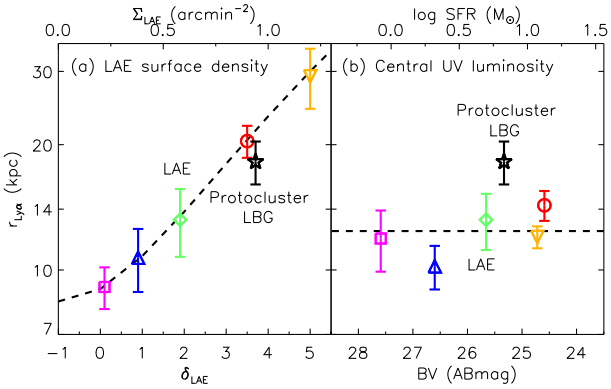

Fig. 20. Lyα scale length as a function of (a) LAE surface density and (b) central UV luminosity based on BV magnitude measured with $2''$ diameter aperture photometry. The dashed lines are $r = 0.6 \times (1 + \delta_{\mathrm{LAE}})^2 + 8.4$ kpc (left) and $r = 12.4$ kpc (right). These trends suggest that the spatial extents of the Lyα haloes are determined by the surrounding Mpc-scale environment rather than the central UV luminosities. The error bars represent 1-σ uncertainties of the exponential profile fitting. The star-formation rate (SFR) is converted from the BV magnitude without dust attenuation correction. This figure is reproduced by permission of the RAS.

that Lyα photons formed via shock compression by gas outflows or cooling radiation by gravitational gas inflows may partly contribute to illuminate the Lyα haloes; however, most of their Lyα luminosity can be explained by photo-ionization by ionizing photons or scattering of Lyα photons produced in H II regions in and around the central galaxies. Regardless of the source of Lyα photons, if the Lyα haloes trace the overall gaseous structure following the dark matter distributions, it is not surprising that the Lyα spatial extents depend more strongly on the surrounding Mpc-scale environment than on the activities of the central galaxies.

Bibliography

[4] Matsuda, Y., et al. 2012 Monthly Notices Roy. Astron. Soc., 425, 878–883

Intrinsic Shape of Star-forming BzK Galaxies. II. Rest-frame Ultraviolet and Optical Structures in GOODS-South and SXDS [5]

In collaboration with the members of The University of Tokyo, Kyoto University, and National Astronomical Observatory of Japan.

We study statistical intrinsic shape of star-forming BzK galaxies (sBzK galaxies) at $z \sim 2$ in both rest-frame UV and rest-frame optical wavelengths. The sBzK galaxies are selected down to $K_{AB} = 24.0$ mag in the Great Observatories Origins Deep Survey-South (GOODS-S) and Subaru-XMM Deep Survey (SXDS) fields, where high-resolution images from *Hubble Space Telescope* are publicly available. 57% (583) of all 1028 galaxies in GOODS-S show a single component in the Advanced Camera for Survey (ACS)/F850LP image. As Wide Field Camera (WFC3)/F160W images cover only some part of GOODS-S and SXDS, 724/1028 and 2500/29835 sBzK galaxies in the GOODS-S and SXDS have the WFC3 coverage. 86% (626) and 82% (2044) of the sBzK galaxies in WFC3/F160W images appear as a single component in the GOODS-S and SXDS, respectively. Larger fraction of single-component objects in F850LP images represents multiple star-forming regions in galaxies, while they are not so obvious in the F160W image which appears smoother. Most of the single-component sBzK galaxies show Sérsic indices of $n = 0.5 - 2.5$, in agreement with those of local disk galaxies. Their effective radii are $1.0 - 3.0$ kpc and $1.5 - 4.0$ kpc in F850LP and F160W images, respectively, regardless of the observed fields. Stellar surface mass density of the sBzK galaxies is also comparable to that of the local disk galaxies. However, the intrinsic shape of sBzK galaxies is not a round disk as seen in the local disk galaxies. By comparing apparent axial ratio (b/a) distributions of the sBzK galaxies with those by assuming tri-axial model with axes $A > B > C$, we found their intrinsic face-on B/A ratios peak at $B/A = 0.70$ and $B/A = 0.77 - 0.79$ in the rest-frame UV and optical, respectively and are statistically more bar-like than that of the local disk galaxies. The intrinsic edge-on C/A ratios in both rest-frame UV and optical wavelengths peak at 0.26, which is slightly larger than that of the local disk galaxies. Possible origins of this bar-like structure are bar instability, galaxy interaction, or continuous minor mergers. Study of galaxy

structure evolution in cosmological simulations is desirable to examine the most likely scenario.

Bibliography

[5] Yuma, S., et al. 2012, Astrophys. J., 761, 19

Primary Cosmic Ray Group

[Spokesperson : Hiroko Miyahara]
ICRR, The Univ. of Tokyo, Kashiwa, Chiba 277-8582

Tracing the impacts of periodic GCR enhancements during the Maunder Minimum [1]

In collaboration with the members of Univ. of Tokyo and Yamagata Univ.

Annually measured beryllium-10 contents in ice cores have suggested that heliospheric environment could have been changed at the Maunder minimum (AD1645-1715) due to the extremely weakened solar magnetic activity. Beryllium-10 data show characteristic variations possibly associated with the drift effect of GCRs in the heliosphere, showing a component related to the 22-year solar magnetic polarity reversals (Fig.21). The beryllium-10 flux reveals significant enhancements at solar minima but only at qA negative phases. The excesses of the beryllium-10 flux at qA negative phases to the mean of maximal fluxes of neighboring two qA positive cycles are 40, 39, 26 and 39 percent, respectively. The mean duration between the spikes is 28 years. Annually measured carbon-14 contents in tree rings have revealed that the 11-year solar cycles were extended to about 14 years during the Maunder Minimum. The above period of 28 years is therefore consistent with the Hale period during that time. The drift effect in the inner heliosphere is suggested to be able to cause 15-20 percent enhancement, whereas the observed beryllium-10 enhancements are up to 40 percent. We have discussed the possible additional impact from heliosheath, where heliospheric current sheet is accumulated and hence GCR particles may be effectively drifted across the stacked magnetic sectors, and have suggested that it may explain the additional 15-20 percent of enhancements (Fig.22). It would be important to further investigate the accumulation pattern of the heliospheric current sheet in the heliosheath to understand the GCR spikes at the Maunder Minimum. The above enhancements of GCR flux provide unique opportunity to trace the GCR impact on global climate. It is suggested that the response of cloud activities to GCRs are localized, and their impacts are propagated through atmospheric circulations. It is therefore very important to reveal the spatial distribution of the responses to shed light on the GCR impact on climate system. We are now conducting the measurements of stable isotopes in tree rings so that we can reveal the regional responses to GCRs mainly in the Asian region.

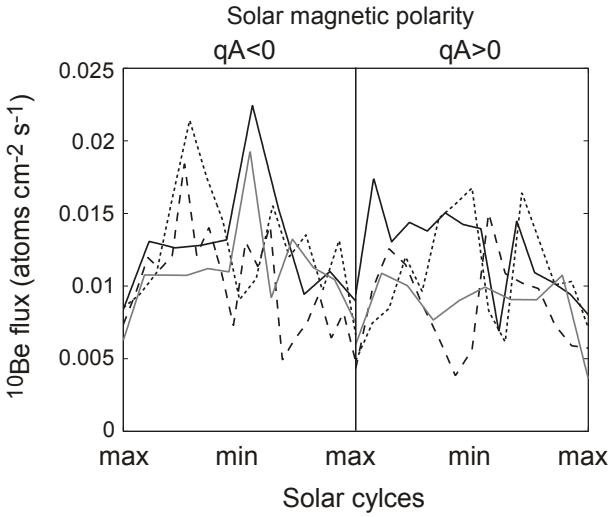

Fig. 21. Time profiles of 10Be flux (Berggren et al., 2009) superposed for qA negative and qA positive solar cycles, around the Maunder Minimum. Note that the plotted time series are tied each other by solar cycle maxima.

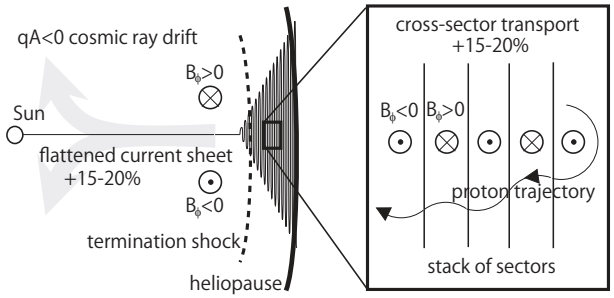

Fig. 22. Vertical cross sectional view of the heliosphere. The termination shock and heliopause are shown with a dashed curve and solid curve, respectively. The percentages given are the increase in cosmic ray intensity during solar minimum of qA negative phase against that of qA positive (The polarity of magnetic field lines and the cosmic ray paths indicated by gray arrows are for qA¡0 phase). The cross-sector transport may cause 15-20 percent increase, while the flattened current sheet is suggested to cause 15-20 percent increase during the qA negative phase.

Bibliography

[1] R. Kataoka, H. Miyahara, et al., Anomalous 10Be spikes during the Maunder Minimum: Possible evidence for extreme space weather in the heliosphere, Space Weather **10** (2012), doi:10.1029/2012SW000835.

Millennial scale sun-climate connection during the last 70,000 years [2]

In collaboration with the members of Univ. of Tokyo and The Univ. of Edinburgh.

Millennial scale climate oscillations are known to correlate well with solar variations with 1000 and 2000 year periods through the current interglacier period, while the records of ice-rafted debris reconstructed for the last glacier period

had been known to show g1500-yearh cycles, for which identifiable external forcing was absent. We therefore re-examined the ice core chronology and conducted a Monte Carlo Simulation. As a result, it turned out that the g1500-yearh cycles were actually 1000 and 2000 year cycles, which are consistent with solar cycles. We find it very interesting that the amplitude of the 1000 and 2000 year climate cycles are much larger at the glacier period, compared to the interglacier period. It may be providing some clues on the processes of solar influence on climate system.

Bibliography

[2] S.P. Obrochta, H. Miyahara, et al., A re-examination of evidence for the North Atlantic g1500-year cycleh at Site 609, Quaternary Science Reviews **55** (2012), doi:10.1016/j.quascirev.2012.08.008.

Theory Group

Overview

We have theoretically studied particle physics (mainly particle physics phenomenology) and astroparticle physics (mainly particle cosmology).

2012 was one of the biggest years for the particle physics phenomenology and the cosmology. The CERN has reported the detection of a Higgs-like scalar boson and also the Planck satellite has released the precise data of the cosmic microwave background (CMB). Although these experiments make us confirm the standard model of particle physics and Big bang Universe, they also give us many implications for extensions of the standard scenarios.

The supersymmetric (SUSY) extension of the standard model (SM) in the particle physics is considered to be one of the most promising models beyond the standard model. It solves the naturalness problem for the Higgs boson mass term in the standard model, and it is also compatible with the grand unified theories (GUTs). Our group has been studying phenomenological and cosmological aspects of the SUSY models.

Recent cosmological observations including the Planck data determine precisely the mean densities of matter and baryon in the Universe, and existence of non-baryonic dark matter is established. Weakly interacting massive particles (WIMPs) are considered to be good candidates of the dark matter. They act as the cold dark matter in the structure formation of the universe. Our group has been studying model building for dark matter and detectability in direct and indirect search experiments.

For understanding of the early universe, a role of the elementary particle physics is crucial. Recent progress in the particle physics such as grand unification theories and supersymmetry leads us to a more deeper insight into the fundamental aspects of the early universe. In the inflationary universe, the quantum fluctuations of the scalar field which drives the inflation become the density fluctuations and lead to formation of the structure observed in the present universe. On the other hand cosmology and astrophysics are used to test new theories in particle physics. Such particle cosmology is one of main subjects of our group.

Big Bang Nucleosynthesis (BBN) is one of the most important subjects in modern cosmology. Predicted abundances of the light elements are very sensitive to the cosmological scenario. On the other hand, physics beyond the standard model predicts the new particles which would have existed at the BBN epoch. Such particles may spoil the success of BBN, which leads to constraints on the new particles and the particle physics models.

The grand unified theories (GUT) predict that our universe undergoes several vacuum phase transitions. In the course of phase transitions topological defects (monopoles, cosmic strings and domain walls) are generally produced depending on symmetries of the vacua. Our group has studied evolution of various topological defects.

Particle Phenomenology

[Spokesperson : M. Ibe]

ICRR, The Univ. of Tokyo, Kashiwa, Chiba 277-8582

Higgs Mass in Supersymmetric Standard Model

• A 125 GeV Higgs Boson Mass and Gravitino Dark Matter in R-invariant Direct Gauge Mediation

In collaboration with the member of IPMU

We discuss the SM-like Higgs boson mass in the MSSM in an R-invariant direct gauge mediation model with the gravitino mass in the O(1) keV range. The gravitino dark matter scenario in this mass range is a good candidate for a slightly warm dark matter. We show that the Higgs boson mass around 125 GeV suggested by the ATLAS and CMS experiments can be easily achieved in the direct gauge mediation model with this gravitino mass range [1].

• The Lightest Higgs Boson Mass in the MSSM with Strongly Interacting Spectators

In collaboration with the members of IPMU

We propose a new mechanism for producing a Higgs boson mass near 125 GeV within the MSSM. By coupling the MSSM Higgs boson to a set of strongly interacting fields, large corrections to the Higgs quartic coupling are induced. Although the Higgs doublets do not participate in the strong dynamics, they feel the effects of the strongly coupled sector via (semi-)perturbative interactions. These same strong dynamics are also capable of generating the μ-term. Additionally, this strong sector is in the conformal window, which drives the couplings to an infrared fixed point and naturally generates model parameters of the appropriate size [2].

• Heavy Squarks and Light Sleptons in Gauge Mediation From the viewpoint of 125 GeV Higgs Boson and Muon $g-2$

In collaboration with the members of IPMU

In the framework of gauge mediation models, we investigate scenarios with heavy squarks and light sleptons, motivated by the recent discovery of the Higgs boson and the deviation of the muon anomalous magnetic moment $(g-2)$ from the SM prediction. We show that only models with a messenger multiplet in the adjoint representation of $SU(5)$ GUT gauge group are the unique possibility that sleptons are light enough to explain the muon $g-2$ in the minimal setup. We also show that, if there is an additional source of the Higgs soft masses, the muon $g-2$ can be explained with messenger multiples in the fundamental representation of $SU(5)$ with the help of the light higgsino. Some phenomenological aspects of these models are also discussed [3].

• Universality in Pure Gravity Mediation

In collaboration with the member of IPMU and Michigan University

If low energy supersymmetry is realized in nature, the apparent discovery of a Higgs boson with mass around 125 GeV points to a supersymmetric mass spectrum in the TeV or multi-TeV range. Multi-TeV scalar masses are a necessary component of supersymmetric models with pure gravity mediation or in any model with strong moduli stabilization. Here, we show that full scalar mass universality remains viable as long as the ratio of Higgs vevs, tan beta is relatively small ($\lesssim 2.5$). We discuss in detail the low energy (observable) consequences of these models [4].

• Focus point gauge mediation in product group unification

In collaboration with the member of IPMU and DESY

In certain models of gauge-mediated supersymmetry breaking with messenger fields in incomplete GUT multiplets, the radiative corrections to the Higgs potential cancel out during renormalization group running. This allows for relatively heavy superpartners and for a 125 GeV Higgs while the fine-tuning remains modest. In this paper, we show that such gauge mediation models with "focus point" behaviour can be naturally embedded into a model of $SU(5) \times U(3)$ product group unification [5].

• Muon $g-2$ and 125 GeV Higgs in Split-Family Supersymmetry

In collaboration with the member of IPMU

We discuss the minimal supersymmetric standard model with "split-family" spectrum where the sfermions in the first two generations are in the hundreds GeV to a TeV range while the sfermions in the third generation are in the range of tens TeV. With the split-family spectrum, the deviation of the muon $g-2$ and the observed Higgs boson mass are explained simultaneously. It is predicted that the gluino and the squarks in the first two generations are within the reach of the LHC experiments in most favored parameter space for the universal gaugino mass, which can be tested by searching for events with missing transverse energy or events with stable charged massive particles. We also point out that the split-family scenario can be consistent with the focus point scenario for the non-universal gaugino masses where the required mu-term is in the hundreds GeV range [6].

Bibliography

[1] M. Ibe and R. Sato, Phys. Lett. B **717**, 197 (2012) [arXiv:1204.3499 [hep-ph]].

[2] J. L. Evans, M. Ibe and T. T. Yanagida, Phys. Rev. D **86**, 015017 (2012) [arXiv:1204.6085 [hep-ph]].

[3] M. Ibe, S. Matsumoto, T. T. Yanagida and N. Yokozaki, JHEP **1303**, 078 (2013) [arXiv:1210.3122 [hep-ph]].

[4] J. L. Evans, M. Ibe, K. A. Olive and T. T. Yanagida, arXiv:1302.5346 [hep-ph].

[5] F. Brümmer, M. Ibe and T. T. Yanagida, arXiv:1303.1622 [hep-ph].

[6] M. Ibe, T. T. Yanagida and N. Yokozaki, arXiv:1303.6995 [hep-ph].

Collider Phenomenology of Supersymmetric Standard Model

• Pure Gravity Mediation of Supersymmetry Breaking at the LHC

In collaboration with the members of IPMU

Supersymmetric theories which can allow for a 125 GeV Higgs mass and also solve the naturalness and susy flavor problems now require a fair degree of complexity. Here we consider the simplest possibility for supersymmetry near the weak scale, but with the requirement of naturalness dropped. In "pure gravity mediation", all supersymmetric particles except for the gauginos lie at tens to thousands of TeV, with the gauginos obtaining loop suppressed masses automatically by anomaly mediation and higgsino threshold corrections. The gauginos are the lightest superpartners, and we investigate the current collider constraints on their masses, as well as the future reach of the LHC. We consider gluino pair production with a jets + missing energy signature, as well as events with disappearing charged tracks caused by charged winos decaying into their neutral partners. We show that presently, gluino masses less than about 1 TeV and wino masses less than about 300 GeV are excluded, and that the 14 TeV LHC can probe gluino masses up to about 2 TeV and wino masses up to 1 TeV [1].

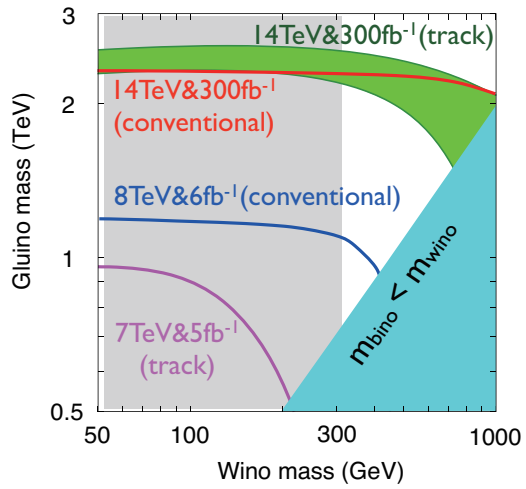

Fig. 23. Expected bounds on the gluino and wino masses obtained with $300 fb^{-1}$ of data at 14 TeV running. In all cases, the gluino is assumed to decay into two light quarks and a charged/neutral wino.

• Mass Splitting between Charged and Neutral Winos at Two-Loop Level

In collaboration with the members of IPMU

The recent result of the higgs search at the LHC experiment has lead to more attention to the supersymmetric standard models with heavy sfermions. Among them, the models with the almost pure wino being the lightest supersymmetric particle (LSP) have been widely discussed due to their success in providing a consistent dark matter candidate. The notable phenomenological feature of the wino LSP is the degeneracy with its charged $SU(2)_L$ partner (the charged wino) in mass. The tiny mass splitting makes the charged wino long-lived, which allows us to detect the wino production at the LHC experiment by searching for the disappearing charged tracks inside the detectors. Since the reach of the experiment is sensitive to the mass splitting, it is mandatory to estimate it very precisely. We therefore perform a full calculation of the mass splitting at two-loop level, and find that the splitting is reduced by a few MeV compared to the one-loop calculation. This reduction leads to about a 30% longer lifetime of the charged wino, with which the current constraint on the wino mass by the ATLAS experiment is improved by about 10%. The recent result of the Higgs search at the LHC experiment has lead to more attention to the supersymmetric standard models with heavy sfermions. Among them, the models with the almost pure wino being the lightest supersymmetric particle (LSP) have been widely discussed due to their success in providing a consistent dark matter candidate. The notable phenomenological feature of the wino LSP is the degeneracy with its charged $SU(2)_L$ partner (the charged wino) in mass. The tiny mass splitting makes the charged wino long-lived, which allows us to detect the wino production at the LHC experiment by searching for the disappearing charged tracks inside the detectors. Since the reach of the experiment is sensitive to the mass splitting, it is mandatory to estimate it very precisely. We therefore perform a full calculation of the mass splitting at two-loop level, and find that the splitting is reduced by a few MeV compared to the one-loop calculation. This reduction leads to about a 10-30% longer lifetime of the charged wino, with which the current constraint on the wino mass by the ATLAS experiment is improved by about 10% [2].

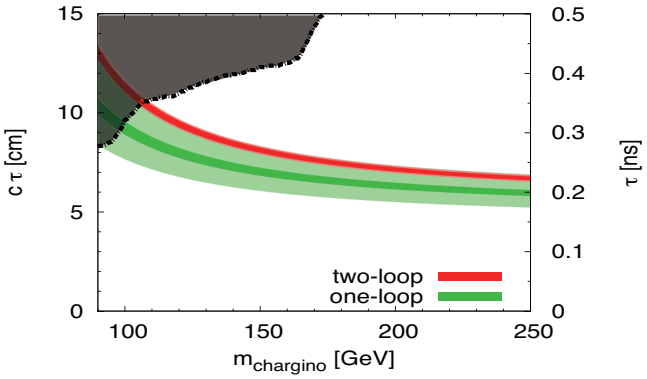

Fig. 24. The lifetime of charged wino evaluated by using δm at the one-loop (green band) and two-loop (red band). We neglected the next-to-leading order corrections to the lifetime of the charged wino estimated in terms of the pion decay rate, which is expected to be a few percent correction. The dark shaded region is excluded by the ATLAS collaboration at 95 % CL.

• Natural SUSY's Last Hope: R-parity Violation via UDD Operators

In collaboration with the members of IPMU

Here, we give a broad overview of the more natural spectra allowed by the LHC when UDD R-parity violation is allowed. Because R-parity violation removes the missing energy signals in colliders, the experimental constraints on the gluino, stops, sbottoms and higgsinos are relatively mild. We also show that UDD R-parity violation and lepton number conservation can be made consistent with grand unification. This feat is achieved through the product unification, $SU(5) \times U(3)$. In this model, mixing of the SM quarks with additional quark like particles charged under the $U(3)$ generate a UDD R-parity violating operator. Furthermore, these models are also capable of generating a 'natural' spectra. The emergence of these more natural low-scale spectra relies heavily on the fact that the gaugino masses are non-universal, a natural consequence of product unification [3].

Bibliography

[1] B. Bhattacherjee, B. Feldstein, M. Ibe, S. Matsumoto and T. T. Yanagida, Phys. Rev. D **87**, 015028 (2013) [arXiv:1207.5453 [hep-ph]].

[2] M. Ibe, S. Matsumoto and R. Sato, Phys. Lett. B **721**, 252 (2013) [arXiv:1212.5989 [hep-ph]].

[3] B. Bhattacherjee, J. L. Evans, M. Ibe, S. Matsumoto and T. T. Yanagida, arXiv:1301.2336 [hep-ph].

Model of Neutrino

• Seesaw Mechanism with Occam's Razor

In collaboration with the member of IPMU

We discuss the seesaw mechanism which includes the minimum number of parameters for successful leptogenesis and three neutrino oscillations in the spirit of Occam's razor. We show that models with two right-handed neutrinos with two texture zeros supported by Occam's razor cannot fit the observed neutrino parameters consistently for the normal light neutrino mass hierarchy. For the inverted light neutrino mass hierarchy, on the other hand, we find that the models can fit the observed neutrino parameters consistently. Besides, we show that the model predicts the maximal Dirac CP-phase of the neutrino mixing matrix in the measurable range in the foreseeable future for the inverted neutrino mass hierarchy. We also show that the predicted effective Majorana neutrino mass responsible for the neutrinoless double beta decay is around 50 meV which is also within reach of future experiments [1].
.

Bibliography

[1] K. Harigaya, M. Ibe and T. T. Yanagida, Phys. Rev. D **86**, 013002 (2012) [arXiv:1205.2198 [hep-ph]].

Cosmology and Astrophysics

[Spokesperson : M. Kawasaki]

ICRR, The Univ. of Tokyo, Kashiwa, Chiba 277-8582

Inflation and Thermal History in the early Universe

• High scale SUSY breaking from topological inflation

In collaboration with the members of ICRR and IPMU

The recently observed mass ~ 125 GeV for the Higgs boson suggests a high-energy scale SUSY breaking, at above $O(10)$ TeV. It is, however, very puzzling why nature chooses such a high energy scale for the SUSY breaking, if the SUSY is a solution to the hierarchy problem. We show that the pure gravity mediation provides us with a possible solution to this puzzle if the topological inflation is the last inflation in the early universe. We briefly discuss a chaotic inflation model in which a similar solution can be obtained [1].

• Gravitational waves from smooth hybrid new inflation

In collaboration with the members of ICRR

We calculate the production of the gravitational waves from a double inflation model with lattice simulations. Between the two inflationary stages, gravitational waves with a characteristic frequency are produced by fluctuations of the scalar fields enhanced through parametric resonance. The wavelength of the produced gravitational waves gets extra redshift during the second inflationary stage and it can be in the observable range for the direct gravitational wave detectors. It is found that there is a possibility for the produced gravitational waves to be detected in the planned experiments [2].

• Smooth hybrid inflation in a supersymmetric axion model

In collaboration with the members of ICRR, IPMU and University of Tokyo

We show that the smooth hybrid inflation is naturally realized in a framework of supersymmetric axion model. Identifying the Peccei-Quinn scalar fields as a part of the infaton sector, successful inflation takes place reproducing the amplitude and spectral index of the curvature perturbation observed by WMAP. A relatively large axion isocurvature perturbation and its non-Gaussianity are predicted in our model. The saxion coherent oscillation has a large amplitude and dominates the Universe. The subsequent decay of the saxion produces huge amount of entropy, which dilutes unwanted relics. Winos, the lightest supersymmetric particles in this scenario, are produced non-thermally in the decay and account for dark matter [3].

• Heavy gravitino in hybrid inflation

In collaboration with the members of ICRR, IPMU and University of Tokyo

It is known that supersymmetric hybrid inflation model may require severe tunings on the initial condition for large gravitino mass of order 100 - 1000 TeV due to the constant term in the superpotential. We propose a modified hybrid inflation model, where the constant term is suppressed during inflation and generated after inflation by replacing a constant term with dynamical field. In this modified model, successful inflation consistent with large gravitino mass takes place without severe tunings on the initial condition. Constraint from cosmic strings is also relaxed [4].

• Primordial black hole formation from an axion-like curvaton model

In collaboration with the members of ICRR and IPMU

We argue that the existence of the cold dark matter is explained by primordial black holes. We show that a significant number of primordial black holes can be formed in an axion-like curvaton model, in which the highly blue-tilted power spectrum of primordial curvature perturbations is achieved. It is found that the produced black holes with masses $\sim 10^{20} - 10^{38}$ g account for the present cold dark matter. We also argue the possibility of forming the primordial black holes with mass $\sim 10^5 M_\odot$ as seeds of the supermassive black holes [5].

• Chaotic Inflation with a Fractional Power-Law Potential in Strongly Coupled Gauge Theories

In collaboration with the members of IPMU Models of chaotic

inflation with a fractional power-law potential are not only viable but also testable in the foreseeable future. We show that such models can be realized in simple strongly coupled supersymmetric gauge theories. In these models, the energy scale during inflation is dynamically generated by the dimensional transmutation due to the strong gauge dynamics. Therefore, such models not only explain the origin of the fractional power in the inflationary potential but also provide a reason why the energy scale of inflation is much smaller than the Planck scale. Models of chaotic inflation with a fractional power-law potential are not only viable but also testable in the foreseeable future. We show that such models can be realized in simple strongly coupled supersymmetric gauge theories. In these models, the energy scale during inflation is dynamically generated by the dimensional transmutation due to the strong gauge dynamics. Therefore, such models not only explain the origin of the fractional power in the inflationary potential but also provide a reason why the energy scale of inflation is much smaller than the Planck scale [6].

• Stochastic Approach to Flat Direction during Inflation

In collaboration with the members of ICRR.

We revisit the time evolution of a flat and non-flat direction system during inflation. In order to take into account quantum noises in the analysis, we base on stochastic formalism and solve coupled Langevin equations numerically. We focus on a class of models in which tree-level Hubble-induced mass is not generated. Although the non-flat directions can block the growth of the flat direction's variance in principle, the blocking effects are suppressed by the effective masses of the non-flat directions. We find that the fate of the flat direction during inflation is determined by one-loop radiative corrections and non-renormalizable terms as usually considered, if we remove the zero-point fluctuation from the noise terms [7].

• Remarks on Hubble Induced Mass from Fermion Kinetic Term and MSSM plasma

In collaboration with the members of ICRR and Tohoku Univ.

We evaluate the effective mass of a scalar field which interacts with visible sector via Planck-suppressed coupling in supergravity framework. We focus on the radiation-dominated (RD) era after inflation and the contribution from a fermionic field in the thermal bath. We find that, in RD era, the fermion kinetic term gives the effective mass of the order of Hubble scale to the scalar field [8].

We also evaluate the effective mass of a scalar field ϕ coupled to thermal plasma through Planck-suppressed interactions. We find it useful to rescale the coupled fields so that all the ϕ-dependences are absorbed into the yukawa and gauge couplings, which allows us to read off the leading order contributions to the effective mass $\tilde{m}_\phi$ from the 2-loop free energy calculated with the rescaled couplings. We give an analytical expression for $\tilde{m}_\phi$ at a sufficiently high temperature in the case where ϕ is coupled to the MSSM chiral superfields through non-minimal Kähler potential. We find that $|\tilde{m}_\phi^2|$ is about $10^{-3}H^2 \sim 10^{-2}H^2$ at the leading order in terms of the couplings for typical parameter sets, where H is the Hubble expansion rate in the radiation-dominated era [9].

• A Simple Solution to the Polonyi Problem in Gravity Mediation

In collaboration with the members of IPMU

The Polonyi field is a necessary ingredient in any viable scenario of gravity mediated supersymmetry breaking. However, it is known that the presence of the Polonyi field leads to several serious cosmological problems, which are collectively referred to as the Polonyi problem. We show that the Polonyi problem can be solved if the Polonyi field couples to a pseudo modulus in the superpotential and this pseudo modulus has a large field expectation value during inflation. To illustrate our idea, we construct an explicit model which can be readily connected to scenarios of gravity mediation. The generation of the mass parameters contained in our model by strong gauge dynamics is also commented on. The Polonyi field is a necessary ingredient in any viable scenario of gravity mediated supersymmetry breaking. However, it is known that the presence of the Polonyi field leads to several serious cosmological problems, which are collectively referred to as the Polonyi problem. We show that the Polonyi problem can be solved if the Polonyi field couples to a pseudo-modulus in the superpotential and this pseudo-modulus has a large field expectation value during inflation. To illustrate our idea, we construct an explicit model which can be readily connected to scenarios of gravity mediation. The generation of the mass parameters contained in our model by strong gauge dynamics is also commented on [10].

Bibliography

[1] K. Harigaya, M. Kawasaki and T. T. Yanagida, Phys. Lett. B **719**, 126–130 (2013) [arXiv:1211.1770 [hep-ph]].

[2] M. Kawasaki, K. Saikawa and N. Takeda, Phys. Rev. D **87** (2013) 103521 [arXiv:1208.4160 [astro-ph.CO]].

[3] M. Kawasaki, N. Kitajima and K. Nakayama, Phys. Rev. D **87**, 035010 (2013) [arXiv:1211.6516 [hep-ph]].

[4] M. Kawasaki, N. Kitajima, K. Nakayama and T. T. Yanagida, arXiv:1301.6281 [hep-ph].

[5] M. Kawasaki, N. Kitajima and T. T. Yanagida, Phys. Rev. D **87**, 063519 (2013) [arXiv:1207.2550 [hep-ph]].

[6] K. Harigaya, M. Ibe, K. Schmitz and T. T. Yanagida, Phys. Lett. B **720**, 125 (2013) [arXiv:1211.6241 [hep-ph]].

[7] M. Kawasaki and T. Takesako, JCAP **1208**, 031 (2012) [arXiv:1207.1165 [hep-ph]].

[8] M. Kawasaki and T. Takesako, Phys. Lett. B **718**, 522 (2012) [arXiv:1208.1323 [hep-ph]].

[9] M. Kawasaki, F. Takahashi and T. Takesako, JCAP **1304**, 008 (2013) [arXiv:1211.4921 [hep-ph]].

[10] K. Harigaya, M. Ibe, K. Schmitz and T. T. Yanagida, Phys. Lett. B **721**, 86 (2013) [arXiv:1301.3685 [hep-ph]].

Dark Matter, Baryogenesis, Big-Bang nucleosynthesis

• Axion cosmology with long-lived domain walls

In collaboration with the members of ICRR, YITP and Nagoya Univ.

We investigate the cosmological constraints on axion models where the domain wall number is greater than one. In these models, multiple domain walls attached to strings are formed, and they survive for a long time. Their annihilation occurs due to the effects of explicit symmetry breaking term which might be raised by Planck-scale physics. We perform three-dimensional lattice simulations and compute the spectra of axions and gravitational waves produced by long-lived domain walls. Using the numerical results, we estimated relic density of axions and gravitational waves. We find that the existence of long-lived domain walls leads to the overproduction of cold dark matter axions, while the density of gravitational waves is too small to observe at the present time. Combining the results with other observational constraints, we find that the whole parameter region of models are excluded unless an unacceptable fine-tuning exists [1].

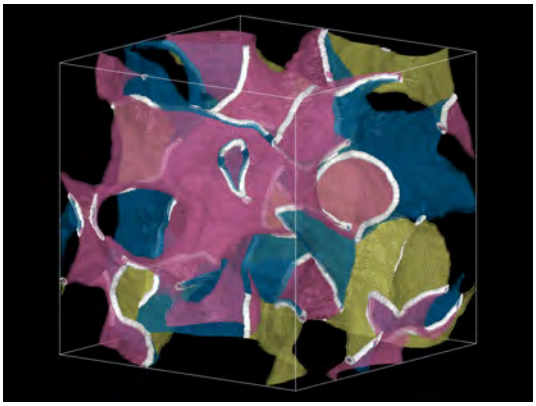

Fig. 25. A visualization of the simulation which shows the spatial configurations of topological defects. The white lines correspond to the position of the core of strings and the domain walls are represented by surfaces with various colors.

• Evolution and thermalization of dark matter axions in the condensed regime

In collaboration with the members of ICRR and Titech

We discuss the possibility that dark matter axions form a Bose-Einstein condensate (BEC) due to the gravitational self-interactions. The formation of BEC occurs in the condensed regime, where the transition rate between different momentum states is large compared to the energy exchanged in the transition. The time evolution of the quantum state occupation

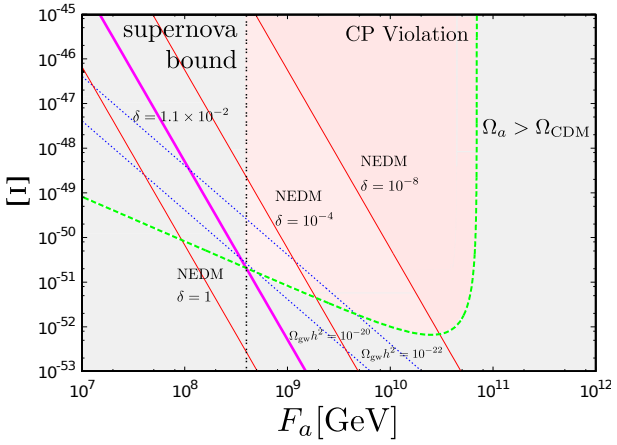

Fig. 26. The various observational constraints in the parameter space of the axion models F_a (axion decay constant) and Ξ (a bias parameter which relates a pressure on walls).

number of axions in the condensed regime is derived based on the in-in formalism. We recover the expression for the thermalization rate due to self interaction of the axion field, which was obtained in the other literature. It is also found that the leading order contributions for interactions between axions and other species vanish, which implies that the axion BEC does not give any significant modifications on standard cosmological parameters [2].

• Axino dark matter and baryon number asymmetry from Q-ball decay in gauge mediation

In collaboration with the members of ICRR, IPMU and Kanagawa Univ.

We investigate the Q-ball decay into the axino dark matter in the gauge-mediated supersymmetry breaking. In our scenario, the Q ball decays mainly into nucleons and partially into axinos to account for the baryon asymmetry and the dark matter of the universe simultaneously. The Q ball decays well before the big bang nucleosynthesis so that it is not affected by the decay. The decay into the supersymmetric particles of the minimal supersymmetric standard model is kinematically prohibited until the very end of the decay, and we could safely make their abundances small enough for the successful big bang nucleosynthesis. We show the regions of axino model parameters and the Q-ball parameters which realize this scenario [3].

• Q ball Decay Rates into Gravitinos and Quarks

In collaboration with the members of ICRR and IPMU.

The Affleck-Dine mechanism, which is one of the most attractive candidates for the baryogenesis in supersymmetric theories, often predicts the existence of baryonic Q balls in the early universe. In this scenario, there is a possibility to explain the observed baryon-to-dark matter ratio because Q balls decay into supersymmetric particles as well as into quarks. If the gravitino mass is small compared to the typical interaction energy, the longitudinal component of the gravitino

behaves like the massless goldstino. We numerically calculate the goldstino production rates from Q balls in the leading semi-classical approximation without using large radius limit or effective coupling. We also calculate the quark production rates from Q balls in the Yukawa theory with a massive fermion. In deriving the decay rate we also take into account the scalar field configuration of the Q ball. These results are applied to a realistic model in the gauge-mediated supersymmetry breaking and yield the branching ratio of the Q ball decay into the gravitino. We obtain the branching ratio much smaller than the one estimated in the previous analysis [4].

• Revisiting the gravitino dark matter and baryon asymmetry from Q-ball decay in gauge mediation

In collaboration with the members of ICRR, IPMU, Kanagawa Univ, and Max Planck Inst.

We reinvestigate the scenario that the amount of the baryons and the gravitino dark matter is naturally explained by the decay of the Q balls in the gauge-mediated SUSY breaking. Equipped by the more correct decay rates into gravitinos and baryons recently derived, we find that the scenario with the direct production of the gravitino dark matter from the Q-ball decay works naturally [5].

• Opening the window to the cogenesis with Affleck-Dine mechanism in gravity mediation

In collaboration with the members of ICRR and IPMU.

The observed baryon and dark matter densities are equal up to a factor of 5. This observation indicates that the baryon asymmetry and dark matter have the same origin. The Affleck-Dine baryogenesis is one of the most promising mechanisms in this context. Q balls, which are often formed in the early Universe associated with the Affleck-Dine baryogenesis, decay both into supersymmetric particles and into quarks. Recently, it was pointed out that annihilation of squarks into quarks gives a dominant contribution to the Q-ball decay rate and the branching ratio of Q-ball decay into supersymmetric particles changes from the previous estimate. In this paper, the scenario of baryon and dark matter cogenesis from Q ball in gravity mediation is revisited in respect of the improved Q-ball decay rates. It is found that the successful cogenesis takes place when a wino with mass 400-600 GeV is dark matter [6].

• Updated constraint on a primordial magnetic field during big bang nucleosynthesis and a formulation of field effects

In collaboration with the members of ICRR and NAOJ.

A new upper limit on the amplitude of primordial magnetic field (PMF) is derived by a comparison between a calculation of elemental abundances in big bang nucleosynthesis (BBN) model and the latest observational constraints on the abundances. Updated nuclear reaction rates are adopted in the calculation. Effects of PMF on the abundances are consistently taken into account in the numerical calculation with the precise formulation of changes in physical variables. We find that abundances of ^{3}He and ^{6}Li increase while that of ^{7}Li decreases when the PMF amplitude increases, in the case of the baryon-to-photon ratio determined from the measurement of cosmic microwave background radiation. We derive a constraint on the present amplitude of PMF, i.e., $B(0) < 1.5\ \mu$G [corresponding to the amplitude less than 2.0×10^{11} G at BBN temperature of $T = 10^9$ K] based on the rigorous calculation [7].

The effect of PMF on BBN through the energy density is studied in order to derive constraints on models for PMF generations. We assume a PMF with a power law (PL) distribution in wave number defined with a field strength, a PL index, and maximum and minimum scales at a generation epoch. We then show a relation between PL-PMF parameters and the scale invariant (SI) strength of PMF. We perform a BBN calculation, and show abundances as a function of baryon-to-photon ratio. Degeneracies between the PL-PMF parameters in the PMF effect are then discussed. In addition, we study a general case in which both of the existence and a dissipation of PMF are possible [8].

• Solution to Big-Bang nucleosynthesis in hybrid axion dark matter model

In collaboration with the members of ICRR, Univ. Wisconsin, Madison, NAOJ, Univ. Tokyo, Mimar Sinan Fine Arts Univ. Besiktas.

The primordial ^{7}Li abundance predicted in standard big bang nucleosynthesis (BBN) model for the baryon-to-photon number ratio determined from the cosmic microwave background WMAP observations is higher than those observed in old halo stars. Recently a new solution to the lithium puzzle was proposed, which is a mechanism for the cooling of photons in the epoch between the end of BBN and the last photon scattering. An axion could form a Bose-Einstein condensate (BEC) and may have cooled the photons in the epoch. The baryon-to-photon ratio would then be smaller in BBN epoch than that measured by WMAP. We adopted a limit on the sum of primordial abundances of D and ^{3}He taken from an observational abundance for the protosolar cloud, and showed that the constraint excludes the original axion BEC model. We calculated BBN in a hybrid axion and decaying exotic relic particle model in which the axion cools the photons and the particle produces nonthermal photons to eliminate the high D abundance in the original axion BEC model. It is found that calculated abundances of all nuclides including D and ^{7}Li can be simultaneously in ranges of adopted observational constraints [9].

• Production of ^{9}Be through α-fusion reaction of metal-poor cosmic ray and stellar flare

In collaboration with the members of ICRR.

Spectroscopic observations of metal-poor stars have indicated possible ^{6}Li abundances which are much larger than the primordial abundance predicted in standard big bang nucleosynthesis model. Possible mechanisms of ^{6}Li production in metal-poor stars include pregalactic and cosmological cosmic

ray (CR) nucleosynthesis and nucleosynthesis by flare accelerated nuclides. We study the ^{9}Be production by two-step α-fusion reactions of CR or flare accelerated ^{3,4}He through ^{6}He and ^{6,7}Li, in pregalactic structure, intergalactic medium and stellar surfaces. We solve transfer equations of CR or flare particles and calculate nuclear yields of ^{6}He, ^{6,7}Li and ^{9}Be taking account of probabilities of processing ^{6}He and ^{6,7}Li into ^{9}Be via fusions with α particles. Yield ratios, i.e., ^{9}Be/^{6}Li, are then calculated for the CR and flare nucleosynthesis models. We suggest that the future observations of ^{9}Be in metal-poor stars may find enhanced abundances originating from metal-poor CR or flare activities [10].

Bibliography

[1] T. Hiramatsu, M. Kawasaki, K. Saikawa and K. Sekiguchi, JCAP **1301** (2013) 001 [arXiv:1207.3166 [hep-ph]].

[2] K. Saikawa and M. Yamaguchi, Phys. Rev. D **87** (2013) 085010 [arXiv:1210.7080 [hep-ph]].

[3] S. Kasuya, E. Kawakami and M. Kawasaki, arXiv:1202.4067 [hep-ph].

[4] M. Kawasaki and M. Yamada, Phys. Rev. D **87**, 023517 (2013) [arXiv:1209.5781 [hep-ph]].

[5] S. Kasuya, M. Kawasaki and M. Yamada, arXiv:1211.4743 [hep-ph].

[6] A. Kamada, M. Kawasaki and M. Yamada, Phys. Lett. B **719**, 9 (2013) [arXiv:1211.6813 [hep-ph]].

[7] M. Kawasaki and M. Kusakabe, Phys. Rev. D **86**, 063003 (2012) [arXiv:1204.6164 [astro-ph.CO]].

[8] D. G. Yamazaki and M. Kusakabe, Phys. Rev. D **86**, 123006 (2012) [arXiv:1212.2968 [astro-ph.CO]].

[9] M. Kusakabe, A. B. Balantekin, T. Kajino and Y. Pehlivan, Phys. Lett. B **718**, 704 (2013) [arXiv:1202.5603 [astro-ph.CO]].

[10] M. Kusakabe and M. Kawasaki, Astrophys. J. **767**, 5 (2013) [arXiv:1208.4210 [astro-ph.CO]].

Cosmic Strings

• Gravitational lensing due to cosmic strings

In collaboration with the members of University of Tokyo, RESCEU, YITP, Hirosaki University, and Kumamoto University

We study the observational signature of the effect of weak gravitational lensing. In the presence of vector perturbations, the non-vanishing signals for B-mode cosmic shear and curl-mode deflection angle, which have never appeared in the case of scalar metric perturbations, naturally arise. As a possible source for seeding vector perturbations, we then consider a cosmic string network, and discuss its detectability from upcoming weak lensing and CMB measurements. We find that the weak lensing signals are enhanced for a smaller intercommuting probability of the string network, P, and they are potentially detectable from the upcoming cosmic shear and CMB lensing observations [1]. On the other hand, if a cosmic string with the deflection angle $8\pi G\mu \sim 10-18$ exists around the line of sight a gamma-ray burst, we may observe characteristic interference patterns caused by gravitational lensing in the energy spectrum of the gamma-ray burst, so-called femto-lensing [2].

• Forecast constraints on cosmic strings from future CMB, pulsar timing and gravitational wave direct detection experiments

In collaboration with the members of ICRR, RESCEU, Nagoya Univ., Kumamoto Univ. and Institut d' Astrophysique.

We study future observational constraints on cosmic string parameters from various types of next-generation experiments. In addition to GW direct detection on the ground, we also consider that by space-based interferometers, GW background detection in pulsar timing experiments and cosmic string contributions to the cosmic microwave background (CMB) temperature and polarization anisotropies. These different types of observations offer independent probes of cosmic strings and may enable us to investigate cosmic string properties if the signature is detected. In these papers, we evaluate the power of future experiments to constrain cosmic string parameters, such as the string tension $G\mu$, the initial loop size α, and the reconnection probability p, by performing Fisher information matrix calculations. We find that combining the information from the different types of observations breaks parameter degeneracies and provides more stringent constraints on the parameters. We also find future space-borne interferometers independently provide a highly precise determination of the parameters [3].

• Cosmological and astrophysical constraints on superconducting cosmic strings

In collaboration with the members of ICRR and Univ. of Tokyo.

We investigate the cosmological and astrophysical constraints on superconducting cosmic strings (SCSs). SCS loops emit strong bursts of electromagnetic waves, which might affect various cosmological and astrophysical observations. We take into account the effect on the CMB anisotropy, CMB blackbody spectrum, BBN, observational implications on radio wave burst and X-ray or gamma-ray events, and stochastic gravitational wave background measured by pulsar timing experiments. We then derive constraints on the parameters of SCS from current observations and estimate prospects for detecting SCS signatures in on-going observations. As a result, we find that these constraints exclude broad parameter regions, and also that on-going radio wave observations can probe large parameter space [4].

Bibliography

[1] D. Yamauchi, T. Namikawa and A. Taruya, JCAP **1210**, 030 (2012) [arXiv:1205.2139 [astro-ph.CO]].

[2] C. -M. Yoo, R. Saito, Y. Sendouda, K. Takahashi and D. Yamauchi, PTEP **2013**, 013E01 (2013) [arXiv:1209.0903 [astro-ph.CO]].

[3] S. Kuroyanagi, K. Miyamoto, T. Sekiguchi, K. Takahashi and J. Silk, Phys. Rev. D **87**, 023522 (2013) [arXiv:1210.2829 [astro-ph.CO]].

[4] K. Miyamoto and K. Nakayama, arXiv:1212.6687 [astro-ph.CO].

Primordial non-Gaussianity

• Non-Gaussianity from axionic curvaton

In collaboration with the members of ICRR, Tohoku Uni. and CITA.

We study non-Gaussianity of density perturbations generated by an axionic curvaton, focusing on the case that the curvaton sits near the hilltop of the potential during inflation. Such hilltop curvatons can generate a red-tilted density perturbation spectrum without invoking large-field inflation. We show that, even when the curvaton dominates the Universe, the non-Gaussianity parameter $f_{\rm NL}$ is positive and mildly increases towards the hilltop of the curvaton potential, and that $f_{\rm NL} = \mathcal{O}(10)$ is a general and robust prediction of such hilltop axionic curvatons. In particular, we find that the non-Gaussianity parameter is bounded as $f_{\rm NL} \lesssim$ 30-40 for a range of the scalar spectral index, $n_s = 0.94$-0.99, and that $f_{\rm NL} =$ 20-40 is realized for the curvaton mass $m_\sigma = 10$-10^6 GeV and the decay constant $f = 10^{12}$-10^{17} GeV. One of the plausible candidates for the axionic curvaton is an imaginary component of a modulus field with mass of order 10-100 TeV and decay constant of $10^{16\text{-}17}$GeV. We also discuss extreme cases where the curvaton drives a second inflation and find that $f_{\rm NL}$ is typically smaller compared to non-inflating cases [1].

• CMB constraint on non-Gaussianity in isocurvature perturbations

In collaboration with the members of ICRR, Nagoya Univ. and Saga Univ.

We study CMB constraints on non-Gaussianity from isocurvature perturbations of general types. Specifically, we study CDM/neutrino isocurvature perturbations which are uncorrelated or totally correlated with adiabatic ones. Using the data from the WMAP 7-year observation at V and W bands, we obtained optimal constraints on the nonlinearity parameters of adiabatic and isocurvature perturbations. We also discuss implications our results on the axion CDM isocurvature model [2, 3].

• Full bispectra from primordial scalar and tensor perturbations in the most general single field inflation model

In collaboration with the members of ICRR, RESCEU, Nagoya Univ., Rikkyo Univ., Titech, and Astroparticule et Cosmologie.

We compute the full bispectra, namely both auto- and cross-bispectra, of primordial curvature and tensor perturbations in the most general single-field inflation model whose scalar and gravitational equations of motion are of second order. The formulae in the limits of k-inflation and potential driven inflation are also given. These expressions are useful for estimating the full bispectra of temperature and polarization anisotropies of the cosmic microwave background radiation [4].

• CMB power spectra induced by primordial cross-bispectra between metric perturbations and vector fields

In collaboration with the members of ICRR, and Nagoya Univ.

We study temperature and polarization anisotropies of the cosmic microwave background (CMB) radiation sourced from primordial cross-bispectra between metric perturbations and vector fields, which are generated from the inflation model where an inflaton and a vector field are coupled. In case the vector field survives after the reheating, both the primordial scalar and tensor fluctuations can be enhanced by the anisotropic stress composed of the vector fields during radiation dominated era. We show that through this enhancement the primordial cross-bispectra generate not only CMB bispectra but also CMB power spectra. In general, we can expect such cross-bispectra produce the non-trivial mode-coupling signals between the scalar and tensor fluctuations. However, we explicitly show that such mode-coupling signals do not appear in CMB power spectra. Through the numerical analysis of the CMB scalar-mode power spectra, we find that although signals from these cross-bispectra are smaller than primary non-electromagnetic ones, these have some characteristic features such as negative auto-correlations of the temperature and polarization modes, respectively. On the other hand, signals from tensor modes are almost comparable to primary non-electromagnetic ones and hence the shape of observed B-mode spectrum may deviate from the prediction in the non-electromagnetic case. The above imprints may help us to judge the existence of the coupling between the scalar and vector fields in the early Universe [5].

• Statistics of general functions of a Gaussian field - application to non-Gaussianity from preheating-

In collaboration with the members of ICRR, and RESCEU.

We provide a general formula for calculating correlators of arbitrary function of a Gaussian field. This work extends the standard leading-order approximation based on the delta N formalism to the case where truncation of the delta N at some low order does not yield the correct answer. As an application of this formula, we investigate 2, 3 and 4-point functions of the primordial curvature perturbation generated in the

massless preheating model by approximating the mapping between the curvature perturbation and the Gaussian field as a sum of the many spiky normal distribution functions as suggested by lattice calculations. We also discuss observational consequences of this case and show that trispectrum would be a key observable to search signature of preheating in the CMB map. It is found the forms of the curvature correlation functions for any delta N, at the leading order in the correlator of the Gaussian field, coincide with the standard local type ones. Within this approximation, it is also found that the standard formula for the non-linearity parameters given by the product of the derivatives of the e-folding number still holds after we replace the bare e-folding number appearing in the original delta N expansion with the one smoothed in the field space with a Gaussian window function [6].

• Non-Gaussianity bubble in the sky

In collaboration with the members of Kyoto University

We point out a possible generation mechanism of non-Gaussian bubbles in the sky due to bubble nucleation in the early universe. We consider a curvaton scenario for inflation and assume that the curvaton field, whose energy density is subdominant during inflation but which is responsible for the curvature perturbation of the universe, is coupled to another field which undergoes false vacuum decay through quantum tunneling. For this model, we compute the skewness of the curvaton fluctuations due to its interaction with the tunneling field during tunneling, that is, on the background of an instanton solution that describes false vacuum decay. We find that the resulting skewness of the curvaton can become large in the spacetime region inside the bubble. We then compute the corresponding skewness in the statistical distribution of the CMB temperature fluctuations. We find a non-vanishing skewness in a bubble-shaped region in the sky. It can be large enough to be detected in the near future, and if detected it will bring us invaluable information about the physics in the early universe [7].

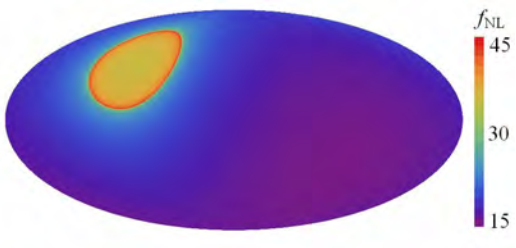

Fig. 27. Localized non-Gaussian bubble in the sky. The color shows the amplitude of the skewness of the primordial fluctuations.

• Implications of Planck results for models with local type non-Gaussianity

In collaboration with the members of ICRR, RESCEU, Titech, and Saga Univ..

We discuss implications of Planck results for models with local type non-Gaussianity. In light of the recent results of the Planck satellite, we constrain model parameters of several representative models and give the prediction of trispectrum, in particular, gNL. We also consider interesting possibilities that trispectrum appears as the first signature of the non-Gaussianities of the curvature perturbations, that is, fNL is small while gNL can be significantly large [8].

Bibliography

[1] M. Kawasaki, T. Kobayashi and F. Takahashi, JCAP **1303**, 016 (2013) [arXiv:1210.6595 [astro-ph.CO]].

[2] C. Hikage, M. Kawasaki, T. Sekiguchi and T. Takahashi, arXiv:1211.1095 [astro-ph.CO].

[3] C. Hikage, M. Kawasaki, T. Sekiguchi and T. Takahashi, JCAP **1303**, 020 (2013) [arXiv:1212.6001 [astro-ph.CO]].

[4] X. Gao, T. Kobayashi, M. Shiraishi, M. Yamaguchi, J. 'i. Yokoyama and S. Yokoyama, arXiv:1207.0588 [astro-ph.CO].

[5] M. Shiraishi, S. Saga and S. Yokoyama, JCAP **1211**, 046 (2012) [arXiv:1209.3384 [astro-ph.CO]].

[6] T. Suyama and S. Yokoyama, arXiv:1303.1254 [astro-ph.CO].

[7] K. Sugimura, D. Yamauchi and M. Sasaki, Europhys. Lett. **100**, 29004 (2012) [arXiv:1208.3937 [astro-ph.CO]].

[8] T. Suyama, T. Takahashi, M. Yamaguchi and S. Yokoyama, arXiv:1303.5374 [astro-ph.CO].

Structure formation in the Universe

• Testing general scalar-tensor gravity and massive gravity with cluster lensing

In collaboration with the members of RESCEU, Rikkyo University, and YITP

We explore the possibility of testing modified gravity exhibiting the Vainshtein mechanism against observations of cluster lensing. We work in the most general scalar-tensor theory with second-order field equations (Horndeski's theory), and derive static and spherically symmetric solutions, for which the scalar field is screened below a certain radius. It is found that the essential structure of the problem in the most general case can be captured by the program of classifying Vainshtein solutions out of different solutions to a quintic equation, as has been performed in the context of massive gravity. The key effect on gravitational lensing is that the second derivative of the scalar field can substantially be large at the transition from screened to unscreened regions, leaving a dip in the convergence. This allows us to put observational constraints on parameters characterizing the general scalar-tensor modification of gravity [1].

• Scale-dependent bias with higher order primordial non-Gaussianity: Use of the Integrated Perturbation Theory

In collaboration with the members of ICRR, and Nagoya Univ.

We analytically derive a more accurate formula for the power spectrum of the biased objects with the primordial non-Gaussianity parameterized not only by the non-linearity parameter fNL, but also by gNL and tauNL which characterize the trispectrum of the primordial curvature perturbations. We adopt the integrated perturbation theory which was constructed in Matsubara (2011). We discuss an inequality between fNL and tauNL in the context of the scale-dependent bias, by introducing a stochasticity parameter. We also mention higher order loop corrections into the scale-dependency of the bias parameter [2].

We also consider the other type of primordial non-Gaussianity as a source of the large scale modulation of the halo bias parameter. Anisotropic stress perturbations induced by primordial Gaussian vector fields create non-Gaussianity in curvature perturbations. We found that such non-Gaussianity closely resembles the local-type non-Gaussianity parametrized by $f_{\rm NL}$, and generates scale-dependent bias in large-scale structures. We also found a simple relationship between the scale-dependent bias and the power spectrum of the vector fields. When the vector fields are interpreted as primordial magnetic fields, the effective $f_{\rm NL}$ is shown to be always negative. The scale-dependent bias provides a new approach to probing primordial vector fields [3].

• Imprints of Non-thermal Wino Dark Matter on Small-Scale Structure

In collaboration with the member of IPMU

We study how "warm" the wino dark matter is when it is non-thermally produced by the decays of the gravitino in the early Universe. We clarify the energy distribution of the wino at the decay of the gravitino and the energy loss process after their production. By solving the Boltzmann equation, we show that a sizable fraction of the wino dark matter can be "warm" for the wino mass $m_{\tilde{w}} \sim 100 - 500$ GeV. The "warmness" of the wino dark matter leaves imprints on the matter power spectra and may provide further insights on the origin of dark matter via the future 21 cm line survey. Our calculations can be applied [4].

Bibliography

[1] T. Narikawa, T. Kobayashi, D. Yamauchi and R. Saito, Phys. Rev. D **87**, 124006 (2013) [arXiv:1302.2311 [astro-ph.CO]].

[2] S. Yokoyama and T. Matsubara, Phys. Rev. D **87**, 023525 (2013) [arXiv:1210.2495 [astro-ph.CO]].

[3] M. Shiraishi, S. Yokoyama, K. Ichiki and T. Matsubara, arXiv:1301.2778 [astro-ph.CO].

[4] M. Ibe, A. Kamada and S. Matsumoto, arXiv:1210.0191 [hep-ph].

OBSERVATORIES and A RESEARCH CENTER

Location of the Institute and the Observatories in Japan

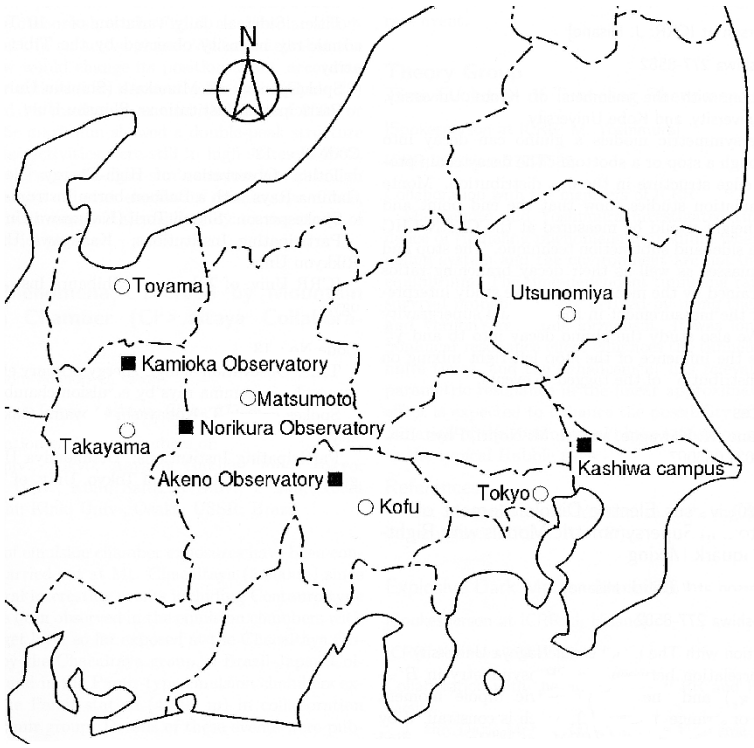

Norikura Observatory

Location:	Iwaitani, Nyukawa-cho, Takayama-shi, Gifu Prefecture 506-2254 N 36°06′, E 137°33′, 2770 m a.s.l.
Telephone (Fax):	+263-33-7456
Telephone (satellite):	090-7721-5674
Telephone (car):	090-7408-6224

Akeno Observatory

Location:	5259 Asao, Akeno-machi, Hokuto-shi, Yamanashi Prefecture 407-0201 N 35°47′, E 138°30′, 900 m a.s.l.
Telephone / Fax:	+551-25-2301 / +551-25-2303

Kamioka Observatory

Location:	456 Higashi-mozumi, Kamioka-cho, Hida-shi, Gifu Prefecture 506-1205 N 36°25′26″, E 137°19′11″, 357.5 m a.s.l.
Telephone / Fax:	+578-85-2116 / +578-85-2121

Research Center for Cosmic Neutrinos

Location:	5-1-5 Kashiwanoha, Kashiwa, Chiba Prefecture 277-8582
Telephone / Fax:	+4-7136-3138 / +4-7136-3115

NORIKURA OBSERVATORY

Introduction

Norikura Observatory (36.10°N and 137.55°E) was founded in 1953 and attached to ICRR in 1976. It is located at 2770 m above sea level, and is the highest altitude manned laboratory in Japan. Experimental facilities of the laboratory are made available to all the qualified scientists in the field of cosmic ray research and associated subjects. The AC electric power is generated by the dynamo and supplied throughout the observatory. In 1996, two dynamos of 70 KVA each were replaced with the new ones. The observatory can be accessed easily by car and public bus in summer (July-September). The 50th anniversary of Norikura Observatory was celebrated in 2003.

Fig. 1. Norikura Observatory.

The feasibility of the automatic operation of Norikura Observatory during winter period has been tested since winter 2004 in order to study the possibilities to reduce maintenance and labor costs without seriously damaging to the use of researches. A long-distance (∼40km) wireless LAN system (11M bps) was set up in 2003. Two new easy-to-handle and easy-to-maintain dynamos of 115 KVA each were installed in 2004 as well. The unmanned operation of Norikura Observatory has been mostly successful in winter, during which the battery backed-up solar panels and/or wind power generators kept supplying the electricity to the wireless LAN and on-going cosmic-ray experiments.

Present major scientific interests of the laboratory is focused on the modulation of high energy cosmic rays in the interplanetary space associated with the solar activity and the generation of energetic particles by the solar flares, both of which require long-term monitoring. This research has been carried out by the group of universities, where ICRR provides them with laboratory facility. A part of the facility has been open for the environmental study at high altitude such as aerosol-related mechanism in the atmosphere, observation of total ozone and UV solar radiation, for botanical study in the high-altitude environment, etc.

Fig. 2. A dynamo of 115KV.

Cosmic Ray Physics

A neutron monitor has been continuously operated to study the correlation of solar activities and cosmic ray flux for a long time. It is the only active one in Japan now. The neutron monitor data are open to researchers worldwide as a world observation network point (WDC). In addition, space weather observation is actively made by a 25 m^2 muon hodoscope at Norikura Observatory[1], [2], [3], [4], [5], [6], [7], [8], [9].

The anisotropy observed with the global muon detector network (GMDN) provides us with a unique information of the spatial gradient of the GCR density which reflects the large-scale magnetic structure in the heliosphere. The solar cycle variation of the gradient gives an important information on the GCR transport in the heliosphere, while the short-term variation of the gradient enables us to deduce the large-scale geometry of the magnetic flux rope and the interplanetary coronal mass ejection (ICME). Real-time monitoring of the precursory anisotropy which has often been observed at the Earth preceding the arrival of the ICME accompanied by a strong shock may provide us with useful tools for forecasting the space weather with a long lead time. By using a self-supporting power system utilizing the solar panels and batteries, we keep a 25 m^2 muon hodoscope running at the Mt. Norikura Cosmic Ray Observatory as an important component detector of the GMDN. The total power consumption of

this detector has been suppressed as low as 36 Watt by replacing all amplifier boards with those using CMOS ICs and by introducing a new recording system using the FPGA. This new system, in which the observation has been automatically carried out by a PC connected with the internet, also enabled us to monitor the data on the real-time basis for the space weather study.

The Sun is the nearest site to the Earth capable of accelerating particles up to high energies. When the Sun becomes active, flares are frequently observed on its surface. The flare accelerates the proton and ion to high energy and they are detected on the Earth soon after the flare. Among the particles generated by the flare, high energy neutrons provide the most direct information about the acceleration mechanism as they come straight from the flare position to the Earth without deflected by the magnetic field.

Observation of solar neutron has been conducted at the Norikura Observatory since 1990. Neutron is used to clarify the acceleration mechanism of high energy particles in association with solar flares, because the neutron is not reflected by the interplanetary magnetic field. The 64m^2 solar neutron telescope was constructed in 1996, which is one of 7 solar neutron telescopes deployed at different longitudes to make up a network of 24 hour observation of solar neutrons. The Norikura 64m^2 solar neutron telescope has been operated by solar batteries and windmills since 2004.

This collaborative work has started since fiscal 2007 succeeding to the previous project titled 'Observation of solar neutrons by using a new method.' Although solar cycle 24 has started since 2008, the solar activity has continued to be inactive, and no new solar neutron event has been detected by the network since 2006. The last solar neutron event was on September 7, 2005. This event is unique because it indicates ions were accelerated or trapped at the acceleration region longer than electrons. The summary of 11 solar neutron events detected until 2005 shows that it may not be probable that a very efficient acceleration such as the shock acceleration works for ions at solar flares. This is given by deriving the energy spectrum of neutrons at the solar surface for each solar neutron event with a power law. Power law indices obtained span from 3 to 7. The energy spectrum of the original ions is softer than that of neutron. Therefore an efficient acceleration has not been detected by the observation of solar neutrons so far.This work continues in solar cycle 24 to accumulate more events to obtain definite results related with particle acceleration at the solar surface.

Another effort aiming at observation of highest-energy solar cosmic rays started at the Norikura Observatory. The Sun is an accelerator of protons and electrons in the universe. In association with large solar flares, protons and electrons are accelerated into high energies. It is known that protons are accelerated over 50 GeV in the largest solar flares[24]. These high energy particles produce the Ground Level Enhancement (GLE).

In order to understand the acceleration mechanism of protons, we have prepared several solar neutron telescopes at the high altitude laboratories in the world. They are located at Gornergrat (3,135m), Mt. Aragats in Armenia (3,200m), Tibet (4,200m), Mauna-Kea in Hawaii (4,200m), Mt. Chacaltaya in Bolivia (5,250m), and at Mt. Sierra Negra in Mexico (4,900m). We have constructed a solar neutron telescopes at Mt. Norikura Cosmic Ray Observatory (2,770m) in 1990 and operated it until 2004[21]. However due to the lack of power supply during the winter time since 2005, the first solar neutron telescope (36 m^2) has not been operated. From 2008 to 2009, we have decided to make a new solar neutron telescope to utilize the large amount of the plastic scintillator (0.5m^3), as shown in Fig. 3, left at the observatory.

Fig. 3. 0.5-m^2 plastic scintillation counter for a new neutron telescope.

The new solar neutron telescope with use of the recycled plastic scintillator consists of main target where neutrons are converted into protons and of the anti-counters surrounding the target. The signals of neutrons converted into protons are observed by using one photomultiplier from bottom side to reduce the electric power. Furthermore a lead plate with the thickness of 1cm is located over the target and the lead plate is sandwiched by two layers of the plastic scintillator to identify gamma-rays from neutrons. The new solar neutron telescope has a function to reject charged particles with an efficiency of 90%. Therefore the new solar neutron telescope has capability of 1/3 of the 64m^2 large solar neutron telescope located at the same place. We are waiting large solar flares over our detectors.

In addition to the long-term cosmic-ray observations mentioned above, various kinds of short-dated experiments are carried out every year taking an advantage of the high alti-

tude of the observatory.

High-energy radiations from thunderstorms have been observed by flight measurement, high-mountain observations and ground-based measurement. There are two types of those radiations associated with thunderstorms. One is short-duration radiations with duration of 1 ms or less. The other is long-duration emissions lasting for a few seconds to a few minutes, or a few tens of minutes on rare occasions. It is believed that both emissions originate from electrons accelerated in strong electric fields formed in lightning and thunderclouds. However, compared with the former, the latter has remained less understood due to lack of a large sample of observations.

To investigate production mechanism of long-duration emissions and the relevant electron acceleration, we installed at Norikura Cosmic-ray Observatory a radiation detection system and environmental sensors to measure light and electric fields during 2008−2010. The radiation system consists of a spherical NaI scintillator and a thin plastic scintillator that is placed just above the NaI counter. During the period, the system detected one long-duration bursts as well as five short-duration events.

Fig. 4 (top) shows the long-duration event observed during thunderstorms on 2008 September 20th [25]. The event lasted for 90 sec. Fig. 4 (bottom) represents an observed photon spectrum extending from 10 keV to 10 MeV. This indicates that electrons can be accelerated to at least 10 MeV in a quasi-stable thundercloud electric field. In addition, we compared the observed spectrum with model ones, and concluded that a gamma-ray source is located 60 m−130 m (at 90% confidence level) apart from our detector. Given these results, the observed emission was found to consist of not only gamma rays but also electrons. This was the first simultaneous observation of gamma rays and electrons in long-duration bursts

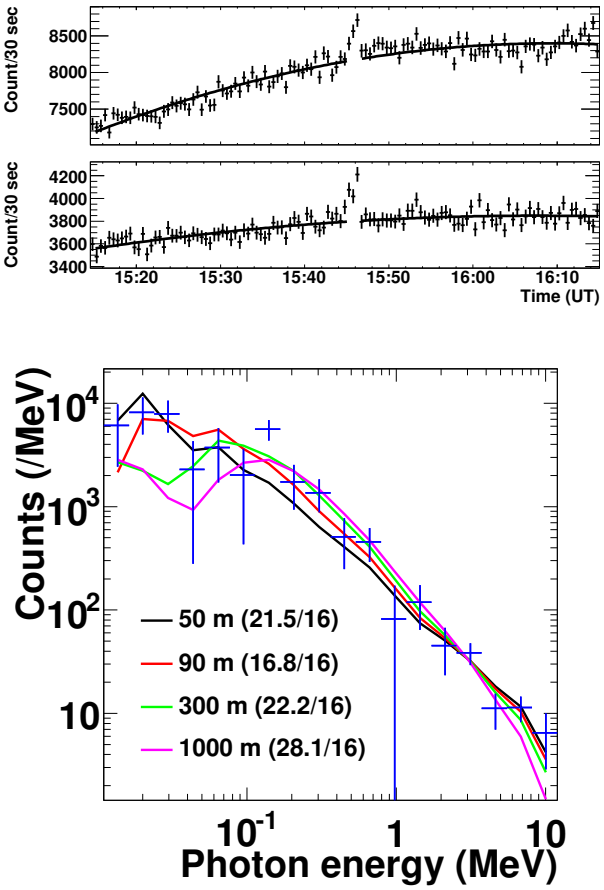

Fig. 4. (Top) Count rates per 30 sec observed by the >10 keV NaI scintillator (upper) and > 100 keV plastic one (lower). (Bottom) The photon spectrum observed by the NaI scintillator.

Observation of night sky background is carried out at Mt. Norikura for basic study of ultra high energy cosmic-ray physics.

The JEM-EUSO mission is going on in order to study ultra high energy cosmic rays (UHECRs), especially above 10^{20}eV. A 2.5m telescope with 60° FoV will be attached to the International Space Station in 2017 and detect fluorescence in near UV band from extensive air showers induced by UHECRs. Observation of UHECRs from a satellite orbit has not been done yet, so that the knowledge of background light intensity is important to realize the observation. We have measured it from a balloon altitude, but the opportunity is limited. We started the background measurement at Mt. Norikura.

Two 1 inch multi-anode photomultipliers (MAPMTs) developed for EUSO was used with UV filters. The center wavelengths of the filters were 337, 350, 358, 370, 380, 391, 400nm with 10nm band width. In addition BG3 filter was used to detect light in wider range from 330nm to 430nm. The MAPMTs were collimated to 7° FoV. The data was taken with the photon counting method.

We have observed several nights for three years. The intensity at zenith was almost constant at 600-800 photons/ ns sr m^2 for BG3 filter. The spectral intensity was about 1.5-2 times larger than those measured at La Palma and Namibia. The estimated portion of star light and zodiacal light was ∼30% and artificial light and nightglow at upper atmosphere may be the main components at Mt.Norikura.

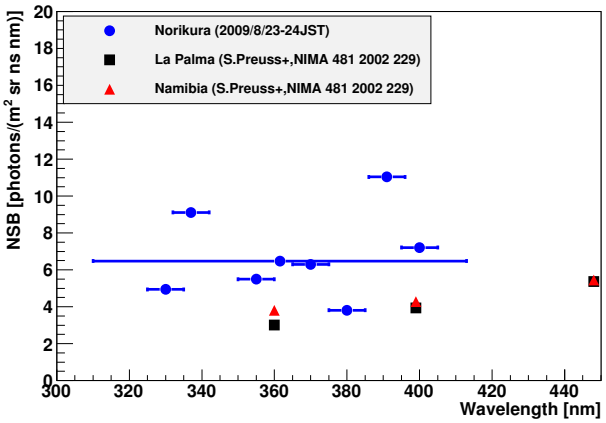

Fig. 5. Spectrum of night sky background measured at Mt.Norikura compared with those at La Palma and Namibia.

Environmental Study

One of the interesting topics is atmospheric environment especially relating with atmospheric aerosol particles and water soluble gases. The cosmic ray observatory at Mt. Norikura provides us very unique opportunity for the observations of atmosphere at free-tropospheric conditions with its high altitude, AC power supply at the site, accommodation facility, and easy accessibility. From year 2000 to 2007, we conducted continuous monitoring (mostly mid-May to mid-October) of meteorological parameters, number-size distribution of aerosols, aerosol chemical composition, ozone and radon concentrations, and column amount of aerosols from sky radiometer and ceilometers. We also collected rain, fog, water-condensed aerosol samples. These samples combined with other observed parameters were used in publications in the following subjects [26, 27, 28]:

(1) Polluted air pumping effects over central Japanese Alps in summer
(2) Seasonal variation of aerosol chemistry in free troposphere
(3) Vertical profiles of aerosols and clouds near the top of the atmospheric boundary layer.

Ceilometer (lidar with small output energy) was installed in summer 2002, and was operated in 6 summer seasons. The aerosol and cloud profiles near the top of the atmospheric boundary layer have been observed. Some events of Asian dust were detected.

Observations of total ozone and UV solar radiation with Brewer spectrophotometer on the Norikura mountains are also made[29, 30, 31]. Aerological Observatory started "Observations of total ozone and UV solar radiation with Brewer spectrophotometer at Norikura mountains" as a joint project with Institute for Cosmic Ray Research (ICRR), University of Tokyo at the Norikura Observatory of ICRR (Brewer site: 36.11 N, 137.56 E, 2,772 m a.s.l.), locating at the Northern Japanese Alps in every summer seasons from 2009 (Ito *et al.*: 2011). Purpose of this study is based on the concept of developing Regional Brewer Calibration Centre in Asia and study of total ozone, total sulfur oxide and global/diffuse UV included solar radiation on the high mountains. Observation results by using Brewer spectrophotometers and other instruments for the observation period of three summer seasons of recent three years between 2009 to 2011 are summarized as follows;

(1) Daily means of ds O_3 (total ozone) at Norikura for the observation periods were approx. 280 to 290 m atm-cm and were running on the lower values of approx. -3 to -6% compared to the value at Tsukuba (36.06 N, 140.13 E, 39 m a.s.l.) at almost same latitude. Day-to-day variations at Norikura were also small against Tsukuba. On the other hand, daily mean of ds SO_2 (total sulfur oxide) values were not recognized at Norikura.

(2) Absolute calibration of Brewers for ds O_3 and ds SO_2 observations could be carried out within the range of air mass from 7.928 (maximum) to 1.028 (minimum) at Norikura in the clear day. O_3 and SO_2 Extra-Terrestrial Coefficients (=ETC) of Brewers could be produced as about 10 samples satisfying the condition of "$R^2 > 0.9997$" by the calibrations. As an example of the calibration in 2011, the average of O_3 ETC of Brewers was identical within 1% to the currently used coefficient.

(3) In comparison to the data acquired at Tsukuba, the average of daily total GL_{UV} (global UV, e.g. CIE) for the observation periods indicated the intensities of approx. +23 % in 2009 to -6 % in 2011. The low intensity in 2011 was due to the bad weather on the Norikura Mountain. In the case of clear days, the GL_{UV} at Norikura indicated high intensities of approx. +35 to +52 % against the values at Tsukuba. On the other hand, the GL_{UV} increased in the short wavelength range at Norikura against the average at Tsukuba. The altitudinal increasing rate of GL_{UV} in the clear day indicated the calculated amounts of approx. +13 to +18 % per 1,000 m.

This joint project had been clarifying the low total O_3, high UV in clear day, low turbidity and etc. at Norikura against the value at Tsukuba. Those environmental conditions are useful for the intercomparison and the absolute calibrations with Brewers. The continuous observations with Brewers and other instrument are very important for the clarification of the seasonal variation and the coefficient trends.

Botanical Study

Effects of snow cover on pine shrub Pinus pumila in the alpine region of Mt. Norikura

High mountainous habit is one of the most severe habits for plant life and sometimes dwarf shrubs cannot survive. In the alpine regions of Japan, the dwarf shrub Pinus pumila (Japanese name : Haimatsu) forms communities together with small alpine plants, whereas dwarf shrubs occur only in the transition zone between the alpine region and the subalpine forest in Europe and North America. This characteristic of alpine vegetation is considered to be owing to winter heavy snow in the alpine regions of Japan. The purpose of this study is to elucidate how snow cover protects Haimatsu from winter environmental stresses in the alpine region of Mt. Norikura.

Study site

Tree height of Haimatsu and snow depth differ greatly as a result of slight difference in topography. Two site of the study area were selected. (i) site P (wind-protected) and (ii) site E (wind-exposed). At site P, mean tree height was 1.1 m. There was a lot of snow accumulation and Haimatsu was almost entirely covered with snow during the winter. Needle browning and death occurred rarely. At site E, mean tree height was 0.4 m. Snow accumulation was minimal, and Haimatsu was not entirely covered with snow. Needle browning and death was observed frequently.

Winter needle death in Haimatsu[32]

At site E, the browning and death of needles of Haimatsu occurred mainly in early spring at the point where the shoot protrudes from the snowpack. They are thought to be caused by excessive water loss due to mechanical damage to the cu-

ticle and/or to a thinner cuticle. However, needle browning and death in Haimatsu were not related to mechanical damage of the cuticle but might be due to changes in the quality and structure of the cuticle wax and resultant increase in water loss from needle cells.

Photosynthetic capacity in Haimatsu[33]

At site E, needles of Haimatsu had lower biomass, nitrogen, Rubisco (enzyme) and cell wall per unit area, and had higher photosynthetic capacity and shorter needle life-span than Haimatsu at site P. These results suggest that Haimatsu at wind-exposed site produces needles at low cost with high productivity to compensate for a short leaf life-span which may be imposed by wind stress when needles appear above the snow surface in winter.

Bibliography

[1] K. Munakata, S. Yasue, C. Kato, J. Kota, M. Tokumaru, M. Kojima, A. A. Darwish, T. Kuwabara and J. W. Bieber, "On the cross-field diffusion of galactic cosmic rays into the magnetic flux rope of a CME", *Advances in Geosciences*, 2, 115-124, eds. W. H. Ip and M. Duldig (World Scientific Publishing Co., USA), (2006).

[2] T. Kuwabara, J. W. Bieber, J. Clem, P. Evenson, R. Pyle, K. Munakata, S. Yasue, C. Kato, S. Akahane, M. Koyama, Z. Fujii, M. L. Duldig, J. E. Humble, M. R. Silva, N. B. Trivedi, W. D. Gonzalez and N. J. Schuch, "Real-time cosmic ray monitoring system for space weather", *Space Weather*, 4, S08001-1 10, (2006).

[3] M. R. Da Silva, A. Dal Lago, E. Echer, A. de Lucas, W. D. Gonzalez, N. J. Schuch, K. Munakata, L. E. A. Vieira, and F. L. Guarnieri, "Muon and neutron observations in connection with the corotating interaction regions", *Adv. Space Res.*, 40, pp348-352, (2007).

[4] Y. Okazaki, A. Fushishita, T. Narumi, C. Kato, S. Yasue, T. Kuwabara, J. W. Bieber, P. Evenson, M. R. Da Silva, A. Dal Lago, N. J. Schuch, Z. Fujii, M. L. Duldig, J. E. Humble, I. Sabbah, J. Kta and K. Munakata, "Drift effects and the cosmic ray density gradient in a solar rotation period: First observation with the Global Muon Detector Network (GMDN)", *Astrophys. J.*, 681, 693-707, (2008).

[5] T. Kuwabara, J. W. Bieber, P. Evenson, K. Munakata, S. Yasue, C. Kato, A. Fushishita, M. Tokumaru, M. L. Duldig, J. E. Humble, M. R. Silva, A. Dal Lago, and N. J. Schuch, "Determination of ICME Geometry and Orientation from Ground Based Observations of Galactic Cosmic Rays", *J. Geophys. Res., 114*, A05109-1 10, doi:10.1029/2008JA013717, (2009).

[6] A. Fushishita, T. Kuwabara, C. Kato, S. Yasue, J. W. Bieber, P. Evenson, M. R. Da Silva, A. Dal Lago, N. J. Schuch, M. Tokumaru, M. L. Duldig, J. E. Humble, I. Sabbah, H. K. Al Jassar, M. M. Sharma, and K. Munakata, "Precursors of the Forbush Decrease on 2006 December 14 observed with the Global Muon Detector Network (GMDN)", *Astrophys. J.*, 715, 1239-1247, (2010).

[7] A. Fushishita, Y. Okazaki, T. Narumi, C. Kato, S. Yasue, T. Kuwabara, J. W. Bieber, P. Evenson, M. R. Da Silva, A. Dal Lago, N. J. Schuch, M. Tokumaru, M. L. Duldig, J. E. Humble, I. Sabbah, J. Kta, and K. Munakata, "Drift effects and the average features of cosmic ray density gradient in CIRs during successive two solar minimum periods", *Advances in Geosciences*, eds. W. H. Ip and M. Duldig (World Scientific Publishing Co., USA), 21, 199-210, (2010).

[8] M. Tokumaru, M. Kojima, K. Fujiki, K. Munakata, T. Kuwabara and K. Marubashi, "Relation between loop-shaped interplanetary disturbances and the magnetic flux rope", *Advances in Geosciences*, eds. W. H. Ip and M. Duldig (World Scientific Publishing Co., USA), 21, 21-32, (2010).

[9] M. Rockenbach, A. Dal Lago, W. D. Gonzalez, K. Munakata, C. Kato, T. Kuwabara, J. W. Bieber, N. J. Schuch, M. L. Duldig, J. E. Humble, H. K. Al Jassar, M. M. Sharma, and I. Sabbah, "Geomagnetic Storms Precursors Observed from 2001 to 2007 with the Global Muon Detector Network GMDN", *Geophys. Res. Lett.*, 38, L16108-1 4, doi:10.1029/2011GL048556, (2011).

[10] "Solar neutron events of OctoberNovember 2003", Watanabe, K. *et al.*, Astrophys. J., **636**, 1135–1144, 2006.

[11] " Solar neutron events in association with large solar flares in November 2003", Watanabe, K. *et al.*, Adv. Space Res., **38**, 425–430, 2006.

[12] "Long-lived solar neutron emission in comparison with electron-produced radiation in the 2005 September 7 solar flare", Sako, T. *et al.*, Astrophys. J., **651**, L69–L72, 2006.

[13] " Highly significant detection of solar neutrons on 2005 September 7", Watanabe, K. *et al.*, Adv. Space Res., **39**, 1462–1466, 2007.

[14] " A solar neutron telescope in Tibet and its capability examined by the 1998 November 28th event", Muraki, Y. *et al.*, Astroparticle Phys., **28**, 119–131, 2007.

[15] " Simultaneous detection of high-energy solar neutrons and protons at Chacaltaya observatory on April 15, 2001", Muraki, Y. *et al.*, in Proc. 30th Int. Cosmic Ray Conf, Merida, **1**, 25–28, 2007.

[16] " Search for solar neutrons associated with series of X-class flares during the declining period of solar cycle 23", Matsubara, Y. *et al.*, in Proc. 30th Int. Cosmic Ray Conf, Merida, **1**, 29–32, 2007.

[17] " Ion acceleration and neutral emission mechanisms for 2005 September 7 flare", Watanabe, K. *et al.*, in Proc. 30th Int. Cosmic Ray Conf, Merida, **1**, 45–48, 2007.

[18] " Emission profile of solar neutrons obtained from the ground-based observations for the 7 September 2005 event", Sako, T. *et al.*, in Proc. 30th Int. Cosmic Ray Conf, Merida, **1**, 53–56, 2007.

[19] " Energy spectrum for the solar neutron event of September 7 2005, derived from the SNT at Sierra Negra", Gonzalez, L. X. *et al.*, in Proc. 30th Int. Cosmic Ray Conf, Merida, **1**, 57–60, 2007.

[20] " Status of the world-wide network of solar neutron telescopes in solar cycle 24", Matsubara, Y. *et al.*, in Proc. 31st Int. Cosmic Ray Conf, Lodz, **1**, On Conference homepage, 2009.

[21] " Detection of high-energy solar neutrons and protons by ground level detectors on April 15, 2001", Muraki, Y. *et al.*, Astropart. Phys., **29**, 229–242, 2008.

[22] " Solar neutron events as a tool to study particle acceleration at the Sun", Valdes-Galicia, J. F. *et al.*, Adv. Space Res., **43**, 565–572, 2009.

[23] " Physics of ion acceleration in the solar flare on 2005 September 7 determines γ-ray and neutron production", Watanabe, K. *et al.*, Adv. Space Res., **44**, 789–793, 2009.

[24] " Observation of solar neutrons associated with the large flare on 1991 June 4", Muraki, Y. *et al.*, ApJ, **400**, L75-L78 , 1992.

[25] " Observation of an energetic radiation burst from mountain-top thunderclouds", H. Tsuchiya *et al.*, Phys. Rev. Lett. **102**, 255003 (2009), Citation Index:13.

[26] Nishita, C., K. Osada, K. Matsunaga, Y. Iwasaka, e, J. Geophys. Res., **113**, D06202, doi:10.1029/2007JD009302, 2008.

"Nucleation mode particles in up-slope valley winds at Mt. Norikura, Japan: implications for the vertical extent of new particle formation events in the lower tropospher", Nishita, C., K. Osada, K. Matsunaga, Y. Iwasaka, J. Geophys. Res., **113**, D06202, doi:10.1029/2007JD009302, 2008.

[27] "Temporal variation of water-soluble ions of free tropospheric aerosol particles over central Japan", Osada, K., Kido, M., Nishita, C., Matsunaga, K., Iwasaka, Y., Nagatani, M., Nakada, H., Tellus, **59B**, 742-754, 2007.

[28] "Number-size distributions of free tropospheric aerosol particles at Mt. Norikura, Japan: effects of precipitation and air-mass transportation pathways", Nishita, C., K. Osada, K. Matsunaga, Y. Iwasaka, J. Geophys. Res., 112, doi:10.1029/2006JD007969, 2007.

[29] " Observations of total ozone and UV solar radiation with Brewer spectrophotometers on the Norikura mountains in 2009.", Ito, M., M. Takano, H. Oguri, M. Takita, H. Shimodaira and H. Ishitsuka, Jour. of the Aerological Observatory, **69**, 41-54 2011.

[30] " Observations of total ozone and UV solar radiation with Brewer spectrophotometers on the Norikura mountains, Northern Japanese Alps, from 2009.", Ito, M., S. Shimizu, Y. Noto, T. Shimamura, M. Takano, M. Takita, H. Shimodaira and H. Ishitsuka, The 13th WMO Biennial Brewer Workshop, Beijing, China in 2011, 2011.

[31] " Total ozone and UV solar radiation with Brewer spectrophotometers at Norikura of Northern Japanese Alps, in recent three years.", Ito, M., S. Shimizu, Y. Noto, T. Shimamura, M. Takita, H. Shimodaira and H. Ishitsuka, Jour. of the Aerological Observatory, **70**, in contribution.

[32] "Needle browning and death in Pinus pumila in the alpine region of central Japan were not related to mechanical damage of cuticle and cuticle thickness.", Nakamoto A., Ikeda T., Maruta E., Can. J. For. Res. 42, 167-178 (2012).

[33] "Needle traits of an evergreen, coniferous shrub growing at wind-exposed and protected sites in a mountain region: does Pinus pumila produce needles with greater mass per area under wind-stress conditions?", Nagano S., Nakano T., Hikosaka K and Maruta E., Plant Biology 11(Suppl.1), 94-100, (2009).

AKENO OBSERVATORY

Introduction

The Akeno Observatory is situated in Akeno of Hokuto-city, 20 km northwest of Kofu and 130 km west of metropolitan Tokyo. The location is at the longitude of 138.5°E and the latitude of 35.8°N. The altitude is ∼900 m above sea level. It was established in 1977 as a research center for air shower studies in the very high energy region, and it has been administered by the ICRR as a facility of joint-university-use.

Akeno Air Shower Experiments

The Akeno Air Shower Experiment started in 1979 with an array covering 1 km^2 area (the 1 km^2 array, see Fig.1). The array was enlarged to 20 km^2 in 1984 and was gradually expanded to Akeno Giant Air Shower Array (AGASA) of approximately 100 km^2 area by 1990. The AGASA was built

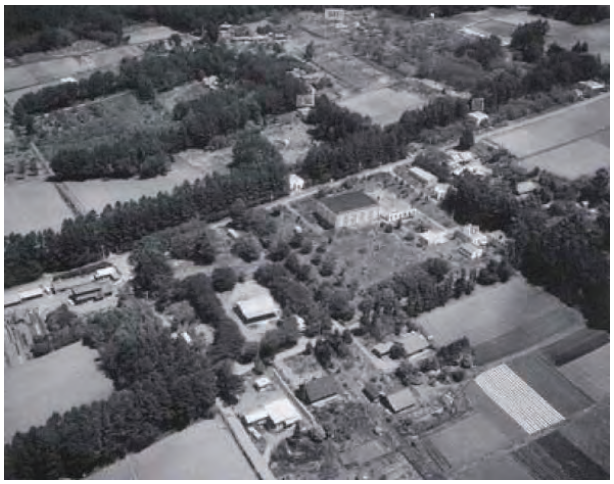

Fig. 1. Aerial View of Akeno Observatory and 1 km^2 Array Area

to detect Ultra-High Energy Cosmic Rays (UHECRs) in the energy range of 10^{20} eV.

One of the distinctive features of Akeno experiments is that the measurements were made over five decades of energies well covering 10^{15} eV - 10^{20} eV by using both the surface detector for electromagnetic component, and the shielded detector for muon component (Fig.2). The wide energy coverage was accomplished by the arrays of scintillation detectors of various inter-detector spacings from 3 m to 1 km and with different triggering conditions. This feature of Akeno air shower measurement is well demonstrated in Fig.3, in which the spectra from Akeno 1 km^2 array for $10^{14.5}$ eV - $10^{18.8}$ eV [10] and AGASA for $10^{18.5}$ eV - $10^{20.3}$ eV [11] are plotted.

*[10] M. Nagano et al., J. Phys. **G10**, 1295 (1984); M. Nagano et al., J. Phys. **G18**, 423 (1992).
*[11] M. Takeda et al., Astropart. Phys. **19**, 447 (2003).

Fig. 2. One of the muon detector housings with concrete shielding.

AGASA

The AGASA was composed of 111 surface detectors, each with plastic scintillator of 2.2 m^2 area and 5 cm thickness. The counters were deployed with ∼1 km spacing covering the ground area of about 100 km^2 in the suburban area of Akeno, outside of the observatory campus. All counters were connected with optical fibers for the timing measurement and digital data transfer to the observatory. The AGASA served as the largest air shower array in the world since its commissioning in 1990 until it stopped data taking in January 2004, when the construction of the succeeding experiment, Telescope Array (TA), started in Utah. It was dismantled in 2007 together with other Akeno air shower arrays.

An exposure of 5.8 $\times$ 10^{16} m^2 s sr above 10^{19} eV was accumulated by AGASA in 13 years of operation. Extensive air showers with zenith angles smaller than 45° and with core locations inside the array area were used for the analysis. The AGASA reported an extension of the energy spectrum beyond the predicted Greisen-Zatsepin-Kuzmin (GZK) cutoff in 1998 [12] and a total of eleven UHECR events were observed above 10^{20} eV by 2003.

Measurement of UHECRs

Since the AGASA measurement in 1998, High Resolution Fly's Eye (HiRes) [13], Pierre Auger Observatory (PAO) [14], and Telescope Array (TA) [15] measured the energy spectra of UHECRs with higher statistics.

The HiRes observed the UHECR using the fluorescence telescope. The PAO and TA measure the spectrum using the surface array consisting of either water tanks (PAO) or plastic

*[12] M. Takeda et al., Phys. Rev. Lett. **81**, 1163 (1998).
*[13] R.U. Abbasi et al., Phys. Rev. Lett. **100**, 101101 (2008).
*[14] J. Abraham et al., Phys. Lett. **B685**, 239 (2010).
*[15] T. Abu-Zayyad et al., arXiv:1205.5067v1 (2012).

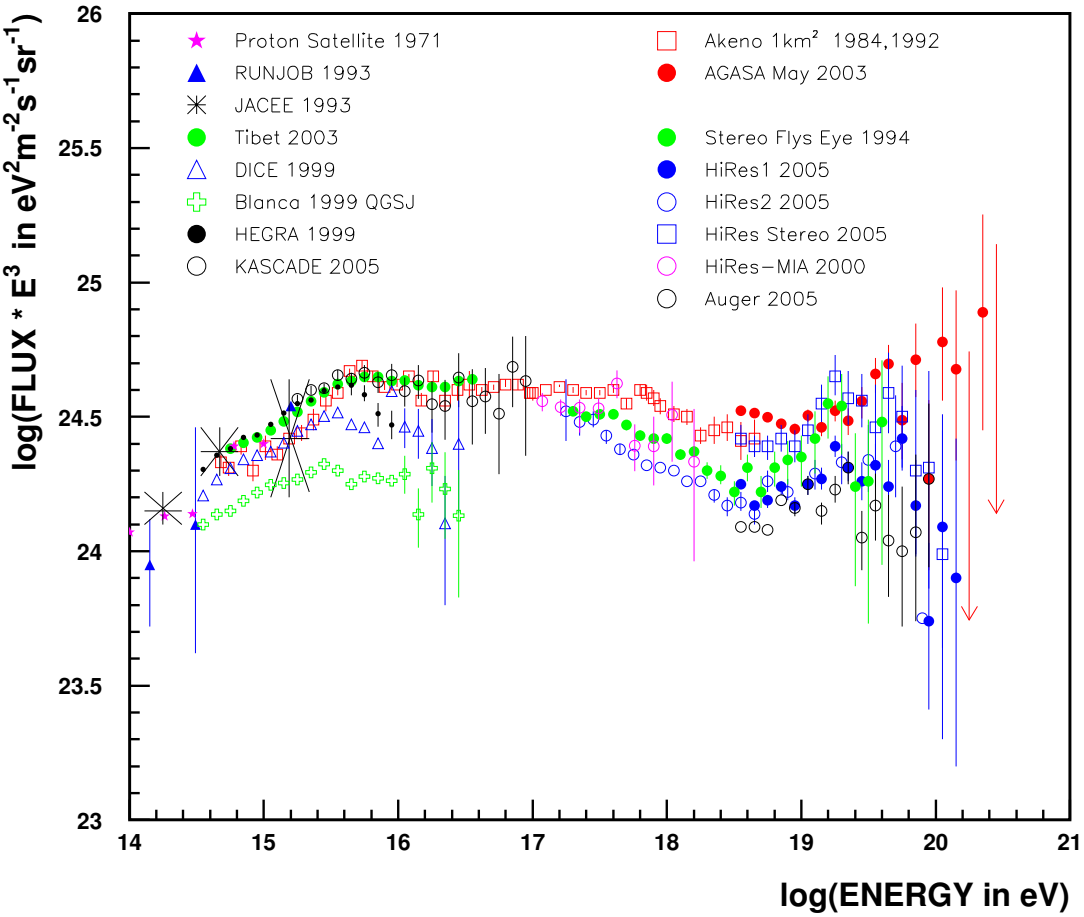

Fig. 3. Akeno energy spectrum measurements for 10^{15} eV - 10^{20} eV.

scintillators (TA), but the energy scale of the array is determined by the fluorescence telescope using a subset of events observed by the fluorescence telescope and surface array at the same time. The adoption of the energy scale by the fluorescence telescopes is based on its small dependence on the air shower simulation.

The energy spectra above 10^{18} eV by AGASA and other experiments are compiled and compared by the working group represented by UHECR experiments in the UHECR-2012 symposium held at CERN for Feb. 13th - 16th, 2012 [16]. The result is plotted in Fig.4 with the energy scale of each experiment adjusted to a reference energy, which is set halfway between the PAO and TA/HiRes.

Following factors were applied for the energy scale; $\times 1.10$ for PAO, $\times 0.91$ for TA and HiRes, $\times 0.65$ for AGASA and $\times 0.56$ for Yakutsk.

As seen in Fig.4, the overall agreement between experiments is good, and a "dip" structure was seen around $10^{18.7}$ eV by all experiments. The HiRes, PAO and TA confirmed a strong flux suppression above approximately $10^{19.7}$ eV. Although the AGASA spectrum does not demonstrate the cutoff structure, the number of events above 10^{20} eV became only two after the energy rescaling, making the claim of the extended spectrum statistically insignificant. The estimate of systematic uncertainty of the energy measurement is approximately 20% for all the experiments, and rescalings for the TA/HiRes and PAO are within this limit. Rescaling of the surface array energy, $\times 0.65$ for AGASA and $\times 0.56$ for Yaktsuk, indicates that there exist larger systematic uncertainties than originally estimated by running the air shower simulation. This difference of energy scale obtained by the surface array and by the fluorescence telescope remains as a basic question in the understanding of the air shower phenomena.

Recent Research Activities

The study of UHECRs by AGASA in Akeno was succeeded by the Telescope Array (TA) experiment in Utah, USA since 2008. After the cessation of AGASA, the Akeno observatory has been used for small scale cosmic ray experiments, astrophysical observations and as a test and maintenance facility of TA by the ICRR and university researchers. Research activities in JFY 2012 (April 2012 - March 2013) are described in the following.

*[16] http://indico.cern.ch/conferenceDisplay.py?confId=152124

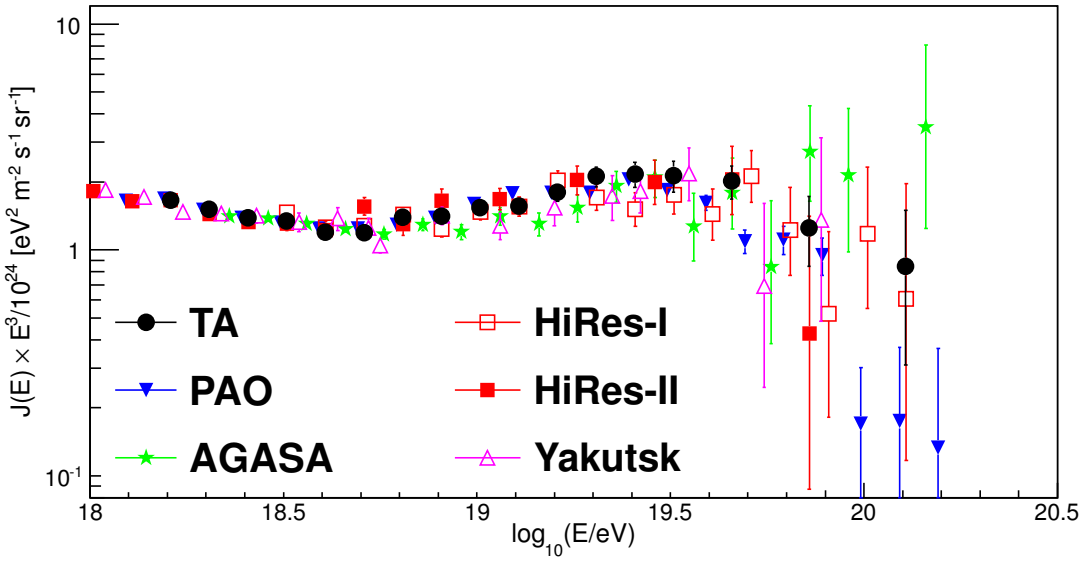

Fig. 4. Recent compilation of UHECR energy spectra. The energy scale of each experiment is adjusted as described in the text.

Research and development for the Telescope Array observation in Utah by the TA collaboration

All the fluorescence imaging cameras and a part of the surface detectors of TA were assembled in the Akeno observatory by the TA collaboration team. The detectors were tested in Akeno and shipped to the Utah observation site for the installation. All the unit mirrors of the TA fluorescence telescope were tested in Akeno and the atmospheric monitoring lidar of TA using YAG laser was developed in Akeno. In JFY 2012, totally 35 TA SDs were assembled and were sent to Utah. A part of the experimental hall was prepared for the test and temporary storage of KAGRA gravitational antenna equipment.

Observation by the multi-color imager for transients, survey and monstrous explosions (MITSuME) by N. Kawai (Tokyo Institute of Technology) et al.

One of the three MITSuME robotic telescopes was installed in the Akeno observatory in 2003 on the roof of the unused concrete muon house. The telescope has an aperture of 50 cm, an FOV of 28' $\times$ 28' and is equipped with a tricolor CCD camera capable of $g'R_CI_C$-bands photometry. It is operated remotely from the Tokyo Tech using dedicated ADSL connections. Upon receiving a GRB alert from Swift or Fermi satellite, it quickly directs the telescope (9°/s maneuverability) toward the GRB direction, and makes a prompt observation of the GRB and its afterglow. Since its commissioning in 2004, the MITSuME telescope in Akeno has been making more than $\sim$10 GRB follow-up observations every year, and detected more than 10 GRB afterglows. Between January and December in 2012, the MITSuME was triggered by 29 GRBs including GRBs during cloudy days and succeeded to observe afterglows of 2 GRBs. It also followed up a new black hole, MAXI J1910-057. It has been joining the multi-wavelength campaign for observing AGNs and other transient objects as well. The ADSL line at the telescope site was replaced to optical fiber line.

Observation of galactic cosmic rays by large area muon telescope by S. Shibata (Chubu University) et al.

Four layers of proportional counter telescopes, each with 25 m^2 area, were installed in three muon houses in Akeno (Fig.2) and have been continuously measuring the cosmic ray muons since 2003. The mode energy of the primary cosmic rays is approximately 25 GeV corresponding to 2m thick concrete ceiling of the muon house and the latitude of Akeno observatory. The measurement in Akeno is combined with a simultaneous measurement in Ooty, India, and the modulation effects of galactic cosmic rays by the solar activity such as the Forbush decrease and its precursor have been continuously monitored [17]. In JFY 2012, the observation was continued.

Research and development for a small atmospheric Cherenkov telescope in Akeno observatory by T. Yoshikoshi, M. Ohishi (ICRR) and K.Nishijima (Tokai University) et al.

A small alt-azimuth telescope is being setup in Akeno for prototype tests with atmospheric Cherenkov observations of gamma rays [18]. Refurbishing of the telescope control system, the unit mirror and optics was made in 2010 and 2011. Aluminum deposit was performed on all remaining mirrors. The mirrors were mounted on the telescope, for which the operation was tested.

*[17] T. Nonaka.et al, Proc. of the 29th ICRC, **1**, 363-366 (2005).
*[18] T. Yoshikoshi et al., Proc. of the 32nd ICRC, Beijing, **9**, 226-229 (2011).

KAMIOKA OBSERVATORY

Kamioka observatory is located at 1000 m underground (2700 m water equivalent) in the Kamioka Mine, Gifu prefecture, about 200 km west of Tokyo. The observatory was established in 1995 in order to operate Super-Kamiokande experiment (SK). The underground laboratories are located under Mt.Ikeno-yama and accessible to the experimental site through a 1.7 km horizontal tunnel. The observatory also has surface research buildings and a dormitory located at the distance of 15 minutes drive from the entrance of the underground laboratories.

The Super-Kamiokande experiment had discovered neutrino oscillations through the observations of atmospheric and solar neutrinos (see the section for Neutrino and Astroparticle Division). The atmospheric neutrino oscillation was confirmed by the long baseline neutrino oscillation experiment, K2K, using accelerator neutrino beam, which was conducted between 1999 and 2004. A new long baseline neutrino oscillation experiment (the T2K experiment) using a high intensity beam, 50 times of the K2K neutrino beam, by the J-PARC proton accelerator has started in 2009. In 2011, the experiment has observed 6 ν_e appearance events indicating non-zero θ_{13} which was as yet determined the last neutrino oscillation parameter. In 2012, the collaboration accumulated more electron neutrino appearance events and strengthen the discovery of non-zero θ_{13}.

The low cosmic ray flux and low seismic noise environment in the underground site enables us to conduct various researches. There is a 100 m long laser interferometer, which is a proto-type of the 3 km gravitational wave antenna (see section of Astrophysics Gravity Division) under construction. Using the low radioactive background environment in the Kamioka Mine, a dark matter experiment, called XMASS is operated in Lab-C. The XMASS group constructed a 800kg liquid xenon detector and started commissioning run in late 2010. In 2012 they have started an improvement of the detector to remove unexpected backgrounds. The R&D study of a tracking type detector for dark matter detection lead by the Kobe University group (the NEWAGE experiment) has also been performed in Lab-B. The commissioning run of the CANDLE experiment in Lab-D (Osaka Univ.), a double beta decay experiment is now conducted. The study to improve the neutrino detection sensitivity by adding gadolinium to Super-Kamiokande is on going. Especially in 2010, a new 200 ton test tank in Lab-E dedicated for the R&D study of the gadolinium project was completed and continuously used for the feasibility study. In order to support those experiments and also related R&D works, the Observatory is equipped with low background Germanium detector in Lab-1 and Lab-A, ICP-MS and so on to measure extremely low radioactive backgrounds.

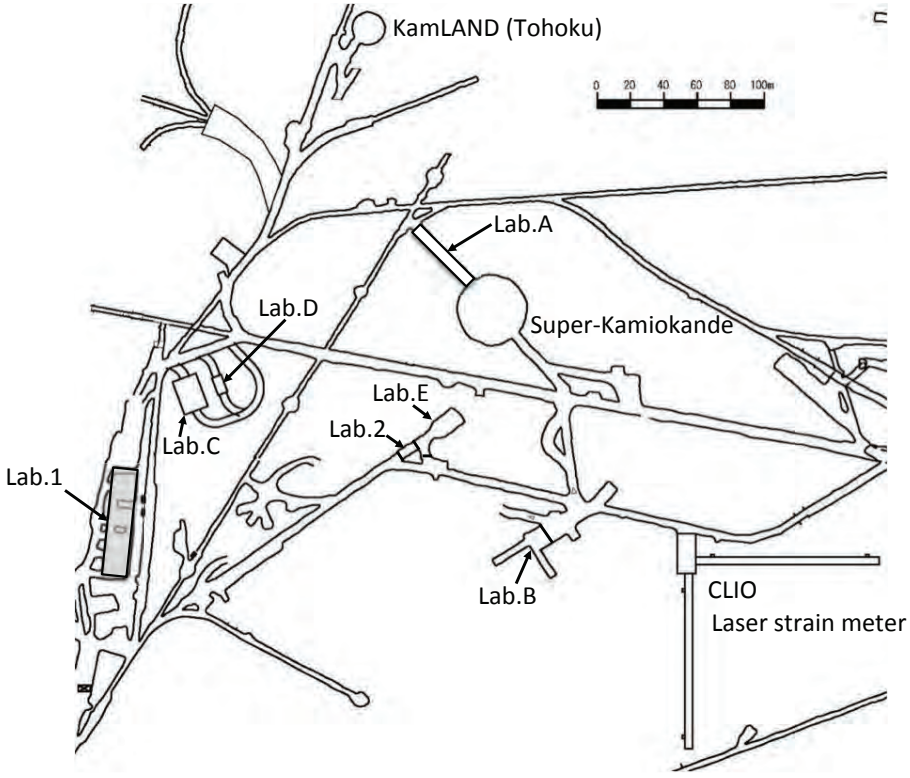

Fig. 1. Kamioka Underground Observatory.

RESEARCH CENTER FOR COSMIC NEUTRINOS

The Research Center for Cosmic Neutrinos (RCCN) was established in April, 1999. The main objective of this center is to study neutrinos based on data from various observations and experiments. In order to promote studies of neutrino physics, it is important to provide the occasion to discuss theoretical ideas and experimental results on neutrino physics. Therefore, one of the most important tasks of this center is the organization of neutrino-related meetings. On March 15, 2013, we hosted this year's domestic neutrino workshop, whose topics were (1) the IceCube observation of very high energy neutrinos and (2) "θ_{13}" and future neutrino oscillation experiments. About 40 physicists participated in this meeting.

Members of this center have been involved in the Super-Kamiokande and T2K experiments, carrying out researches in neutrino physics. (Please see the Super-Kamiokande and T2K pages for the scientific results.) It is recognized that atmospheric neutrino data give one of the most precise pieces of information on neutrino oscillations. Therefore, several new experiments have been proposed in the world. In 2012, we calculated the atmospheric neutrino flux at the potential future experimental sites; the INO, South Pole and Pyhasalmi sites.

It is important that the general public knows about the achievements of the present science. For this reason, we hold public lectures every year. From FY 2009, two public lectures per year have been co-sponsored by ICRR and the Kavli Institute for the Physics and Mathematics of the Universe. The spring lecture is co-organized by RCCN and the Public Relation Office of ICRR. The 2012 public lecture was held on April 14, 2012. The topics of the lectures were observational cosmology with the Subaru Telescope and the TeV gamma-ray astronomy.

RCCN, together with the computer committee of ICRR, is in charge of operating the central computer system in ICRR. In FY 2012, the system was operated without any serious trouble. The system has been highly utilized for the analyses and simulations of various researches in cosmic-ray physics. RCCN also supports the users of the computer system, including physicists in the cosmic ray community in Japan.

Since 2004, RCCN has been acting as a body for accepting the ICRR inter-university programs related to the low-background underground facility in the Kashiwa campus. The facility is currently equipped with 4 Ge detectors mainly for the measurements of cosmic radioactive isotopes. The scientific activities related to this facility is described elsewhere.

APPENDICES

A. ICRR Workshops and Ceremonies

2nd Korea Japan workshop on KAGRA

Date: May 28-29, 2012
Place: ICRR, the University of Tokyo, Japan

Outline: The workshop consisted of three sessions: Current status of the collaboration research, Relevant research, and Discussion about the future collaboration. A lab tour at ICRR was also held. In the discussion session, we agreed to continue/initiate the collaboration research in the field of Laser, Data analysis, Data branch, Vibration isolation, Interferometer, Quantum optics, and Detector characterization for KAGRA.

Participants: 26 participants.

EliTES 1st General Meeting

Date: Oct 3-4, 2012
Place:Eureopean Union delegation in Japan & Sanjo Conference Hall, the University of Tokyo, Japan

Outline: The ELiTES program is initiated by partners; European Gravitational Observatory sponsored by Italy and France, ICRR (Japan), Universit di Roma "La Sapienza" (Italy), Friedrich-Schiller Universitaet, Jena (Germany), University of Glasgow (UK), FOM (Nitherland), MPG (Germany), Universit degli Studi del Sannio (Italy), University of West Scotland (UK).

The acronym ELiTES stands for ET LCGT interferometric Telescopes: Exchanges of Scientists. It is an initiative supported (2012-2016) by the European Commission under FP7-people. In particular, ELiTES is supported as IRSES: International Research Staff Exchange Scheme (RISE in H2020). ELiTES supports the exchange of GW scientists between EU and Japan (and the Japanese counterpart set-up a mirror initiative, consequent to ELiTES). ELiTES idea born during the second ET general meeting, focusing on the ET-KAGRA common aspects:

- Cryogenics and Underground facilities
- Very active and productive links are sustained through

ELiTES consists of four working packages, WP1: Suspensions design and test, WP2: Suspensions materials and fibers, WP3: Infrastructures & Vacuum apparatuses and WP4: organization. Under this ELiTES program, we have one technical workshop in Europe and one general meeting in Japan. In this financial year, ICRR hosted the first general meeting in Tokyo. Since the program is sponsored by EU, the first day was held in EU representative house in Tokyo (as shown in the picture). First half of the beginning session of the first day consisted of invited talks. First one was given by Dr. Barbara Rhode who is the Head of Science and Technology Section of the delegation of EU to Japan (EU house in Tokyo). The second one was given by the director of the Scientific Research Institutes Devision, Research Promotion Bureau, Ministry of Eduation, Culture, Sports, Science and Technology. The third one was by Science & Technology Attache of Embassy of Italy, Dr. Arberto Mengoni. The second day, the meeting venue was moved to Sanjo Hall in Hongo campus of UTokyo.

Participants: 80people 7 countries.

3rd Japan Korea workshop on KAGRA

Date: Dec 21-22, 2012
Place: Sogang University, Seoul, Korea

Outline: The workshop consisted of four sessions: Plenary talk, Current status of collaboration research, Relevant research, and Discussion about the future collaboration. A lab tour at Sogang University was also held. In the Discussion session, we agreed to continue the existing collaboration research, and also agreed that we should keep submitting individual proposals and have more exchange of people to promote the collaboration research.

Participants: 20 participants.

B. ICRR Seminars

1. May 22, 2012: Alessandro De Angelis (Udine University), "Gamma Ray Astronomy and Fundamental Physics"
2. May 30, 2012: Naba Mondal (Tata Institute of Fundamental Research), "India-Based neutrino Observatory (INO) Project"
3. June 14, 2012: Rieko Momose (ICRR, the University of Tokyo), "The resolved Kennitutt-Schmidt law in nearby galaxies"
4. June 26, 2012: Yousuke Itoh (Research Center for the Early Universe, the University of Tokyo),"Gravitational lensing of gravitational waves"
5. June 27, 2012: Mohammad Sajjad Athar (Aligarh Muslim University), "Importance of cross section in predicting the neutrino event rates"
6. July 5, 2012: Akio Hosoya (Tokyo Institute of Technology), "Uncertainty Relation and Weak Value"
7. July 27, 2012: Kimiaki Masuda (Solar-Terrestrial Environment Laboratory, Nagoya University), "A signature of cosmic-ray increase in AD775 from tree rings in Japan"
8. August 24, 2012: Shoei Nakayama (ICRR, University of Tokyo), "Latest results from T2K"
9. August 30, 2012: Aya Ishihara (Chiba University), "Searches for ultra-high energy cosmic neutrinos with the IceCube neutrino detector"
10. September 19, 2012: Mineo Imamura (National Museum of Japanese History), "Variations of atmospheric 14C and the climate in Yayoi period"
11. October 17, 2012: Stefan Goßler (Leibniz Universität Hannover and Max-Planck-Institute for Gravitational Physics), "Gravitational-wave detection"
12. October 22, 2012: Yifang Wang (Institute of High Energy Physics, Chinese Academy of Sciences), "Latest Daya Bay results and its future prospects"
13. November 8, 2012: Yasushi Suto (The University of Tokyo), "Deciphering colors of a pale blue dot"
14. November 9, 2012: George W.-S. Hou (National Taiwan University), "NuTel, Ashra-1, and NTA"
15. November 16, 2012: David Reitze (California Institute of Technology & University of Florida), "The Coming Global Gravitational-wave Detector Network with an Emphasis on Advanced LIGO"
16. December 4, 2012: Takayuki Saitoh (Tokyo Institute of Technology), Dr. Makoto Miyoshi (National Astronomical Observatory of Japan), "Part I: Flaring up of the Compact Cloud G2 (Saitoh)", "Part II: Caravan Project for Sgr A* Observation (Miyoshi)"
17. December 4, 2012: Anatael Cabrera (IN2P3/CNRS-APC, Paris), "Reactor θ_{13}: the Ultimate Measurement?"

C. List of Publications

(a) Papers Published in Journals

1. "Radon Removal from Gaseous Xenon with Activated Charcoal", XMASS Collaboration (K. Abe (Tokyo U., ICRR) et al.)., Nucl. Instr. and Meth. in Phys.Res. A**661** 50-57 (2012).
2. "Development of New Data Acquisition System for Nearby Supernova Bursts at Super-Kamiokande", T. Tomura et al., Physics Procedia **37**, 1398 (2012).
3. "Light WIMP search in XMASS", XMASS Collaboration (K. Abe (Tokyo U., ICRR) et al.)., Phys.Lett. B**719** 78-82 (2013), [arXiv:1211.5404].

4. “XMASS detector”, XMASS Collaboration (K. Abe (Tokyo U., ICRR) et al.)., Accepted at Nucl. Instr. and Meth. in Phys.Res. A, [arXiv:1301.2815v1].

5. “Measurements of the T2K neutrino beam properties using the INGRID on-axis near detector”, T2K Collaboration(K.Abe et al.), Nucl.Instrum.Meth. A**694** 211-223 (2012), [arXiv:1111.3119].

6. “First Muon-Neutrino Disappearance Study with an Off-Axis Beam”, T2K Collaboration(K.Abe et al.), Phys. Rev. D**85** 031103 (2012), [arXiv:1201.1386].

7. “The T2K Neutrino Flux Prediction”, T2K Collaboration(K.Abe et al.), Phys.Rev. D**87** (2013) 012001, [arXiv:1211.0469].

8. “Measurement of the Inclusive NuMu Charged Current Cross Section on Carbon in the Near Detector of the T2K Experiment”, T2K Collaboration(K.Abe et al.), Submitted to Phys. Rev. D, [arXiv:1302.4908v1].

9. “A Measurement of the Appearance of Atmospheric Tau Neutrinos by Super-Kamiokande”, Super-Kamiokande Collaboration (K. Abe (Tokyo U., ICRR & Tokyo U., IPMU) et al.)., Phys. Rev. latt. [arXiv:1206.0328].

10. “Supernova relic neutrino search at super-Kamiokande”, Super-Kamiokande Collaboration(K. Bays et al.), Phys. Rev. D**85** 052007 (2012)., [arXiv:1111.5031].

11. “Search for proton decay via p$\rightarrow \mu^+ + K^0$ in Super-Kamiokande I, II, and III, Super-Kamiokande”, Collaboration (Regis, C et al.), Phys. Rev. D**86** 012006 (2012), [arXiv:1205.6538].

12. “Search for Nucleon Decay into Charged Anti-lepton plus Meson”, in Super-Kamiokande I and II, Super-Kamiokande Collaboration (H. Nishino et al.), Astropart.Phys. **36** 131-136 (2012), [arXiv:1203.4030].

13. “Search for GUT Monopoles at Super-Kamiokande”, Super-Kamiokande Collaboration (K. Ueno (Tokyo U., ICRR) et al.), Phys. Rev. D**85** 112001 (2012), [arXiv: 1203.0940].

14. “On the origin of the Kamiokande experiment and neutrino astrophysics”, T. Kajita, M. Koshiba and A. Suzuki, Eur. Phys. J. H**37**, 33-73 (2012).

15. “Atmospheric neutrinos”, Takaaki Kajita, Adv. High Energy Phys. 504715, 2012 (2012).

16. “Atmospheric neutrino flux at INO, South Pole and Pyhasalmi”, M. Sajjad Athar, M. Honda, T. Kajita, K. Kasahara and S. Midorikawa, Phys. Lett. B**718**, 1375-1380 (2013), [arXiv:1210.5154[hep-ph]].

17. “Very high energy gamma-ray observation of the peculiar transient event Swift J1644+57 with the MAGIC telescopes and AGILE”, MAGIC Collaboration (K.Saito, M.Teshima, et al.) Astronomy & Astrophysics, Volume 552, id.A112, p. 6 (2013).

18. “Gamma-ray burst science in the era of the Cherenkov Telescope Array”, S. Inoue, M.Teshima et al. Astroparticle Physics, Volume 43, p. 252-275 (2013).

19. “Introducing the CTA concept”, CTA Consortium (M.Hayashida, H.Ohoka, M. Ohishi, K.Saito, M. Teshima, T. Yoshikoshi), Astroparticle Physics, Volume 43, p. 3-18 (2013).

20. “Monte Carlo design studies for the Cherenkov Telescope Array”, T.Yoshikoshi et al., Astroparticle Physics, Volume 43, p. 171-188 (2013).

21. “Observations of the magnetars 4U 0142+61 and 1E 2259+586 with the MAGIC telescopes”, MAGIC Collaboration (K. Saito, M.Teshima et al.) Astronomy & Astrophysics, Volume 549, id.A23, 4 pp (2013).

22. “Light sensors selection for the Cherenkov Telescope Array: PMT and SiPM”, M.Shayduk, M.Teshima et al., Nuclear Instruments and Methods in Physics Research A, Volume 695, p. 109-112 (2012).

23. “SiPM interdisciplinary application in the fields of astroparticle physics and bio-molecular science”, H. Miyamoto, M.Teshima et al., Nuclear Instruments and Methods in Physics Research A, Volume 695, p. 87-90 (2012).

24. “Large area UV SiPMs with extremely low cross-talk”, B. Dolgoshein, M.Teshima et al., Nuclear Instruments and Methods in Physics Research A, Volume 695, p. 40-43 (2012).

25. “Discovery of VHE -rays from the blazar 1ES 1215+303 with the MAGIC telescopes and simultaneous multi-wavelength observations”, MAGIC Collaboration (K. Saito, M. Teshima et al.) Astronomy & Astrophysics, Volume 544, id.A142, 10 pp (2012).

26. “MAGIC observations of the giant radio galaxy M 87 in a low-emission state between 2005 and 2007”, MAGIC Collaboration (K. Saito, M.Teshima et al.), Astronomy & Astrophysics, Volume 544, id.A96, 8 pp (2012).

27. “High zenith angle observations of PKS 2155-304 with the MAGIC-I telescope”, MAGIC Collaboration (K.Saito, M.Teshima et al.), Astronomy & Astrophysics, Volume 544, id.A75, 9 pp (2012).

28. “Detection of VHE -Rays from HESS J0632+057 during the 2011 February X-Ray Outburst with the MAGIC Telescopes”, MAGIC Collaboration (K. Saito, M.Teshima et al.), The Astrophysical Journal Letters, Volume 754, Issue 1, article id. L10, 6 pp (2012).

29. “Mrk 421 active state in 2008: the MAGIC view, simultaneous multi-wavelength observations and SSC model constrained”, MAGIC Collaboration (K.Saito, M.Teshima et al.), Astronomy & Astrophysics, Volume 542, id.A100, 11 pp (2012).

30. “Constraining cosmic rays and magnetic fields in the Perseus galaxy cluster with TeV observations by the MAGIC telescopes”, MAGIC Collaboration (K. Saito, M. Teshima et al.), Astronomy & Astrophysics, Volume 541, id.A99, 12 pp (2012).

31. “Morphological and spectral properties of the W51 region measured with the MAGIC telescopes”, MAGIC Collaboration (K. Saito, M.Teshima et al.), Astronomy & Astrophysics, Volume 541, id.A13, 11 pp (2012).

32. “A Tunable Delay Line for Fast Analog Pulses as Key Element of a New Sum-Trigger for Cherenkov Telescopes”, D. Haefner, M. Teshima et al., IEEE Transactions on Nuclear Science, vol. 59, issue 2, pp. 289-293 (2012).

33. “Phase-resolved energy spectra of the Crab pulsar in the range of 50-400 GeV measured with the MAGIC telescopes”, MAGIC Collaboration (K. Saito, M.Teshima et al.), Astronomy & Astrophysics, Volume 540, id.A69, 6 pp (2012).

34. “Searches for very high energy gamma rays from blazars with CANGAROO-III telescope in 2005-2009”, CANGAROO Collaboration (M. Ohishi, T. Yoshikoshi et al.), Astroparticle Physics, Volume 35, Issue 9, p. 563-572 (2012).

35. “Determination of the Point-spread Function for the Fermi Large Area Telescope from On-orbit Data and Limits on Pair Halos of Active Galactic Nuclei”, Fermi Collaboration (M. Hayashida et al.), The Astrophysical Journal, Volume 765, Issue 1, article id. 54, 19 pp. (2013).

36. “Search for anisotropy of Ultrahigh energy cosmic rays with the Telescope Array experiment”, T. Abu-Zayyad et al. (TA collaboration), Astrophys. J. **757**:26(11pp), 2012, [arXiv:1205.5984v1[astro-ph.HE]].

37. ”The energy spectrum of Telescope Array’s Middle Drum detector and the direct comparison to the High Resolution Fly’s Eye experiment”, T. Abu-Zayyad et al. (TA collaboration), Astropart. Phys. **39-40**,109-119 (2012), [arXiv:1202.5141v1[astro-ph.IM]].

38. “The surface detector array of the Telescope Array experiment”, T. Abu-Zayyad et al. (TA collaboration), Nucl. Instr. and Methods A**689**, 87-97 (2012).

39. “Cherenkov τ shower earth-skimming method for PeV-EeV ν_τ observation”, Asaoka, Y. and Sasaki, M., Astroparticle Physics, 2013, [arXiv:1202.5656 [astro-ph.HE]].

40. “Is the large-scale sidereal anisotropy of the galactic cosmic-ray intensity really instable at TeV energies?”, M. Amenomori et al., Astroparticle Physics, **36**, 237-241 (2012).

41. “Calculation of thermal radiation input via funneling through a duct shield with baffles for KAGRA”, Yusuke Sakakibara, Nobuhiro Kimura, Kazuhiro Yamamoto, Toshikazu Suzuki, Takayuki Tomaru, Shinji Miyoki,Takashi Uchiyama, Kazuaki Kuroda, Classical and Quantum Gravity, IOP Publishing, **29** 205019, (2012).

42. “Material and surface processing in J-PARC vacuum system”, Y. Saito, F. Naito, C. Kubota, S. Meigo, H. Fujimori, N. Ogiwara, J. Kamiya, M. Kinsho, Z. Kabeya, T. Kubo, M. Shimamoto, Y. Sato, Y. Takeda, M. Uota, Y. Hori, VACUUM 86 817-821 (2012).

43. “Reduction of thermal fluctuations in a cryogenic laser interferometric gravitational wave detector”, Takashi Uchiyama, Shinji Miyoki, Souichi Telada, Kazuhiro Yamamoto, Masatake Ohashi, Kazuhiro Agatsuma, Koji Arai, Masa-Katsu Fujimoto, Tomiyoshi Haruyama, Seiji Kawamura, Osamu Miyakawa, Naoko Ohishi, Takanori Saito, Takakazu Shintomi, Toshikazu Suzuki, Ryutaro Takahashi, Daisuke Tatsumi, Phys. Rev. Lett., **108** 141101 (5pp) (2012).

44. “High accuracy measurement of the quantum efficiency using radiation pressureh, Kazuhiro Agatsuma, Takumi Mori, Stefan Ballmer, Giulia DeSalvo4, Shihori Sakata, Erina Nishida, and Seiji Kawamura, J. Phys.: Conf. Ser. **363**, 012002 (2012).

45. “Development of a high power optical cavity for optomechanical QND experimenth, T Mori, K Agatsuma, S Ballmer, S Sakata, O Miyakawa, S Kawamura, A Furusawa and N Mio, J. Phys.: Conf. Ser. **363** 012015 (2012).

46. “First low-latency LIGO+Virgo search for binary inspirals and their electromagnetic counterparts”, J. Abadie, S. Kawamura, et al., Phys. Rev. D**85**, 122001 (2012).

47. “IMPLICATIONS FOR THE ORIGIN OF GRB 051103 FROM LIGO OBSERVATIONS”, J. Abadie, S. Kawamura, et al., Astrophys. J. **755**, 2 (2012).

48. “Search for gravitational waves from intermediate mass binary black holes”, J. Abadie, S. Kawamura, et al., Phys. Rev. D**85**, 102004 (2012).

49. “All-sky search for gravitational-wave bursts in the second joint LIGO-Virgo run”, J. Abadie, S. Kawamura, et al., Phys. Rev. D**85**, 122007 (2012).

50. “The characterization of Virgo data and its impact on gravitational-wave searches”, J Aasi, S. Kawamura, et al., Class. Quantum Grav. **29**, 155002 (2012).

51. “SWIFT FOLLOW-UP OBSERVATIONS OF CANDIDATE GRAVITATIONAL-WAVE TRANSIENT EVENTS”, P. A. Evans, S. Kawamura, et al., ApJS **203**, 28 (2012).

52. “SEARCH FOR GRAVITATIONAL WAVES ASSOCIATED WITH GAMMA-RAY BURSTS DURING LIGO SCIENCE RUN 6 AND VIRGO SCIENCE RUNS 2 AND 3”, J. Abadie, S. Kawamura, et al., Astrophys. J. **760**, 12 (2012).

53. “Einstein@Home all-sky search for periodic gravitational waves in LIGO S5 data”, J. Aasi, S. Kawamura, et al., Phys. Rev. D**87**, 042001 (2012).

54. “Search for gravitational waves from binary black hole inspiral, merger, and ringdown in LIGO-Virgo data from 2009-201”, J. Aasi, S. Kawamura, et al., Phys. Rev. D**87**, 022002 (2013) .

55. “Evidence for Low Extinction in Actively Star-forming Galaxies at $z > 6.5$”, Walter, F., et al., Astrophys. J., **752**, 93, 2012, [arXiv:1204.3426 [astro-ph.CO]].

56. “The First Systematic Survey for Lyα Emitters at $z = 7.3$ with Red-sensitive Subaru/Suprime-Cam”, Shibuya, T., et al., Astrophys. J., **752**, 114, 2012, [arXiv:1112.3997 [astro-ph.CO]].

57. “NIR Spectroscopy of Star-Forming Galaxies at $z \sim 1.4$ with Subaru/FMOS: The Mass-Metallicity Relation”, Yabe, K., et al., Publ. Astron. Soc. Japan, **64**, 60, 2012, [arXiv:1112.3704 [astro-ph.CO]].

58. “The Spitzer Extragalactic Representative Volume Survey (SERVS): Survey Definition and Goals”, Mauduit, J.-C., et al., Publ. Astron. Soc. Pacific, **124**, 714-736, 2012, [arXiv:1206.4060 [astro-ph.CO]].

59. “A Dual-Narrowband Survey for Hα Emitters at Redshift of 2.2: Demonstration of the Technique and Constraints on the Hα Luminosity Function”, Lee, J. C., et al., Publ. Astron. Soc. Pacific, **124**, 782-797, 2012, [arXiv:1205.0017 [astro-ph.CO]].

60. “Initial Results from Nobeyama Molecular Gas Observations of Distant Bright Galaxies”, Iono, D., et al., Publ. Astron. Soc. Japan, **64**, L2, 2012, [arXiv:1206.3840 [astro-ph.CO]].

61. “Diffuse Lyα haloes around Lyα emitters at $z = 3$: do dark matter distributions determine the Lyα spatial extents?”, Matsuda, Y., et al., Monthly Notices Roy. Astron. Soc., **425**, 878-883, 2012, [arXiv:1204.4934 [astro-ph.CO]].

62. “Intrinsic Shape of Star-forming BzK Galaxies. II. Rest-frame Ultraviolet and Optical Structures in GOODS-South and SXDS”, Yuma, S., et al., Astrophys. J., **761**, 19, 2012, [arXiv:1210.2750 [astro-ph.CO]].

63. “Physical Conditions in Molecular Clouds in the Arm and Interarm Regions of M51”, Koda, J., et al., Astrophys. J., **761**, 41, 2012, [arXiv:1210.6349 [astro-ph.CO]].

64. “Black Hole Mass and Eddington Ratio Distribution Functions of X-Ray-selected Broad-line AGNs at $z \sim 1.4$ in the Subaru XMM-Newton Deep Field”, Nobuta, K., et al., Astrophys. J., **761**, 143, 2012, [arXiv:1211.0069 [astro-ph.CO]].

65. “The Abundance of Star-forming Galaxies in the Redshift Range $8.5 - 12$: New Results from the 2012 Hubble Ultra Deep Field Campaign”, Ellis, R., et al., Astrophys. J. (Letters), **763**, L7, 2013, [arXiv:1211.6804 [astro-ph.CO]].

66. “A Water Maser and NH_3 Survey of GLIMPSE Extended Green Objects”, Cyganowski, C. J., et al., Astrophys. J., **764**, 61, 2013, [arXiv:1210.5528 [astro-ph.GA]].

67. "Nebular Attenuation in Hα-selected Star-forming Galaxies at $z = 0.8$ from the NewHα Survey", Momcheva, I. G., et al., Astron. J., **145**, 47, 2013, [arXiv:1207.5479 [astro-ph.CO]].

68. "Gas Motion Study of Lyα Emitters at $z \sim 2$ Using FUV and Optical Spectral Lines", Hashimoto, T., Ouchi, M., et al., Astrophys. J., **765**, 70, 2013, [arXiv:1206.2316 [astro-ph.CO]].

69. "New Constraints on Cosmic Reionization from the 2012 Hubble Ultra Deep Field Campaign", Robertson, B., et al., to be published in Astrophys. J., 2013, [arXiv:1301.1228 [astro-ph.CO]].

70. "First Spectroscopic Evidence for High Ionization State and Low Oxygen Abundance in Lyα Emitters", Nakajima, K., Ouchi, M., et al., to be published in Astrophys. J., 2013, [arXiv:1208.3260 [astro-ph.CO]].

71. "The UV Luminosity Function of Star-forming Galaxies via Dropout Selection at Redshifts $z \sim 7$ and 8 from the 2012 Ultra Deep Field Campaign", Schenker, M. A., et al., to be published in Astrophys. J., 2013, [arXiv:1212.4819 [astro-ph.CO]].

72. "Extended analysis of CMB constraints on non-Gaussianity in isocurvature perturbation", C. Hikage, M. Kawasaki, T. Sekiguchi and T. Takahashi, JCAP **1303**, 020 (2013) [arXiv:1212.6001 [astro-ph.CO]].

73. "Opening the window to the cogenesis with Affleck-Dine mechanism in gravity mediation", A. Kamada, M. Kawasaki and M. Yamada, Phys. Lett. B **719**, 9 (2013) [arXiv:1211.6813 [hep-ph]].

74. "Mass Splitting between Charged and Neutral Winos at Two-Loop Level", M. Ibe, S. Matsumoto and R. Sato, Phys. Lett. B **721**, 252 (2013) [arXiv:1212.5989 [hep-ph]].

75. "Smooth hybrid inflation in a supersymmetric axion model", M. Kawasaki, N. Kitajima and K. Nakayama, Phys. Rev. D **87**, 035010 (2013) [arXiv:1211.6516 [hep-ph]].

76. "Effects of power law primordial magnetic field on big bang nucleosynthesis", D. G. Yamazaki and M. Kusakabe, Phys. Rev. D **86**, 123006 (2012) [arXiv:1212.2968 [astro-ph.CO]].

77. "Chaotic Inflation with a Fractional Power-Law Potential in Strongly Coupled Gauge Theories", K. Harigaya, M. Ibe, K. Schmitz and T. T. Yanagida, Phys. Lett. B **720**, 125 (2013) [arXiv:1211.6241 [hep-ph]].

78. "Hubble-induced mass from MSSM plasma", M. Kawasaki, F. Takahashi and T. Takesako, JCAP **1304**, 008 (2013) [arXiv:1211.4921 [hep-ph]].

79. "Non-Gaussianity from Attractor Curvaton", K. Harigaya, M. Ibe, M. Kawasaki and T. T. Yanagida, Phys. Rev. D **87**, 063514 (2013) [arXiv:1211.3535 [hep-ph].

80. "High Scale SUSY Breaking From Topological Inflation", K. Harigaya, M. Kawasaki and T. T. Yanagida, Phys. Lett. B **719**, 126 (2013) [arXiv:1211.1770 [hep-ph]].

81. "CMB constraint on non-Gaussianity in isocurvature perturbations", C. Hikage, M. Kawasaki, T. Sekiguchi and T. Takahashi, to be published in JCAP (2013) [arXiv:1211.1095 [astro-ph.CO]].

82. "Heavy Squarks and Light Sleptons in Gauge Mediation From the viewpoint of 125 GeV Higgs Boson and Muon g-2 ", M. Ibe, S. Matsumoto, T. T. Yanagida and N. Yokozaki, JHEP **1303**, 078 (2013) [arXiv:1210.3122 [hep-ph]].

83. "Scale-dependent bias with higher order primordial non-Gaussianity: Use of the Integrated Perturbation Theory", S. Yokoyama and T. Matsubara, Phys. Rev. D **87**, 023525 (2013) [arXiv:1210.2495 [astro-ph.CO]].

84. "Imprints of Non-thermal Wino Dark Matter on Small-Scale Structure", M. Ibe, A. Kamada and S. Matsumoto, Phys. Rev. D **87**, 063511 (2013) [arXiv:1210.0191 [hep-ph]].

85. "Q ball Decay Rates into Gravitinos and Quarks", M. Kawasaki and M. Yamada, Phys. Rev. D **87**, 023517 (2013) [arXiv:1209.5781 [hep-ph]].

86. "CMB power spectra induced by primordial cross-bispectra between metric perturbations and vector fields", M. Shiraishi, S. Saga and S. Yokoyama, JCAP **1211**, 046 (2012) [arXiv:1209.3384 [astro-ph.CO]].

87. "Femto-lensing due to a Cosmic String", C. -M. Yoo, R. Saito, Y. Sendouda, K. Takahashi and D. Yamauchi, PTEP **2013**, 013E01 (2013) [arXiv:1209.0903 [astro-ph.CO]].

88. "Production of 9Be through alpha-fusion reaction of metal-poor cosmic ray and stellar flare", M. Kusakabe and M. Kawasaki, Astrophys. J. **767**, 5 (2013) [arXiv:1208.4210 [astro-ph.CO]].

89. "Gravitational waves from smooth hybrid new infation", M. Kawasaki, K. Saikawa and N. Takeda, to be published in Phys. Rev. D (2013) [arXiv:1208.4160 [astro-ph.CO]].

90. "Non-Gaussian bubbles in the sky", K. Sugimura, D. Yamauchi and M. Sasaki, Europhys. Lett. **100**, 29004 (2012) [arXiv:1208.3937 [astro-ph.CO]].

91. Remarks on Hubble Induced Mass from Fermion Kinetic Term, M. Kawasaki and T. Takesako, Phys. Lett. B **718**, 522 (2012) [arXiv:1208.1323 [hep-ph]].

92. "Pure Gravity Mediation of Supersymmetry Breaking at the LHC", B. Bhattacherjee, B. Feldstein, M. Ibe, S. Matsumoto and T. T. Yanagida, Phys. Rev. D **87**, 015028 (2013) [arXiv:1207.5453 [hep-ph]].

93. "Axion cosmology with long-lived domain walls", T. Hiramatsu, M. Kawasaki, K. Saikawa and T. Sekiguchi, JCAP **1301**, 001 (2013) [arXiv:1207.3166 [hep-ph]].

94. "Primordial black hole formation from an axion-like curvaton model" M. Kawasaki, N. Kitajima and T. T. Yanagida, Phys. Rev. D **87**, 063519 (2013) [arXiv:1207.2550 [hep-ph]].

95. "Weak lensing generated by vector perturbations and detectability of cosmic strings", D. Yamauchi, T. Namikawa and A. Taruya, JCAP **1210**, 030 (2012) [arXiv:1205.2139 [astro-ph.CO]].

96. "Updated constraint on a primordial magnetic field during big bang nucleosynthesis and a formulation of field effects" M. Kawasaki and M. Kusakabe Phys. Rev. D **86**, 063003 (2012) [arXiv:1204.6164 [astro-ph.CO]].

97. "A 125 GeV Higgs Boson Mass and Gravitino Dark Matter in R-invariant Direct Gauge Mediation" M. Ibe and R. Sato, Phys. Lett. B **717**, 197 (2012) [arXiv:1204.3499 [hep-ph]].

98. "Solution to Big-Bang Nucleosynthesis in Hybrid Axion Dark Matter Model", M. Kusakabe, A. B. Balantekin, T. Kajino and Y. Pehlivan, Phys. Lett. B **718**, 704 (2013) [arXiv:1202.5603 [astro-ph.CO]].

99. "Forecast constraints on cosmic string parameters from gravitational wave direct detection experiments", S. Kuroyanagi, K. Miyamoto, T. Sekiguchi, K. Takahashi and J. Silk, Phys. Rev. D **87**, 023522 (2013) [arXiv:1210.2829 [astro-ph.CO]].

100. "Revisiting the cosmological coherent oscillation", M. Kawasaki, N. Kitajima and K. Nakayama, Phys. Rev. D **87**, 023513 (2013) [arXiv:1112.2818 [hep-ph]].

101. "Non-Anomalous Discrete R-symmetry Decrees Three Generations", J. L. Evans, M. Ibe, J. Kehayias and T. T. Yanagida, Phys. Rev. Lett. **109**, 181801 (2012) [arXiv:1111.2481 [hep-ph]].

102. "Stochastic Approach to Flat Direction during Inflation", M. Kawasaki and T. Takesako, JCAP **1208**, 031 (2012) [arXiv:1207.1165 [hep-ph]].

103. "Seesaw Mechanism with Occam's Razo", K. Harigaya, M. Ibe and T. T. Yanagida, Phys. Rev. D **86**, 013002 (2012) [arXiv:1205.2198 [hep-ph]].

104. "The Lightest Higgs Boson Mass in the MSSM with Strongly Interacting Spectators", J. L. Evans, M. Ibe and T. T. Yanagida, Phys. Rev. D **86**, 015017 (2012) [arXiv:1204.6085 [hep-ph]].

105. "Production of dark matter axions from collapse of string-wall system", T. Hiramatsu, M. Kawasaki, K. Saikawa and T. Sekiguchi, Phys. Rev. D **85**, 105020 (2012) [arXiv:1202.5851 [hep-ph]].

106. "Non-Gaussian isocurvature perturbations in dark radiatio", E. Kawakami, M. Kawasaki, K. Miyamoto, K. Nakayama and T. Sekiguchi, JCAP **1207**, 037 (2012) [arXiv:1202.4890 [astro-ph.CO]].

107. "Primordial seeds of supermassive black hole", M. Kawasaki, A. Kusenko and T. T. Yanagida, Phys. Lett. B **711**, 1 (2012) [arXiv:1202.3848 [astro-ph.CO]].

108. "Forecast constraints on cosmic string parameters from gravitational wave direct detection experiment", S. Kuroyanagi, K. Miyamoto, T. Sekiguchi, K. Takahashi and J. Silk, Phys. Rev. D **86**, 023503 (2012) [arXiv:1202.3032 [astro-ph.CO]].

109. "Pure Gravity Mediation with $m_{3/2} = 10 - 100$TeV", M. Ibe, S. Matsumoto and T. T. Yanagida, Phys. Rev. D **85**, 095011 (2012) [arXiv:1202.2253 [hep-ph]].

110. "A 125GeV Higgs Boson and Muon g-2 in More Generic Gauge Mediation", J. L. Evans, M. Ibe, S. Shirai and T. T. Yanagida, Phys. Rev. D **85**, 095004 (2012) [arXiv:1201.2611 [hep-ph]].

111. “Hubble Induced Mass in Radiation Dominated Univers”, M. Kawasaki and T. Takesako, Phys. Lett. B **711**, 173 (2012) [arXiv:1112.5823 [hep-ph]].

112. “The Lightest Higgs Boson Mass in Pure Gravity Mediation Mode”, M. Ibe and T. T. Yanagida, Phys. Lett. B **709**, 374 (2012) [arXiv:1112.2462 [hep-ph]].

113. “Resonant annihilation of long-lived massive colored particles through hadronic collision”, M. Kusakabe and T. Takesako, Phys. Rev. D **85**, 015005 (2012) [arXiv:1112.0860 [hep-ph]].

114. “The GeV-scale dark matter with B-L asymmetry”, M. Ibe, S. Matsumoto and T. T. Yanagida, Phys. Lett. B **708**, 112 (2012) [arXiv:1110.5452 [hep-ph]].

115. “Multi-field open inflation model and multi-field dynamics in tunneling”, K. Sugimura, D. Yamauchi and M. Sasaki, JCAP **1201**, 027 (2012) [arXiv:1110.4773 [gr-qc]].

116. “Prospects for determination of thermal history after inflation with future gravitational wave detectors”, S. Kuroyanagi, K. Nakayama and S. Saito, Phys. Rev. D **84**, 123513 (2011) [arXiv:1110.4169 [astro-ph.CO]].

117. “Weak lensing of CMB by cosmic (super-)strings”, D. Yamauchi, K. Takahashi, Y. Sendouda and C. -M. Yoo, Phys. Rev. D **85**, 103515 (2012) [arXiv:1110.0556 [astro-ph.CO]].

118. “Full-sky lensing reconstruction of gradient and curl modes from CMB maps”, T. Namikawa, D. Yamauchi and A. Taruya, JCAP **1201**, 007 (2012) [arXiv:1110.1718 [astro-ph.CO]].

119. “Cyclotron resonant interactions in cosmic particle accelerators”, T. Terasawa and S. Matsukiyo, Space Science Rev. **173**, 623, Nov 2012.

120. “The 2009-2010 MU radar head echo observation programme for sporadic and shower meteors: radiant densities and diurnal rates”, J. Kero, C. Szasz, T. Nakamura, D. Meisel, M. Ueda, Y. Fujiwara, T. Terasawa, K. Nishimura, and J. Watanabe, Monthly Notices of the Royal Astronomical Society, Volume 425, Issue 1, pp. 135-146, Sep 2012.

121. “Magnetic field decay with Hall drift in neutron star crusts”, Y. Kojima, Y., and S. Kisaka, Monthly Notices of the Royal Astronomical Society, Volume 421, Issue 3, pp. 2722-2730, Apr 2012.

122. “TeV cosmic-ray electrons from millisecond pulsars”, S. Kisaka, and N. Kawanaka, Monthly Notices of the Royal Astronomical Society, Volume 421, Issue 4, pp. 3543-3549, Apr 2012.

(b) Conference Papers

1. “T2K: New physics results”, Shoei Nakayama (on behalf of the T2K Collaboration), Proceedings of the 12th International Conference on Topics in Astroparticle and Underground Physics (TAUP2011), Journal of Physics: Conference Series 375 (2012) 042070.

2. “The Hyper-Kamiokande project,” M. Shiozawa, Nucl. Phys. B (Proc. Suppl.) 237-238 (2013) 289-294.

3. “Low Energy Investigations at Kamioka Observatory”, Hiroyuki Sekiya, Proceedings of the the 6th International Symposium on large TPCs for Low Energy Rare Event Detection, 2012, [arXiv:1301.7125, [astro-ph.IM]].

4. “Status of the XMASS experiment”, K. Hiraide, Proceedings of the 8th Patras Workshop on Axions, WIMPs and WISPs, July 2012.

5. “Recent results from XMASS”, K. Hiraide, Proceedings of the 48th Rencontres de Moriond, March 2013.

6. “Hybrid Photo-Detectors for the Hyper-Kamiokande Project”, Y. NISHIMURA, PoS(PhotoDet 2012)050, 2012.

7. “Results from the Telescope Array experiment”, H. Tokuno for The Telescope Array Collaboration, Proceedings of the 36th International Conference on High Energy Physics (ICHEP2012), July 4-11, 2012, Melbourne, Australia.

8. “Energy spectrum of UHECRs measured by newly constructed fluorescence detectors in Telescope Array experiment”, T. Fujii for the Telescope Array Collaboration, Proceedings of the XVII International Symposium on Very High Energy Cosmic Ray Interactions (ISVHECRI2012), August 10-15, 2012, Berlin, Germany.

9. “TeV cosmic-ray electrons from millisecond pulsars”, S. Kisaka, and N. Kawanaka, Proceedings of the International Astronomical Union, Volume 291, pp. 419-421, Mar 2013.

10. "Cosmic-ray Electrons and Atmospheric Gamma-rays in 1-30 GeV observed with Balloon-borne CALET prototype detector", T. Niita, H. Fuke, K. Yoshida, Y. Katayose, S. Torii, Y. Akaike, K. Kasahara, T. Tamura, Y. Ueyama, S. Ozawa, Y. Shimizu,M. Kyutan, H. Murakami, D.Ito, M. Karube, K. Kondo, 39th COSPAR Scientific Assembly. Held 14-22 July 2012, in Mysore, India. Abstract C2.1-5-12, p.1371.

11. "The MU radar meteor head echo observation programme", J. Kero, T. Nakamura, K. Nishimura, D. Meisel, T. Terasawa, M. Ueda, Y. Fujiwara, C. Szasz, and J. Watanabe, 39th COSPAR Scientific Assembly. Held 14-22 July 2012, in Mysore, India. Abstract C0.3-3-12, p.909.

12. "Development of a Ranging System for the Forward Scattering Meteor Radio Echo Observation Using a GPS-Synchronized Multiple Receiving Stations", T. Usui, H. Yoshida, H. Miyamoto, N. Yaguchi, T. Terasawa, and I. Yoshikawa, Asteroids, Comets, Meteors 2012, Proceedings of the conference held May 16-20, 2012 in Niigata, Japan. LPI Contribution No. 1667, id.6099.

13. "The Forward Scattering Meteor Radio Echo Observation Using a GPS-Synchronized Multiple Receiving Stations", H. Yoshida, T. Terasawa, H. Miyamoto, T. Usui, N. Yaguchi, and I. Yoshikawa, Asteroids, Comets, Meteors 2012, Proceedings of the conference held May 16-20, 2012 in Niigata, Japan. LPI Contribution No. 1667, id.6187.

14. "Stellar-Mass Metallicity Relation at $z \sim 1.4$", Ohta, K., et al., ASP Conference Proceedings, 458, 87, 2012.

15. "Spectroscopic confirmation of three z-dropout galaxies at $z = 6.844 - 7.213$: Demographics of Lyα emission in $z \sim 7$ galaxies", Ono, Y., AIP Conference Proceedings, 1480, 277-280, 2012.

16. "The Resolved Kennicutt-Schmidt Law in Nearby Galaxies", Momose, R., et al., Proceedings of the International Astronomical Union, 292, 335, 2013.

17. "Effect of exotic long-lived sub-strongly interacting massive particles in big bang nucleosynthesis and a new solution to the Li problem," M. Kawasaki and M. Kusakabe, EPJ Web Conf. **20**, 04001 (2012).

(c) ICRR Reports

1. ICRR-Report-612-2012-1
   "Void bias from primordial non-Gaussianities"
   Toyokazu Sekiguchi, and Shuichiro Yokoyama.

2. ICRR-Report-613-2012-2
   "A 125GeV Higgs Boson Mass and Gravitino Dark Matter in R-invariant Direct Gauge Mediation"
   Masahiro Ibe, and Ryosuke Sato.

3. ICRR-Report-614-2012-3
   "The Lightest Higgs Boson Mass in MSSM with Strongly Interacting Spectators"
   Jason L. Evans, Masahiro Ibe, and Tsutomu T. Yanagida.

4. ICRR-Report-615-2012-4
   "Seesaw Mechanism with Occam's Razor"
   Keisuke Harigaya, Masahiro Ibe, and Tsutomu T. Yanagida.

5. ICRR-Report-616-2012-5
   "Primordial black hole formation from an axion-like curvaton model"
   Masahiro Kawasaki, Naoya Kitajima, Tsutomu T. Yanagida.

6. ICRR-Report-617-2012-6
   "Stochastic Approach to Flat Direction during Inflation"
   Masahiro Kawasaki, Tomohiro Takesako.

7. ICRR-Report-618-2012-7
   "Remarks on Hubble Induced Mass from Fermion Kinetic Term"
   Masahiro Kawasaki, Tomohiro Takesako.

8. ICRR-Report-619-2012-8
   "Full bispectra from primordial scalar and tensor perturbations in the most general single-field inflation model"
   Xian Gao, Tsutomu Kobayashi, Maresuke Shiraishi, Masahide Yamaguchi, Jun'ichi Yokoyama, Shuichiro Yokoyama.

9. ICRR-Report-620-2012-9
"Axion cosmology with long-lived domain walls"
Takashi Hiramatsu, Masahiro Kawasaki, Ken'ichi Saikawa, Toyokazu Sekiguchi.

10. ICRR-Report-621-2012-10
"Updated constraint on a primordial magnetic field during big bang nucleosynthesis and a formulation of field effects"
Masahiro Kawasaki, Motohiko Kusakabe.

11. ICRR-Report-622-2012-11
"Pure Gravity Mediation of Supersymmetry Breaking at the LHC"
Biplob Bhattacherjee, Brian Feldstein, Masahiro Ibe, Shigeki Matsumoto, Tsutomu T. Yanagida.

12. ICRR-Report-623-2012-12
"Non-Gaussian bubbles in the sky"
Kazuyuki Sugimura, Daisuke Yamauchi, Misao Sasaki.

13. ICRR-Report-624-2012-13
"Production of 9Be through alpha-fusion reaction of metal-poor cosmic ray and stellar flare"
Kusakabe, Motohiko; Kawasaki, Masahiro.

14. ICRR-Report-625-2012-14
"Femto-lensing due to a Cosmic String"
Chul-Moon Yoo, Ryo Saito, Yuuiti Sendouda, Keitaro Takahashi, Daisuke Yamauchi.

15. ICRR-Report-626-2012-15
"CMB power spectra induced by primordial cross-bispectra between metric perturbations and vector fields"
Maresuke Shiraishi, Shohei Saga, Shuichiro Yokoyama.

16. ICRR-Report-627-2012-16
"Q ball Decay Rates into Gravitinos and Quarks"
Masahiro Kawasaki, Masaki Yamada.

17. ICRR-Report-628-2012-17
"Imprints of Non-thermal Wino Dark Matter on Small-Scale Structure"
Masahiro Ibe, Ayuki Kamada, Shigeki Matsumoto.

18. ICRR-Report-629-2012-18
"Heavy Squarks and Light Sleptons in Gauge Mediation $\sim$ From the viewpoint of 125 GeV Higgs Boson and Muon g-2 $\sim$"
Masahiro Ibe, Shigeki Matsumoto, Tsutomu T. Yanagida, Norimi Yokozaki.

19. ICRR-Report-630-2012-19
"Non-Gaussianity from Attractor Curvaton"
Keisuke Harigaya, Masahiro Ibe, Masahiro Kawasaki, Tsutomu T. Yanagida.

20. ICRR-Report-631-2012-20
"Scale-dependent bias with higher order primordial non-Gaussianity: Use of the Integrated Perturbation Theory"
Shuichiro Yokoyama, Takahiko Matsubara.

21. ICRR-Report-632-2012-21
"Evolution and thermalization of dark matter axions in the condensed regime"
Ken'ichi Saikawa, Masahide Yamaguchi.

22. ICRR-Report-633-2012-22
"Non-Gaussianity from Axionic Curvaton"
Masahiro Kawasaki, Takeshi Kobayashi, Fuminobu Takahashi.

23. ICRR-Report-634-2012-23
"CMB constraint on non-Gaussianity in isocurvature perturbations"
Chiaki Hikage, Masahiro Kawasaki, Toyokazu Sekiguchi, Tomo Takahashi.

24. ICRR-Report-635-2012-24
"High Scale SUSY Breaking From Topological Inflation"
Keisuke Harigaya, Masahiro Kawasaki, Tsutomu T. Yanagida.

25. ICRR-Report-636-2012-25
"Hubble-induced mass from MSSM plasma"
Masahiro Kawasaki, Fuminobu Takahashi, Tomohiro Takesako.

26. ICRR-Report-637-2012-26
"Study of the neutrino mass hierarchy with the atmospheric neutrino data observed in Super-Kamiokande"
Lee Ka Pik.

27. ICRR-Report-638-2012-27
"Revisiting the gravitino dark matter and baryon asymmetry from Q-ball decay in gauge mediation"
Shinta Kasuya, Masahiro Kawasaki, Masaki Yamada.

28. ICRR-Report-639-2012-28
"Smooth hybrid inflation in a supersymmetric axion model"
Masahiro Kawasaki, Naoya Kitajima, Kazunori Nakayama.

29. ICRR-Report-640-2012-29
"Opening the window to the cogenesis with Affleck-Dine mechanism in gravity mediation"
Ayuki Kamada, Masahiro Kawasaki, Masaki Yamada.

30. ICRR-Report-641-2012-30
"Mass Splitting between Charged and Neutral Winos at Two-Loop Level"
Masahiro Ibe, Shigeki Matsumoto, Ryosuke Sato.

31. ICRR-Report-642-2012-31
"Extended analysis of CMB constraints on non-Gaussianity in isocurvature perturbations"
Chiaki Hikage, Masahiro Kawasaki, Toyokazu Sekiguchi, Tomo Takahashi.

32. ICRR-Report-643-2012-32
"Axions : Theory and Cosmological Role"
Masahiro Kawasaki, Kazunori Nakayama.

33. ICRR-Report-644-2012-33
"Testing general scalar-tensor gravity and massive gravity with cluster lensing"
Tatsuya Narikawa, Tsutomu Kobayashi, Daisuke Yamauchi, Ryo Saito.

34. ICRR-Report-645-2012-34
"Scale-dependent bias due to primordial vector field"
Maresuke Shiraishi, Shuichiro Yokoyama, Kiyotomo Ichiki, Takahiko Matsubara.

35. ICRR-Report-646-2012-35
"Heavy gravitino in hybrid inflation"
M. Kawasaki, N. Kitajima, K. Nakayama and T. T. Yanagida.

36. ICRR-Report-647-2012-36
"Forecast constraints on cosmic strings from future CMB, pulsar timing and gravitational wave direct detection experiments"
Sachiko Kuroyanagi, Koichi Miyamoto, Toyokazu Sekiguchi, Keitaro Takahashi, Joseph Silk.

37. ICRR-Report-648-2012-37
"Statistics of general functions of a Gaussian field -application to non-Gaussianity from preheating-"
Teruaki Suyama, Shuichiro Yokoyama.

38. ICRR-Report-649-2012-38
"Gravitational waves from a curvaton model with blue spectrum"
Masahiro Kawasaki, Naoya Kitajima, Shuichiro Yokoyama.

39. ICRR-Report-650-2012-39
"Probing small scale fluctuations with 21cm absorption lines"
Hayato Shimabukuro, Kiyotomo Ichiki, Susumu Inoue, Shuichiro Yokoyama.

40. ICRR-Report-651-2012-40
"Muon g-2 and 125 GeV Higgs in Split-Family Supersymmetry"
Masahiro Ibe, Tsutomu T. Yanagida, Norimi Yokozaki.

D. Doctoral Theses

1. “Precision solar neutrino measurements with Super-Kamiokande-IV”, Takaaki Yokozawa, Ph.D Thesis, Mar. 2013.
2. “Study of the neutrino mass hierarchy with the atmospheric neutrino data observed in Super-Kamiokande”, Lee Ka Pik, Ph.D Thesis, Oct. 2012.
3. “Forecast constraints on cosmic string parameters from observations of gravitational waves and CMB”, K. Miyamaoto, Ph.D Thesis, Mar. 2013.
4. “Production and evolution of axion dark matter in the early universe”, K. Saikawa, Ph.D Thesis, Mar. 2013.

E. Public Relations

(a) ICRR News

ICRR News is a quarterly publication written in Japanese about scientific and educational activities at ICRR. It includes :

1. reports on scientific activities of ICRR staff members and those conducted at one or more of its facilities,
2. reports of international conferences on topics relevant to ICRR’s research activities,
3. reports on topics discussed at ICRR’s Committees,
4. list of publications published by ICRR [ICRR-Report],
5. list of seminars held at ICRR,
6. announcements, and
7. other items of relevance.

Below lists the main topics in the issues published in FY 2012:

No.81 (June 30, 2012)

- Demonstration of thermal noise reduction in CLIO (Cryogenic Laser Interferometer Observatory), Takashi Uchiyama.
- Report of 2011 ICRR graduate student workshop, Hideo Itoh.
- Staff reassignment.
- ICRR-Seminar.
- ICRR-Report.

No.82 (Jan 1, 2013)

- The search for very high energy neutrinos with Ashra, Makoto Sasaki.
- Activity report of Ashra group at Toho University, Satoru Ogawa.
- Report of 2012 Kashiwa Open Campus, Misato Hayashida.
- Staff reassignment.
- ICRR-Seminar.
- ICRR-Report.

No.83 (Feb 28, 2013)

- Report of FY2012 ICRR Workshop on Inter-University Research Activities, Masatake Ohashi.

- Status report and future prospects of XMASS experiment, Hiroshi Ogawa & Masaki Yamashita.
- String cosmology with high precision observations, Daisuke Yamauchi.
- Staff reassignment.

No.84 (Mar 31, 2013)

- Report of ICRR External Review Meeting 2013, Masahiro Teshima.
- New developments of deep universe survey with Hubble Space Telescope I, Yoshiaki Ono & Masami Ouchi.
- Staff reassignment.
- ICRR-Report.

(b) Public Lectures

- "Dark Matter", June 11, 2012, Tokyo Institute of Technology, Tokyo, Yoichiro Suzuki (ICRR, the University of Tokyo).
- "SSH Toyounaka High School", Sep 10, 2012, Kamioka-cho, Hida-city, Gifu, Makoto Miura and Jun Kameda (ICRR, the University of Tokyo).
- "SSH Senior High School Attached to Kyoto University of Education", Aug. 22, 2012, Kamioka-cho, Hida-city, Gifu, Yosuke Koshio (ICRR, University of Tokyo).
- "SSH ikuno High School", Aug. 20, 2012, Kamioka-cho, Hida-city, Gifu, Koh Abe (ICRR, the University of Tokyo).
- "SSH Sanda Shounkan High School", Aug. 9, 2012, Kamioka-cho, Hida-city, Gifu, Hiroyuki Sekiya (ICRR, the University of Tokyo).
- "Yoshiki High School", Jul. 14, 2011, Kamioka-cho, Hida-city, Gifu, Koh Abe (ICRR, the University of Tokyo).
- "SSH Shizuoka-kita High School", Apr. 26, 2012, Kamioka-cho, Hida-city, Gifu, Makoto Miura (ICRR, the University of Tokyo).
- "SSH Fujishima Senior High School", Aug. 1, 2012, Kamioka-cho, Hida-city, Gifu, Jun Kameda (ICRR, the University of Tokyo).
- "SSH Kariya Upper Secondary School", Aug. 7, 2012, Kamioka-cho, Hida-city, Gifu, Makoto Miura (ICRR, the University of Tokyo).
- "SSH Tochigi Ashikaga High School", Aug. 27, 2012, Kamioka-cho, Hida-city, Gifu, Yosuke Koshio (ICRR, the University of Tokyo).
- "SSH Senri Senior High School", Aug. 27, 2012, Kamioka-cho, Hida-city, Gifu, Koh Abe (ICRR, the University of Tokyo).
- "The Large Object Himiko", June 2, 2012, Asahi Culture Center, Tokyo, Masami Ouchi (ICRR, the University of Tokyo).
- "The Largest Network in the Universe—Large Scale Structures—", Nov. 3, 2012, The University of Tokyo Public Lecture, Masami Ouchi (ICRR, the University of Tokyo).

(c) Visitors

KASHIWA Campus (Total: 5 groups, 208 peoples)

- Chiba Career Challenge School
- The University of Tokyo staff competency development program
- Shimane Izumo High School
- Others: 2 groups

KAMIOKA Observatory (Total: 177 groups, 2869 peoples)

- Yumeno Tamago Jyuku (Hida Academy for High School Students)
- MEXT Super Science High School (SSH) project: total 13 schools
- Schools and Universities: total 12 groups
- Researchers: total 14 groups
- Others: 137 groups

F. Inter-University Research Activities

Numbers of Researchers

	Number of Applications	Number of Adoptions	Number of Researchers
Facility Usage			
Kamioka Observatory	35	33	954
Akeno Observatory	4	4	53
Norikura Observatory	7	7	54
Low-Level Radioisotope Measurement Facility	6	6	41
Cryogenic Laser Interferometer in Kashiwa	15	15	173
Laboratorial Facility in Kashiwa	10	10	240
Computer Facility in Kashiwa	12	12	187
Conference Facility in Kashiwa	7	7	327
Over Sea Facilities	11	11	263
Annual Sums	107	105	2292

Collaborative Research			
Neutrino and Astroparticle Research	36	34	958
High Energy Cosmic Ray Research	43	43	868
Astrophysics and Gravity Research	17	17	353
Research Center for Cosmic neutrinos	11	11	113
Annual Sums	107	105	2292

Research Project Titles

1. Study for Supernova monitor
2. Study in upward-going muons and high energy neutrinos
3. 3-flavor oscillation study in atmospheric neutrinos
4. Neutrino workshop
5. Study of flavor identification of atmospheric and beam neutrinos
6. Study of the low energy solar neutrinos
7. Tokai to Kamioka Long Baseline Experiment T2K
8. Study of Supernova Relic Neutrinos
9. Study of atmospheric neutrino flux and neutrino oscillations
10. Search for proton decay via $e + \pi^0$ mode
11. R&D of Mton water Cherenkov Detector Hyper-Kamiokande
12. Study of Solar Neutrino Flux
13. Calibration study of liquid xenon detector
14. Development of low concentration radon detection system
15. Study of solar neutrino energy spectrum
16. Study for the electron neutrino appearance search in the T2K experiment
17. Neutrino interaction study using accelerator data

18. Precise measurement of Day/Night effect for B8 solar neutrinos
19. Study of simulation for atmospheric neutrino
20. Study of nucleon decay $p \to \nu K$
21. Sidereal daily variation of $\sim$10TeV galactic cosmic ray intensity observed by the Super-Kamiokande
22. Energy Calibration for Super-Kamiokande
23. Study for upgrade of XMASS detector
24. Strain, tilt, seismic measurement in Kamioka-mine
25. Analysis of Spatial Distribution of Radon Family Underground and Its Dosimetry
26. Integration of crustal activity observation around the Atotsugawa fault
27. Study for double beta decay of ^{48}Ca
28. A Search for Dark Matter using Liquid Xenon Detector
29. Study for lowering backgrounds of radioisotopes in large volume detectors
30. Development of radon detector for purified gases
31. A study on decay time of liquid xenon scintillation
32. Direction-sensitive dark matter search experiment
33. Microanalysis of gaseous contaminant in Xe
34. Study of energy calibration for dark matter search detector
35. Reconstruction of the optical system of a small Cherenkov telescope at the Akeno Observatory
36. Multi-Color Imager for Transients, Survey and Monstrous Explosions
37. Observation of Galactic Cosmic Rays by Large Area Muon Telescope
38. R&D for a Small Atmospheric Cherenkov Telescope in Akeno Observatory
39. Observations of total ozone and UV solar radiation with Brewer spectrophotometer on the Norikura mountains
40. Thunderstorm-related energetic radiation and cosmic rays
41. In-Situ Conservation–Establishment of handling method of chicks for one month after hatching by cage captivity
42. Observation of solar neutrons in solar cycle 24
43. Dynamics of Abies mariesii forests at forest line of Mt. Norikura
44. Space weather observation using muon hodoscope at Mt. Norikura
45. Evaluation of altitude dependent doses of secondary cosmic neutrons
46. Study of the composition of cosmic-rays at the Knee
47. Experimental Study of High-energy Cosmic Rays in the Tibet ASγ Experiment
48. Study on High Energy Cosmic Ray Sources by Observations in Space
49. A study on variation of interplanetary magnetic field with the cosmic-ray shadow by the sun
50. Study of Galactic Diffuse Gamma Rays
51. Cosmic ray interactions in the knee and the highest energy regions
52. Sidereal daily variation of $\sim$10TeV galactic cosmic ray intensity observed by the Tibet air shower array
53. Observations of high-energy cosmic-ray electrons with emulsion chambers

54. CTA-Japan Physics-Monte Carlo Simulation Joint Research
55. High Energy Gamma-ray Observations of Celestial Objects with the MAGIC telescope
56. Development of the photodetector and readout system for CTA LST
57. Development of camera for CTA small-sized telescopes
58. CTA Project R&D
59. Development of advanced photon counter for the future IACT
60. Study of Very-High Energy Gamma Rays in Australia
61. Workshop on High Energy Gamma-Ray Astrophysics and Fundamental Physics
62. Study of radio detection of highest energy cosmic rays
63. Research and development of detectors for microwave radiations induced by cosmic ray air showers
64. Bolivian Air Shower Joint Experiment
65. Observation of airshower fluorescence light at the TA FD site by using an Imaging UV telescope
66. Study of Extremely-high Energy Cosmic Rays by Telescope Array
67. Study of absolute energy calibration of air shower by a compact electron linac
68. Calibration for TA FD with RC helicopter
69. A R&D for a new atmospheric monitoring system
70. Development of new surface detector for observation of ultra high energy cosmic ray at Telescope Array site
71. Comparative study of astrophysical particle acceleration processes
72. Comprehensive study of particle acceleration process in Crab nebula/pulsar
73. Test and installation of image pipeline for Ashra observation
74. Integration of the optical fiber trigger system for Ashra
75. Test of the sensor to detect cosmic rays for Ashra observation
76. Observation with the All-sky Survey High Resolution Air-shower detector (Ashra)
77. Study of cosmic-ray influence on the growth of tropospheric clouds
78. Gravitational Wave Detector in Kamioka (XI)
79. Study for LCGT data analysis and Research for its System (II)
80. Development of optical cavities for ultranarrow stable lasers
81. Research of Large-scale Gravitational wave Telescope (II)
82. Development of Sapphire Mirror Suspension for LCGT (VIII)
83. Study of quantum noise and quantum non-demolition scheme for LCGT
84. Development of precision profiler for mirrors of LCGT interferometer 2
85. Data analysis using CLIO data (III)
86. Research on ultra-low frequency anti-vibration system for LCGT
87. Research of the Earth's free oscillations based on simultaneous observations with a laser strainmeter and a superconducting gravimeter
88. Measurement of low-temperature mechanical Q for mirror coatings in gravitational-wave detector

89. Development of an evaluation system of a high-quality sapphire for LCGT
90. Real time control for interferometer using computers
91. Research of Cryogenic Silicon mirror for 3rd generation GWDs II
92. Research on cryogenic payload for LCGT
93. Development of Very Low Vibration Cryo-Cooler System
94. Cosmic Reionization Probed with Large Optical Near-Infrared Telescopes
95. Continuous Measurement of Underground Laboratory Environment
96. Evaluation of the erupted radio activities into the environment
97. Detection of time variations for cosmogenic Be-7
98. Detection of low level radioisotopes in tree rings
99. Frontier of the planetary material science
100. Chemical study for Antarctic meteorites and micrometeorites
101. Determination of ^{26}Al in Antarctic meteorite and micrometeorite samples
102. Study of solar activity, cosmic rays and climate change based on the analyses of cosmogenic nuclides and stable isotopes
103. Precise calculation of the atmospheric neutrino flux
104. Simulation Study for the IceCube Neutrino Observatory
105. Future plan town meeting for cosmic ray research

G. List of Committee Members

(a) Board of Councillors

KAJITA, Takaaki	ICRR, the University of Tokyo
FUKUSHIMA, Masaki	ICRR, the University of Tokyo
KAWASAKI, Masahiro	ICRR, the University of Tokyo
NAKAHATA, Masayuki	ICRR, the University of Tokyo
AIHARA, Hiroaki	The University of Tokyo
MATSUMOTO, Yoichiro	The University of Tokyo
YAMAUCHI, Masanori	KEK
KUGO, Taichi	YITP, Kyoto University
HAYASHI, Masahiko	National Astronomical Observatory of Japan
YUDA, Toshinori	The University of Tokyo
MURAKI, Yasushi	Nagoya University
MASAIKE, Akira	Kyoto University
MAKINO, Fumiyoshi	Institute of Space and Astronautical Science
SUGIYAMA, Naoshi	Nagoya University
KOMAMIYA, Yukio	ICEPP, the University of Tokyo

(b) Advisory Committee

KAJITA, Takaaki	ICRR, the University of Tokyo
HISANO, Junji	Nagoya University
SUGIYAMA, Naoshi	Nagoya University
HAZUMI, Masashi	KEK
KISHIMOTO, Tadafumi	Osaka University
YOKOYAMA, Masashi	The University of Tokyo
KANDA, Nobuyuki	Osaka City University
ITOW, Yoshitaka	Nagoya University
NISHIJIMA, Kyoshi	Tokai University
OGIO, Shoichi	Osaka City University
SUZUKI, Yoichiro	ICRR, the University of Tokyo
KURODA, Kazuaki	ICRR, the University of Tokyo
NAKAHATA, Masayuki	ICRR, the University of Tokyo
KAWASAKI, Masahiro	ICRR, the University of Tokyo
TERASAWA, Toshio	ICRR, the University of Tokyo
TESHIMA, Masahiro	ICRR, University of Tokyo

(c) Inter-University Research Advisory Committee

NISHIJIMA, Kyoshi	Tokai University
MUNAKATA, Kazuoki	Shinshu University
TAJIMA, Hiroyasu	Nagoya University
MASUDA, Kimiaki	Nagoya University
YAMAMOTO, Tokonatsu	Konan University
ANDO, Masaki	National Astronomical Observatory of Japan
TSUNESADA, Yoshiki	Tokyo Institute of Technology
KUBO, Hidetoshi	Kyoto University
TERASAWA, Toshio	ICRR, the University of Tokyo
TAKITA, Masato	ICRR, the University of Tokyo
SAGAWA, Hiroyuki	ICRR, the University of Tokyo
OHASHI, Masatake	ICRR, the University of Tokyo
KISHIMOTO, Yasuhiro	ICRR, the University of Tokyo

H. List of Personnel

Director KAJITA, Takaaki,

Vice-Director TERASAWA, Toshio,

Kamioka Observatory (Neutrino and Astroparticle Division)

Scientific Staff	ABE, Ko,	HAYATO, Yoshinari,	HIRAIDE, Katsuki,
	KAMEDA, Jun,	KISHIMOTO, Yasuhiro,	KOBAYASHI, Kazuyoshi,
	KOSHIO, Yusuke,	MIURA, Makoto,	MORIYAMA, Shigetaka,
	NAKAHATA, Msayuki,	NAKAYAMA, Shoei,	OGAWA, Hiroshi,
	SEKIYA, Hiroyuki,	SHIOZAWA, Masato,	SUZUKI, Yoichiro,
	TAKEDA, Atsushi,	TANAKA, Hidekazu,	TOMURA, Tomonobu,
	YAMASHITA, Masaki,	WENDELL, Roger Alexandre	
Administrative Staff	TAKAKURA, Koji,	TANAKA, Masahiro,	
Technical Staff	NOZAWA, Noriyuki,	ONOUE, Tatsuya,	TAMORI, Yukio,
Research Fellow	BAI, Lili,	MARTIMAGRO, Lluis,	TAKENAGA, Yumiko,
	UENO, Koh,	YANG, Byeongsu,	
Secretary	MAEDA, Yukari,	OKURA, Yoko,	TANIMURA, Naoko,
	YONEZAWA, Keiko,		

Research Center for Cosmic Neutrinos (Neutrino and Astroparticle Division)

Scientific Staff	ATHAR, Mohammad Sajjad,	KAJITA, Takaaki,	MASUDA, Kimiaki,
	NISHIMURA, Yasuhiro,	OKUMURA, Kimihiro,	
Technical Staff	SHINOHARA, Masanobu,		
Research Fellow	KAJI, Hiroshi,	LEE, Ka Pic,	McLACHLAN, Thomas Fukuei
Secretary	KITSUGI, Atsuko,	WATANABE, Keiko,	

High Energy Cosmic Ray Division

Scientific Staff	ASAOKA, Yoichi,	ENOMOTO, Ryoji,	FUKUSHIMA, Masaki,
	HAYASHIDA, Masaaki,	KAWATA, Kazumasa	NONAKA, Toshiyuki,
	TAKEDA, Masahiro,	TAKITA, Masato,	TERASAWA, Toshio,
	TESHIMA, Masahiro,	OHNISHI, Munehiro,	OHISHI, Michiko,
	SASAKI, Makoto,	SHIBATA, Tatsunobu,	YOSHIKOSHI, Takanori,
Technical Staff	AOKI, Toshifumi,	KOBAYASHI, Takahide,	OOKI, Kaoru,
Research Fellow	AITA, Yuichi,	AKAIKE, Yosui,	CHEN, Ding,
	FUJII, Toshihiro,	IKEDA, Daisuke,	INOUE, Susumu,
	KIDO, Eiji,	KISAKA, Shota,	MIYAMOTO, Hideaki,
	SAITO, Koji,	TAMEDA, Yoichiro,	
Secretary	KOKUBUN, Yayoi,	OKAMURA, Takako,	SUGAHARA, Midori,

Akeno Observatory (High Energy Cosmic Ray Division)

Scientific Staff	SAGAWA, Hiroyuki,		
Tecnical Staff	OHOKA, Hideyuki,	SHIMIZU, Kanetoshi,	

Norikura Observatory (High Energy Cosmic Ray Division)

Technical Staff	AGEMATSU, Yoshiaki,	ISHITSUKA, Hideki,	OKAZAKI, Nao,
	SHIMODAIRA, Hideaki,	TOKOKU, Chihiro,	USHIMARU, Tsukasa,

Astrophysics and Gravity Division

Scientific Staff	IBE, Masahiro,	KAWAMURA, Seiji,	KAWASAKI, Masahiro,
	KIMURA, Nobuhiro,	KURODA, Kazuaki,	MIYAHARA, Hiroko,
	MIYAKAWA, Osamu,	MIYOKI, Shinji,	NAKATANI, Ichiro,
	OHASHI, Masatake,	OISHI, Naoko,	ONO, Yoshiaki,
	OUCHI, Masami,	SAITO, Yoshio,	SUZUKI, Toshikazu,
	TAKAHASHI, Ryutaro,	UCHIYAMA, Takashi,	YAMAMOTO, Kazuhiro,
Technical Staff	FURUTA, Kiyoshi,	IWASAKI, Utako,	KAMIIZUMI, Masahiro,
	SAKAI, Akiko,		
Research Fellow	FRIEDRICH, Daniel Dieter,	HIROSE, Eiichi,	KUSAKABE, Motohiko,
	MOMOSE, Rieko,	NISHIDA, Erina,	SHIOMI, Sachie,
	SUGIYAMA, Shohei,	YAMAUCHI, Daisuke,	YOKOYAMA, Shuichiro,
	YUMA, Suraphong,		
Secretary	KAWAKAMI, Akiko,	KIKUCHI, Rie,	MASHIMA, Chieko,
	OKINAKA, Mihoko	SATO, Ritsuko,	

Graduate Students

Doctor	IRVINE, Tristan James,	IYOGI, Kazuki,	KIDO, Eiji,
	KAWAKAMI, Etsuko,	KITAJIMA, Naoya,	MIYAMOTO, Koichi,
	OBI, Yoshio,	RICHARD, Euan Neil,	SAIKAWA, Kenichi,
	SAKAKIBARA, Yusuke,	SEKIGUCHI, Takanori,	SHINOZAKI, Akihiro,
	TAKEDA, Naoyuki,	TAKESAKO, Tomohiro,	YOKOZAWA, Takaaki,
Master	CHEN, Dan,	HAGA, Yuto,	HIEDA, Keisuke,
	HIGUCHI, Chika,	HIRANO, Shigetoshi,	KAMETANI, Isao,
	KONNO, Akira,	MIKAMI, Ryo,	NAITO, Yoshiaki,
	NAKAGAWA, Katsuma,	NAKANO, Masayuki,	NAKANO, Yuki,
	NAKAO, Yuta,	OKA, Naoya,	TAKACHIO, Osamu,
	TAKEISHI, Ryuji,	TEJIMA, Koudai,	TSUYUKI, Takanao,
	UMEMOTO, Daigo,	YAMADA, Masaki,	YOSHINO, Kazuyoshi,

Administration Division

Scientific Staff	ITOH, Hideo,		
Administrative Staff	AKIYAMA, Makiko,	FUJIE, Tamiko,	IRIMAJIRI, Aki,
	MARUMORI, Yasuko,	MATSUZAWA, Noboru,	MORITSUBO, Shigeru,
	NAKAMURA, Saori,	OCHI, Masashi,	OGURA, Satoshi,
	SAITO, Akiko,	TAKANO, Eri,	WATANABE, Wataru,
	YAMAGUCHI, Akiko,		
Outreach Staff	HAYASHIDA, Misato		